Exact Open Quantum System Dynamics – Investigating Environmentally Induced Entanglement

Richard Hartmann

Technische Universität Dresden

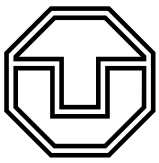

Institut für Theoretische Physik
Gruppe Prof. Dr. Walter Strunz, Theoretische Quantenoptik

Dissertation

Exact Open Quantum System Dynamics – Investigating Environmentally Induced Entanglement

Richard Hartmann

1. Gutachter Prof. Dr. Walter Strunz
Institut für Theoretische Physik
Technische Universität Dresden

2. Gutachter Prof. Dr. Michael Thorwart
Institut für Theoretische Physik
Universität Hamburg

Betreut von Prof. Dr. Walter Strunz

Version vom 1. März 2022

Richard Hartmann

Exact Open Quantum System Dynamics – Investigating Environmentally Induced Entanglement

Dissertation, (eingereicht am 8. November 2021)
Gutachter: Prof. Dr. Walter Strunz und Prof. Dr. Michael Thorwart

Technische Universität Dresden
Gruppe Prof. Dr. Walter Strunz, Theoretische Quantenoptik
Institut für Theoretische Physik
Zellescher Weg 17
01069 Dresden

Abstract

When calculating the dynamics of a quantum system, including the effect of its environment is highly relevant since virtually any real quantum system is exposed to environmental influences. It has turned out that the widely used perturbative approaches to treat such so-called open quantum systems have severe limitations. Furthermore, due to current experiments which have implemented strong system-environment interactions the non-perturbative regime is highly topical. Therefore, determining the exact dynamics of an open quantum system is of fundamental relevance.

The hierarchy of pure states (HOPS) formalism amounts to such an exact approach. Its novel and detailed derivation, as well as several numerical aspects constitute the main methodical part of this work. Furthermore, motivated by fundamental issues but also due to practical relevance for real world devices exploiting quantum effects, the entanglement dynamics of two qubits in contact with a common environment is investigated extensively.

The HOPS formalism is based on the exact stochastic description of open quantum system dynamics in terms of the non-Markovian quantum state diffusion (NMQSD) theory. The distinguishing and numerically beneficial features of the HOPS approach are its stochastic nature, the implicit treatment of the environmental dynamics and, related to this, the enhanced statistical convergence (importance sampling), as well as the fact that only pure states have to be propagated. In order to claim that the HOPS approach is exact, we develop schemes to ensure that the numerical errors can be made arbitrarily small. This includes the sampling of Gaussian stochastic processes, the multi-exponential representation of the bath correlation function and the truncation of the hierarchy. Moreover, we incorporated thermal effects on the reduced dynamics by a stochastic Hermitian contribution to the system Hamiltonian. In particular, for strong system-environment couplings this is very beneficial for the HOPS. To confirm the accuracy assertion we utilize the seemingly simple, however, non-trivial spin-boson model to show agreement between the HOPS and other methods. The comparison shows the HOPS method's versatile applicability over a broad range of model parameters including weak and strong coupling to the environment, as well as zero and high temperatures.

With the reassurance that the HOPS method is versatile and accurately applicable, we investigate the specific case of two qubits while focusing on their entanglement dynamics. It is well known that entanglement, the relevant property when exploiting

quantum effects in fields like quantum computation, communication and metrology, is fragile when exposed to environmental noise. On the other hand, a common environment can also mediate an effective interaction between the two parties featuring entanglement generation. In this work we elucidate the interplay between these competing effects, focusing on several different aspects. For the perturbative (weak coupling) regime we enlighten the difficulties inherent to the frequently used rotating wave approximation (RWA), an approximation often applied to ensure positivity of the reduced state for all times. We show that these difficulties are best overcome when simply omitting the RWA. The seemingly unphysical dynamics can still be used to approximate the exact entanglement dynamics very well. Furthermore, the influence of the renormalizing counter term is investigated. It is expected that under certain conditions (adiabatic regime) the generation of entanglement is suppressed by the presence of the counter term. It is shown, however, that for a deep sub-Ohmic environment this expectation fails. Leaving the weak coupling regime, we show that the generation of entanglement due to the influence of the common environment is a general property of the open two-spin system. Even for non-zero temperatures it is demonstrated that entanglement can still be generated and may last for arbitrary long times. Finally, we determine the maximum of the steady state entanglement as a function of the coupling strength and show how the known delocalization-to-localization phase transition is reflected in the long time entanglement dynamics. All these results require an exact treatment of the open quantum system dynamics and, thus, contribute to the fundamental understanding of the entanglement dynamics of open quantum systems.

Zusammenfassung

Reale Quantendynamik, wie sie in Experimenten zu beobachten ist, wird stets von äußeren Einflüssen mitbestimmt. Es zeigt sich, dass die häufig verwendeten störungstheoretischen Ansätze zur Berücksichtigung dieser Einflüsse nur bedingt gute Ergebnisse liefern. Entsprechend ist die exakte Bestimmung der Dynamik sogenannter offener Quantensysteme von grundlegender Bedeutung. Im Rahmen einer solchen exakten Beschreibung lässt sich außerdem das Regime starker Wechselwirkung zwischen dem System und seiner Umgebung behandeln. Neben dem fundamentalen Interesse, stark wechselwirkende Systeme theoretisch zu beschreiben, führen neuartige Experimente in diesem Regime zu zunehmender praktischer Relevanz.

Einen exakten numerischen Zugang für offene Quantendynamik stellt der *hierarchy of pure states* (HOPS) Formalismus dar. Dessen neuartige und detaillierte Herleitung, sowie diverse nummerische Aspekte werden im methodischen Teil dieser Arbeit dargelegt. In vielerlei Hinsicht relevant folgt als Anwendung eine umfangreiche Untersuchung der Verschränkungsdynamik zweier Qubits unter dem Einfluss einer gemeinsamen Umgebung. Vor allem im Hinblick auf die mittlerweile experimentell realisierbare starke Kopplung mit der Umgebung ist dieses Analyse von Interesse.

Der HOPS-Formalismus basiert auf der stochastischen Beschreibung der Dynamik offener Quantensysteme im Rahmen der *non-Markovian quantum state diffusion* (NMQSD) Theorie. Der stochastische Charakter der Methode, die implizite Berücksichtigung der Umgebungsdynamik, sowie das damit verbundene *Importance Sampling*, als auch die Tatsache, dass lediglich reine Zustände propagiert werden müssen, unterscheidet diese Methode maßgeblich von anderen Ansätzen und birgt numerische Vorteile. Um zu behaupten, dass die HOPS-Methode exakte Ergebnisse liefert, müssen die auftretenden numerischen Fehler beliebig klein gemacht werden können. Ein grundlegender Teil der hier vorgestellten methodischen Arbeit liegt in der Entwicklung diverser Schemata, die genau das erreichen. Dazu zählen die numerische Realisierung von gauß'schen stochastischen Prozessen, die Darstellung der Badkorrelationsfunktion als Summe von Exponentialfunktionen sowie das Abschneiden der Hierarchie. Außerdem wird gezeigt, dass sich der temperaturabhängige Einfluss der Umgebung durch einen stochastischen hermiteschen Beitrag zum System-Hamiltonoperator berücksichtigen lässt. Vor allem bei starker Kopplung ist diese Variante besonders geeignet für den HOPS-Zugang. Um die Genauigkeitsbehauptung der HOPS-Methode zu überprüfen, wird die Übereinstimmung mit anderen Methode gezeigt, wobei das vermeintlich einfachste, jedoch nicht triviale

Spin-Boson-Modell als Testsystem verwendet wird. Diese Untersuchung belegt, dass die HOPS-Methode für eine Vielzahl an Szenarien geeignet ist, wie zum Beispiel schwache und starke Kopplung an die Umgebung, sowie Temperatur null als auch hohe Temperaturen.

Mit der gewonnenen Sicherheit, dass die HOPS-Methode vielseitig einsetzbar ist und genaue Ergebnisse liefert, wird anschließend der spezielle Fall zweier Qubits untersucht. Im Hinblick auf die Ausnutzung von Quanteneffekten in Bereichen wie Quantencomputern, Kommunikation oder Messtechnik liegt der primäre Fokus auf der Dynamik der Verschränkung zwischen den Qubits. Es ist bekannt, dass durch von außen induziertes Rauschen die Verschränkung im Laufe der Zeit abnimmt. Andererseits weiß man auch, dass eine gemeinsame Umgebung zu einer effektiven Wechselwirkung zwischen den Qubits führt, welche Verschränkung aufbauen kann. In dieser Arbeit wird das Wechselspiel zwischen diesen beiden gegensätzlichen Effekten untersucht, wobei die folgenden Aspekte beleuchtet werden. Für den Fall schwacher Kopplung, wo eine störungstheoretische Behandlung in Frage kommt, werden die Probleme der *rotating wave approximation* (RWA) analysiert. Diese Näherung wird häufig verwendet, um die Positivität des reduzierten Zustands für alle Zeiten zu gewährleisten. Es wird gezeigt, dass die negativen Auswirkungen der RWA am besten durch einfaches Weggelassen dieser umgangen werden können. Die auf den ersten Blick nicht-physikalische Dynamik ist sehr gut geeignet, um die exakte Verschränkungsdynamik näherungsweise wiederzugeben. Des Weiteren wird der Einfluss der Renormalisierung durch den sogenannten *counter*-Term untersucht. Unter bestimmten Voraussetzungen (adiabatisches Regime) ist zu erwarten, dass der Verschränkungsaufbau durch den *counter*-Term verhindert wird. Es zeigt sich jedoch, dass für eine sehr subohm'sche Umgebung (deep sub-Ohmic regime) diese Erwartung nicht zutrifft. Mit praktischer Relevanz für neuartige Experimente wird der Fall starker Kopplung zwischen dem Zwei-Qubit-System und der Umgebung betrachtet. Die Berechnungen zeigen das generelle Bild, dass sich zwei nicht wechselwirkende Qubits durch den Einfluss einer gemeinsamen Umgebung verschränken. Selbst bei Temperaturen größer als null kann Verschränkung aufgebaut werden und auch für beliebig lange Zeiten erhalten bleiben. Als spannende letzte Frage wird das Maximum der stationären Verschränkung (Langzeit-Limes) in Abhängigkeit der Kopplungsstärke bestimmt. Die Berechnungen zeigen außerdem, dass eine qualitative Änderung in der Langzeitdynamik der Verschränkung mit dem bekannten Phasenübergang von Delokalisierung zu Lokalisierung einhergeht. All diese Erkenntnisse erfordern eine exakte Behandlung der offenen Systemdynamik und ermöglichen ein erweitertes Verständnis der Verschränkungsdynamik offener Quantensysteme.

Contents

1 Introduction

At the microscopic scale, numerous experiments report effects which clash with our classical intuition from the macroscopic world. They include, for example, the wave-particle-dualism or the quantization of energy. Importantly, the theory of quantum mechanics predicts that a quantum system can be prepared in a superposition of states, with consequences most radically illustrated by Schrödinger's famous thought experiment [Sch35]. The thrilling implications for multi-partite (many-body) quantum states have been discussed manifold in the literature, most prominently under the keywords *Einstein-Podolsky-Rosen-Paradoxon* [EPR35; Boh35] and *Bell inequalities* [Bel64]. The experimental verification that in our world Bell inequalities can indeed be violated [CS78; AGR82; Hen+15] has motivated one of the most fascinating applications of modern physics – the exploitation of *entanglement* to supersede classical computation and communication [NC00]. Although, in principal, the evolution and manipulation of quantum systems and, thus, the dynamical behavior of entanglement is understood, real world implementations suffer from environmental noise. Therefore, investigating the exact entanglement dynamics while including the effect of an environment poses an exciting field which sets the overall scope of the research presented here.

From a fundamental point of view, the system of interest and its surrounding should be modeled on equal grounds [CL83; BP07; Wei08]. This means that the dynamics of the joint global system is governed by the Schrödinger equation as well. As we are interested in the system only, the environmental degrees of freedom can be averaged out. The resulting so-called *reduced dynamics* contains all information to determine the expectation value of any system observable, i.e., any measurable system quantity. Thinking of the surrounding being composed of a very large number of degrees of freedom, which we will refer to as a *macroscopic environment*, obviously precludes a straightforward explicit quantum mechanical treatment of everything. It is the primary task of the field of *open quantum system dynamics* to still calculate the dynamics of the reduced state [BP07; Wei08]. Beyond a perturbative treatment of the system-environment interaction this amounts to an exceptionally difficult task. Various presumably exact approaches have been developed, each with a limited range of applicability. To name but a few, the quasi-adiabatic propagator path integral (QUAPI) [Mak95; MM95] as well as the related time-evolving matrix product operator (TEMPO) approach [Str+18] assume a finite memory length of the environment, which usually holds approximately only. The family of time-

dependent Hatree methods, in particular the multilayer multiconfiguration time-dependent Hartree (ML-MCTDH) approach [WT03] provides a powerful tool to solve the Schrödinger equation of the global system for a very large, but, finite set of environmental oscillators modeling the macroscopic surrounding. Although this approach is well suited to treat a strong system-environment interaction in combination with long lasting environmental correlations [WT10; WS19], it seems unfeasible to account for thermal initial environmental states. In contrast, the hierarchical equations of motion (HEOM) approach [Tan06; Tan14] can treat thermal initial states but becomes impractical for low temperatures. While recent variants have improved on this deficit [Tan+15; RK19], the inherent matrix character of the HEOM approach sets limits on the possible system dimension as well as the coupling strength to the environment.

These limits can be improved by means of a pure state description for the reduced dynamics. The price to pay is the *stochastic* nature of the resulting non-Markovian quantum state diffusion (NMQSD) [Str96; DGS98; SDG99] formalism. As we will show in this theses, a very promising approach to actually solve the NMQSD equation and, with this, unravel the reduced density matrix in terms of pure states, is the hierarchy of pure states (HOPS), first introduced by D. Süß et al. [SES14]. The salient point of the HOPS formalism is to replace the numerically impractical functional derivative appearing in the NMQSD equation by a set of auxiliary states, an approach inspired by the HEOM [Tan06; Tan14]. The evolution equation for these auxiliary states includes yet another set of auxiliary states. In that way an infinite hierarchical structure of coupled differential equations emerges – the HOPS. Note that due to its stochastic nature, the HOPS method can easily be parallelized and is, thus, well suited for modern super computers, allowing us to push the limits on the coupling strength between the system and the environment.

As a first result of this thesis the HOPS approach is elevated to the level of a generally applicable (arbitrary system Hamiltonian and environment, wide range of temperatures, including zero temperature) and numerically exact (in principal, errors can be made arbitrarily small) method. We derive the formalism independently of the existing pathways in Ch. 2 by employing an iterative, and with that, time-discrete formulation of the evolution. In that way the NMQSD equation as well as the HOPS are obtained very transparently (Sec. 2.1). Subsequently, we show how to incorporate non-zero temperature into any zero temperature formalism, e.g., the NMQSD/HOPS approach, by introducing a stochastic contribution to the system Hamiltonian (Sec. 2.2). For the HOPS this is particularly relevant because it leaves the hierarchical structure invariant. This conceptional part is completed by elucidating various other results derived from the NMQSD equation (Sec. 2.3) which are promising on their own and conceivably contribute to alternative descriptions of the reduced dynamics.

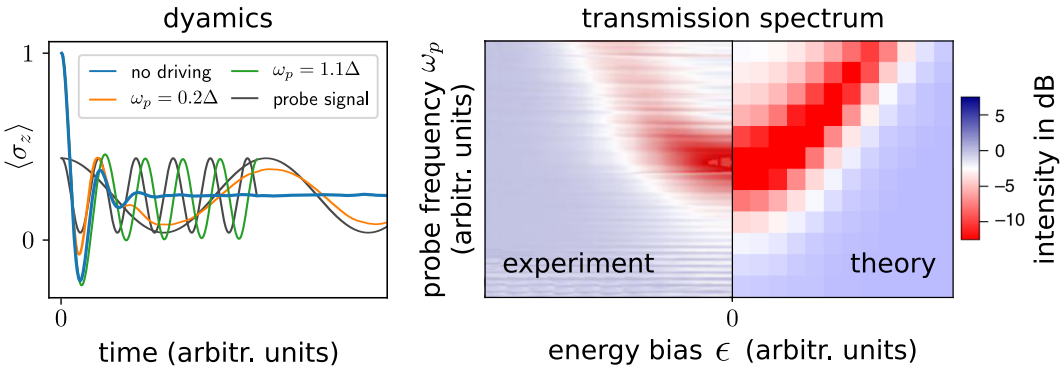

Fig. 1.1: Inspired by a recent experiment from Magazzù et al. [Mag+18] we consider a single spin strongly coupled to a macroscopic environment and show its dynamics obtained from the HOPS (blue line) in the left panel. Strongly damped oscillatory dynamics is clearly visible. When further including an external harmonic probe driving (black lines, two different probe driving frequencies ω_p as examples) the spin dynamics (orange and green lines) exhibits the same periodicity as the probe signal, however, with different amplitude and phase shift. From the amplitude and phase shift, the transmission coefficient can be deduced [Mag+18]. By varying the energy bias ϵ of the spin system and the probe frequency ω_p the transmission spectrum (right panel) follows. Since the spectrum is symmetric around zero, the theoretical data is plotted mirrored to the experimental results from Ref. [Mag+18]. Thus, overall agreement between the theoretical and the experimental data is shown. The rather broad width on the frequency axis, seen in experimental as well as theoretical data, indicates the strong coupling regime which in general requires a non-perturbative, i.e., exact treatment of the open system model.

Besides fundamental interests, exact methods beyond the weak coupling regime, such as the HOPS, are motivated by recent experimental progress focusing on strong system-environment interaction [Fri+19]. In particular, L. Magazzù et al. [Mag+18] achieved to *strongly* couple a superconducting flux qubit to a transmission line which amounts to an implementation of the very prominent spin-boson model (SBM) [Leg+87] (see Sec. 4.1 for details on the model). The strong damping of the spin polarization due to the strong system-environment interaction is reflected in the width of the measured transmission spectrum (see Fig. 1.1). For a theoretical prediction the driven SBM has to be solved. The amplitude/phase relation between the long time spin polarization and the driving signal allows one to deduce the transmission spectrum. The theoretical prediction obtained using the HOPS agrees qualitatively with the experimental data. As seen in the left panel of Fig. 1.1 the associated spin dynamics is strongly damped. This shows that open quantum system dynamics far beyond the perturbative regime has become relevant for experimentalists, too. Noteworthily, also weakly damped quantum systems designed with the intention to serve as building blocks for quantum information tasks [DS13; NMG16], where entanglement plays a crucial role, might require a non-perturbative treatment, as we elucidate in Sec. 5.1.

In order to trust the results of the HOPS formalism, numerical errors need to be controllable which is of particular relevance for the strong coupling regime mentioned above. It is the second major aspect of this thesis (Ch. 3) to elevate the HOPS formalism to serve as an *exact method* in the sense that numerical errors can be made arbitrarily small.

This includes a scheme to reliably sample stochastic processes, which are complex valued, stationary and Gaussian distributed. In Sec. 3.1 we develop two different such sampling schemes. Importantly, for both of them the accuracy can be controlled such that the auto correlation function of the numeric realizations agree with the given one up to a certain tolerance. An implementation of the presented sampling schemes is freely available at `github.com/cimatosa/stocproc`.

Further, the hierarchical structure of the HOPS is governed by the model for the environmental interaction, i.e., the spectral density (SD) or equivalently the bath correlation function (BCF). The particular structure is tightly related to a multi-exponential representation of the BCF where the size of the hierarchy scales with the number of exponential terms. It is, thus, desirable to find a highly accurate representation with as few as possible exponential terms. Here we focus on the commonly used class of Ohmic and sub-Ohmic SDs [Leg+87]. Notably, other approaches, like the HEOM [Tan06; Tan14], require such an exponential representation as well. It is often obtained indirectly via a Maier-Tannor approximation of the SD where this particular form of the SD results exactly in a multi-exponential representation of the BCF [MT99]. However, using this approach for sub-Ohmic SDs, poor results for the dynamics have been noted [Tan+15]. In addition, low temperatures are numerically unfeasible. It is shown in Sec. 3.2 that these limits can be overcome by fitting the multi-exponential representation directly in the time domain. Although this path is numerically very demanding, we find exceptionally good (nearly exponential) convergence of the error with the number of exponential terms used. Based on this, we are able to check convergence of the reduced dynamics with respect to the accuracy of the BCF representation.

Of course, the infinite set of differential equations needs to be truncated for a numerical treatment. Besides discussing general aspects of truncating the hierarchy in Sec. 3.3, we propose a flexible truncation scheme which allows one to tweak the convergence rate with respect to the number of auxiliary states for Ohmic as well as sub-Ohmic SDs. Related to the truncation of the hierarchy, we highlight in Sec. 3.4 the significant numerical benefit of incorporating non-zero temperature effects by means of a stochastic contribution to the system Hamiltonian. This approach outperforms the previously proposed thermo field (TF) method [SU83; TU96] which yields the same NMQSD equation as for zero temperature, but, with the non-zero temperature BCF instead [DGS98].

Since the error due to the stochastic process sampling, the multi-exponential representation of the BCF and the truncation of the hierarchy can be made arbitrarily small, the HOPS method is regarded exact. The wide range of applicability of the HOPS approach is demonstrated in Ch. 4 by solving the so-called spin-boson model (SBM), i.e., a two-level system (spin) in contact with a bosonic environment. As environment we consider the challenging sub-Ohmic case. The comparison with various other approaches yields agreement over a wide range of situations reaching from weak to strong coupling to the environment, as well as zero to high temperature for the initial environmental state.

After having derived, refined and tested the HOPS method we are able to explore in Ch. 5 novel physical effects related to one of the most fascinating properties of quantum mechanics – entanglement. As mentioned at the very beginning, entanglement is the crucial resource when exploiting quantum mechanics to supersede classical applications in fields like computation, communication and metrology. Unfortunately, it has turned out that entanglement is a fragile property which degrades under the influence of a macroscopic environment [Zur03; Min+05]. Even worse, it has been demonstrated that after *finite* time, entanglement may be lost completely [YE09], a phenomenon known as sudden death of entanglement. In contrast, it has been shown that for two *non-interacting* separable qubits, entanglement can still develop due to the interaction with a common environment [Bra02; Isa09]. The interplay between these competing effects poses an exciting field of research.

Similar to many other open systems concerns, the subject has been first addressed by utilizing master equations to model the reduced dynamics (e.g. in Refs. [BF05; LW06; BFM10]). This formalism reveals that the non-unitary contribution to the dynamics (action of the so-called dissipator) results in the decay of entanglement whereas the environmentally induced unitary part (often called Lamb-shift Hamiltonian) can explain the buildup of entanglement. Interestingly, it has been shown also that for two non-interacting qubits the evolution under the dissipator only can generate entanglement, too [BFP03]. However, a few puzzling questions emerged alongside these seminal findings. For example, the success of the quantum optical master equation (QOME) (Born-Markov and rotating wave approximation (RWA)) to describe the decay of a single atom (modeled effectively as two-level system) motivates the application of the same series of approximations to the two-qubit model. Due to the RWA, entanglement generation can only be found for resonant qubits, i.e., qubits with the same energy splitting. Even an infinitesimal detuning of the qubit frequencies results in no entanglement generation at all, which seems not plausible [BFM10]. This deficiency of the RWA to adequately describe bipartite correlations has been noted for a multitude of systems [Ma+12; Eas+16; Dod+18]. As a result, various other master equations circumventing the RWA, while still retaining the Gorini-Kossakowski-Sudarshan-Lindblad (GKSL)-form, i.e., assuring completely

positive dynamics, have been proposed [SB08; BFM09; TB15; Dav20]. Alternatively, the Redfield equation (RFE) can be used, which is sound in a perturbative sense but does not guarantee positivity of the reduced state for all times. Although all of these approaches can resolve the inconsistency related to slightly detuned qubits, it is not obvious which equation is most appropriate. With reference to the exact dynamics obtained from the HOPS we show in Sec. 5.1 that the RFE should be the perturbative method of choice and elucidate the shortcomings of the other approaches. As a remark, the results are in agreement with the thorough accuracy assessment [HS20a] for the same selection of master equations, however, considering a single pseudo-mode environment (single Lorentzian SD). The only difference observed is that for the sub-Ohmic environment considered here, negative eigenvalues of the reduced state approximation from the RFE appear already when the error is still acceptably small. Since the magnitude of the negative and, thus, unphysical contribution is significantly smaller than the error between the exact and the approximate state, the occurrence of the negative contributions does not contradict the usefulness of the RFE. Still, it should be kept in mind that the overall error of the reduced state obtained from the RFE scales linearly with the coupling strength [FC11; HS20a; Dav20; Tup+21]. Therefore, the behavior of the asymptotic entanglement, which is shown in Sec. 5.4 to increase linearly with the coupling strength, cannot be predicted correctly. The same holds true for the other perturbative approaches as well.

Another issue concerns the effect of the so-called counterterm. Originating from the model of a trapped particle in contact with a harmonic environment, the counterterm is included to compensate the change of the potential felt by the particle due to the presence of the environment [Wei08]. For the open two-spin model this corresponds to a compensation of the environmental induced Hamiltonian contribution (Lamb-shift). As mentioned above, this contribution is primarily responsible for the generation of entanglement. Consequently, one expects that including the counterterm inhibits the buildup of entanglement [KA14]. We show in Sec. 5.2 that the effect of including the counterterm depends crucially on the model for the environment, i.e., the kind of SD $J(\omega) \sim \omega^s$. Wile for the Ohmic case ($s = 1$) the inhibition is evident, nearly no effect of the counterterm on the entanglement dynamics is seen in the deep sub-Ohmic regime $s = 0.3$. Utilizing the RFE, we can explain this behavior by showing that the remaining contribution of the Lamb-shift Hamiltonian plus the counterterm is related to the flatness of $S(\omega)$ over the interval containing all transition frequencies of the system Hamiltonian. The function $S(\omega)$ denotes the half sided Fourier transform of the BCF and is, thus, determined by the SD. Remarkably, we find the unexpected result that even in the adiabatic limit, i.e., $S(\omega)$ becomes effectively flat, for resonant qubit and a sub-Ohmic environment, entanglement generation beyond purely dissipative effects remains [HS20b].

As a next step we investigate the entanglement dynamics far beyond the perturbative regime. We analyze a broad range of model parameters, showing that the HOPS approach suits many scenarios encountered by current experiments featuring strong system-environment interactions [Mag+18]. Furthermore, the strong coupling regime is methodically relevant since for this case inconsistencies between several other numerical methods have been noted recently [Zho+18]. In Sec. 5.3 we show the exact entanglement dynamics for a broad range of coupling strengths and various detuning parameters. The buildup of a significant amount of entanglement appears to be the general case. The significant difference between resonant and detuned qubits, observed for weak coupling, disappears. When including non-zero temperature, entanglement generation can still be observed. As intuitively expected, increasing the temperature leads to less entanglement being generated. Nonetheless, our results show that the generation of entanglement is far from being a zero-temperature phenomenon.

As mentioned above, the entanglement of the steady state is inaccessible by perturbative approaches, here referred to master equations of first order in the coupling strength (second order in the interaction Hamiltonian) [FC11; HS20a]. This motivates us to investigate the asymptotic entanglement by means of HOPS in Sec. 5.4. It is estimated from a sufficiently long real time propagation of the reduced state. Unfortunately, a direct calculation of the steady state within the HOPS formalism is not straightforward. We find that the asymptotic entanglement increases linearly from zero when increasing the coupling strength. Note that it is plausible that for zero coupling strength, i.e., the qubits are isolated from the environment, the asymptotic entanglement is zero since no entanglement can be induced by the environment. The limit of infinite coupling strength can be treated analytically, too, by simply neglecting the system Hamiltonian. The resulting dephasing-like model results in no dynamics at all for the particular initial condition of the two spins oriented in z-direction. Consequently, the reduced states remains separable for all times. It follows that the asymptotic entanglement as a function of the coupling strength must exhibit a maximum. By means of the HOPS formalism we find the location and the value of that maximum for the two exemplary cases of an Ohmic and a sub-Ohmic ($s = 0.3$) environment. In other words, for two qubits with no direct interaction we deduce the particular coupling strength between the system and the environment at which the long-time entanglement between the qubits becomes largest. For both cases ($s = 1$ and $s = 0.3$) the maximum was found in the vicinity of the coupling strength $\eta \approx 0.5$ (see Eq. (3.25) for a definition of η). Further we show that the asymptotic entanglement is nearly independent of the detuning of the two qubits. This is particularly remarkable in the weak coupling regime where the intermediate path to the asymptotic state, the entanglement dynamics as such, is very sensitive to the detuning. With respect to the presence of the counterterm, in the weak coupling regime its diverse effects on the dynamics (elucidated in Sec. 5.2) are reflected by

the asymptotic entanglement, too. Since the counterterm, which mimics a direct interaction between the qubits, scales with the coupling strength, a different overall behavior is expected in the strong coupling regime. Our calculation shows that the asymptotic entanglement arising when including the counter term increases monotonically with the coupling strength, i.e., no maximum is observed.

While examining the asymptotic entanglement for the special case of zero temperature, and with that the asymptotic state, we are able to connect our dynamical results to the known phase transition of the two-spin system [Ort+10; WR14; Zho+18]. In spirit of other works concerning a single spin [WT08; WT10; Str+18] we use the asymptotic spin polarization of, for example, spin A $\langle\sigma_z^A\rangle$ as an order parameter. For a sub-Ohmic environment we find that $\langle\sigma_z^A\rangle$ remains zero (delocalized phase) upon increasing the coupling strength until a critical value η_c is reached. Beyond that, $\langle\sigma_z^A\rangle$ increases continuously (localized phase) which reflects the second order phase transition. We find that the critical coupling strength coincides with the position of the maximum of the asymptotic entanglement. Notably, passing the critical coupling strength is also reflected in a qualitative change of the entanglement dynamics. For $\eta < \eta_c$ the entanglement approaches the steady state quickly (on the scale η^{-1}). Contrarily, for $\eta > \eta_c$ an additional exponential relaxation appears with a decay rate vanishing as η approaches η_c from above. The sudden appearance of this additional decay is responsible for a kink in the asymptotic entanglement as a function of the coupling strength. Since this slow decay is very sensitive to the accuracy of the multi-exponential representation of the sub-Ohmic BCF (Sec. 3.2), determining the asymptotic entanglement in the regime of localization is numerically very demanding. For an Ohmic SD the phase transition appears at a larger coupling strength while the location of the maximum of the asymptotic entanglement remains nearly unchanged. Determining the exact value of the critical coupling strength of the phase transition by means of real time dynamics remains challenging, as for the single spin case [Str+18].

As a summary, the results presented in Ch. 5 concern a) the applicability of perturbative master equations (Sec. 5.1), b) the anomalous behavior in the adiabatic regime where the renormalizing counterterm is expected to inhibit entanglement generation (Sec. 5.2), c) the entanglement dynamics beyond the weak coupling regime for various model parameters, including zero and non-zero temperature (Sec. 5.3) and d) the asymptotic entanglement while drawing the connection to the known phase transition of the two-spin-boson model (Sec. 5.4).

From a methodical point of view, these results demonstrate the wide range of applicability of the HOPS approach and show how far the limits of exact open quantum system dynamics approaches have been pushed. The thesis closes with conclusions and an outlook on future project arising from our results.

Open Quantum System Dynamics

2

Perfectly isolating a quantum system from its surrounding is an idealized concept. Therefore, in order to calculate the dynamics of a *real* quantum system it is inevitable to including external influences which result in dissipation of energy and decoherence of quantum states. For a fully quantum mechanical description of such open quantum systems the environment is commonly modeled by a set of harmonic oscillators. Note that this oscillator model has one of its roots in the classical description of a particle exhibiting Brownian motion due to environmental influences [Ull66]. In the standard model the system and the environment are coupled by a Hermitian interaction linear in the creation (annihilation) operator $a_\lambda^\dagger$ (a_λ) of the environmental mode λ [Leg+87; BP07; Wei08; CDG98]. The unitary dynamics of the composite system, system of interest and environment, is governed by the so-called microscopic Hamiltonian

$$\begin{aligned} H &= H_{\text{sys}} + H_{\text{interaction}} + H_{\text{env}} \\ &= H_{\text{sys}} + \sum_\lambda (g_\lambda^* L a_\lambda^\dagger + \text{h.c.}) + \sum_\lambda \omega_\lambda a_\lambda^\dagger a_\lambda \ . \end{aligned} \tag{2.1}$$

H_{sys} denotes the system Hamiltonian and L the coupling operator, both acting on the Hilbert space of the system. L can be Hermitian but does not have to be. The coupling constants g_λ account for the individual coupling strength between the system and the mode with frequency ω_λ. For convenience, units are used where $\hbar$ (reduced Planck constant) and k_B (Boltzmann constant) become unity.

To model the effect of a genuine environment, leading to dissipation and decoherence, the discrete set of environmental modes needs to become infinite with a dense distribution of the frequencies ω_λ [Wei08] – the so-called continuous limit. This leads to the concept of the spectral density (SD) where the individual coupling strengths g_λ are captured by a, in general, continuous function in ω

$$J(\omega) := \pi \sum_\lambda |g_\lambda|^2 \delta(\omega - \omega_\lambda) \ . \tag{2.2}$$

Note, the factor π is solely conventional. It has its origin in the derivation of perturbative master equations and was kept to relate this work more easily to the literature.

The equation of motion given by the microscopic Hamiltonian [Eq. (2.1)], in particular in the continuous $J(\omega)$ limit, can, in general, not be solved explicitly as

of its infinite dimension. Even a suitable truncation of each harmonic oscillator does not solve this problem. However, since the original motivation is to model the dynamics of the system part including dissipation, the primary task is to calculate the non-unitary dynamics of the *reduced density matrix*

$$\rho_{\mathrm{sys}}(t) \coloneqq \mathrm{Tr}_{\mathrm{env}}\rho(t) \tag{2.3}$$

where the total state $\rho(t)$ evolves unitarily according to the von-Neumann equation $\mathrm{i}\dot{\rho}(t) = [H, \rho(t)]$ and $\mathrm{Tr}_{\mathrm{env}}$ denotes the partial trace over the environmental modes. Under suitable conditions (weak coupling and/or an effectively flat SD) the reduced dynamics can be calculated efficiently in a perturbative manner using time local master equations [Red57; Dav74; SB08; Dav20] (see also App. D). However, when leaving the perturbative regime the calculation of the reduced dynamics becomes substantially more challenging. Not only theoretical interest but also the growing number of experiments considering non-trivial environmental influences ([Eng+07; Nie+10; MM13; Bay+17; Mag+18] to list a few only) has encouraged the development of non-perturbative methods. Without doubt, the steady increase of computational power over the last decades has contributed to the successful application and further refinement of such methods as well.

The non-perturbative methods fall mainly into two categories. On the one hand, for so-called explicit methods the continuous environment is approximated by a sufficiently large but finite set of modes. It is the challenge of such methods to calculate the dynamics governed by the still very large microscopic Hamiltonian in a sophisticated way. Consequently, the reduced dynamics is simply obtained by explicitly performing the trace over the environmental degrees of freedom. Among the most prominent candidates for that group are variants of the time-dependent Hartee (TDH) formalism [MMC90; WT03], the time-dependent numerical renormalization group (TD-NRG) [AS05; AS06] and the multi-Davydov-Ansatz [Sun+15; Gro+16; WG18].

On the other hand, evolution equations for the reduced state alone can also be constructed. These so-called reduced methods usually involve the BCF (here for zero temperature)

$$\alpha(\tau) \coloneqq \frac{1}{\pi}\int_0^\infty \mathrm{d}\omega\, J(\omega)e^{-\mathrm{i}\omega\tau} \tag{2.4}$$

which contains, just like the SD, all the necessary information about the coupling to the environment. Successfully applied methods from that group include the quasi-adiabatic propagator path integral (QUAPI) [Mak95; MM95], its variant based on matrix product states – the time-evolving matrix product operator (TEMPO) approach [Str+18] and the hierarchical equations of motion (HEOM) [Tan06; Tan14] including several variants [Tan+15; RK19].

As a side note, the two categories are opposing in the sense that frequency and time are conjugate variables. Further details have been discussed in a cooperation with Michael Werther and Frank Großmann [Har+19] where a path towards an intermediate picture has been proposed.

Although the pool of available methods seems rich, each approach has its limits. The explicit methods, for example, struggle with non-zero temperature. The QUAPI approach requires a sufficiently short memory time for the environment and the HEOM approach, in its traditional form, makes use of the Maier-Tannor decomposition [MT99] for the SD and, thus, does not work for low temperatures. Also, since the reduced methods are usually based on auxiliary density matrices computational storage limits are reached quickly.

Yet another very promising line of reasoning aims for a *stochastic representation* of the reduced state. Suitable for the non-perturbative regime (usually referred to as non-Markovian in the literature) the fundamental non-Markovian quantum state diffusion (NMQSD) formalism [Str96; DGS98; SDG99] yields, as we will show, the generally applicable and numerically exact HOPS method [SES14; HS17] – the principal method of this thesis. It allows one, for example, to treat *both* zero and non-zero temperature environments. Although the method can be considered as a reduced method, it is based on pure states instead of density matrices at the cost of being a stochastic method. This, however, can easily be coped with by numeric parallelization. Also, in a stochastic sense, the global microscopic state can be recovered. Remarkably, as a consequence of realizing an importance sampling scheme a non-linear evolution equation emerges which allows for an efficient treatment of strong environmental interactions.

The central steps to derive the HOPS in linear and non-linear form are presented in the following section 2.1 by using a time-discrete formulation. This new time-discrete path represents an independent and highly transparent derivation of the NMQSD / HOPS formalism. Equally important, in section 2.2 a novel and numerically highly favorable way to treat non-zero temperature initial environmental states follows. These two sections provide the fundamentals for the HOPS formalism. In addition, section 2.3 contains various different aspects related to the NMQSD and HOPS theory intended to inspire future investigations. Nonetheless, special notice should be given to the Karhunen-Loève expansion Schrödinger equation (KLESEQ) derived in Sec. 2.3.1 which provides a new approach especially suited for environments with long memory times and is, thus, complementary to the well studied Markovian regime. It is particularly interesting since it is based explicitly on the BCF but has the notion of a discrete environment, however, with time-dependent coupling strengths.

2.1 Derivation of the Hierarchy of Pure States (HOPS) Formalism

The HOPS was first derived by D. Süß et al. [SES14] from the NMQSD approach [Str96; DGS98; SDG99]. Despite the NMQSD framework being well known, here we derive the NMQSD equation as well as the HOPS in an independent manner. By utilizing a time-discrete scheme the NMQSD/HOPS formalism follows in a clear and self-contained way. In addition, this novel time-discrete formulation contributes on a more fundamental level, too. We are able to relate the reduced dynamics to a so-called time-oscillator model – instead of a static coupling to the environment, the sought after reduced dynamics is also obtained when the system couples dynamically to a new oscillator at each time step (see Sec. 2.3.2).

2.1.1 Time-Discrete Non-Markovian Quantum State Diffusion (NMQSD) Equation

The main achievement of the NMQSD theory is to express the reduced density matrix as ensemble average over dyads of stochastic pure states where the evolution of these states is governed by the NMQSD equation.

Starting point is the formal expression of the reduced state [Eq. (2.3)] where the trace over the environment has been made explicit in terms of Bargmann coherent states [Bar61] $|z_\lambda\rangle := e^{z_\lambda a_\lambda^\dagger}|0\rangle_\lambda$ with the *coherent state labels* $z_\lambda \in \mathbb{C}$ and $|0\rangle_\lambda$ denoting the ground state of the mode with index λ,

$$\rho_{\mathrm{sys}}(t) = \mathrm{Tr}_{\mathrm{env}}(|\Psi(t)\rangle\langle\Psi(t)|) = \int \mathrm{d}^2\mathbf{z}\frac{e^{-|\mathbf{z}|^2}}{\pi^{N_B}}\langle\mathbf{z}|\Psi(t)\rangle\langle\Psi(t)|\mathbf{z}\rangle \ . \tag{2.5}$$

Note, to ensure unambiguous notation the number of environmental oscillators N_B enters explicitly. The boldface notation is used to express the vector character of $\mathbf{z} := (z_1, \dots z_{N_B})^T$. In addition $|\mathbf{z}\rangle$ is meant to abbreviate the tensor product $|\mathbf{z}\rangle := |z_1\rangle \dots |z_{N_B}\rangle$ and $\mathrm{d}^2 z_\lambda := \mathrm{d}\,\mathrm{Re}(z_\lambda)\,\mathrm{d}\,\mathrm{Im}(z_\lambda)$. To eliminate the oscillator dynamics, the interaction picture with respect to the environmental Hamiltonian H_{env} is chosen for the total state $|\Psi(t)\rangle$. Thus, $|\Psi(t)\rangle$ evolves according to the following Schrödinger equation

$$\begin{aligned} \mathrm{i}\partial_t|\Psi(t)\rangle &= U_{\mathrm{env}}^\dagger(t)(H - H_{\mathrm{env}})U_{\mathrm{env}}(t)|\Psi(t)\rangle \\ &= \Big(H_{\mathrm{sys}} + \sum_\lambda g_\lambda^* e^{\mathrm{i}\omega_\lambda t} L a_\lambda^\dagger + g_\lambda e^{-\mathrm{i}\omega_\lambda t} L^\dagger a_\lambda\Big)|\Psi(t)\rangle \ . \end{aligned} \tag{2.6}$$

Since the propagator $U_{\mathrm{env}}(t) = e^{-\mathrm{i}H_{\mathrm{env}}t}$ acts on the environment only, the reduced state is unaffected by that particular choice of interaction picture.

Reading the integral (2.5) in a Monte-Carlo sense turns the coherent state labels into complex valued Gaussian distributed random variables with zero mean and covariances

$$\mathcal{M}(z_\lambda z_{\lambda'}) = \mathcal{M}(z_\lambda^* z_{\lambda'}^*) = 0 \quad \text{and} \quad \mathcal{M}(z_\lambda z_{\lambda'}^*) = \delta_{\lambda,\lambda'} \; . \tag{2.7}$$

Consequently, the reduced state appears as an ensemble average, generally denoted by $\mathcal{M}$, over the coherent state labels

$$\rho_{\mathrm{sys}}(t) = \mathop{\mathcal{M}}_{\mathbf{z}} \left(|\psi(\mathbf{z}^*,t)\rangle\langle\psi(\mathbf{z},t)| \right) \tag{2.8}$$

of the dyads of the *stochastic pure state*

$$|\psi(\mathbf{z}^*,t)\rangle \coloneqq \langle \mathbf{z}|\Psi(t)\rangle \; . \tag{2.9}$$

For completeness, it is a property of the Bargmann coherent states that $\langle\Psi(t)|\mathbf{z}\rangle$ is holomorphic in $\mathbf{z}$ and, thus, does not depend on $\mathbf{z}^*$. This is of importance, e.g., for the non-linear theory (Sec. 2.1.3) and explains the notation $|\psi(\mathbf{z}^*,t)\rangle$ for the stochastic pure state.

Therefore the dynamics of the reduced state can be obtained if the dynamics of the stochastic pure state is known. Using that $\langle\mathbf{z}|a_\lambda|\Psi\rangle = \partial_{z_\lambda^*}\langle\mathbf{z}|\Psi\rangle$ and $\langle\mathbf{z}|a_\lambda^\dagger|\Psi\rangle = z_\lambda^*\langle\mathbf{z}|\Psi\rangle$, its evolution equation follows from the Schrödinger equation (2.6) and reads

$$\partial_t\psi(\mathbf{z}^*,t) = \left[-\mathrm{i}H_{\mathrm{sys}} + \eta^*(\mathbf{z}^*,t)L - \mathrm{i}L^\dagger \sum_\lambda g_\lambda e^{-\mathrm{i}\omega_\lambda t}\partial_{z_\lambda^*} \right] \psi(\mathbf{z}^*,t) \tag{2.10}$$

where the microscopic definition of the *stochastic process* $\eta^*(t)$, a scalar complex function,

$$\eta^*(\mathbf{z}^*,t) \coloneqq -\mathrm{i}\sum_\lambda g_\lambda^* z_\lambda^* e^{\mathrm{i}\omega_\lambda t} \tag{2.11}$$

has been introduced. In order to clarify notation, we choose the symbol η^* for the stochastic process which differs from the notation established in the literature [DGS98; SDG99] where z^* has been chosen. Here, we reserve the symbol $\mathbf{z}^*(t)$ for the vector of co-moving coherent state labels only (see Sec. 2.1.3). Note that for reasons of convenience the "bra-ket" notation of the stochastic pure state will be omitted whenever the notion as "ket"-vector is clear, i.e., $|\psi(\mathbf{z}^*,t)\rangle \stackrel{\triangle}{=} \psi(\mathbf{z}^*,t)$.

Although the stochastic pure state is an element of the system Hilbert space, the number of bath modes is still present in the above expression (2.10) by means of

the coherent state labels. Crucially, this $\mathbf{z}^*$ dependence (frequency domain) can be cast into a functional dependence on the stochastic process η^* (time domain) and with that a dependence on the BCF only. In order to show that, a factorized initial pure state is assumed, i.e.,

$$|\Psi_0\rangle = |\psi_0\rangle \bigotimes_{\lambda}^{N_B} |0\rangle_\lambda \,, \tag{2.12}$$

with an arbitrary system state $|\psi_0\rangle$ and a zero temperature environment corresponding to the ground states $|0\rangle_\lambda$ of the environmental modes. Note that an initial thermal environmental condition can be dealt with as well by still making use of the zero temperature formalism (see Sec. 2.2.2). The expressions derived next do not contain the number of bath modes N_B anymore and, thus, intrinsically allow for the continuous limit ($N_B \to \infty$) of the SD.

The derivation presented here departs from the original lines of reasoning by using a time-discrete scheme instead of keeping the differential form. For a fixed Δt the index n is used to enumerate equally spaced time points $t_n := n\Delta t$ and with that

$$\psi_n(\mathbf{z}^*) := \psi(\mathbf{z}^*, t_n), \qquad \eta_n^*(\mathbf{z}^*) := \eta^*(\mathbf{z}^*, t_n) = -\mathrm{i}\sum_\lambda g_\lambda^* z_\lambda^* e^{\mathrm{i}\omega_\lambda n\Delta t} \,. \tag{2.13}$$

It follows from the evolution equation (2.10) that up to first order in Δt the propagation from t_n to t_{n+1} becomes

$$\begin{aligned} \psi_{n+1}(\mathbf{z}^*) &= [1 + \Delta t K_n]\, \psi_n(\mathbf{z}^*) \\ K_n &:= -\mathrm{i}H_{\mathrm{sys}} + \eta_n^*(\mathbf{z}^*)L - \mathrm{i}L^\dagger \sum_\lambda g_\lambda e^{-\mathrm{i}\omega_\lambda n\Delta t}\partial_{z_\lambda^*} \,. \end{aligned} \tag{2.14}$$

To elucidate the change of variables for the stochastic pure state from $\mathbf{z}^*$ to the functional η^* the successive iteration of equation (2.14) is considered. From the initial condition $|\Psi(0)\rangle = |\psi_0\rangle|\mathbf{0}\rangle$ it follows that the stochastic pure state at time $t = 0$ coincides with the initial state of the system $\psi_0(\mathbf{z}^*) = |\psi_0\rangle\langle\mathbf{z}|\mathbf{0}\rangle = |\psi_0\rangle$ and, thus, does not depend on $\mathbf{z}^*$. As a consequence the partial derivative with respect to z_λ^* acting on ψ_0 vanishes and it follows

$$\psi_1(\mathbf{z}^*) = [1 + \Delta t(-\mathrm{i}H_{\mathrm{sys}} + \eta_0^*(\mathbf{z}^*)L)]\psi_0 \,. \tag{2.15}$$

Evidently, ψ_1 depends on $\mathbf{z}^*$ solely by means of the complex scalar η_0^*. Concerning the next iteration $\psi_2 = [1 + \Delta t K_1]\psi_1$, this can be used to express the partial derivative acting on ψ_1. By using the chain rule it follows that

$$-\mathrm{i}\sum_\lambda g_\lambda e^{-\mathrm{i}\omega_\lambda t_1}\partial_{z_\lambda^*}\, \psi_1(\eta_0^*(\mathbf{z}^*)) = -\sum_\lambda |g_\lambda|^2 e^{-\mathrm{i}\omega_\lambda(t_1 - t_0)}\partial_{\eta_0^*}\psi_1(\eta_0^*) \,. \tag{2.16}$$

Realizing that the right hand side contains the zero temperature bath correlation function $\alpha(\tau)$ introduced in Eq. (2.4), results in

$$\psi_2(\mathbf{z}^*) = \left[1 + \Delta t \left(-\mathrm{i}H_{\mathrm{sys}} + \eta_1^*(\mathbf{z}^*)L - L^\dagger \alpha(t_1 - t_0)\partial_{\eta_0^*}\right)\right] \psi_1(\eta_0^*(\mathbf{z}^*)) \tag{2.17}$$

which shows that ψ_2 depends on $\mathbf{z}^*$ through η_0^* and η_1^*. In the same way it follows that: given ψ_n depends on $\eta_0^* \dots \eta_{n-1}^*$ then ψ_{n+1} takes the form

$$\psi_{n+1}(\eta^*|_0^n) = \left[1 + \Delta t \left(-\mathrm{i}H_{\mathrm{sys}} + \eta_n^* L - L^\dagger \sum_{m=0}^{n-1} \alpha(t_n - t_m)\partial_{\eta_m^*}\right)\right] \psi_n(\eta^*|_0^{n-1}) \tag{2.18}$$

and, thus, depends on $\eta_0^* \dots \eta_n^*$ (shorthand notation $\eta^*|_0^n$). By mathematical induction it follows that for any $n \geq 0$, ψ_{n+1} depends on $\eta^*|_0^n$.

Although the time-discrete evolution equation (2.18) does not depend explicitly on the infinite number of random variables z_λ, it does so implicitly through $\eta^*|_0^n$. However, since η_k^* depends linearly on the original Gaussian random variables $\mathbf{z}^*$, η_k^* is also Gaussian distributed. Therefore, the statistical properties of η_k^* are fully determined by its first and second moment. From the definition of the stochastic process η^* [Eq. (2.11)] and the statistics of z_λ^* [Eq. (2.7)] it follows that

$$\mathcal{M}(\eta_k^*) = 0, \quad \mathcal{M}(\eta_k^*\eta_l^*) = 0 = \mathcal{M}(\eta_k\eta_l) \quad \text{and} \quad \mathcal{M}(\eta_k\eta_l^*) = \alpha(t_k - t_l)\,. \tag{2.19}$$

This shows that equation (2.18) is fully characterized by H_{sys}, L and the BCF $\alpha(\tau)$.

Taking the limit $\Delta t \to 0$ leads to the known differential form of the NMQSD equation

$$\partial_t \psi_t[\eta^*] = \left[-\mathrm{i}H_{\mathrm{sys}} + \eta^*(t)L - L^\dagger \int_0^t \mathrm{d}s\, \alpha(t-s)\frac{\delta}{\delta\eta^*(s)}\right] \psi_t[\eta^*]\,. \tag{2.20}$$

The random variables η_k^* turn into a time continuous, complex valued, Gaussian distributed and stationary stochastic process $\eta^* = \eta^*(t)$ with zero mean and only one non-vanishing second moment

$$\mathcal{M}(\eta(t)\eta^*(s)) = \alpha(t-s)\,. \tag{2.21}$$

Consequently, the stochastic pure state becomes a functional of the stochastic process η^* indicated by the squared brackets. Although the equation is local in time with respect to the stochastic pure state, it contains a convolution-like integral which probes how the stochastic pure state at time t depends on the entire history of the stochastic process.

At this stage, we have derived the evolution equation for the stochastic pure states, the NMQSD equation (2.20). Solving this equation independently for many different

realizations of the stochastic process $\eta^*(t)$ and taking the ensemble average over their dyads yields the sought after reduced dynamics. However, due to the integral over the functional derivative the NMQSD equation cannot be solved straightforwardly. In the following we show how to overcome this difficulty by introducing auxiliary states comprising the complicated terms, eventually leading to the hierarchy of pure states (HOPS). As acknowledging note, this strategy was inspired by the HEOM [TK89; Tan06] – a reduced method based on (auxiliary) density matrices rather than pure states.

2.1.2 Time-Discrete HOPS

Here the HOPS is deduced from the time-discrete NMQSD equation (2.18). This derivation is very transparent because it involves only partial rather than functional derivatives. Of course, both approaches are equivalent, especially, since the functional derivative is defined as the limiting case of infinitely many partial derivatives.

As a remark, the explicit expression defining the auxiliary states is related to a particular representation of the BCF. If it is possible to represent the BCF and its derivative in terms of a *finite* set of functions a HOPS can be constructed which yields the exact reduced dynamics. However, since the numerical effort to propagate the HOPS scales with the number of such functions a small set is desirable. Hence, the case of an approximate representation, where the error decreases while increasing the number of involved functions, is also of relevance. Finding an optimal representation for the BCF is a non-trivial task which has been investigated in relation to the HEOM, too [Tan+15; Dua+17].

Here, an expansion in terms of exponential functions is considered, i.e.,

$$\alpha(\tau) = \sum_{\mu=1}^{N} G_\mu e^{-W_\mu \tau} \quad \text{with} \quad G_\mu, W_\mu \in \mathbb{C} \quad \text{and} \quad \tau \geq 0\,. \tag{2.22}$$

Obviously, for each function $e^{-W_\mu \tau}$ its derivative is trivially represented by the set of functions, too. It turns out that this simple expansion is very well suited for a wide range of BCF and, thus, for a variety of environments (see Sec. 3.2 for more details).

The representation of the BCF with N exponentials [Eq. (2.22)] gives rise to the definition of N independent auxiliary states. This is most conveniently done by

introducing the combined partial derivative (action of the convolution-like integral and the functional derivatives)

$$D_\mu^n := \begin{cases} 0 & n = 0 \\ \bar{g}_\mu \sum_{m=0}^{n-1} e^{-W_\mu (n-m)\Delta t} \partial_{\eta_m^*} & n > 0 \end{cases} \tag{2.23}$$

where n and m correspond to discrete time indices, μ is the index from the bath correlation function representation and $\bar{g}_\mu \sim \sqrt{G_\mu}$ is an arbitrary scaling which ensures that the auxiliary states have the same unit as the stochastic pure state. In order to ease readability, the explicit dependence of the stochastic pure state on the random variables η_k^* is dropped $\psi_n(\eta^*|_0^{n-1}) \to \psi_n$ which, for the time-discrete NMQSD equation, yields

$$\psi_{n+1} = \psi_n + \Delta t \left(-\mathrm{i}H_{\mathrm{sys}} + \eta_n^* L\right) \psi_n - \Delta t L^\dagger \sum_{\mu=1}^{N} \frac{G_\mu}{\bar{g}_\mu} D_\mu^n \psi_n \, . \tag{2.24}$$

This expression motivates the definition of the auxiliary states $\psi_n^{\mathbf{e}_\mu} := D_\mu^n \psi_n$ with index vector $\mathbf{e}_\mu$ which denotes the N-dimensional unit vector in μ direction. It turns out useful to define a general auxiliary state indexed by the vector $\mathbf{k} = (k_1, \dots k_N)$ with $k_\mu \geq 0$ and $k_\mu \in \mathbb{N}$ as

$$\psi_n^{\mathbf{k}} := \prod_{\mu=1}^{N} \left(D_\mu^n\right)^{k_\mu} \psi_n \tag{2.25}$$

where, as a consequence of the partial derivatives, the sequence of applying the D operators is arbitrary. The total number of successive applications reflects the order of the partial derivatives and is given by $l = \sum_\mu k_\mu$ (later also referred to as the hierarchy level).

With the help of the recursion relation

$$D_\mu^{n+1} = e^{-W_\mu \Delta t} \left(\bar{g}_\mu \partial_{\eta_n^*} + D_\mu^n\right) \tag{2.26}$$

the evolution for the auxiliary states can be determined. Combining the above equations yields

$$\begin{aligned} \psi_{n+1}^{\mathbf{k}} = \prod_{\mu=1}^{N} \left(D_\mu^{n+1}\right)^{k_\mu} \psi_{n+1} = \prod_{\mu=1}^{N} e^{-k_\mu W_\mu \Delta t} \left(\bar{g}_\mu \partial_{\eta_n^*} + D_\mu^n\right)^{k_\mu} \times \\ \left[1 + \Delta t \left(-\mathrm{i}H_{\mathrm{sys}} + \eta_n^* L - L^\dagger \sum_{\mu=1}^{N} \frac{G_\mu}{\bar{g}_\mu} D_\mu^n\right)\right] \psi_n \, . \end{aligned} \tag{2.27}$$

It has been pointed out earlier that ψ_n does not depend on η_n^*. Therefore, the partial derivative $\partial_{\eta_n^*}$ acts only on the linear occurrence of η_n^* in equation (2.27) which

means that higher than first order partial derivatives with respect to η_n^* vanish. Consequently, we group the terms of the product derivative operator according to powers of $\partial_{\eta_n^*}$

$$\prod_{\mu=1}^{N}\left(\bar{g}_\mu\partial_{\eta_n^*}+D_\mu^n\right)^{k_\mu}=\prod_{\mu=1}^{N}\left(D_\mu^n\right)^{k_\mu} + \sum_{\mu=1}^{N}k_\mu\bar{g}_\mu\partial_{\eta_n^*}\left(D_\mu^n\right)^{-1}\prod_{\nu=1}^{N}\left(D_\nu^n\right)^{k_\nu}+\sim\partial_{\eta_n^*}^2+\cdots+\sim\partial_{\eta_n^*}^l\,. \tag{2.28}$$

For reasons of compact notation the expression D^{-1} as been introduced which acts like $D^{-1}D^k\equiv D^{k-1}$ for $k>0$. Note, $(\partial_{\eta_n^*}+D^n)^0=1=(D^n)^0$ holds for $k=0$. Therefore the term $0\cdot\partial_{\eta_n^*}(D^n)^{-1}(D^n)^0$ does not appear when "expanding" $(\bar{g}_\mu\partial_{\eta_n^*}+D_\mu^n)^0$ and it is consistent to define $kD^{-1}D^k\equiv 0$ for $k=0$. Keeping only terms up to first order in Δt yields

$$\begin{aligned}\psi_{n+1}^{\mathbf{k}}=&\left(1-\sum_{\mu=1}^{N}k_\mu W_\mu\Delta t\right)\left(1+\sum_{\mu=1}^{N}k_\mu\bar{g}_\mu\partial_{\eta_n^*}\left(D_\mu^n\right)^{-1}\right)\\ &\times\left[1+\Delta t\left(-\mathrm{i}H_{\mathrm{sys}}+\eta_n^*L-L^\dagger\sum_{\mu=1}^{N}\frac{G_\mu}{\bar{g}_\mu}D_\mu^n\right)\right]\psi_n^{\mathbf{k}}\\ =&\psi_n^{\mathbf{k}}+\Delta t\left(-\mathrm{i}H_{\mathrm{sys}}-\sum_{\mu=1}^{N}k_\mu W_\mu+\eta_n^*L\right)\psi_n^{\mathbf{k}}\\ &-\Delta tL^\dagger\sum_{\mu=1}^{N}\frac{G_\mu}{\bar{g}_\mu}\psi_n^{\mathbf{k}+\mathbf{e}_\mu}+\Delta tL\sum_{\mu=1}^{N}k_\mu\bar{g}_\mu\psi_n^{\mathbf{k}-\mathbf{e}_\mu}\,.\end{aligned} \tag{2.29}$$

Taking the limit $\Delta t\to 0$ recovers the set of coupled differential equations known as the *(linear) Hierarchy of Pure state* (HOPS) [SES14; HS17]:

$$\begin{aligned}&\dot{\psi}_t^{\mathbf{k}}=A\psi_t^{\mathbf{k}}+B\sum_{\mu=1}^{N}\frac{G_\mu}{\bar{g}_\mu}\psi_t^{\mathbf{k}+\mathbf{e}_\mu}+C\sum_{\mu=1}^{N}k_\mu\bar{g}_\mu\psi_t^{\mathbf{k}-\mathbf{e}_\mu},\\ &\text{with}\quad A=-\mathrm{i}H_{\mathrm{sys}}-\sum_{\mu=1}^{N}k_\mu W_\mu+\eta_t^*L,\qquad B=-L^\dagger,\qquad C=L,\\ &\mathcal{M}(\eta_t^*)=0,\qquad\mathcal{M}(\eta_t^*\eta_s^*)=0=\mathcal{M}(\eta_t\eta_s),\qquad\mathcal{M}(\eta_t\eta_s^*)=\alpha(t-s)\,.\end{aligned} \tag{2.30}$$

As a remark, the scalars $\bar{g}_\mu$ have been introduced to account for the unit of $[G_\mu]=[\omega]^2$. If g_μ has the unit of a frequency the auxiliary states are unitless. Nonetheless, the HOPS remains valid for any value of g_μ. This allows one to recover the exact form of the HOPS from the seminal paper of D. Süß et al. [SES14] by setting $g_\mu=G_\mu$.

The structure of the above equations reveals that an auxiliary state of level $l=\sum_\mu k_\mu$ couples to other auxiliary states with level $l\pm 1$ only. Thus, the different levels of

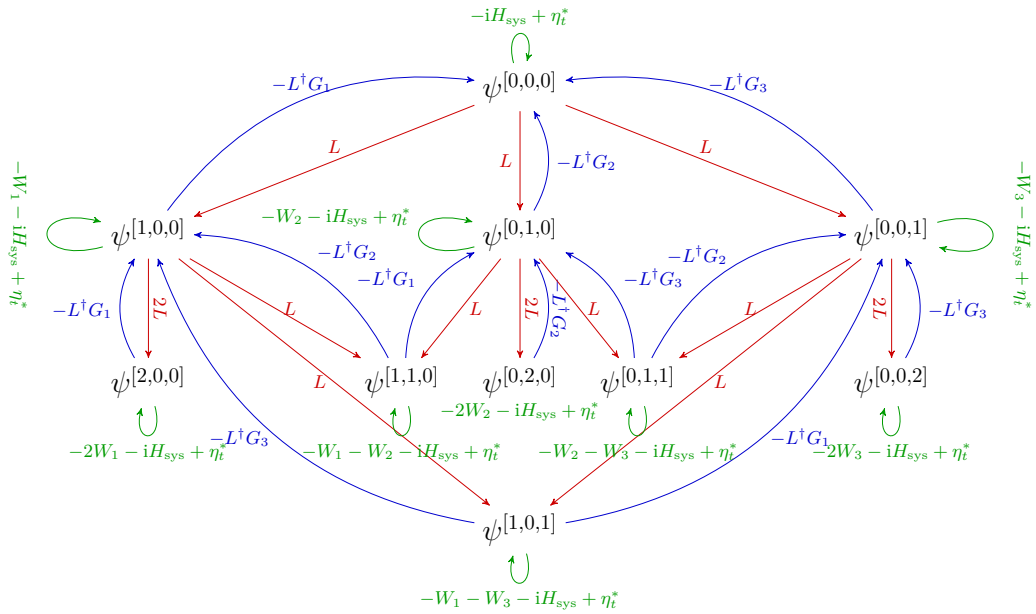

Fig. 2.1: This graph shows the hierarchical structure of the HOPS for an exemplary BCF representation with $N = 3$ exponential terms up to a hierarchical depth $l = 2$. The tuple in brackets corresponds to the index vector $\mathbf{k}$. The very top node with index vector $\mathbf{0}$ corresponds to the stochastic pure state needed to calculate the reduced state.

auxiliary states depend on each other in a hierarchical manner (see Fig. 2.1 for a graph visualization of the hierarchical structure).

In order to solve the above set of differential equations (the HOPS) the initial condition needs to be specified. Recall, the initial condition for the stochastic pure state coincides with the initial state for the system. Further, by definition [Eqs. (2.23) and (2.25)] the auxiliary states are zero at $t = 0$. Thus, the initial condition for the HOPS reads

$$\begin{aligned} \psi_0^{\mathbf{k}} &= |\psi_0\rangle \qquad \text{for } \mathbf{k} = \mathbf{0} \\ \psi_0^{\mathbf{k}} &= 0 \qquad\quad \text{for } \mathbf{k} \neq \mathbf{0}\,. \end{aligned} \tag{2.31}$$

In summary, based on a multi-exponential representation of the BCF [Eq. (2.22)] we have shown that the stochastic pure states, being solutions to the NMQSD equation, can equivalently be obtained from the HOPS – an a-priory infinite set of coupled differential equations. Further details regarding its use as numerical method and its comparison to other approaches are discussed in Ch. 3 and Ch. 4 respectively. We continue on the conceptual side by showing how to modify the NMQSD / HOPS formalism in order to ensure that each sample contributes with equal weight to the ensemble average, a property which is highly desirable for numerics and has turned out necessary in the strong coupling regime.

2.1.3 Importance Sampling and the Non-Linear HOPS

In the previous section, the HOPS formalism has been derived as a method to solve the NMQSD equation (2.20). The resulting stochastic pure states ψ_t yield the reduced dynamics by averaging the dyads $|\psi_t\rangle\langle\psi_t|$. Crucially, it follows from the NMQSD equation that the norm of the stochastic pure states $\sqrt{\langle\psi_t|\psi_t\rangle}$ is not preserved. As a consequence the dyads contribute with different weight to the ensemble average. This is easily seen by trivially rewriting Eq. (2.8) in terms of normalized dyads (actual projectors)

$$\rho_{\mathrm{sys}}(t) = \mathcal{M}\left(\langle\psi_t|\psi_t\rangle \frac{|\psi_t\rangle\langle\psi_t|}{\langle\psi_t|\psi_t\rangle}\right) = \int \mathrm{d}^2\mathbf{z} \frac{e^{-|\mathbf{z}|^2}}{\pi^{N_B}} \langle\psi_t|\psi_t\rangle \frac{|\psi_t\rangle\langle\psi_t|}{\langle\psi_t|\psi_t\rangle} \,, \tag{2.32}$$

where the squared norm $\langle\psi_t|\psi_t\rangle$ expresses the time dependent weights for each contribution. Note that we distinguish between a general dyadic product $|\psi_t\rangle\langle\psi_t|$ and the dyadic product of normalized states $|\psi_t\rangle\langle\psi_t|/\langle\psi_t|\psi_t\rangle$, referred to exclusively as projectors.

Especially for strong system-environment interactions the norm may differ drastically between different realizations of ψ_t. When using a finite number of samples to estimate the ensemble mean, as necessary for a numeric method, a single stochastic pure state can dominate the entire ensemble and ruin the statistical significance. As demonstrated in Sec. 4.5 an improved stochastic convergence becomes inevitable for a numeric treatment of the strong coupling regime.

Remarkably, it has been shown that the NMQSD formalism can be modified such that each sample does, in fact, contribute with the same weight to the ensemble [DGS98; deV+05], i.e., the so-called importance sampling is realized. The resulting equation is usually referred to as the non-linear NMQSD equation. By revising the steps for the NMQSD formalism we eventually obtain the corresponding HOPS.

Starting point is, again, the expression for the reduced state by taking the trace over the environmental degrees of freedom in terms of Bargmann coherent states. As indicated above, averaging over projectors can be trivially achieved by dividing $|\psi(\mathbf{z}^*,t)\rangle \equiv \langle\mathbf{z}|\Psi(t)\rangle$ by its norm $\sqrt{\langle\psi(\mathbf{z},t)|\psi(\mathbf{z}^*,t)\rangle}$,

$$\rho_{\mathrm{sys}}(t) = \int \mathrm{d}^2\mathbf{z} \frac{e^{-|\mathbf{z}|^2}}{\pi^{N_B}} \langle\Psi(t)|\mathbf{z}\rangle\langle\mathbf{z}|\Psi(t)\rangle \frac{|\psi(\mathbf{z}^*,t)\rangle\langle\psi(\mathbf{z},t)|}{\langle\psi(\mathbf{z},t)|\psi(\mathbf{z}^*,t)\rangle} \,. \tag{2.33}$$

It is now a crucial observation that the terms in front of the projector correspond precisely to the Husimi function (Q-function) of the multi-mode bath state,

$$\langle\Psi(t)|\mathbf{z}\rangle\langle\mathbf{z}|\Psi(t)\rangle \frac{e^{-|\mathbf{z}|^2}}{\pi^{N_B}} = \langle\mathbf{z}|\left(\mathrm{Tr}_{\mathrm{sys}}|\Psi(t)\rangle\langle\Psi(t)|\right)|\mathbf{z}\rangle \frac{e^{-|\mathbf{z}|^2}}{\pi^{N_B}} \equiv Q(\mathbf{z},\mathbf{z}^*,t) \,, \tag{2.34}$$

here expressed in terms of Bargmann coherent states $|\mathbf{z}\rangle$. The evolution equation of $Q(\mathbf{z},\mathbf{z}^*,t)$ follows from the Schrödinger equation (2.6) and takes the form of a first order partial differential equation,

$$\begin{aligned}\partial_t Q(\mathbf{z},\mathbf{z}^*,t) &= -\sum_\lambda \left(\mathrm{i}g_\lambda e^{-\mathrm{i}\omega_\lambda t}\partial_{z_\lambda^*}\langle L^\dagger\rangle Q(\mathbf{z},\mathbf{z}^*,t) + \mathrm{h.c.}\right) ,\\ \text{with}\quad \langle L^\dagger\rangle &= \frac{\langle\psi(\mathbf{z},t)|L^\dagger|\psi(\mathbf{z}^*,t)\rangle}{|\psi(\mathbf{z}^*,t)|^2} .\end{aligned} \tag{2.35}$$

Note that $Q(\mathbf{z},\mathbf{z}^*,t)$, being the Husimi function of the environment, can be regarded as a pseudo probability distribution. In particular, it is normalized to 1. Thus, the dynamics in phase space expressed in $(\mathbf{z}^*,\mathbf{z})$ coordinates has to obey a continuity equation, i.e., $\partial_t Q + \mathrm{div}\vec{J} = 0$. Thinking of $Q(\mathbf{z},\mathbf{z}^*,t)$ being realized by a set of individual trajectories $(\mathbf{z}^*(t),\mathbf{z}(t))$ and expressing the current as $\vec{J} := (\dot{\mathbf{z}}^*,\dot{\mathbf{z}})Q$ allows us to identify Eq. 2.35 as the continuity equation if the evolution of the components of $(\mathbf{z}^*(t),\mathbf{z}(t))$ obey

$$\dot{z}_\lambda^*(t) = \mathrm{i}g_\lambda e^{-\mathrm{i}\omega_\lambda t}\langle L^\dagger\rangle \tag{2.36}$$

or its complex conjugate version, respectively. As a remark, the trajectories correspond to the characteristics when solving the partial differential equations (2.35) by means of the method of characteristics [Eva10]. The above reasoning allows us to express the time evolution of $Q(\mathbf{z},\mathbf{z}^*,t)$ in terms of the evolution of the individual trajectories with initial conditions $\mathbf{z}(t=0)=\mathbf{z}_0$, i.e,

$$Q(\mathbf{z},\mathbf{z}^*,t) = \int \mathrm{d}^2\mathbf{z}_0\; Q_0(\mathbf{z}_0,\mathbf{z}_0^*)\delta(\mathbf{z}-\mathbf{z}(t,\mathbf{z}_0)) , \tag{2.37}$$

with $Q_0(\mathbf{z},\mathbf{z}^*) := Q(\mathbf{z},\mathbf{z}^*,0)$. Note that as for the notation of $\mathrm{d}^2\mathbf{z}$ we abbreviate

$$\delta(\mathbf{z}) \equiv \delta(\mathrm{Re}(z_1))\delta(\mathrm{Im}(z_1))\delta(\mathrm{Re}(z_2))\delta(\mathrm{Im}(z_2))\dots . \tag{2.38}$$

In summary, it has been shown that the environmental state, expressed as a phase space distribution (Husimi function), can be represented by a family of phase space trajectories $\mathbf{z}^*(t,\mathbf{z}_0)$, so-called *co-moving coherent state labels*, which are the solutions of the characteristic equation (2.36). Note that the influence of the system on the environmental dynamics, i.e., the characteristics, is hidden in the special expectation value $\langle L^\dagger\rangle$ which has to be taken with respect to the stochastic pure state $\psi(\mathbf{z}^*,t)$ of the system.

It follows that the reduced state can now be expressed as

$$\rho_{\mathrm{sys}}(t) = \int \mathrm{d}^2\mathbf{z}\;\mathrm{d}^2\mathbf{z_0}\; Q_0(\mathbf{z}_0,\mathbf{z}_0^*)\delta(\mathbf{z}-\mathbf{z}(t,\mathbf{z}_0))P(\mathbf{z},\mathbf{z}^*,t) \tag{2.39}$$

with the abbreviation for the stochastic projector

$$P(\mathbf{z},\mathbf{z}^*,t) := \frac{|\psi(\mathbf{z}^*,t)\rangle\langle\psi(\mathbf{z},t)|}{|\psi(\mathbf{z}^*,t)|^2} \,. \tag{2.40}$$

The $\mathbf{z}$ integration collapses due to the δ term causing an evaluation of the projector at the value of the co-moving coherent state labels at time t, i.e., $\mathbf{z}^* \to \mathbf{z}^*(t)$. The integration over $\mathbf{z}_0$ can be understood in a Monte Carlo sense. For the relevant case here where $|\mathbf{0}\rangle$ is considered as initial environmental state, the weight function for the initial values $\mathbf{z}_0$ becomes Gaussian, $Q_0(\mathbf{z}_0,\mathbf{z}_0^*) = \prod_\lambda \frac{e^{-|z_{\lambda,0}|^2}}{\pi}$. This leads to the central conclusion that the reduced state can be written as ensemble average of projectors

$$\rho_{\mathrm{sys}}(t) = \underset{\mathbf{z}_0,\mathbf{z}_0^*}{\mathcal{M}} P(\mathbf{z},\mathbf{z}^*,t)\Big|_{\mathbf{z}^*=\mathbf{z}^*(t,\mathbf{z}_0^*)} \tag{2.41}$$

over the complex valued and Gaussian distributed random variables $z_{\lambda,0}$ with $\mathcal{M}(z_{\lambda,0}) = 0 = \mathcal{M}(z_{\lambda,0}z_{\lambda',0})$ and $\mathcal{M}(z_{\lambda,0}z_{\lambda',0}^*) = \delta_{\lambda,\lambda'}$, The projector is constructed from the dyadic product of the *normalized stochastic pure state*

$$|\tilde{\psi}(\mathbf{z}^*,t)\rangle := \frac{|\psi(\mathbf{z}^*,t)\rangle}{|\psi(\mathbf{z}^*,t)|} \,, \tag{2.42}$$

however, evaluated at $\mathbf{z}^* = \mathbf{z}^*(t)$. To establish a more intuitive picture, recall that by definition the stochastic pure states $|\psi(\mathbf{z}^*,t)\rangle := \langle\mathbf{z}|\Psi(t)\rangle$ are parameterized by the coherent state labels $\mathbf{z}^*$. In that sense, each combination of parameters $\mathbf{z}^*$ can be identified with a different stochastic pure state. Therefore, since the projector in Eq. (2.41) is evaluated at $\mathbf{z}^*(t)$, in general, a different stochastic pure state contributes at each time (see parts of the later Fig. 2.2 for a visualization). Due to their equal weight for the reduced state, the stochastic pure states selected in this way can be regarded as most relevant. Furthermore, since the co-moving coherent state labels reflect the dynamics of the Q-function the exact dynamics of the environment is captured in this approach.

To make use of this statistically favorable rewriting of the reduced state we deduce the evolution equation for the "effective" stochastic pure state which follows the co-moving coherent state labels $|\psi(\mathbf{z}^*(t,\mathbf{z}_0^*),t)\rangle$ and, thus, swipes through many different "ordinary" stochastic pure states $|\psi(\mathbf{z}^*,t)\rangle$. As before, this includes the transformation from the dependence on the infinite dimensional coherent state labels $\mathbf{z}$ to a functional dependence on a stochastic process.

2.1.3.1 Non-Linear NMQSD Equation

To ease notation, the dependence of the co-moving coherent state label on the initial condition $\mathbf{z}_0^*$ is not essential for the following and will, thus, be omitted. Using the evolution equation for a fixed $\mathbf{z}^*$ [Eq. (2.10)] and the expression for $\dot{z}_\lambda^*$ [Eq. (2.36)] yields for the change of the stochastic pure state with a co-moving frame

$$\begin{aligned}\frac{\mathrm{d}}{\mathrm{d}t}\psi(\mathbf{z}^*(t,\mathbf{z}_0^*),t) = \Bigg[\Bigg(&- \mathrm{i}H_{\mathrm{sys}} + \eta^*(\mathbf{z}^*,t)L - \mathrm{i}L^\dagger \sum_\lambda g_\lambda e^{-\mathrm{i}\omega_\lambda t}\partial_{z_\lambda^*}\Bigg)\psi(\mathbf{z}^*,t) \\ &+ \mathrm{i}\langle L^\dagger\rangle_{\psi(\mathbf{z}^*,t)} \sum_\lambda g_\lambda e^{-\mathrm{i}\omega_\lambda t}\partial_{z_\lambda^*}\psi(\mathbf{z}^*,t)\Bigg]_{\mathbf{z}^*=\mathbf{z}^*(t,\mathbf{z}_0^*)} .\end{aligned} \tag{2.43}$$

The subscript at the special normalized expectation value $\langle L^\dagger\rangle_{\psi(\mathbf{z}^*,t)}$ [Eq. (2.35)] is used to highlight its $\mathbf{z}^*$ dependence. Formally, this expression corresponds to the evolution equation of the stochastic pure state with a fixed $\mathbf{z}^*$ [Eq. (2.10)], however, with the replacements $L^\dagger \to L^\dagger - \langle L^\dagger\rangle$ and $\mathbf{z}^* \to \mathbf{z}^*(t)$. As shown in the following, these changes show up in the NMQSD equation, too [DGS98; Str01]. It is, again, instructive to employ the time-discrete scheme to perform the change from the coherent state labels $\mathbf{z}^*$ to the stochastic process η^*. Simply rewriting the above differential equation up to first order in Δt then yields

$$\begin{aligned}\psi_{n+1}(\mathbf{z}^*)\big|_{\mathbf{z}^*=\mathbf{z}^*(t_{n+1})} = \Bigg[\psi_n(\mathbf{z}^*) + \Delta t\Big(&- \mathrm{i}H_{\mathrm{sys}} + \eta_n^*(\mathbf{z}^*)L \\ &- \mathrm{i}\sum_\lambda g_\lambda e^{-\mathrm{i}\omega_\lambda n\Delta t}(L^\dagger - \langle L^\dagger\rangle)\partial_{z_\lambda^*}\Big)\psi_n(\mathbf{z}^*)\Bigg]_{\mathbf{z}^*=\mathbf{z}^*(t_n)} .\end{aligned} \tag{2.44}$$

Ignoring the explicit evaluation of $\mathbf{z}^*$ at $\mathbf{z}^*(t_n)$ for a moment, the equation describes the relation between ψ_n and ψ_{n+1} seen as functions that map a coherent state label $\mathbf{z}^*$ to a vector of the system Hilbert space. Exactly as in the previous Sec. 2.1.1, these functions can be rephrased to depend on the time-discrete stochastic process $\eta_n^*(\mathbf{z}^*)$ [Eq. (2.13)] rather than the coherent state labels $\mathbf{z}^*$. Thus, $\psi_n(\eta^*|_0^{n-1})$ and $\psi_{n+1}(\eta^*|_0^n)$ are related by the time-discrete NMQSD equation (2.18), here, however, with $L^\dagger \to L^\dagger - \langle L^\dagger\rangle$,

$$\begin{aligned}\psi_{n+1}(\eta^*|_0^n) = \Bigg[1 + \Delta t\Big(&- \mathrm{i}H_{\mathrm{sys}} + \eta_n^* L \\ &- (L^\dagger - \langle L^\dagger\rangle)\sum_{m=0}^{n-1}\alpha(t_n - t_m)\partial_{\eta_m^*}\Big)\Bigg]\psi_n(\eta^*|_0^{n-1}) .\end{aligned} \tag{2.45}$$

Recalling that we started with the time derivative of the stochastic pure state with co-moving frame, the additional $\langle L^\dagger \rangle$ term ensures that evaluating ψ_n at $\eta_i^*(\mathbf{z}^* = \mathbf{z}^*(t_n))$ for $0 \leq i < n$ results in the iterated state ψ_{n+1} evaluated at $\eta_i^* = \eta_i^*(\mathbf{z}^*(t_{n+1}))$

$$\begin{aligned}\psi_{n+1}(\eta^*|_0^n)\Big|_{\eta_i^*=\eta_i^*(\mathbf{z}^*(t_{n+1}))} = \Bigg[\Bigg(1 + \Delta t\Big(&- \mathrm{i}H_{\mathrm{sys}} + \eta_n^* L \\ &- (L^\dagger - \langle L^\dagger \rangle) \sum_{m=0}^{n-1} \alpha(t_n - t_m)\partial_{\eta_m^*}\Big)\Bigg)\psi_n(\eta^*|_0^{n-1})\Bigg]_{\eta_i^*=\eta_i^*(\mathbf{z}^*(t_n))}\end{aligned} \tag{2.46}$$

with $0 \leq i \leq n$. Fig. 2.2 attempts to illustrate the relation between the co-moving coherent state labels and the resulting shifted process, i.e, the process in the co-moving frame (see Eq. (2.49) below), as well as the stochastic pure states with and without co-moving coherent state labels. This leads to the known differential form [DGS98; SDG99] for the non-normalized stochastic pure state with co-moving coherent state labels,

$$\begin{aligned}\partial_t \psi_t[\eta^*] = \Bigg[&- \mathrm{i}H_{\mathrm{sys}} + \eta^*(\mathbf{z}^*(t), t)L \\ &- (L^\dagger - \langle L^\dagger \rangle_{\psi_t[\eta^*]}) \int_0^t \mathrm{d}s\, \alpha(t-s) \frac{\delta}{\delta \eta^*(s)}\Bigg|_{\eta^*(\cdot)=\eta^*(\mathbf{z}^*(t),\cdot)}\Bigg] \psi_t[\eta^*]\,.\end{aligned} \tag{2.47}$$

This is the final result. Propagating this equation yields the stochastic pure states with co-moving coherent sate labels. The reduced state is obtained by averaging their normalized dyads, thus, featuring the enhanced statistical convergence discussed above.

Several remarks deserve notice. Since the additional normalized expectation value $\langle L^\dagger \rangle$ [Eq. (2.35)] is taken with respect to the stochastic pure state, the equation (2.47) is non-linear in ψ and, thus, referred to as the *non-linear NMQSD equation*. To distinguish this equation from the previously discussed case (Sec. 2.1.1), the NMQSD equation with fixed coherent state labels $\mathbf{z}^*$ is also called *linear NMQSD equation*.

Another remark concerns the evaluation of the microscopically defined stochastic process for the time evolving co-moving coherent state labels, i.e., $\eta^*(\mathbf{z}^*(t), t)$, which is needed for the non-linear NMQSD equation. Recalling the definition of the stochastic process, $\eta^*(t) \coloneqq -\mathrm{i}\sum_\lambda g_\lambda^* z_\lambda^* e^{\mathrm{i}\omega_\lambda t}$, and setting z_λ^* to the formal solution of the characteristics [Eq. (2.36)]

$$z_\lambda^*(t, z_{\lambda,0}^*) = z_{\lambda,0}^* + \int_0^t \mathrm{d}s\, \mathrm{i}g_\lambda e^{-\mathrm{i}\omega_\lambda s}\langle L^\dagger \rangle_{\psi_s} \tag{2.48}$$

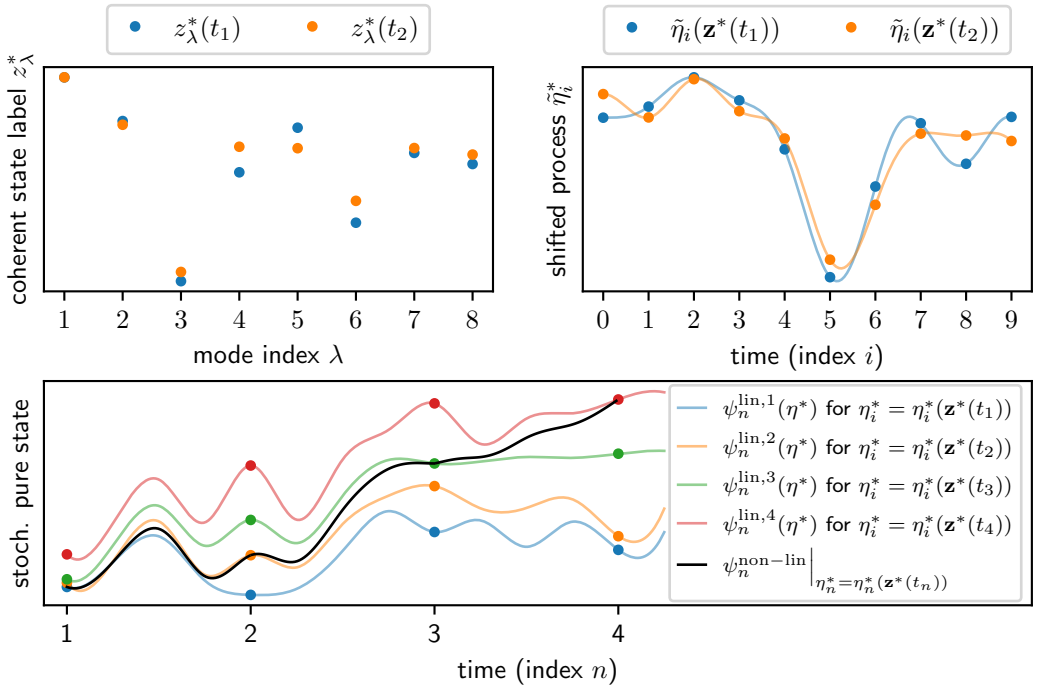

Fig. 2.2: The plots shown here are illustrations only, visualizing various quantities occurring in the co-moving frame and their relation to the linear HOPS. In the co-moving frame, coherent state labels evolve with time, $\mathbf{z}^* \to \mathbf{z}^*(t)$ (upper left panel). Therefore, $\eta^*_i(\mathbf{z}^*(t)) = -\mathrm{i}\sum_\lambda g^*_\lambda z^*_\lambda(t) e^{\mathrm{i}\omega_\lambda t_i}$ (from Eq. (2.13)) generally varies for all i when t changes (upper right panel). Note that $\tilde{\eta}^*_i(t)$ has two independent time variables, the time index i of the process and the time t fixing z^*_λ as $z^*_\lambda(t)$. The NMQSD equation, however, is exposed to the instance $t = t_n$ only, defining the actual shifted stochastic process $\tilde{\eta}^*(t_n) := \eta^*_n(\mathbf{z}^*(t_n))$. The other values ($i < n$) enter indirectly only in terms of the partial derivatives. Their influence can be coped with using the HOPS formalism (see below). The bottom panel shows various stochastic pure states $\psi_n^{\mathrm{lin},k}$ (colored lines) obtained from the linear NMQSD equation for a fixed process $\eta^*_i(\mathbf{z}^*(t_k))$ (fixed t_k). As of the co-moving coherent state labels, the action of the non-linear NMQSD equation propagates the stochastic pure state such that it changes from one solution of the linear NMQSD to another, i.e., $\psi_n^{\mathrm{lin},k=n} = \psi_n^{\mathrm{non-lin}}$. In that way, referring to the importance sampling at each time the "optimal" stochastic pure state is obtained.

results in

$$\begin{aligned} \eta^*(\mathbf{z}^*(t),t) &= -\mathrm{i}\sum_\lambda g^*_\lambda z^*_{\lambda,0} e^{\mathrm{i}\omega_\lambda t} + \int_0^t \mathrm{d}s\, \alpha^*(t-s)\langle L^\dagger\rangle_{\psi_s} \\ \tilde{\eta}^*(t) &:= \eta^*(\mathbf{z}^*(t),t) = \eta^*(t) + \eta^*_{\mathrm{sh}}(t)\,. \end{aligned} \tag{2.49}$$

The first term on the right hand side in the upper line corresponds to a truly stochastic process, microscopically generated by the random numbers $z^*_{\lambda,0}$. Since the $z^*_{\lambda,0}$ are Gaussian distributed with variance one, the process can be identified with the Gaussian process $\eta^*(t)$ known from the linear NMQSD equation [Eq. (2.21)]. The second term shifts the Gaussian process, thus, the stochastic process $\tilde{\eta}(t)$ is called *shifted process*. Note that the shift itself is expressed in terms of a memory

kernel involving the entire history of the stochastic pure state. This makes an explicit evaluation very complicated. However, for a BCF of multi-exponential form [Eq. (2.22)], as required for the HOPS, the time derivative of the shift takes the closed form

$$\begin{aligned} \eta^*_{\mathrm{sh}}(t) &\equiv \sum_{\mu=1}^{N} \eta^*_{\mathrm{sh},\mu}(t) \coloneqq \sum_{\mu=1}^{N} \int_0^t \mathrm{d}s\, G^*_\mu e^{-W^*_\mu (t-s)} \langle L^\dagger \rangle_{\psi_s} \\ \Rightarrow \qquad \dot{\eta}^*_{\mathrm{sh},\mu}(t) &= G^*_\mu \langle L^\dagger \rangle_{\psi_t} - W^*_\mu \eta^*_{\mathrm{sh},\mu}(t)\ . \end{aligned} \tag{2.50}$$

Therefore, it can be propagated along with the stochastic pure state. Note that from a numerical perspective, here the number of exponential terms representing the BCF is not limited to a few terms only, in contrast to the HOPS. Consequently, an appropriate discretization of the SD which also leads to a multi-exponential representation of the BCF may be used, too.

To obtain the stochastic pure state in the co-moving frame the non-linear NMQSD equation (2.47) needs to be solved. As in the linear case, the functional derivative term can be dealt with using the HOPS formalism, shown next.

2.1.3.2 Non-Linear HOPS

Starting from the time-discrete non-linear NMQSD equation (2.45), it is the same line of reasoning as for the linear equation (see Sec. 2.1.2) which leads to the non-linear HOPS. Consequently, its hierarchical structure is identical to the linear HOPS. The only differences emerge from the additional expectation value $\langle L^\dagger \rangle$ and the shifted noise process $\tilde{\eta}^*(t)$. In summary, for a given BCF $\alpha(\tau)$ with a suitable representation as a sum of exponentials $\sum_{\mu=1}^{N} G^*_\mu e^{-W^*_\mu \tau}$ the non-linear HOPS refers to the following set of non-linear differential equations

$$\begin{aligned} \dot{\psi}^{\mathbf{k}}_t &= A\psi^{\mathbf{k}}_t + B\sum_{\mu=1}^{N} \frac{G_\mu}{\bar{g}_\mu} \psi^{\mathbf{k}+\mathbf{e}_\mu}_t + C\sum_{\mu=1}^{N} k_\mu \bar{g}_\mu \psi^{\mathbf{k}-\mathbf{e}_\mu}_t, \\ \dot{\eta}^*_{\mathrm{sh},\mu}(t) &= G^*_\mu \langle L^\dagger \rangle_{\psi_t} - W^*_\mu \eta^*_{\mathrm{sh},\mu}(t), \end{aligned} \tag{2.51}$$

with

$$\begin{aligned} A = -\mathrm{i}H_{\mathrm{sys}} - \sum_{\mu=1}^{N} k_\mu W_\mu + \tilde{\eta}^*_t L, \qquad B = -(L^\dagger - \langle L^\dagger \rangle_{\psi_t}), \qquad C = L, \\ \tilde{\eta}^*(t) = \eta^*(t) + \sum_{\mu=1}^{N} \eta^*_{\mathrm{sh},\mu}(t), \\ \mathcal{M}(\eta^*_t) = 0, \qquad \mathcal{M}(\eta^*_t \eta^*_s) = 0 = \mathcal{M}(\eta_t \eta_s), \quad \text{and} \quad \mathcal{M}(\eta_t \eta^*_s) = \alpha(t-s). \end{aligned} \tag{2.52}$$

Up to now, this set of equations provides the most sophisticated approach to utilize the NMQSD formalism as numeric approach which solves the dynamics of an open quantum system exactly. Based on the details on solving the HOPS provided in Ch. 3, it will be shown in Ch. 4 that the HOPS is well suited for a wide range of situation reaching from weak to strong coupling as well as zero and large temperatures. Our publications concerning these results can be found in Refs. [HS17; Har+19; HS20b].

2.2 Shifted and Thermal Initial Bath States

The derivation of the NMQSD equation (2.20), as provided in the previous section, requires that the environment is initially in its ground state. Obviously, this requirement has to be met for the HOPS as well. However, it has been shown that the NMQSD formalism can also be extended to thermal initial environmental states [DGS98; DS97]. For Hermitian coupling operators $L = L^\dagger$, non-zero temperature is simply accounted for by replacing the zero-temperature BCF by its thermal equivalent. Here, however, a different approach is used to account for initial environmental conditions other than the ground state. It will be shown in the following that a shifted initial condition can be treated with the ground-state formalism, except for an additional time dependent system Hamiltonian. As a consequence of this, for a thermal initial environmental state the time dependence of the additional Hamiltonian is governed by yet another stochastic process. This corresponds to the picture that a thermal environment can be accounted for by a stochastic force [Wei08] which yields a stochastic potential encoded by a time dependent system Hamiltonian.

This approach has two advantages over the earlier one. First, since only the zero-temperature BCF enters the HOPS formalism, a suitable multi-exponential representation has to be obtained only once. In the former approach, each temperature yields a different BCF which, in turn, would require its own multi-exponential representation. As discussed in Sec. 3.2, finding highly accurate representations is a difficult task on its own. Even more importantly, the approach presented here requires significantly less numerical effort when dealing with strong system-environment interactions (see Sec. 4.5).

Noteworthy, this approach is not only particularly suited for the HOPS methods, but can in principal be used by any method which solves the zero-temperature case and allows for a time dependent system Hamiltonian.

2.2.1 Shifted Initial States

As a prerequisite to treat thermal initial conditions, shifted initial states are considered. Suppose the reduced dynamics for an arbitrary initial global state ρ_0 can be calculated. Here we show that this implies that the reduced evolution of the shifted initial condition $\rho_{\mathrm{sh}} := \mathbf{D}\rho_0\mathbf{D}^\dagger$ can be calculated, too, by actually solving the reduced dynamics for ρ_0, however, with an additional time-dependent contribution to the system Hamiltonian. The environmental operator $\mathbf{D} := \otimes_\lambda D_\lambda(y_\lambda)$ denotes the multi-mode displacement operator, where $D_\lambda(y_\lambda) = e^{y_\lambda a_\lambda^\dagger - y_\lambda^* a_\lambda}$ ($y_\lambda \in \mathbb{C}$) acts on the mode λ. This, in particular, implies that coherent states can be dealt with effectively using the ground state as initial condition.

For ρ_{sh} as initial condition, the reduced state at later times t can be expressed by means of the propagator $U(t)$ for the microscopic model [Eq. (2.6)],

$$\rho_{\mathrm{sys}}(t) = \mathrm{Tr}_{\mathrm{env}} U(t)\rho_{\mathrm{sh}}U^\dagger(t) = \mathrm{Tr}_{\mathrm{env}} U(t)\mathbf{D}\rho_0\mathbf{D}^\dagger U^\dagger(t)\ . \tag{2.53}$$

Using that $\mathbf{D}$ is a unitary operator, $\rho_{\mathrm{sys}}(t)$ may also be written as

$$\rho_{\mathrm{sys}}(t) = \mathrm{Tr}_{\mathrm{env}} \tilde{U}(t)\rho_0\tilde{U}^\dagger(t) \tag{2.54}$$

with the transformed time evolution operator $\tilde{U}(t) = \mathbf{D}^\dagger U(t)\mathbf{D}$. Since $U(t)$ obeys the Schrödinger equation (2.6)

$$\mathrm{i}\partial_t U(t) = H(t)U(t)\ , \tag{2.55}$$

$\tilde{U}(t)$ fulfills the same Schrödinger equation with the transformed Hamilton $\tilde{H}(t) := \mathbf{D}^\dagger H(t)\mathbf{D}$. This leads to the final conclusion that the reduced dynamics, formally expressed in Eq. (2.54), can be obtained by evolving the initial state ρ_0 under action of the total Hamilton

$$\tilde{H}(t) = H_{\mathrm{sys}} + H_{\mathrm{sys}}^{\mathrm{shift}}(t,\mathbf{y}) + \left(L\sum_\lambda g_\lambda^* e^{\mathrm{i}\omega_\lambda t}a_\lambda^\dagger + \mathrm{h.c.}\right), \tag{2.56}$$

which includes an additional contributing to the system Hamiltonian, the so-called shift Hamiltonian

$$H_{\mathrm{sys}}^{\mathrm{shift}}(t,\mathbf{y}) := L\sum_\lambda g_\lambda^* y_\lambda^* e^{\mathrm{i}\omega_\lambda t} + \mathrm{h.c.}\ . \tag{2.57}$$

As a specific application of that, recall that the displacement operator acting on the ground state yields a coherent state $|y_\lambda\rangle = D_\lambda(y_\lambda)|0\rangle$. Therefore, the initial state $|\psi\rangle|\mathbf{y}\rangle$ can be expressed by a shift of the ground state,

$$|\psi\rangle\langle\psi|\otimes|\mathbf{y}\rangle\langle\mathbf{y}| \equiv |\psi\rangle\langle\psi|\otimes\mathbf{D}|\mathbf{0}\rangle\langle\mathbf{0}|\mathbf{D}^\dagger = \rho_{\mathrm{sh}}\ . \tag{2.58}$$

This in turn allows us to use the zero-temperature HOPS formalism with the additional Hermitian shift Hamiltonian given in Eq. (2.57) to treat coherent states as initial condition.

Another application of the above consideration appears for an environment initially prepared in a so-called canonical shifted distribution [Wei08; ABV07; NT10]

$$\rho_{\mathrm{sh}} = |\psi_l\rangle\langle\psi_l| \otimes \exp\left(-\beta(H_{\mathrm{env}} - H_{\mathrm{int}}|_{L=l})\right)/\tilde{Z}, \tag{2.59}$$

at inverse temperature β, where the system state $|\psi_l\rangle$ is forced to be the eigenstate of the now Hermitian coupling operator $L = L^\dagger$ with real eigenvalue l while the environment is assumed to be thermalized with respect to the remaining effective environmental Hamiltonian $H_{\mathrm{env}} - H_{\mathrm{int}}|_{L=l}$ (see Eq. (2.1)). By using the properties of the displacement operator, the exponent in the equation above can be rewritten as

$$\begin{aligned} H_{\mathrm{env}} - H_{\mathrm{int}}|_{L=l} &= \sum_\lambda \omega_\lambda a_\lambda^\dagger a_\lambda - l(g_\lambda^* a_\lambda^\dagger + g_\lambda a_\lambda) \\ &= \sum_\lambda \omega_\lambda (a_\lambda^\dagger - l g_\lambda/\omega_\lambda)(a_\lambda - l g_\lambda^*/\omega_\lambda) - l^2|g_\lambda|^2/\omega_\lambda \\ &= \sum_\lambda \omega_\lambda D_\lambda(y_\lambda) a_\lambda^\dagger a_\lambda D_\lambda^\dagger(y_\lambda) + \mathrm{const.} \end{aligned} \tag{2.60}$$

with $y_\lambda = l g_\lambda^*/\omega_\lambda$. Thus, the state considered in Eq. (2.59) belongs to the class of shifted initial conditions

$$\rho_{\mathrm{sh}} = |\psi_l\rangle\langle\psi_l| \otimes \mathbf{D}\rho_\beta\mathbf{D}^\dagger, \qquad \rho_\beta = e^{-\beta H_{\mathrm{env}}}/Z, \qquad Z = \mathrm{Tr} e^{-\beta H_{\mathrm{env}}}, \tag{2.61}$$

and the shift Hamiltonian takes the form

$$H_{\mathrm{sys}}^{\mathrm{shifted}}(t) = L l(t) \tag{2.62}$$

with

$$l(t) \coloneqq l \sum_\lambda |g_\lambda|^2/\omega_\lambda \cos(\omega_\lambda t) = \frac{l}{\pi}\int_0^\infty \mathrm{d}\omega\, \frac{J(\omega)}{\omega}\cos(\omega_\lambda t)\,. \tag{2.63}$$

Note that a thermal initial state appears as an effective initial state for the environment. It will be shown in the following, how a thermal initial state can be dealt with stochastically in a zero-temperature formalism such as the HOPS approach.

2.2.2 Thermal initial states

Using the Glauber-Surdashan P-representation allows us to express a thermal environmental state at inverse temperature β in terms of coherent states. Therefore we can employ the above results for coherent states to obtain an effective description of

a thermal environment while still using a zero temperature open system formalism. The P-representation for a thermal state reads

$$\rho_\beta = \bigotimes_\lambda \int \mathrm{d}^2 y_\lambda \frac{1}{\pi \bar{n}_\lambda} e^{-|y_\lambda|^2/\bar{n}_\lambda} |y_\lambda\rangle\langle y_\lambda| \quad \text{with} \quad \bar{n}_\lambda(\beta) = (e^{\beta\omega_\lambda} - 1)^{-1} \,. \tag{2.64}$$

In spirit of Eq. (2.53), the formal time evolution of the reduced state reads

$$\rho_{\mathrm{sys}}(t) = \prod_\lambda \int \mathrm{d}^2 y_\lambda \frac{1}{\pi \bar{n}_\lambda} e^{-|y_\lambda|^2/\bar{n}_\lambda} \mathrm{Tr}_{\mathrm{env}} U(t) \mathbf{D}(\mathbf{y}) |\psi\rangle\langle\psi| \otimes |\mathbf{0}\rangle\langle\mathbf{0}| \mathbf{D}^\dagger(\mathbf{y}) U^\dagger(t) \,. \tag{2.65}$$

Understanding the integration over y in a Monte-Carlo sense

$$\rho_{\mathrm{sys}}(t) = \mathop{\mathcal{M}}_{\mathbf{y}} \rho_{\mathbf{y}}(t) \tag{2.66}$$

allows us to compute the reduced state as an average over the density matrices $\rho_{\mathbf{y}}(t)$ by sampling the random numbers y_λ according to the Gaussian distribution $\frac{1}{\pi\bar{n}_\lambda} e^{-|y_\lambda|^2/\bar{n}_\lambda}$. In turn, each $\rho_{\mathbf{y}}(t)$ can be obtained by the HOPS formalism as an average over stochastic pure state dyads with the additional shift Hamiltonian

$$H_{\mathrm{sys}}^{\mathrm{shift}}(t, \mathbf{y}) = L \sum_\lambda g_\lambda^* y_\lambda^* e^{\mathrm{i}\omega_\lambda t} + \mathrm{h.c.} \,, \tag{2.67}$$

as elucidated above. In the continuous limit the dependence of the shift Hamiltonian on y_λ is most conveniently expressed in terms of the microscopically defined Gaussian stochastic process

$$\xi(t) := \sum_\lambda g_\lambda y_\lambda e^{-\mathrm{i}\omega_\lambda t} \tag{2.68}$$

with corresponding moments $\mathcal{M}(\xi(t)) = 0 = \mathcal{M}(\xi(t)\xi(s))$ and

$$\mathcal{M}(\xi(t)\xi^*(s)) = \sum_{\lambda,\lambda'} |g_\lambda|^2 \mathcal{M}(y_\lambda y_{\lambda'}) e^{-\mathrm{i}\omega_\lambda (t-s)} = \frac{1}{\pi} \int_0^\infty \mathrm{d}\omega \, \bar{n}(\beta\omega) J(\omega) e^{-\mathrm{i}\omega(t-s)} \,. \tag{2.69}$$

As a remark, for a Hermitian coupling operator $L = L^\dagger$ the shift Hamiltonian becomes

$$H_{\mathrm{sys}}^{\mathrm{shift}} = L\xi^*(t) + L^\dagger \xi(t) = L\bar{\xi}(t) \tag{2.70}$$

with the real valued noise $\bar{\xi}(t) := \xi(t) + \xi^*(t)$ with $\mathcal{M}(\bar{\xi}(t)) = 0$ and

$$\mathcal{M}(\bar{\xi}(t)\bar{\xi}(s)) = \frac{1}{\pi} \int_0^\infty \mathrm{d}\omega \, 2\bar{n}(\beta\omega) J(\omega) \cos(\omega(t-s)) \,. \tag{2.71}$$

It turns out that this correlation function corresponds to the *thermal* part of the non-zero temperature BCF which is generally defined by the two time correlation of the force operator $F(t) = \sum_\lambda g_\lambda a_\lambda e^{-\mathrm{i}\omega_\lambda t} + g_\lambda^* a_\lambda^\dagger e^{\mathrm{i}\omega_\lambda t}$ [FV63; CDG98]

$$\begin{aligned}\alpha(\beta, t-s) &= \mathrm{Tr}\rho_\beta F(t)F(s) \\ &= \frac{1}{\pi}\int_0^\infty \mathrm{d}\omega\, J(\omega)\Big((2\bar{n}(\beta\omega)+1)\cos(\omega(t-s)) - \mathrm{i}\sin(\omega(t-s))\Big)\,.\end{aligned} \tag{2.72}$$

This general expression for the BCF splits into a temperature dependent and temperature independent part,

$$\begin{aligned}\alpha(\beta,\tau) = \mathrm{Tr}\rho_\beta F(t+\tau)F(t) = \alpha(\tau) + \alpha_\beta(\tau) \quad &\text{with} \\ \alpha(\tau) = \lim_{\beta\to\infty}\alpha(\beta,\tau) = \frac{1}{\pi}\int_0^\infty \mathrm{d}\omega\, J(\omega)e^{-\mathrm{i}\omega\tau} \\ \text{and} \quad \alpha_\beta(\tau) = \frac{1}{\pi}\int_0^\infty \mathrm{d}\omega\, 2\bar{n}(\beta\omega)J(\omega)\cos(\omega\tau)\,.\end{aligned} \tag{2.73}$$

The formalism derived here accounts for both contributions in a stochastic manner. The zero-temperature BCF $\alpha(\tau)$ defines the statistics of the noise felt by the system which has a purely quantum origin. Its influence is correctly accounted for by the NMQSD, or, equivalently, the HOPS formalism. The noise induced by the uncertainty of the environmental state, which is reflected by the canonical ensemble, obeys the statistics given by $\alpha_\beta(\tau)$. Its influence can simply be accounted for by the stochastic Hamiltonian contribution which can be interpreted as a classical random force acting on the system. Similar stochastic potentials have been proposed by unraveling the Feynman-Vernon influence functional [SG02; CCS13; MC13] where such a Hermitian contribution arises from the real part of the BCF instead of the thermal part α_β.

In summary, using the HOPS method to calculate the reduced dynamics for a system in contact with a thermal environment amounts to averaging stochastic pure state dyads over the two independent stochastic processes $\eta^*(t)$ and $\xi(t)$, i.e.,

$$\rho_{\mathrm{sys}}(t) = \mathop{\mathcal{M}}_{\eta,\xi}|\psi_t[\eta^*,\xi]\rangle\langle\psi_t[\eta^*,\xi]|\,. \tag{2.74}$$

In order to understand how the HOPS formalism is used as a numerical method solving open spin systems in contact with a Ohmic or sub-Ohmic environment, one can continue directly with Ch. 3. The following section, however, provides more theoretical aspects related to the NMQSD as well as the HOPS formalism with prospects for advancing the existing numerical methods.

2.3 Extending Theoretical Aspects of the NMQSD and HOPS Formalism

To give an overview of the different aspects covered in the following, in Sec. 2.3.1 yet another description of remarkable kind for the reduced dynamics is provided. It has been obtained from the NMQSD formalism by expanding the time-continuous stochastic process η_t^* using the Karhunen–Loève theorem [KMT11; GS12]. The expansion, done for a finite time interval $t \in [0, T]$, yields a discrete-mode-like Schrödinger equation with time dependent coupling strengths between the system and the modes. In contrast to many of the explicit methods, where the particular discretization of the SD is arbitrary, here it is uniquely determined by the BCF.

Inspired by the time-discrete NMQSD equation (2.18), a different angle on how to describe the reduced dynamics in spirit of a collision model [AL07; KLS16], the so-called time-oscillator picture, is presented in Sec. 2.3.2.

With the aim to gain insights into the physical meaning of the auxiliary states of the HOPS, in particular their role when truncation the hierarchy, the case of a finite set of environmental mode is discussed in Sec. 2.3.3. In this case, the auxiliary states are closely related to the Fock state representation of the environment, however, in an inverse sense. An auxiliary state at tire l is a superposition of all Fock states with occupation number $n \geq l$.

As a last result (Sec. 2.3.4), a different kind of hierarchy is derived from the NMQSD equation. Instead of expressing the BCF by a suitable set of functions, higher order derivatives of the BCF itself are used to define the auxiliary states which leads to a different hierarchical structure. This circumvents the need to find a multi-exponential representation for the BCF. A particular use case might be the long time dynamics of the SBM in the localized phase (strong coupling) which has turned out sensitive to the accuracy of the multi-exponential representation (see Sec. 5.4).

All these aspects provide independent results which, we are convinced, will be beneficial to develop further applications of the NMQSD theory.

2.3.1 Karhunen–Loève Expansion – a Bath Discretization with Time Dependent Coupling

As mentioned in the introduction of Ch. 2, the vast number of methods known to solve the dynamics of an open quantum system, either exact or approximately,

can be categorized into two classes. On the one hand, *reduced methods* manage to evolve the reduced state and usually depend on the BCF. Such methods, like HOPS or HEOM [TK89; Tan06; RK19; Tan20], are particularly suited for a smooth SD because the continuous limit for the BCF is well defined. On the other hand, *explicit methods*, which model the continuous SD by a sufficiently large number of modes, have been used successfully, too (to list a few references only [WT03; MM13; Sun+15; Gro+16; WG20]). In order to cope with the resulting very large Hilbert space, the success of such methods depends on a suitable, usually time dependent, choice for the basis vectors. In addition, the particular discretization is known to crucially influence the convergence with respect to the number of modes and with that its numerical cost. We have addressed this topic in a cooperation with Michael Werther and Frank Grossmann [Har+19] where we investigate different discretization schemes and propose an a-priory criterion to assess their quality with respect to the resulting reduced dynamics. This discussion is, however, out of the scope of this theses.

Based on the NMQSD equation (2.20), we propose a novel approach which results in an environment of discrete modes, however, with a time dependent coupling between the system and these modes. By explicitly fixing a finite time interval for the solution of the reduced dynamics, the set of discrete modes and their time dependent coupling is uniquely determined by the BCF. Therefore, a continuous SD can be handled intrinsically, however, the resulting evolution equation is a Schrödinger equation for a system interacting with a discrete set of modes. Importantly, the coupling strength decreases with the mode index which means that a finite set of modes may be used as approximation. Consequently, any explicit method which allows for time-dependent system-mode coupling may be used to solve this particular Schrödinger equation.

The essential step for the derivation is to use the Karhunen–Loève expansion [KMT11; GS12] to express the stochastic process $\eta^*(t)$ occurring in the NMQSD equation (2.20), an idea which has also recently been used in the context of a stochastic Liouville equation [HC18]. The theorem states that a stochastic process considered over the interval $[0, T]$ can be expressed by the infinite sum

$$\eta(t) = \mathrm{i} \sum_{k=1}^{\infty} \sqrt{\lambda_k} Z_k u_k(t) \,, \tag{2.75}$$

where for a zero mean complex-valued Gaussian process $\eta(t)$ the random variables Z_k are independent, complex-valued and Gaussian distributed with

$$\mathcal{M}(Z_k) = 0, \qquad \mathcal{M}(Z_k Z_l) = 0, \quad \text{and} \quad \mathcal{M}(Z_k Z_l^*) = \delta_{k,l} \,. \tag{2.76}$$

Note that the factor i is non-standard but convenient for the following. In general, the expansion may be multiplied with an arbitrary phase without altering the stochastic properties. The orthonormal basis functions u_k are the solutions of the Fredholm equation

$$\int_0^T \mathrm{d}s\, \alpha(t,s) u_k(s) = \lambda_k u_k(t)\ , \tag{2.77}$$

with $\alpha(t,s) = \mathcal{M}(\eta(t)\eta^*(s))$ denoting the correlation function of the stochastic process. Since the kernel $\alpha(t,s)$ is a correlation function, the kernel has to be non-negative and, thus, $\lambda_k \in \mathbb{R}$ with $\lambda_k \geq 0$. In correspondence with the discrete eigenvalue problem, the kernel can be expressed in terms of the eigenfunctions $u_k(t)$ and the corresponding eigenvalues λ_k

$$\alpha(t,s) = \sum_{k=1}^{\infty} \lambda_k u_k(t) u_k^*(s)\ . \tag{2.78}$$

Using these properties, it is easily verified that the stochastic process $\eta^*(t)$, expanded as in Eq. (2.75), fulfills the required statistics $\mathcal{M}(\eta(t)) = 0 = \mathcal{M}(\eta(t)\eta(s))$ and

$$\mathcal{M}(\eta(t)\eta^*(s)) = \sum_{k,k'} \sqrt{\lambda_k \lambda_{k'}}\, \mathcal{M}(Z_k Z_{k'}^*) u_k(t) u_{k'}^*(s) = \sum_{k=1}^{\infty} \lambda_k u_k(t) u_k^*(s) = \alpha(t,s)\ . \tag{2.79}$$

As a remark, a stochastic process can be expanded in terms of any orthonormal set of basis functions of the L^2 Hilbert space of square integrable function over $[0,T]$. However, using the Karhunen–Loève expansion minimizes the total mean squared error when approximating the process by the truncated sum [KMT11; GS12] (see also Sec. 3.1.1 where the sampling of stochastic processes is discussed).

Rewriting the NMQSD equation (2.20) by using the Karhunen-Loève expansion for the stochastic process and the BCF yields

$$\begin{aligned}\partial_t \psi_t[\eta^*] = \Big(&- \mathrm{i}H_{\mathrm{sys}} - \mathrm{i}L \sum_k \sqrt{\lambda_k} Z_k^* u_k^*(t) \\ &- L^\dagger \int_0^t \mathrm{d}s \sum_k \lambda_k u_k(t) u_k^*(s) \frac{\delta}{\delta \eta^*(s)} \Big) \psi_t[\eta^*]\ ,\end{aligned} \tag{2.80}$$

which allows us to perform, again, a variable transformation for the stochastic pure state from the process η^* to the discrete random numbers $\mathbf{Z}^* \coloneqq (Z_1^*, \dots)$. Noting that $-\mathrm{i}\sqrt{\lambda_k} u_k^*(s) = \partial_{Z_k^*} \eta^*(s)$ holds, the integral part becomes

$$\begin{aligned}\int_0^t \mathrm{d}s \sum_k \lambda_k u_k(t) u_k^*(s) \frac{\delta}{\delta \eta^*(s)}\, \psi_t[\eta^*] &= \mathrm{i} \sum_k \sqrt{\lambda_k} u_k(t) \int_0^t \mathrm{d}s\, \frac{\partial \eta^*(s)}{\partial Z_k^*} \frac{\delta}{\delta \eta^*(s)}\, \psi_t[\eta^*(\mathbf{Z}^*)] \\ &= \mathrm{i} \sum_k \sqrt{\lambda_k} u_k(t) \partial_{Z_k^*} \psi_t(\mathbf{Z}^*)\ .\end{aligned} \tag{2.81}$$

The action of Z_k^* and $\partial_{Z_k^*}$ on the stochastic pure state may equally well be mimicked by

$$Z_k^*\psi_t(\mathbf{Z}^*) = \langle \mathbf{Z}|b_k^\dagger|\Phi(t)\rangle \quad \text{and} \quad \partial_{Z_k^*}\psi_t(\mathbf{Z}^*) = \langle \mathbf{Z}|b_k|\Phi(t)\rangle \; . \tag{2.82}$$

The state $|\Phi(t)\rangle$ corresponds to a total state which is an element of the product Hilbert space of the system and formally introduced environmental modes with $\psi_t(\mathbf{Z}^*) \equiv \langle \mathbf{Z}|\Phi(t)\rangle$. The states $|\mathbf{Z}\rangle \coloneqq |Z_1\rangle \otimes |Z_2\rangle \ldots$ are, again, multi-mode Bargmann coherent states of the environment with $|Z_k\rangle = e^{Z_k b_k^\dagger}|0\rangle_k$. The operators b_k and $b_k^\dagger$ behave as usual bosonic annihilation and creation operators ($[b_k, b_{k'}^\dagger] = \delta_{k,k'}$) acting on the Fock states $|n\rangle_k$ of the mode k. These steps correspond precisely to the steps done in order to derive the NMQSD equation (see Sec. 2.1.1), however, in reverse order. It follows that Eq. (2.80) can be written as

$$\langle \mathbf{Z}|\partial_t|\Phi(t)\rangle = -\mathrm{i}\langle \mathbf{Z}|\left(H_{\mathrm{sys}} + L\sum_k \sqrt{\lambda_k} b_k^\dagger u_k^*(t) + L^\dagger \sum_k \sqrt{\lambda_k} u_k(t) b_k\right)|\Phi(t)\rangle \; . \tag{2.83}$$

Since this equation is valid for any $\mathbf{Z}^*$, the following equation must hold,

$$\partial_t|\Phi(t)\rangle = -\mathrm{i}\left(H_{\mathrm{sys}} + L\sum_k \sqrt{\lambda_k} b_k^\dagger u_k^*(t) + L^\dagger \sum_k \sqrt{\lambda_k} b_k u_k(t)\right)|\Phi(t)\rangle \; . \tag{2.84}$$

It has the structure of a Schrödinger equation for the total state $|\phi(t)\rangle$ in the interaction picture with respect to the environmental modes. Henceforth, the above equation (2.84) is called Karhunen-Loève expansion Schrödinger equation (KLESEQ). In contrast to the original microscopic model Hamiltonian [Eq. (2.6)] the phase $g_k e^{-\mathrm{i}\omega_k t}$ is replaced by $\sqrt{\lambda_k}u_k(t)$.

This shows that the exact reduced dynamics of an open quantum system interacting with a continuous environment can be obtained from a model where the environment is accounted for by an a-priory infinite, however, countable set of modes. The time dependent interaction between the modes and the system is uniquely determined by the BCF and the *finite* time interval $[0, T]$ for which the dynamics can be evaluated. What is advantageous about this approach is that the coupling strength $\sqrt{\lambda_k}$ decreases with k (see also Sec. 3.1.1, in particular Fig. 3.4). Therefore truncating the infinite sum yields an approximation and convergence can be checked straightforwardly. Furthermore, the rate at which the $\sqrt{\lambda_k}$ decrease is very large for short times intervals, i.e., small T. Thus, the KLESEQ is particularly suited to calculate the short time dynamics.

Several points should be noted. To reiterate, the state $|\Phi\rangle$ is an object of the product Hilbert space of the system and the formally introduced modes enumerated by the index k. Its meaning for the open quantum system dynamics is established by evolving the initial product state $|\Phi(0)\rangle = |\psi_0\rangle_{\mathrm{sys}} \otimes |\mathbf{0}\rangle_{\mathrm{env}}$ according to the KLESEQ (2.84)

and tracing out the environmental modes, $\rho_{\mathrm{sys}}(t) = \mathrm{Tr}_{\mathrm{env}}|\Phi(t)\rangle\langle\Phi(t)|$. Remarkably, for a Hermitian coupling operator $L = L^\dagger$ this pure state formalism can also be used to cover thermal initial environmental states by simply using the thermal BCF (see Eq. (2.72)). The KLESEQ inherits this property directly from the NMQSD equation [DGS98]. We note in passing that the so-called thermo field (TF) dynamics [SU83; TU96], originally used to derive the NMQSD equation for thermal environments, allows one to treat thermal initial conditions with a zero temperature formalism, too. There, the trick is to introduce a second, however, completely isolated bath. With the help of a suitable Bogoliubov transformation an effective joint environment is constructed such that its ground state (zero temperature) corresponds to the thermal state for the original environment.

It should be kept in mind that the basis functions $u_k(t)$ are defined over the time interval $[0, T]$. Therefore, the KLESEQ allows one to solve the reduced dynamics for that interval only. In terms of numerical effort, the upper bound T significantly influences the number of modes required for a suitable truncation. The smaller T the less modes are required (see e.g. Fig. 3.4). In the limit $T \to \infty$ the original microscopic model is recovered, i.e., $u_k(t) \to e^{-\mathrm{i}\omega_k t}$.

To push the limits of applicability, the KLESEQ could be solved by any of the more advanced explicit methods like the time-dependent Hatree [WT03], the Multi-Davidov [Har+19; WG20] or the time-dependent density matrix renormalization group [AS05] approach, which can treat several thousands of modes. Investigating the advantage of the KLESEQ over a conventional discretization of the SD remains as an exciting project.

2.3.2 The Time-Oscillator Picture

In this section it will be shown, that the reduced state can also be obtained from *successive interactions in time* with mode like degrees of freedom, which is in close relation to so-called collisional models [AL07; KLS16]. This perspective is suggested by the time-discrete form of the NMQSD equation (2.18). The idea is to account for the multiplication with η_i^* and the action of the derivative $\partial_{\eta_i^*}$ within the time-discrete NMQSD equation (2.18), again, by using creation and annihilation operators $b_i^\dagger$ and b_i. In contrast to the above KLESEQ, the index i corresponds to a time index. Thus, the action of, i.e., b_i is tied to the time t_i. Simply replacing $\eta_i^* \to b_i^\dagger$ and $\partial_{\eta_i^*} \to b_i$

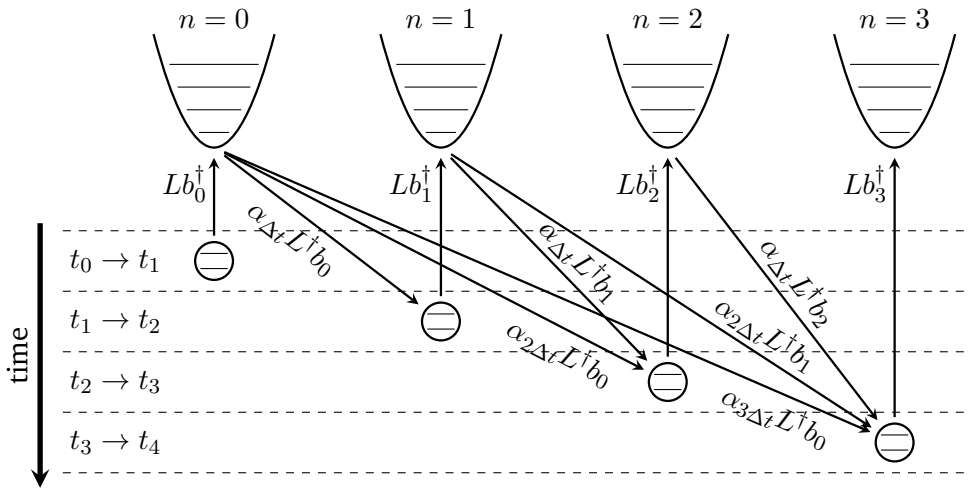

Fig. 2.3: A visualization of the dynamical map [Eq. (2.85)] is shown which iterates from the (not necessarily normalized) state $|\Psi_n\rangle$ to $|\Psi_{n+1}\rangle$. Due to the term $b_n^\dagger$, the system (small circle) excites a new oscillator (index n). In addition all previously excited oscillators (index $m < n$) have a back action on the system scaled by the value of the BCF $\alpha(t_n - t_m)$. In that way memory effects due to the environment are incorporated.

motivates the following map acting on the product Hilbert space of the system and N harmonic "time-oscillators",

$$|\Psi_{n+1}\rangle = \left[1 + \Delta t \left(-\mathrm{i}H_{\mathrm{sys}} + b_n^\dagger L - L^\dagger \sum_{m=0}^{n-1} \alpha(t_n - t_m) b_m\right)\right] |\Psi_n\rangle \quad \text{for} \quad n \leq N \,. \tag{2.85}$$

A visualization of this map is shown in Fig. 2.3.

To obtain the reduced state, on is tempted to take the trace over the environment, i.e, the "time oscillators". Performing the trace in terms of multi-mode Bargmann coherent states $|\mathbf{y}\rangle$ (as in Eq. (2.5) for the NMQSD derivation) yields, by construction, a stochastic pure state with a time-discrete evolution which, on first sight, seems to agree with the NMQSD equation (2.18):

$$\begin{aligned} \mathrm{Tr}_{\mathrm{env}} |\Psi_n\rangle\langle\Psi_n| &= \int \mathrm{d}^2\mathbf{y} \langle\mathbf{y}|\Psi_n\rangle\langle\Psi_n|\mathbf{y}\rangle, \qquad \mathrm{d}^2 y_i := \mathrm{dRe}(y_i)\mathrm{dIm}(y_i)\frac{e^{-|y_i|^2}}{\pi}, \\ \langle\mathbf{y}|\Psi_{n+1}\rangle =: \psi_{n+1} &= \left[1 + \Delta t \left(-\mathrm{i}H_{\mathrm{sys}} + y_n^* L - L^\dagger \sum_{m=0}^{n-1} \alpha(t_n - t_m)\partial_{y_m^*}\right)\right] \psi_n \,. \end{aligned} \tag{2.86}$$

However, the independence of the "time-oscillators" is reflected by independent random variables y_n^* representing the coherent state labels from the trace. This means that the statistics of y_n^*, i.e., $\mathcal{M}(y_n y_m^*) = \delta_{n,m}$ is different from the statistics of the time-discrete process η_n^* of the NMQSD equation, i.e, $\mathcal{M}(\eta_n \eta_m^*) = \alpha(t_n - t_m)$. Consequently, taking the trace over the time-oscillator modes does not yield the

reduced dynamics of the original microscopic model. Nevertheless, the reduced state can be obtained from the following expression

$$\rho_{\mathrm{sys}} = \mathrm{Tr}_{\mathrm{env}} \Upsilon |\Psi_n\rangle\langle\Psi_n| \,, \tag{2.87}$$

where Υ denotes the environmental operator

$$\Upsilon := \int \frac{\mathrm{d}^2\boldsymbol{\eta}}{\pi^N |\boldsymbol{\alpha}|} e^{-\boldsymbol{\eta}^\dagger \boldsymbol{\alpha}^{-1} \boldsymbol{\eta}} |\boldsymbol{\eta}\rangle\langle\boldsymbol{\eta}|, \tag{2.88}$$

with $|\boldsymbol{\eta}\rangle := |\eta_0\rangle \dots |\eta_N\rangle$, $|\eta_\lambda\rangle := e^{\eta_\lambda b_\lambda^\dagger}|0\rangle_\lambda$ and $0 \leq \lambda \leq N$. This leads to the expression for the reduced state

$$\rho_{\mathrm{sys}} = \int \frac{\mathrm{d}^2\boldsymbol{\eta}}{\pi^N |\boldsymbol{\alpha}|} e^{-\boldsymbol{\eta}^\dagger \boldsymbol{\alpha}^{-1} \boldsymbol{\eta}} \langle\boldsymbol{\eta}|\Psi_n\rangle\langle\Psi_n|\boldsymbol{\eta}\rangle = \underset{\boldsymbol{\eta}}{\mathcal{M}} |\psi_n(\boldsymbol{\eta}^*)\rangle\langle\psi_n(\boldsymbol{\eta})| \,. \tag{2.89}$$

Here, $\boldsymbol{\alpha}^{-1}$ denotes the inverse of the correlation matrix $\alpha_{ij} = \alpha(t_i - t_j)$ and $|\boldsymbol{\alpha}|$ its determinant. Reading the integral in a Monte-Carlo sense allows one to identify the vector $\boldsymbol{\eta}$ with a multi-variant complex valued Gaussian distributed random variable obeying $\mathcal{M}(\eta_i) = 0 = \mathcal{M}(\eta_i \eta_j)$ and $\mathcal{M}(\eta_i \eta_j^*) = \alpha_{ij}$. Note that due to the integration over the complex plane, the square root for the normalization is missing compared to a real valued multi-variant Gaussian probability density. By choosing the ground state as the initial condition for the time-oscillator modes it is assured that $\langle\boldsymbol{\eta}|\Psi_n\rangle \equiv |\psi_n\rangle$ depends on $\eta_0^* \dots \eta_{n-1}^*$ only. This shows that the right hand side of Eq. (2.89) is equivalent to the expression for the reduced state obtained by the NMQSD formalism. Consequently, propagating the time-oscillator model [Eq. (2.85)] with the initial condition $|\Psi_0\rangle = |\psi_0\rangle_{\mathrm{sys}}|\mathbf{0}\rangle$ allows one to obtain the reduced state of the microscopic model for open quantum system dynamics [Eq. (2.1)] at time t_n by evaluating

$$\rho_{\mathrm{sys}}(t_n) = \mathrm{Tr}_{\mathrm{env}} \Upsilon |\Psi_n\rangle\langle\Psi_n| \,. \tag{2.90}$$

Of course, the above statement is valid within the time-discrete NMQSD formalism and, thus, requires a sufficiently small step size $\Delta t = t_{n+1} - t_n$.

Although the map [Eq. (2.85)] for the vector $|\Psi_n\rangle$ is mathematically sound, the existence of an experimental implementation is not obvious due to the complicated non-Hermitian generator

$$-\mathrm{i}H_{\mathrm{sys}} + b_n^\dagger L - L^\dagger \sum_{m=0}^{n-1} \alpha(t_n - t_m) b_m \,. \tag{2.91}$$

Nonetheless, the time-oscillator picture presented here might lead to a feasible quantum simulator utilizing successive qubit interactions to emulate open quantum system dynamics. Noteworthily, since each time oscillator is excited only once and

the initial state is the ground state, the vector $|\Psi_n\rangle$ is confined to the two lowest levels of each oscillator. Thus, the oscillators appear as qubits only.

Yet another field of investigation originates from the assumption of a finite correlation length, that is $\alpha(\tau) = 0$ for $\tau > \tau_{\max}$. It seems plausible that this yields a finite dimensional formalism even for an arbitrarily large propagation time and is in the spirit of the QUAPI / TEMPO approach [Mak95; Str+18].

2.3.3 HOPS for a Finite Set of Modes

The goal of this section is to enlighten the meaning of the auxiliary states from a physical perspective and, with this, give reasons to justify the truncation of the hierarchy. As shown in the following, this is easily possible for a finite set of environmental modes. For a continuous environment, however, the physical meaning of the auxiliary states is not obvious. Still, the insights from the discrete case underpin the empiric result (see Sec. 3.3) that the stochastic pure state converges with respect to the number of auxiliary states.

Note that for a discrete SD $J(\omega) = \pi \sum_{\lambda=1}^{N} |g_\lambda|^2 \delta(\omega - \omega_\lambda)$ with N modes, by definition [Eq. (2.4)], the BCF is of multi-exponential kind $\alpha(\tau) = \sum_{\lambda=1}^{N} |g_\lambda|^2 e^{-\mathrm{i}\omega_\lambda \tau}$ such that the parameters entering the HOPS are $G_\lambda = |g_\lambda|^2$ and $W_\lambda = \mathrm{i}\omega_\lambda$ (compare with Eq. (2.22)). The stochastic process $\eta^*(t) = -\mathrm{i} \sum_{\lambda=1}^{N} g_\lambda^* z_\lambda^* e^{\mathrm{i}\omega_\lambda t}$ is defined by the N complex random variables z_λ^* (coherent state labels). This allows one to identify the operator D_λ as the partial derivative with respect to the coherent states labels z_λ^*

$$\frac{\mathrm{i}}{g_\lambda^*} e^{-\mathrm{i}\omega_\lambda n \Delta t} \partial_{z_\lambda^*} = \sum_{m=0}^{n-1} e^{-W_\lambda (n-m)\Delta t} \partial_{\eta_m^*} = D_\lambda^n \tag{2.92}$$

when acting on the stochastic pure state (including a factorized initial condition with a zero temperature environment). The above relation corresponds to simply changing the dependence on the stochastic process η_n^* back to the coherent state labels z_λ^*. As a consequence, for a discrete bath the auxiliary states of the HOPS are related to the Fock-states of the modes by

$$\begin{aligned} \psi_n^{\mathbf{k}} &= \prod_{\lambda=1}^{N} (D_\lambda^n)^{k_\lambda} \, \psi_n(\eta_0, \dots \eta_{n-1}) \\ &\sim \prod_{\lambda=1}^{N} \left(\partial_{z_\lambda^*}\right)^{k_\lambda} \psi_n(z_1^*, \dots z_N^*) = \langle \mathbf{z}| \bigotimes_{\lambda=1}^{N} a_\lambda^{k_\lambda} |\Psi(t_n)\rangle \\ &= \left[\bigotimes_{\lambda=1}^{N} \sum_{n_\lambda=0}^{\infty} \frac{(z_\lambda^*)^{n_\lambda} \sqrt{(n_\lambda + k_\lambda)!}}{n_\lambda!} \langle n_\lambda + k_\lambda| \right] |\Psi(t_n)\rangle \end{aligned} \tag{2.93}$$

where $|z\rangle = \sum_n z^n/\sqrt{n!}|n\rangle$ has been used. This means that an auxiliary state with hierarchy index $\mathbf{k}$ is a superposition of the states $\langle n_1 \dots n_N|\Psi\rangle$ with $n_\lambda \geq k_\lambda$ only. Large values of k_λ imply that only highly excited states contribute. Henceforth, if such states are only marginally populated, auxiliary states of large hierarchy depth are expected to be irrelevant. This reasoning motivates the truncation of the hierarchy which enables a numerical treatment of the HOPS (see also Sec. 3.3).

Is interesting to note that for any fixed set z_λ^*, the auxiliary state vector can be obtained from the Fock-state by a simple matrix multiplication, as seen in Eq. (2.93). Inverting this relation allows one, in principal, to obtain the Fock-space representation, and with it the reduced state $\rho_{\rm sys} = \sum_{n_1,\dots n_N}\langle n_1,\dots n_N|\Psi\rangle\langle\Psi|n_1,\dots n_N\rangle$, from a *single realization* of the HOPS solution, i.e., the stochastic pure state and all corresponding auxiliary states. Recall that in the usual NMQSD / HOPS formalism the reduced state is obtained by averaging over the dyads of different realizations of the stochastic pure state.

The special meaning of the auxiliary states for the discrete environment becomes particularly evident for the choice $z_\lambda^* = 0$. In that case $\psi_n^{\mathbf{k}} \sim \langle \mathbf{0}|\otimes_\lambda a_\lambda^{k_\lambda}|\Psi\rangle \sim \langle \mathbf{k}|\Psi\rangle$ where $|\mathbf{k}\rangle$ denotes the product Fock-state with occupation number k_λ for the mode λ. The HOPS recovers the Schrödinger equation in the Fock-state representation

$$\dot{\psi}_t^{\mathbf{k}} = -\mathrm{i}\left(H_{\rm sys} + \sum_{\lambda=1}^N k_\lambda\omega_\lambda\right)\psi_t^{\mathbf{k}} - \mathrm{i}L^\dagger\sum_{\lambda=1}^N g_\lambda\sqrt{k_\lambda+1}\psi_t^{\mathbf{k}+\mathbf{e}_\lambda} - \mathrm{i}L\sum_{\lambda=1}^N g_\lambda^*\sqrt{k_\lambda}\psi_t^{\mathbf{k}-\mathbf{e}_\lambda}\ . \tag{2.94}$$

Here, the stochastic term has vanished since the coherent state labels have all been chosen to be zero.

2.3.4 HOPS with Derivatives of the Bath Correlation Function

In this section we provide another way to solve the NMQSD equation (2.20) and, thus, the open system model. In the very same spirit as the HOPS approach (Sec. 2.1.2), here we derive a set of hierarchically structured equations where the sought after stochastic pure state amounts to the root of this hierarchy. The crucial difference is that, instead of using a multi-exponential representation for the BCF, higher order derivatives of the BCF are involved. This kind of hierarchy might be of particular relevance for the case where the dynamics depends sensitively on the accuracy of the multi-exponential representation, as noted, e.g., when investigating the long time entanglement dynamics of two qubits in the strong coupling in Sec. 5.4.

Note that in relation with the HEOM, other representations than the multi-exponential form of the BCF have also been used to define auxiliary objects and to derive their hierarchical relation [Tan+15; Cui+19]. As for the HEOM, if the BCF and its derivative can be expressed by a finite set of arbitrary functions a HOPS can be derived, too. For reasons of numerical efficiency the number of such functions should be as small as possible which poses a trade-off between accuracy and efficiency.

In the following we can circumvent this challenging task of finding a suitable representation by deriving a hierarchy based on higher order derivatives of the BCF. It turns out to be useful to define the auxiliary states $\psi_n^{\mathbf{k}}$ at time t_n, where $\mathbf{k} = (k_0, ..., k_\mu, ...)$ denotes an infinite dimensional index vector, as

$$\begin{aligned} \psi_n^{\mathbf{k}} &:= \prod_{\mu=0}^{\infty} \left(D_{n,\mu}\right)^{k_\mu} \psi_n \\ \text{with} \quad D_{n,\mu} &:= \sum_{j=0}^{n-1} \alpha^{(\mu)}((n-j)\Delta t)\partial_{\eta_j^*} \, . \end{aligned} \tag{2.95}$$

Here $\alpha^{(\mu)}$ refers to the μ-th derivative of the BCF. In this notation the time-discrete NMQSD equation (2.18) reads

$$\psi_{n+1} = \left[1 + \Delta t \left(-\mathrm{i}H_{\mathrm{sys}} + \eta_n^* L - L^\dagger D_{n,0}\right)\right] \psi_n \, . \tag{2.96}$$

The evolution of the auxiliary states is obtained by expressing $\psi_{n+1}^{\mathbf{k}}$ by $\psi_n^{\mathbf{k}}$ up to first order in Δt while using the above expression (2.96) of the NMQSD equation. Expanding the μ-th derivative of the BCF at $(n-j)\Delta t$ up to first order in Δt leads to

$$\alpha^{(\mu)}\Big((n+1-j)\Delta t\Big) = \alpha^{(\mu)}\Big((n-j)\Delta t\Big) + \alpha^{(\mu+1)}\Big((n-j)\Delta t\Big)\Delta t + \mathcal{O}(\Delta t^2) \, , \tag{2.97}$$

and yields the recursion relation

$$D_{n+1,\mu} = D_{n,\mu} + \alpha_0^\mu \partial_{\eta_n^*} + \Delta t \left(D_{n,\mu+1} + \alpha_0^{\mu+1}\partial_{\eta_n^*}\right) , \tag{2.98}$$

with $\alpha_0^\mu := \alpha^{(\mu)}(0)$ denoting the value of the μ-th derivative of the BCF at $\tau = 0$. Evaluating the product $\prod_{\mu=0}^{\infty} \left(D_{n+1,\mu}\right)^{k_\mu}$ up to first order in Δt results in

$$\begin{aligned} \prod_{\mu=0}^{\infty} \left(D_{n+1,\mu}\right)^{k_\mu} &= \prod_{\mu=0}^{\infty} \left(D_{n,\mu} + \alpha_0^\mu \partial_{\eta_n^*}\right)^{k_\mu} \\ &\quad + \Delta t \sum_{\mu=0}^{\infty} k_\mu \frac{\prod_{\mu'=0}^{\infty}\left(D_{n,\mu'} + \alpha^{(\mu')}(0)\partial_{\eta_n^*}\right)^{k_{\mu'}}}{D_{n,\mu} + \alpha_0^\mu \partial_{\eta_n^*}} \left(D_{n,\mu+1} + \alpha_0^{\mu+1}\partial_{\eta_n^*}\right) \, , \end{aligned} \tag{2.99}$$

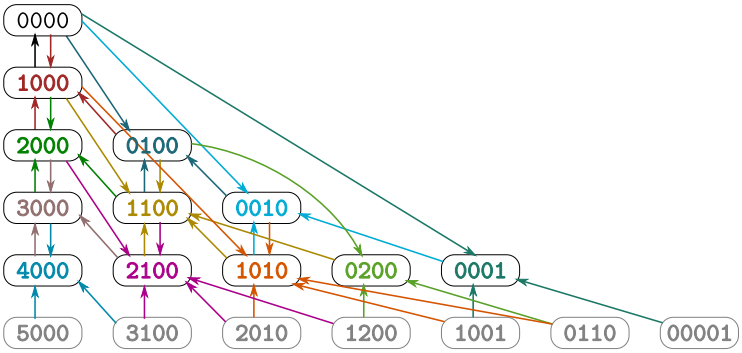

Fig. 2.4: The hierarchical structure of the HOPS based on derivatives of the BCF is shown. In each column the first index k_0 is increased only. The arrangement of the rows was chosen such that for a particular row, the "distance" from each auxiliary state to the stochastic pure state is constant. The term "distance" refers to the minimum number of edges connecting two states in the sense of a mathematical graph.

where the fraction is a formal notation to express the cancellation of the term with index μ in the product. Taking into account that the stochastic pure state at time t_n does not depend on η_n^*, i.e., $\partial\eta_n^*\psi_n = 0$ (see Sec. 2.1.1) leads to

$$\begin{aligned}\psi_{n+1}^{\mathbf{k}} = &\prod_{\mu=0}^{\infty} \left(D_{n,\mu}\right)^{k_\mu} \left[1 + \Delta t \left(-\mathrm{i}H_{\mathrm{sys}} + \eta_n^* L - L^\dagger D_{n,0}\right)\right] \psi_n \\ &+ \Delta t \sum_{\mu=0}^{\infty} k_\mu \frac{\prod_{\mu'=0}^{\infty} \left(D_{n,\mu'}\right)^{k_{\mu'}}}{D_{n,\mu}} \alpha_0^\mu L \psi_n + \Delta t \sum_{\mu=0}^{\infty} k_\mu \frac{\prod_{\mu'=0}^{\infty} \left(D_{n,\mu'}\right)^{k_{\mu'}}}{D_{n,\mu}} \left(D_{n,\mu+1}\right) \psi_n \,.\end{aligned} \tag{2.100}$$

Applying the definition for the auxiliary states, the final expression reads,

$$\begin{aligned}\psi_{n+1}^{\mathbf{k}} = \psi_n^{\mathbf{k}} + \Delta t \left(-\mathrm{i}H_{\mathrm{sys}} + \eta_n^* L\right) \psi_n^{\mathbf{k}} - \Delta t L^\dagger \psi_n^{\mathbf{k}+\mathbf{e}_0} \\ + \Delta t \sum_{\mu=0}^{\infty} k_\mu \left(\alpha_0^\mu L \psi_n^{\mathbf{k}-\mathbf{e}_\mu} + \psi_n^{\mathbf{k}-\mathbf{e}_\mu+\mathbf{e}_{\mu+1}}\right)\end{aligned} \tag{2.101}$$

and becomes, in differential form,

$$\begin{aligned}\partial_t \psi(t)^{\mathbf{k}} = \left(-\mathrm{i}H_{\mathrm{sys}} + \eta_t^* L\right) \psi(t)^{\mathbf{k}} - L^\dagger \psi(t)^{\mathbf{k}+\mathbf{e}_0} \\ + \sum_{\mu=0}^{\infty} k_\mu \left(\alpha_0^\mu L \psi(t)^{\mathbf{k}-\mathbf{e}_\mu} + \psi(t)^{\mathbf{k}-\mathbf{e}_\mu+\mathbf{e}_{\mu+1}}\right) \,.\end{aligned} \tag{2.102}$$

Note that only values of the derivatives of the BCF at $\tau = 0$ enter the hierarchy as parameters.

As for the HOPS with an exponential representation of the BCF, the initial condition reads

$$\begin{aligned} \psi_0^{\mathbf{k}} &= |\psi_0\rangle \qquad \text{for } \mathbf{k} = (0,0,\dots) \\ \psi_0^{\mathbf{k}} &= 0 \qquad\quad \text{for } \mathbf{k} \neq (0,0,\dots)\ . \end{aligned} \tag{2.103}$$

The structure of this HOPS is depicted in Fig. 2.4. Note that the stochastic pure state is directly influenced by the auxiliary state with $\mathbf{k} = (1,0,\dots)$ only. Henceforth, only this auxiliary state belongs to the hierarchy level with depth one. In turn, its time derivative depends on the stochastic pure state and the two new auxiliary states with $\mathbf{k} = (2,0,\dots)$ and $\mathbf{k} = (0,1,0,\dots)$. These two new auxiliary states constitute the hierarchy level with depth two. In general, since each auxiliary state with $\mathbf{k} = (k_0, k_1, \dots)$ depends, among others, on the auxiliary state with $\mathbf{k} = (k_0 + 1, k_1, \dots)$, increasing the first index by one increases the hierarchy level by one, too (see the columns in Fig. 2.4). The influence of lower hierarchy levels on the auxiliary state $\psi_n^{\mathbf{k}}$ is determined by the index $\mathbf{k} - \mathbf{e}_\mu$. In contrast to the standard HOPS (Sec. 2.1.2), $\mathbf{k} - \mathbf{e}_\mu$ enumerates auxiliary states from *different* hierarchy levels. With reference to Fig. 2.4, each non-vanishing index vector component of $\mathbf{k} - \mathbf{e}_\mu$ results in an incoming arrow from "above". On the other hand, the index $\mathbf{k} - \mathbf{e}_\mu + \mathbf{e}_{\mu+1}$ labels an auxiliary state with belongs to the next hierarchy level. This reasoning motivates the following expression for the hierarchy depth

$$l = \sum_{\mu=0}^{\infty} \mu \cdot k_\mu\ . \tag{2.104}$$

In the sense of a mathematical graph, this quantity reflects the smallest number of (directed) edges connecting an auxiliary state of index $\mathbf{k}$ with the root index $\mathbf{k} = (0,0,\dots)$. In other words, it reflects how many intermediate auxiliary states are present for an auxiliary state with index $\mathbf{k}$ to influence the stochastic pure state. Thus, the quantity l seems suitable to serve as the hierarchy level.

In contrast to the HOPS based on a multi-exponential BCF representation, here, the coupling between the auxiliary states is not bi-directional (see Fig. 2.4). In particular, an auxiliary state of level l may directly depend on an auxiliary state from a lower level l' with a level difference *larger* than 1, i.e., $l - l' > 1$. However, these connections never appear in the opposite direction, since an auxiliary state with level l is only influenced from states of larger level l' with a level difference of 1.

When truncating the set of differential equations (2.102), the hierarchical scheme presented here can serve as a numerical method to solve the NMQSD equation (2.20). The importance sampling (non-linear NMQSD formalism) discussed in Sec. 2.1.3 as well as the stochastic treatment of a thermal initial environmental states

(Sec. 2.2.2) can be incorporated as well. It remains as an exciting project to explore the advantages of this kind of hierarchy for real open system scenarios.

Solving the HOPS Numerically

3

In the previous Chapter it has been shown that the HOPS yields an exact description for the reduced dynamics. It is the goal of this Chapter to discuss in detail how the HOPS formalism can be used as a numerical method to calculate the exact dynamics of an open quantum system. To be precise, with "exact" we refer to the intrinsic exactness of the method. Any explicit numeric evaluation will contain some degree of error. However, as of the "exactness" of the HOPS method, this error can, in principle, be made arbitrarily small. Undeniably, the price to pay is the numerical effort.

To begin with, numerical techniques to sample stochastic processes are elucidated in Sec. 3.1. As for the relation to the HOPS, the focus lies on complex valued stationary Gaussian processes defined in terms of their correlation function. Two approaches are considered. The Karhunen-Loève expansion (Sec. 3.1.1) works well for any kind of correlation function and needs the least amount of random numbers as input to sample a particular realization of the stochastic process. However, the method requires one to solve an eigenvalue problem. This limits its applicability since the dimension of this eigenvalue problem scales with the size of the time interval for which the process is defined. In Sec. 3.1.2 a second approach based on the numerical Fourier Transform is analyzed. Whenever the fast Fourier transform (FFT) algorithm is applicable, this method is very efficient (Sec. 3.1.2.1). For an effective SD which diverges at $\omega = 0$, the FFT becomes inefficient due to the implied midpoint rule with equidistant nodes ω_i. As a remark, such SDs become relevant when sampling the thermal noise $\xi(t)$ [Eq. (2.69)] for a sub-Ohmic SD [Eq. (3.25)]. Since the numeric integration of a function with poles can efficiently be done using the tanh-sinh (TS) substitution, a Fourier Transform method based on the TS integration scheme proves to be efficient (Sec. 3.1.2.2).

Another central ingredient for the (standard) HOPS formalism is the multi-exponential representation of the BCF. For the widely used class of Ohmic and sub-Ohmic SDs [Leg+87; BTV03; CT06; WT08; Tan+15; Str+18; Mag+18], also considered in Ch. 4 and Ch. 5, the BCF decays algebraically $\alpha(\tau) \sim \tau^{-(s+1)}$ with $0 < s \leq 1$. As a consequence, an exponential representation may serve as an approximation only. In Sec. 3.2 it is shown how to find highly accurate multi-exponential representations by directly fitting the BCF in time domain. Analyzing the error of the approximation

reveals an efficient convergence with the number of exponential terms. Explicit values for the fits are provided in App. C.

In Sec. 3.3 the truncation of the HOPS is discussed. Along with general considerations on how to check convergence with respect to the truncation, a flexible truncation scheme is proposed and tweaked for Ohmic and sub-Ohmic SDs.

In a final remark (Sec. 3.4), the two approaches, mentioned earlier in Sec. 2.2, for a thermal initial environmental state are compared using the spin-boson model with a sub-Ohmic environment as test bed. It is shown that, in particular for a strong system-environment interaction, the stochastic potential (SP) approach (Sec. 2.2.2) converges significantly faster with respect to the hierarchy depth as compared to the NMQSD variant utilizing the thermal BCF [DGS98]. This is plausible since the real part of the BCF increases with temperature which results in an effective increase of the coupling strength between the auxiliary states. Hence, the stochastic method should be considered the method of choice to incorporate non-zero temperature.

Implementing the tweaks presented in this chapter allow to employ the HOPS formalism to solve the dynamics of an open quantum system far beyond the weak coupling regime. In particular, the development of these tools was necessary to trustworthily determine the entanglement dynamics of two qubits in contract with a common environment over a broad range of system parameters, which sets the overall scope for the application of the HOPS in this theses (see Ch. 5).

3.1 Stochastic Process Sampling

An essential role of the HOPS formalism is taken by the stochastic process. Recall that each realization of the stochastic process yields another stochastic pure state. The reduced dynamics is obtained by averaging over the dyads of such stochastic pure states. Evidently, from a numerical perspective the microscopic definition of the stochastic process $\eta^*(t) = -\mathrm{i}\sum_\lambda g_\lambda^* z_\lambda^* e^{\mathrm{i}\omega_\lambda t}$ [Eq. (2.11)] is of no use for a truly continuous SD. In that case the characterization of the process by its moments is more suitable. The Gaussian distribution of the random variables z_λ^* results in a Gaussian process which is fully characterized by its first and second moments. Therefore, the aim is to develop an accurate method for sampling such Gaussian stochastic processes that fulfill the statistics required by the NMQSD equation

$$\mathcal{M}(\eta(t)) = 0, \quad \mathcal{M}(\eta(t)\eta(s)) = 0 \quad \text{and} \quad \mathcal{M}(\eta(t)\eta^*(s)) = \alpha(t-s) \tag{3.1}$$

for a given BCF $\alpha(\tau)$.

Two different approaches are considered. One possibility is to approximate the stochastic process in terms of the truncated Karhunen-Loève expansion [KMT11; GS12]. The accuracy is then controlled by the number of expansion terms. A second approach makes use of the representation of the BCF in terms of a Fourier integral. The stochastic process is obtained by a modified version of this particular Fourier transform, where the accuracy of such a representation is determined by the discretization of the corresponding integral. An implementation of the methods presented here is publicly available at `github.com/cimatosa/stocproc`.

3.1.1 Karhunen–Loève Expansion

The Karhunen-Loève theorem states that for a fixed time interval $[0, T]$ the expansion of the stochastic process

$$\eta(t) = \sum_{k}^{\infty} g_k Z_k u_k(t), \tag{3.2}$$

with decreasingly ordered g_k and basis functions u_k defined by the continuous eigenvalue problem

$$\int_0^T \mathrm{d}s\, \alpha(t-s) u_k(s) = |g_k|^2 u_k(t), \tag{3.3}$$

is optimal in the sense that any truncation minimizes the total mean squared error ϵ with respect to any other basis expansion. To avoid misconception, in order to comply with common notation the symbols g_k are used here, too, which have a different meaning than the coupling constants of the microscopic Hamiltonian [Eq. (2.1)]. Note that the eigenvalues $|g_k|^2$ are real. Thus, g_k is specified up to an arbitrary phase only so we assume $g_k \in \mathbb{R}$. The complex-valued random variables Z_k have to be Gaussian distributed with $\mathcal{M}(Z_k) = 0 = \mathcal{M}(Z_k Z_l)$ and $\mathcal{M}(Z_k Z_l^*) = \delta_{kl}$ to yield the desired statistics for the process, i.e., $\mathcal{M}(\eta(t)\eta^*(s)) = \alpha(t-s)$. The total mean squared error is defined as

$$\epsilon := \int_0^T \mathrm{d}s\ \mathcal{M}(|\epsilon_N(t)|^2) \tag{3.4}$$

with $\epsilon_N = \eta(t) - \eta_N(t)$. Here, $\eta_N(t)$ denotes the numerically accessible truncated expansion using the first N expansion terms,

$$\eta_N(t) := \sum_{k=1}^{N} g_k Z_k u_k(t)\ . \tag{3.5}$$

The defining equation (3.3) for the eigenfunctions u_k belongs to the class of Fredholm equations. Although this kind of equation has been studied thoroughly [Mik+14], analytical solutions are only known for very limited scenarios. Therefore,

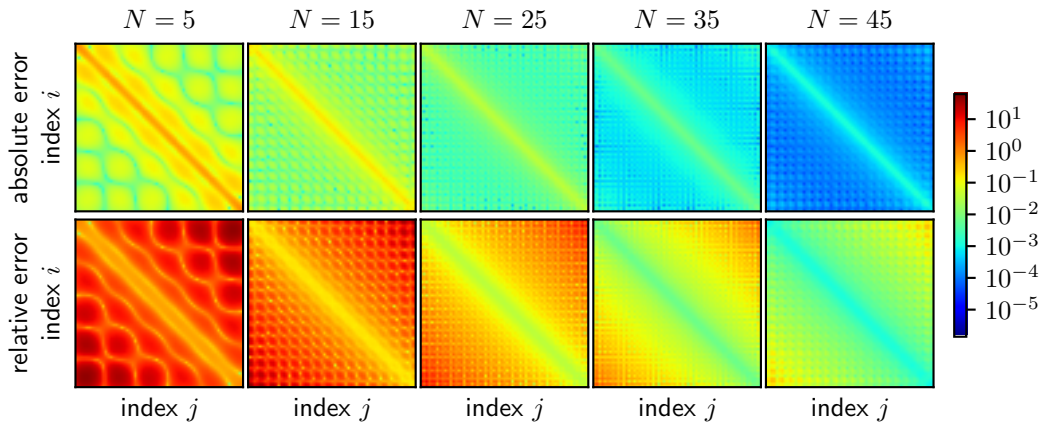

Fig. 3.1: The deviation of the second moment of the truncated Karhunen-Loève expansion from the given BCF is shown for various numbers of expansion terms N. The absolute error is maximal on the diagonal $i = j$, the relative error in the off diagonal corners. As expected, using more terms for the expansion decreases the error. A grid with $M = 257$ equidistant grid points and equal weights (mid-point rule) has been used ($\alpha(\tau) \sim (1 + \mathrm{i}\tau)^{-2}$, $T = 30$).

an accurate numerical scheme is desirable and will be presented in the following. For an arbitrary BCF the eigenfunctions u_k can be obtained by discretizing the integral and solving the resulting eigenvalue problem [Pre+07]

$$\sum_{i=1}^{M} h_j \alpha(t_i - t_j) u_k(t_j) = g_k^2 u_k(t_i) \; . \tag{3.6}$$

In terms of numerical quadrature the times $t_i \in [0, T]$ represent the nodes and h_i the corresponding weights. It is instructive to write the above equation in matrix form $RD^2 u_k = g_k^2 u_k$ where $R_{ij} = \alpha(t_i - t_j)$ and $D_{ij} = \delta_{ij}\sqrt{h_j}$. Multiplication with D from the left yields an eigenvalue equation for the Hermitian matrix $\tilde{R} = DRD$ with eigenvectors $\tilde{u}_k = Du_k$ and intrinsically real eigenvalues g_k^2. Since the integral kernel α originates from the expectation value $\mathcal{M}(\eta(t)\eta^*(s))$, the eigenvalues g_k^2 are non-negative. Without loss of generality, the coefficients g_k are chosen to be the positive root of the numerically obtained g_k^2. As noted earlier, using $e^{\mathrm{i}\varphi_k} g_k$ as coefficients for the expansion [Eq. (3.2)] is equivalent in terms of the moments of the stochastic process.

For a given quadrature scheme, i.e, fixing the nodes t_i and the corresponding weights h_i, the time-discrete numerical estimate for the stochastic process $\eta_N(t_i)$ [Eq. (3.5)] depends on two parameters: the number of nodes M used to discretize the integral and the number of expansion terms N. Its correlation function

$$\alpha_{\mathrm{aprx}}(t_i - t_j) \coloneqq \mathcal{M}(\eta_N(t_i)\eta_N^*(t_j)) = \sum_{k=1}^{N} g_k^2 u_k(t_i) u_k^*(t_j) \tag{3.7}$$

approximates the exact values $\alpha(t_i - t_j)$. The absolute error $|\alpha_{\mathrm{aprx}} - \alpha|$ scales with the missing eigenvalues $|g_k|^2$ ($k > N$) and becomes zero for $N = M$. As an example, for the most simple quadrature rule, the mid-point rule with equally weighted nodes, the error dependence on N is shown in Fig. 3.1 for an algebraically decaying BCF $\alpha(\tau) \sim (1 + \mathrm{i}\tau)^{-2}$. In addition to the absolute error we show the relative error $|\alpha_{\mathrm{aprx}} - \alpha|/|\alpha|$, too. Whereas the absolute error has its maximum on the diagonal $i = j$ the relative error becomes largest at the off-diagonal corners. Note that in order to capture the algebraic decay over a given time interval, the relative error should be used to assess the accuracy. However, when trying to estimate the statistics of the stochastic process in practice by drawing a finite number of N_s samples, the second moment estimate shows an absolute overall noise level which scales with $1/\sqrt{N_s}$. This means that unfeasibly many samples are necessary to see the algebraic decay of the correlations over a large time interval. With respect to using these sample in a numerical methods it appears, thus, consistent to use the maximum *absolute* error, i.e.,

$$\epsilon := \max_{i,j} \left| \sum_{k=1}^{N} g_k^2 u_k(t_i) u_k^*(t_j) - \alpha(t_i - t_j) \right| , \tag{3.8}$$

to quantify the accuracy of the numerical approximation of the stochastic process. It is clear that for any discretization of the Fredholm integral, using the whole set of eigenfunctions ($N = M$) restores the discrete kernel exactly, whereas for $N < M$ the error depends on the quadrature rule. It is shown in Fig. 3.2 (upper row) that the error of the tanh-sinh (TS) scheme [Mor05] (see Sec. 3.1.2.2 for details on the TS quadrature) decreases the fastest when increasing the number of expansion terms N. Remarkably, among the equidistant methods (mid-point, Simpson and 4-point scheme), the very simple mid-point rule performs best.

To be precise, the above statements refer to the case where the stochastic process is evaluated *on the grid points* t_i specified by the quadrature scheme. However, the stochastic processes entering the HOPS approach are continuous in time. In particular, when using adaptive numeric solvers for the set of differential equations, i.e., the HOPS, this property needs to be captured by the numeric estimate of the stochastic process, too. Interpolating the time-discrete eigenfunctions as suggested in Ref. [Pre+07], i.e.,

$$u_k(t) = \frac{1}{g_k^2} \sum_{i=1}^{M} h_j \alpha(t - t_j) u_k(t_j) , \tag{3.9}$$

achieves this task with unexpected consequences for the accuracy (see Fig. 3.2 and 3.3). Comparing the maximum absolute error for the *interpolated* stochastic process (lower row in Fig. 3.2) reveals that the advantage of the TS scheme is nullified whereas the mid-point rule is to be favored slightly over all other considered schemes.

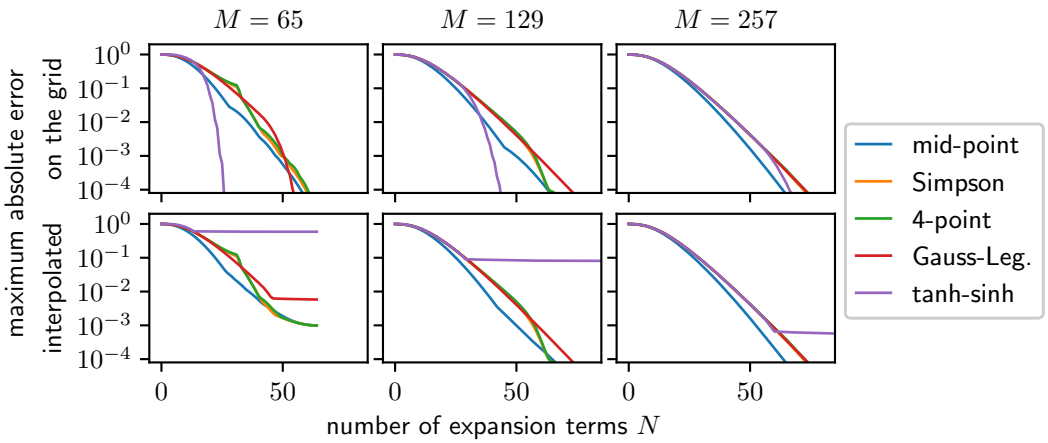

Fig. 3.2: The maximum absolute error ϵ of the correlation kernel as a function of the number of expansion terms N is shown for various numbers of nodes M and quadrature schemes. For the upper row the correlation kernel was evaluated on the quadrature scheme-dependent time grid only. For the lower row three additional times placed equidistantly between two neighboring grid points were considered. It is clear that on the grid points (upper row) the error becomes zero for $N = M$. For $N < M$ differences between the quadrature become evident. In contrast, including intermediate times (lower row) reveals that the maximum error remains larger than zero even for $N = M$. Its particular value depends on the fineness of the grid controlled by the overall number of nodes M and the quadrature scheme, which is expected. The plots suggest to favor the mid-point rule over the other schemes considered ($\alpha(\tau) \sim (1 + \mathrm{i}\tau)^{-2}$, $T = 30$).

To demonstrate the drastic impact of the interpolation on the accuracy of the second moment, the error along the diagonal α_{ii} is shown in Fig. 3.3 for the mid-point and the TS scheme. While for the mid-point scheme the error at interpolated times is roughly the same as for the times on the grid, the TS scheme behaves entirely different. For times close to the middle of the time interval, the error for an intermediate point is larger by several orders of magnitude than the error at the grid point and even exceeds the error of the mid-point rule. This leads to the final conclusion that equally distributed times with equal weights are most suited to numerically solve the Fredholm equation (3.3) with the aim to numerically sample a continuous-time stochastic process by means of the Karhunen-Loève expansion. It seems plausible that this statement is not particularly related to the kind of correlation function considered here, but holds in general.

It is important to note that the numerical effort increases when increasing the length T of the time interval $[0, T]$ for which the stochastic process is evaluated. Numerically analyzing the spectrum $|g_k|^2$ of the correlation kernel as a function of T reveals that the number of eigenvalues larger than a certain threshold scales linearly with T, as shown in Fig. 3.4 for two different kinds of BCFs. Since this threshold roughly controls the error of the truncation, doubling T requires twice as many expansion terms in order to maintain a given degree of accuracy. This behavior is accompanied by the fact that the interpolation error is related to the node density. Thus, the

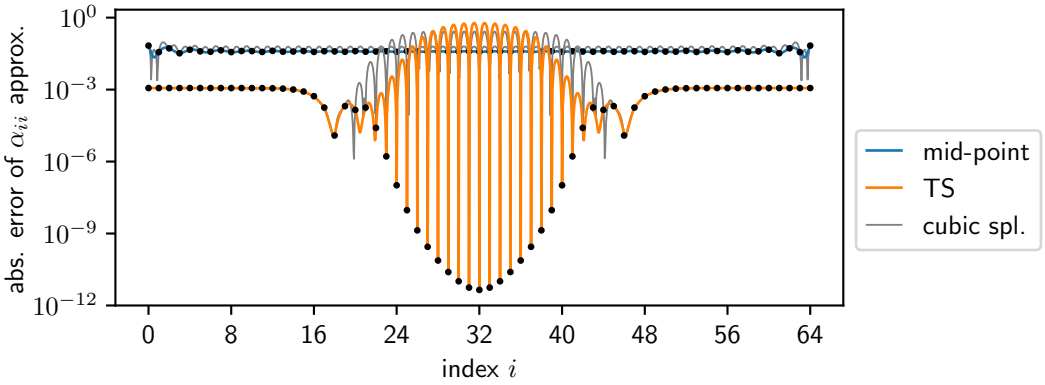

Fig. 3.3: The error of the correlation kernel $\mathcal{M}(\eta_N(t)\eta_N^*(s))$ for $t = s$ is shown using $M = 65$ nodes and $N = 25$ expansion terms. The time axis is labeled by the index of the quadrature scheme-dependent grid points (black dots). This means that for the TS scheme the highly increased node density near the ends of the time interval results in a non-linear relation between the time and the index i. To estimate the error for the continuous time stochastic process, 31 intermediate points between neighboring grid points were used. The two methods under consideration show a completely different behavior. While the error for the mid-point scheme remains roughly constant for the intermediate times, for the TS scheme the error at intermediate times is larger by several orders of magnitude than the error at the grid points. To rule out that this is not a defect of the special interpolation scheme [Eq. (3.9)], cubic splines were used to interpolate the eigenfunctions u_k (gray lines), too, which show a similar behavior ($\alpha(\tau) \sim (1 + \mathrm{i}\tau)^{-2}$, $T = 30$).

number of nodes M needs to increase with T, too. This suggests a linear scaling of the matrix size M with the length of the time interval T. The complexity of general eigenvalue routines is $\mathcal{O}(M^3)$[PC99]. Consequently, doubling the interval length T results in an 8-fold of computation time. In practice, this limits the size of M to several thousand. Notably, exploiting that the correlation kernel of a stationary process is of Toeplitz kind $\alpha_{ij} = \alpha_{i-j}$ reduces the complexity of the eigenvalue problem to $\mathcal{O}(M^2 \log M)$[PC99]. Obviously, the use of such a specialized algorithm is highly desirable. Unfortunately, since the commonly known collections of numerical algorithm do not contain such an implementation, exploiting the Toeplitz property of the kernel for generating stochastic processes remains an open task.

The numerical limits set by the eigenvalue problem can be traded for a less “optimal” expansion in terms of a discrete Fourier Transform discussed next.

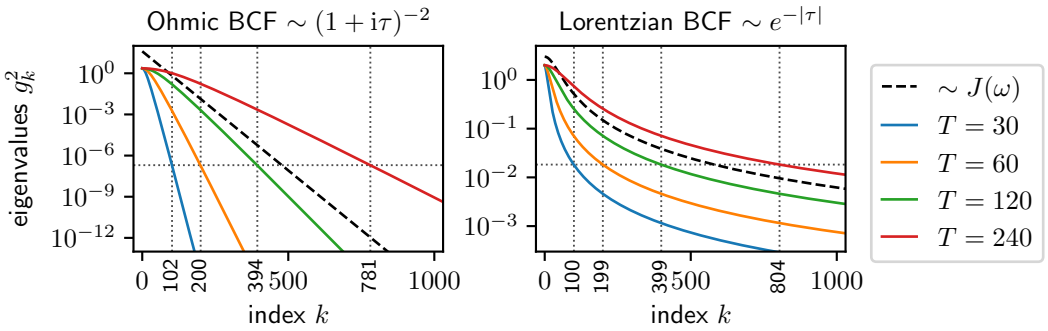

Fig. 3.4: The decrease of the eigenvalues $|g_k|^2$ with the index k is shown for different time intervals $[0, T]$ and two different kinds of BCFs corresponding to an Ohmic SD and a Lorentzian SD. Increasing T results in a slower decay of the spectrum. In particular, the number of eigenvalues above a certain threshold scales linearly with T as indicated by the dotted lines. The black dashed line is proportional to the decay of the SD (exponential in the Ohmic case and algebraic in the Lorentzian case) which matches the decay of the eigenvalues.

3.1.2 Fourier Integral Methods

The Fourier integral approach works for the case where the correlation function can be expressed as the Fourier transform of a positive function $I(\omega)$

$$\alpha(\tau) = \frac{1}{\pi}\int_{-\infty}^{\infty} \mathrm{d}\omega\, I(\omega) e^{-\mathrm{i}\omega\tau}\,. \tag{3.10}$$

Note that this is always the case when the correlation function corresponds to the bath correlation function (BCF) for open quantum system dynamics. The numerical approximation of the stochastic process corresponds to an expansion in terms of Fourier modes, i.e.,

$$\eta_N(t) := \sum_{k=0}^{N-1} g_k Z_k e^{-\mathrm{i}\omega_k t}, \qquad g_k = \sqrt{\frac{h_k I(\omega_k)}{\pi}}\,. \tag{3.11}$$

The random variables Z_k are complex valued and Gaussian distributed with $\mathcal{M}(Z_k) = 0 = \mathcal{M}(Z_k Z_{k'})$ and $\mathcal{M}(Z_k Z_{k'}^*) = \delta_{kk'}$. The expansion coefficients g_k are chosen such that the correlation function of the numerical estimate $\eta_N(t)$ approximates the integral defining the given correlation function [Eq. (3.10)]

$$\mathcal{M}(\eta_N(t)\eta_N^*(s)) = \frac{1}{\pi}\sum_{k=0}^{N-1} h_k I(\omega_k) e^{-\mathrm{i}\omega_k(t-s)} \approx \frac{1}{\pi}\int_{-\infty}^{\infty} \mathrm{d}\omega\, I(\omega) e^{-\mathrm{i}\omega(t-s)} = \alpha(t-s)\,. \tag{3.12}$$

In terms of numerical quadrature, h_k denotes the weights and ω_k the nodes. Note that if $I(\omega)$ corresponds to a physically meaningful SD $J(\omega)$, the lower bound of the integral can be set to zero, since $J(\omega) = 0$ for $\omega \leq 0$. Nonetheless, an effective SD $I(\omega)$ with non-vanishing values for negative frequencies may be useful, too, for example to incorporate non-zero temperature effects (see Sec. 3.4).

3.1.2.1 Fast Fourier Transform

For equally spaced nodes ω_k the stochastic process expansion given in Eq. (3.11) can be evaluated using the fast Fourier transform (FFT) algorithm. Even though the Fourier mode expansion of the stochastic process is not optimal, the efficiency of the FFT algorithm ($\mathcal{O}(N \log N)$ complexity) allows for significantly more expansion terms which easily compensates for this deficiency.

In principal any quadrature scheme with equally spaced nodes can be used. It turns out, however, that it is not beneficial to use more involved schemes as compared to the very simple midpoint rule. This is true especially for large τ where the fast oscillating phase $e^{-\mathrm{i}\omega\tau}$ permits a high degree polynomial interpolation of the integrand between the nodes required by an advanced Newton–Cotes formula.

In terms of numerical evaluation, the improper integral [Eq. (3.12)] needs to be truncated $\int_{-\infty}^{\infty} \mathrm{d}\omega \;\rightarrow\; \int_{\omega_{\min}}^{\omega_{\max}} \mathrm{d}\omega$. Using N nodes results in the node density $h_k = (\omega_{\max} - \omega_{\min})/N =: \Delta\omega$. Therefore, the stochastic process estimation based on the FFT algorithm reads

$$\eta_l := \eta_N(t_l) = \sqrt{\frac{\Delta\omega}{\pi}} e^{-\mathrm{i}t_l\omega_{\min}} \,\mathtt{FFT}\left(\sqrt{J(\omega_k)} Z_k\right) \tag{3.13}$$

with $\omega_k = \omega_{\min} + k\Delta\omega$. The non-vanishing second moment

$$\mathcal{M}(\eta_l \eta_{l'}^*) = \frac{\Delta\omega}{\pi} \sum_{k=0}^{N-1} J(\omega_k) e^{-\mathrm{i}\omega_k(t_l - t_{l'})} =: \alpha_{\mathrm{aprx}}(t_l - t_{l'}) \tag{3.14}$$

approximates the given correlation function $\alpha(\tau)$. For the time interval of interest $[0, T]$, the maximum absolute error

$$\epsilon_{\mathrm{intgr}} = \max_{0 \le \tau_l \le T} |\alpha_{\mathrm{aprx}}(\tau_l) - \alpha(\tau_l)| \tag{3.15}$$

represents the error due to the numerical integration using the FFT algorithm and, thus, can be made arbitrarily small for a suitable choice of $\omega_{\max}$, $\omega_{\min}$ and N. Note that for the FFT algorithm, the times t_l take the values $t_l = \frac{2\pi l}{\omega_{\max} - \omega_{\min}}$ with its largest value $t_{N/2} = \frac{\pi N}{\omega_{\max} - \omega_{\min}}$. Therefore, for a given N, the difference $\omega_{\max} - \omega_{\min}$ needs to be large enough to fulfill $t_{N/2} \ge T$. This imposes an additional condition on $\omega_{\max}$ and $\omega_{\min}$.

Furthermore, in order to provide a truly time-continuous stochastic process the time-discrete process η_l [Eq. (3.13)] needs to be interpolated. The error induced by

the interpolation can easily be obtained for any interpolation scheme which is linear in η_l

$$\eta_N(t) = S(\eta_0, \cdots \eta_{N/2}, t) = \sum_{l=0}^{N/2} a_l(t)\eta_l \ . \tag{3.16}$$

This is in particular true for cubic splines [SB02]. The functions a_l are in general non-linear in t and depend on the partition t_l of the interval $[0, T]$. Note that the linearity in η_l justifies the applicability of the interpolation scheme for complex data sets, too. For the interpolated stochastic process, the non-vanishing second moment reads

$$\mathcal{M}(\eta_N(t)\eta_N^*(s)) = \sum_{l=0}^{N/2}\sum_{l'=0}^{N/2} a_l(t)a_{l'}(s)\alpha_{\mathrm{aprx}}(t_l - t_{l'}) \tag{3.17}$$

which corresponds to the interpolation of the correlation kernel. Therefore, $\Delta t = 2\pi/(\omega_{\max} - \omega_{\min})$ needs to be small enough to assure that the interpolation error

$$\epsilon_{\mathrm{intpol}} = \max_{t,s\in[0,T]} \left| \sum_{l=0}^{N/2}\sum_{l'=0}^{N/2} a_l(t)a_{l'}(s)\alpha(t_l - t_{l'}) - \alpha(t-s) \right| \tag{3.18}$$

stays below a given threshold. Using the exact BCF instead of α_{aprx} is justified if $\epsilon_{\mathrm{intgr}}$ is smaller than $\epsilon_{\mathrm{intpol}}$. Controlling the error of the interpolation imposes yet another condition for a suitable choice of $\omega_{\max}$, $\omega_{\min}$ and N.

In summary, the accuracy of the numerical realization of a truly time-continuous stochastic process using the FFT algorithm in combination with cubic spline interpolation can be controlled. Given the effective SD $I(\omega)$ of the correlation function, the parameters $\omega_{\max}$, $\omega_{\min}$ and N can be determined such that two error criteria with given thresholds $\epsilon_{\mathrm{intgr}}$ and $\epsilon_{\mathrm{intpol}}$ are met. In that way it is assured that the error of the correlation function of $\eta_N(t)$ is in the vicinity of $\epsilon_{\mathrm{intgr}} + \epsilon_{\mathrm{intpol}}$ or smaller.

3.1.2.2 Tanh-Sinh Integration

The applicability of the FFT-based approach crucially depends on the convergence properties of the midpoint quadrature. For the case where the effective SD $I(\omega)$ corresponds to a physically meaningful SD ($J(\omega) = 0$ for $\omega \leq 0$ and cutoff above a particular cutoff frequency) the quadrature converges in the expected manner, i.e, $\mathcal{O}(\Delta\omega^2)$. However, if the BCF accounts for the influence of a thermal environment, this behavior can change. In particular, for the class of sub-Ohmic SDs, the effective SD diverges at $\omega = 0$ (see Sec. 3.4) which drastically worsens the convergence properties as shown in Fig. 3.5.

In order to efficiently treat effective SDs with such singularities, quadrature schemes with non-equidistant nodes can be used. The tanh-sinh (TS) scheme [Mor05] is particularly suited for that case and, hence, will be discussed in the context of sampling stochastic processes numerically.

In general, the convergence properties of a numerical quadrature scheme are enhanced if the integrand rapidly decays to zero at the integral boundaries. The TS method exploits this feature in the most optimal way [TM73] by applying a variable transformation which maps a definite integral, here from 0 to $\omega_{\max}$, to an indefinite integral with a doubly exponentially decaying asymptotic behavior for the integrand. The variable transformation $\omega \to y$ "stretches" the vicinity of the singularity at $\omega = 0$ to the real axis ($\lim_{y\to\infty} \omega(y) = 0$) such that the new effective integrand decays doubly exponentially, i.e.,

$$\begin{gathered} \omega(y) = \omega_{\max}(1 - \tanh(s(y))), \quad s(y) = \pi \sinh(y)/2 \quad \text{and} \\ \int_0^{\omega_{\max}} \mathrm{d}\omega\, I(\omega) e^{-\mathrm{i}\omega\tau} = \omega_{\max} \int_0^{\infty} \mathrm{d}y\, I(\omega(y)) e^{-\mathrm{i}\omega(y)\tau} \frac{\pi \cosh(y)}{2\cosh^2(s(y))} \,. \end{gathered} \tag{3.19}$$

In order to evaluate the integral using double precision floats, the truncation at $y = 4$ is generally sufficient. At that value the additional factor $\pi\cosh(y)/(2\cosh^2(s(y))) = |\mathrm{d}\omega/\mathrm{d}y|$ evaluates to $\approx 10^{-35}$. The remaining definite integral has the desired property of a fast decaying integrand in the vicinity of the integral boundaries and, thus, can be evaluated very accurately using the simple trapezoidal rule, i.e.,

$$\begin{aligned} \alpha(\tau) &\approx \frac{1}{\pi} \int_0^{\omega_{\max}} \mathrm{d}\omega\, I(\omega) e^{-\mathrm{i}\omega\tau} \\ &\approx \frac{\omega_{\max}}{\pi} \int_0^{4} \mathrm{d}y\, I(\omega(y)) e^{-\mathrm{i}\omega(y)\tau} \frac{\pi\cosh(y)}{2\cosh^2(s(y))} \approx \frac{1}{\pi} \sum_{k=0}^{N} h_k I(\omega_k) e^{-\mathrm{i}\omega_k\tau} \,, \end{aligned} \tag{3.20}$$

with

$$h_k = \frac{4\omega_{\max}}{N-1} \frac{\pi\cosh(y_k)}{2\cosh^2(s(y_k))}, \quad \omega_k = \omega(y_k) \quad \text{and} \quad y_k = \frac{4k}{N-1} \,. \tag{3.21}$$

Note that for the trapezoidal rule h_0 and h_N need to be weighted with an additional factor $1/2$. The derived expression [Eq. (3.20)] is of the general form of a discrete Fourier transform which approximates a given correlation function [Eq. (3.12)]. Therefore, the stochastic process $\eta_N(t) = \sum_{k=0}^{N-1} g_k Z_k e^{-\mathrm{i}\omega_k t}$ with $g_k = \sqrt{\frac{h_k I(\omega_k)}{\pi}}$ serves as a numerical estimate (see Eq. (3.11)). Its error is controlled by the integral truncation $\omega_{\max}$ and the number of nodes N and can be made arbitrarily small.

In contrast to the FFT approach, here the time t is still a continuous parameter. However, for reasons of efficiency it is advisable to specify a maximum interpolation tolerance which determines the grid size acceptable for a cubic spline interpolation,

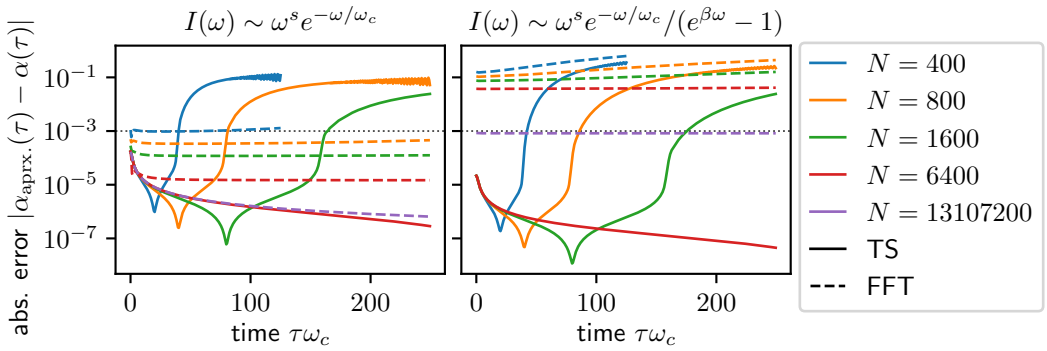

Fig. 3.5: The error resulting from the approximation of the correlation function $\alpha(\tau)$ by a discrete Fourier transform is shown for the FFT and the TS method. In both cases the indefinite integral is truncated at $10\omega_c$. As expected, increasing the number of nodes N used for the discretization results in a better approximation. Even though the TS method is more accurate for the zero-temperature SD (left panel), the error of the FFT method is still well acceptable. However, in case of a sub-Ohmic SD weighted with the thermal occupation number (right panel), the singularity at $\omega = 0$ causes a significant slow down of the convergence rate of the FFT method. Whereas the FFT methods requires more than 13 million nodes to reach an error of 10^{-3}, for the TS approach 6400 nodes are sufficient. Lowering s and/or β worsens the convergence of the FFT method. In contrast, for $s = 1$ the effective SD $I(\omega)$ remains finite at $\omega = 0$ for any β such that the difficulty disappears and the FFT method is still applicable (not shown). The parameters for the plots are $s = 0.5$ and $\beta\omega_c = 0.2$.

as for the FFT approach. When drawing a new sample of the stochastic process, $\eta_N(t)$ is evaluated for each grid point only once, enabling an efficient evaluation for any time within the interval $[0, T]$ by interpolation.

Notably, for $\tau = 0$ the integral approximation using the TS scheme is highly efficient in terms of the required number of nodes. As for the oscillatory behavior of the integrand, for larger τ the error of the TS quadrature increases drastically with τ. This problem, however, is inherent to all Fourier transform based approaches. It is sensible that the interval of a single period $2\pi/\tau$ requires at least some nodes within that interval. Although the node density is not necessarily constant, it does increase linearly with N. The resulting linear relation between the largest acceptable τ and the overall number of nodes N can be seen in Fig. 3.5, too.

To summarize, the Karhunen-Loève expansion and the discrete Fourier transform representation (FFT or TS integration) of the correlation function can be used to sample a time-continuous complex-valued Gaussian stochastic processes numerically. For all three approaches the error over a finite time interval can be made arbitrarily small. Nonetheless, the scope of application may be different for each method. The efficiency of the FFT algorithm qualifies the FFT approach for most purposes and allows for a very large time interval. However, in case of an effective SD with singular points, the poor convergence of the simple midpoint rule inherent to the

FFT algorithm might require the TS integration scheme instead. In contrast to the two Fourier transform based approaches, the Karhunen Loève expansion does not require the knowledge of the effective SD. The approach is solely based on the correlation function and ensures that the number of expansion terms and, with it, the number of complex-valued random variables, is optimal.

All three approaches yield numerical realizations for the stochastic process entering the HOPS method (Sec. 2.1.2). Their controllable accuracy is an important feature which allows us to claim that the HOPS formalism is exact up to numerical errors which, in turn, can be made arbitrarily small.

3.2 Exponential Representation for (Sub-) Ohmic Bath Correlation Functions

In order to employ the HOPS formalism for the widely used class of Ohmic and sub-Ohmic SDs to model the structure of the environment [Leg+87; BTV03; WT08; WT10; Mag+18], the algebraically decaying BCF needs to be accurately represented by as few as possible exponential terms. In this section, it will be shown that the zero-temperature BCF of such SDs, i.e., SDs with a power law behavior for small frequencies $\sim \omega^s$ and an exponential cutoff, can be represented well by a sum of exponential terms as required for the HOPS formalism (see Sec. 2.1.2). Since the BCF of such a SD decays algebraically, whereas any finite sum of exponential terms decays exponentially, it is not obvious that the exponential representation converges efficiently with respect to the number of terms used. Because other methods, like HEOM [Tan06; Tan14] or the non-equilibrium Green's function formalism [XDR02], rely on an exponential representation of the BCF, too, various possibilities to obtain the desired form have been reported (see Ref. [MT99; HXY10; RE14; Cui+19] for a small selection). They all have in common that the exponential form of the BCF is obtained indirectly by means of the SD. That is, the (zero-temperature) SD is expanded in terms of special kinds of functions. The resulting effective BCF if exactly of exponential form and, thus, serves as approximation of the actual BCF. Importantly, the number of relevant summands does not only depend on the particular SD but also on the temperature of the initial environmental Gibbs state by means of summing over Matsubara frequencies [Col15]. Low temperatures result in a large number of such terms which prevents a numerical application in that regime. Although recent developments improve on the numerical limits [Cui+19], zero temperature is not feasible in this approach.

It is the aim of the following to show that this limitation can be overcome by searching a suitable representation directly in the time domain [Har+19]. For the

real time propagation of the reduced state, which is the main purpose of the HOPS method, this approach is more reasonable. From the NMQSD equation (2.20) it follows that in order to propagate the reduced state over the time interval $[0, T]$, it is sufficient to know the BCF for that time interval only. Therefore, if the error of an approximation of the BCF can be made arbitrarily small for all $\tau \in [0, T]$, the error of the reduced dynamics becomes arbitrarily small, too, for that interval of time. Surely, the short (long) time behavior of the BCF is primarily determined by the large (small) frequency behavior of the SD. Nonetheless, the relation between the approximation of the SD (frequency domain) and the accuracy of the reduced dynamics (time domain) is not obvious. A detailed numerical study concerning this topic was carried out in a cooperation with Michael Werther and Frank Großmann, and can be found in Ref. [Har+19].

It turns out that finding a suitable representation for a given BCF $\alpha(\tau)$ in the time domain can be achieved by simply using standard minimization algorithms for the mean p-norm difference, i.e.,

$$d(G_\mu, W_\mu) := \frac{1}{M} \left(\sum_{i=1}^{M} \left| f(\tau_i) \Big(\alpha_{\mathrm{aprx}}(G_\mu, W_\mu, \tau_i) - \alpha(\tau_i) \Big) \right|^p \right)^{\frac{1}{p}} , \tag{3.22}$$

where the minimization is performed with respect to the complex valued parameters G_μ and W_μ of the exponential expansion, i.e.,

$$\alpha_{\mathrm{aprx}}(G_\mu, W_\mu, \tau) := \sum_{k=1}^{N} G_\mu e^{-W_\mu \tau} \quad \text{for} \quad \tau \geq 0 \, . \tag{3.23}$$

The discrete times τ_i, not necessarily equidistant, should cover the time interval $[0, T]$ of interest for the dynamics. An additional weight function $f(\tau)$ is included, for example, to distinguish between the absolute ($f(\tau) = 1$) and the relative difference ($f(\tau) = |\alpha(\tau)|^{-1}$). To rigorously quantify the error of the approximation, the maximum deviation

$$\epsilon := \max_{\tau \in [0,T]} \left| f(\tau) \Big(\alpha_{\mathrm{aprx}}(G_\mu, W_\mu, \tau) - \alpha(\tau) \Big) \right| \tag{3.24}$$

is used. Note, the maximum norm is disadvantageous for numerical minimization since it is not a smooth function of the parameters G_μ and W_μ. Thus, the smooth approximation in terms of the p-norm [Eq. (3.22)] is used where the limit $p \to \infty$ yields the maximum norm. However, choosing p too large results in a highly structured deviation surface $d(G_\mu, W_\mu)$ which is challenging for any minimization routine.

Since such minimization routines converge to a local minimum only, which by chance might be the global minimum, the minimization procedure has to be repeated with

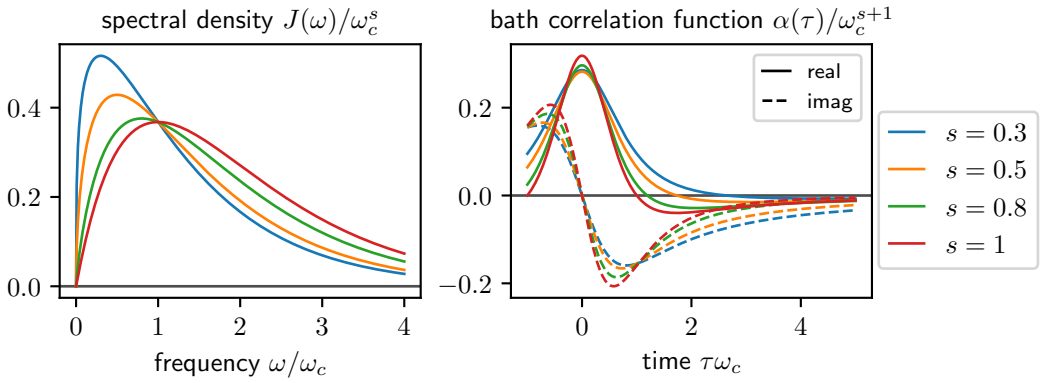

Fig. 3.6: As an overview for the class of sub-Ohmic and Ohmic environments, the SD and its corresponding BCF is shown for various parameters s. This parameter determines the low frequency power law of the SD, i.e., $J(\omega) \sim \omega^s$ and with that the long time behavior of the BCF which amounts to the algebraic decay $\alpha(\tau) \sim (1 + \mathrm{i}\omega_c\tau)^{-1-s}$.

different initial conditions. They are generated most efficiently using a quasi-random low-discrepancy sequence [Sob67; JK03; JK08]. In contrast to randomly chosen initial conditions such a deterministic sequence samples the parameter space "more uniformly". Significant speedup is easily achieved by executing the individual minimization processes on many computational units in parallel.

In the following, particular focus is given to the class of Ohmic ($s = 1$) and sub-Ohmic ($0 < s < 1$) SDs with exponential cutoff (see Fig. 3.6 for example plots), i.e.,

$$J(\omega) = \eta\omega^s e^{-\frac{\omega}{\omega_c}} , \tag{3.25}$$

where ω_c denotes the cutoff frequency and η the coupling strength. Note, in the literature the coupling strength is usually scaled with ω_c^{1-s} which assures that for any value of s the SD has the dimension of a frequency while the coupling strength is dimensionless [EW92; BTV03; WT10]. However, as already pointed out by Leggett et al. [Leg+87] the physically relevant quantity is the entire prefactor η which motivates the notation used here.

The power law behavior at low frequencies results in an algebraic decay of the BCF which, for the exponential cutoff, takes the simple expression

$$\alpha(\tau) = \frac{1}{\pi}\int_0^\infty \mathrm{d}\omega\, J(\omega)e^{-\mathrm{i}\omega\tau} = \frac{\eta}{\pi}\left(\frac{\omega_c}{1 + \mathrm{i}\omega_c\tau}\right)^{s+1}\Gamma(s+1) , \tag{3.26}$$

where Γ denotes the Gamma function. It is evident that the asymptotic behavior of this class of BCFs cannot be reproduced by a finite sum of exponential functions. However, for the finite time interval of the propagation the algebraic decay can indeed be mimicked with high precision by a finite exponential expansion. Following the algebraic decay for a longer time requires more expansion terms in order to

maintain a certain accuracy. In practice this limits the rigorous approach of following the algebraic decay over the entire time interval of the propagation. However, it can also be argued that if the maximum absolute error of the BCF approximation is small enough the effect on the dynamics will be small as well, independent of the propagation time. Of course, in each case, convergence of the reduced dynamics needs to be checked by successively lowering the error ϵ of the BCF approximation.

3.2.1 Numerical Details

The numerical effort of the minimization can be reduced by choosing the number of times τ_i (see Eq. (3.22)) as small as possible while still capturing the main features of the BCF. As shown in Fig. 3.7, distributing the times τ_i on a shifted logarithmic scale fulfills that requirement. From the probability density $p(\tau) \sim 1/(\tau + \tau_0)$ for $\tau \in [0, T]$, the shift parameter τ_0 is chosen such that the fraction $\tilde{u}$ of times τ_i is smaller than a given threshold $\tilde{\tau}$. This ensures that no matter how large the time interval $[0, T]$ is chosen, a fixed portion of times τ_i accounts for the initial behavior ($\tau < \tilde{\tau}$) of the BCF (see Fig. 3.7). For uniformly spaced parametric times $u_i \in [0, 1]$, the real times read

$$\tau_i = \tau_0 \left(e^{a u_i} - 1\right) \quad \text{with} \quad a = \ln\left(\frac{T + \tau_0}{\tau_0}\right) \tag{3.27}$$

where up to first order in $\tau_0/\tilde{\tau}$ the shift parameter can be determined as

$$\tau_0 = \frac{e^b}{1 + c e^b} \quad \text{with} \quad b = \frac{\tilde{u}\ln(T) - \ln(\tilde{\tau})}{\tilde{u} - 1} \quad \text{and} \quad c = \frac{\frac{1}{\tilde{\tau}} - \frac{\tilde{u}}{T}}{\tilde{u} - 1} \,. \tag{3.28}$$

Further it is sufficient to fit the specific BCF

$$\tilde{\alpha}(\tau) = (1 + \mathrm{i}\tau)^{-(s+1)} \approx \sum_{\mu=1}^{N} \tilde{G}_\mu e^{-\tilde{W}_\mu \tau} \,, \tag{3.29}$$

which depends on s only, and deduce the exponential representation of the general (sub-) Ohmic BCF [Eq. (3.26)], i.e.,

$$G_\mu = \frac{\eta}{\pi}\Gamma(s+1)\omega_c^{s+1}\tilde{G}_\mu \quad \text{and} \quad W_\mu = \omega_c \tilde{W}_\mu \quad . \tag{3.30}$$

It has turned out convenient to specify the time interval considered for the optimization $[0, T]$ by the order of magnitude of the decay of the BCF. In the following this quantity will be named *decay threshold* and denoted by D,

$$|\alpha(T)| = 10^{-\mathrm{D}} |\alpha(0)| \,. \tag{3.31}$$

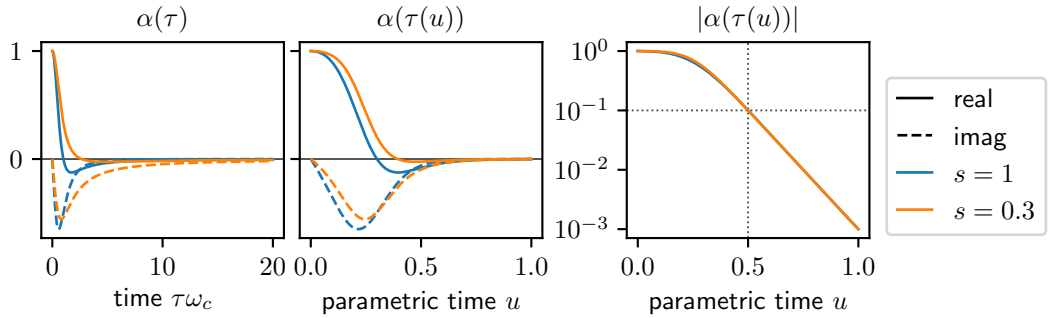

Fig. 3.7: The typical behavior of a (sub-) Ohmic BCF is shown, i.e., real and imaginary part reach a minimum smaller than zero followed by the algebraic decay such that $|\alpha(\tau)| \sim \tau^{-(s+1)}$ (see the left panel). To weight the important initial behavior while still capturing the algebraic decay over several orders of magnitude, the time points τ_i are distributed on a shifted logarithmic scale [Eq. (3.27)] and parameterized by $u \in [0, 1]$ (middle and right panel). The effect of the parametric time u is best seen by the logarithmic plots of the right panel. As an example, the decay is captured over three orders of magnitude, i.e., $|\alpha_s(T)|/|\alpha_s(0)| = 10^{-3}$. Due to the different values for s, this amounts to significantly different "real" time intervals $\omega_c T_{s=1} \approx 32$ and $\omega_c T_{s=0.3} \approx 203$. The threshold time $\tilde{\tau}$, which specifies what is considered as initial behavior, was also chosen in terms of the relative decay $|\alpha_s(\tilde{\tau})|/|\alpha_s(0)| = 0.1$ (horizontal dotted line). The weight for the initial behavior was set to $\tilde{u} = 0.5$ (vertical dotted line).

It can be argued crudely that for different BCF, fits with the same value D are comparable in terms of accuracy since they correctly account for the decay of the BCF up to a certain threshold.

When implementing the optimization numerically, we found that a representation of the complex parameters $\tilde{G}_\mu$, $\tilde{W}_\mu$ by polar coordinates with a logarithmic radial component is well suited,

$$\tilde{G}_\mu(x_{\mu,1}, x_{\mu,2}) = 10^{x_{\mu,1}} e^{\mathrm{i}x_{\mu,2}}, \qquad \tilde{W}_\mu(x_{\mu,3}, x_{\mu,4}) = 10^{x_{\mu,3}} e^{\mathrm{i}x_{\mu,4}} \,. \tag{3.32}$$

By means of standard minimization algorithms provided by scipy [Sci+20], a first estimate is obtained quickly by using the quasi-Newton method with Broyden-Fletcher-Goldfarb-Shanno (BFGS) algorithm. Its output serves as initial condition for the Sequential Least SQuares Programming (SLSQP) method polishing the result. The initial conditions for the phases can be confined to $-\pi < x_{\mu,2} \leq \pi$ and $0 < x_{\mu,4} \leq \pi$ since a decaying BCF requires a positive valued real part for each $\tilde{W}_\mu$. The bounds for the radial magnitudes are not as obvious. Highly accurate fits with an absolute error of $\sim 10^{-4}$ have been obtained by choosing initial values such that $-5 \leq x_{\mu,1} \leq 0$ and $-4 \leq x_{\mu,3} \leq 1$. Reaching for an even better accuracy might require a smaller value for the lower bound.

As an example, the plots in Fig. 3.8 show that increasing the number of summands N in Eq. (3.23) allows for a representation of the BCF with smaller relative error.

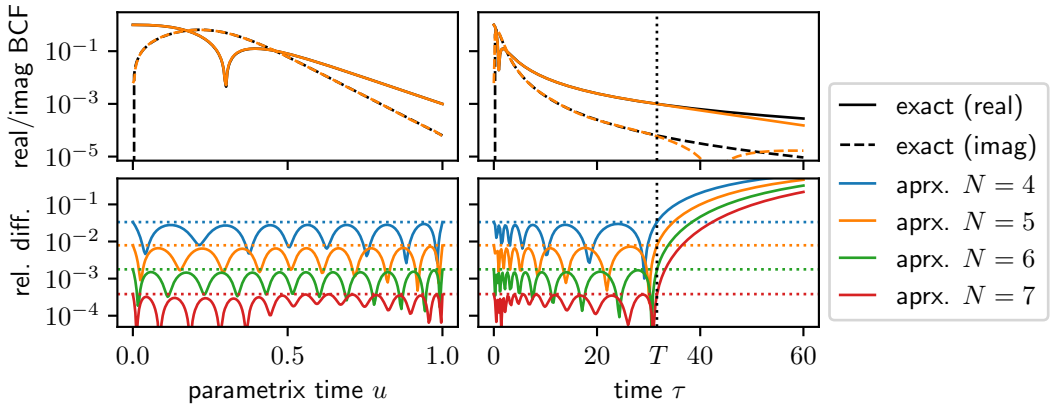

Fig. 3.8: For an Ohmic SD ($s = 1$) various approximations of the BCF in terms of a multi-exponential representation are shown. As weight function $f(\tau) = |\alpha(\tau)|^{-1}$ was chosen which results in an evenly distributed relative error (lower left panel). The decay threshold of 3 used here sets the time interval of interest to $[0, T \approx 32/\omega_c]$. As shown, increasing the number of summands N decreases the maximum relative error ϵ and, thus, results in an approximation with higher accuracy for the time interval $[0, T]$. For times $\tau > T$ the exponential decay of the approximation becomes evident and is reflected in the drastic increase of the relative error (lower right panel).

Evidently, the algebraic decay is reproduced with increasing precision over the entire relevant time interval. As showcase, $\mathrm{D} = 3$ was chosen, which means that the algebraic decay is mimicked with high accuracy over three orders of magnitude. For $\tau > T(\mathrm{D})$ deviations from the algebraic decay become visible on the semi-log plot of the BCF and result in an apparent increase of the relative error.

If the accuracy is quantified by the maximum absolute error ($f(\tau) = 1$) the situation changes slightly. Since the exponential approximation as well as the exact algebraic BCF approach zero asymptotically, their absolute difference tends to zero, too. This allows us to obtain fits where the maximum absolute error is bound for all $\tau \geq 0$. As convention for the following, the maximum error ϵ of a fit obtained by minimizing the absolute difference always refers to the maximum error for all times. Consequently, if the maximum absolute error can be decreased, the approximation follows the algebraic decay for a longer time, too.

As a remark, significant speed up for the global search of the minimum relative error is achieved by using initial guesses based on extrapolating known fit data. Based on heuristic investigation, the error of the optimal fit decreases exponentially with N (see left panel of Fig. 3.10). For such "optimal" fits, most of the parameters $\tilde{G}_\mu$ and $\tilde{W}_\mu$ follow a simple pattern when increasing N as shown in Fig. 3.9. Sampling a few hundred initial guesses only in the vicinity of the extrapolated pattern usually yields a fit where the error follows the heuristically found exponential behavior $\log \epsilon_N \sim -N$. In contrast, when minimizing the absolute difference the parameters of the best fits found do not follows such a simple pattern. Although the error

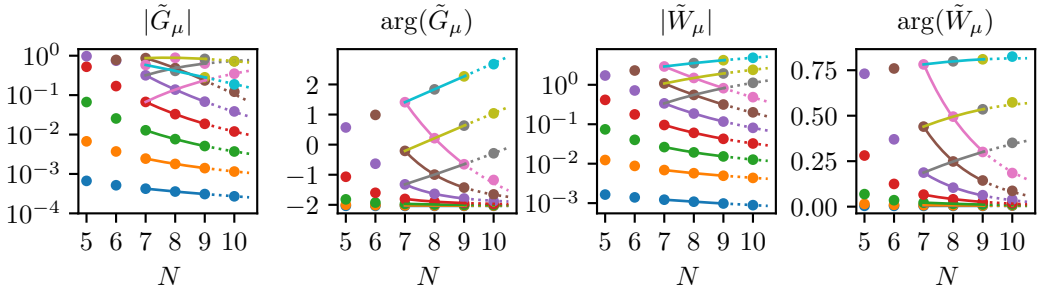

Fig. 3.9: The "optimal" parameters $\tilde{G}_\mu$ and $\tilde{W}_\mu$ for the multi-exponential representation of the sub-Ohmic BCF ($s = 0.3$) minimizing the relative difference over 4 orders of decay ($\mathrm{D} = 4$) are shown. The striking pattern can be used to generate promising initial guesses for the minimization. As example, the fits with $N = 6, 7, 8$ where used for extrapolation (dotted lines). The dots at $N = 9$ correspond to the optimal fit for which the error follows an exponential behavior $\log \epsilon_N \sim -N$.

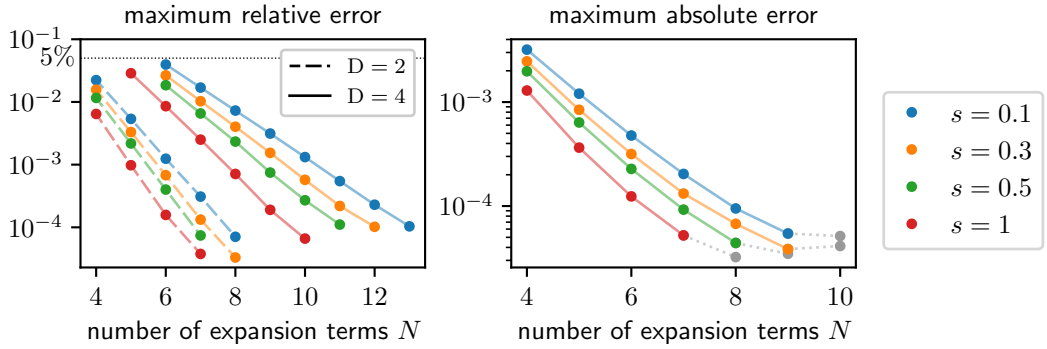

Fig. 3.10: For the multi-exponential representation the dependence of the maximum error on the number of expansion terms N is shown. Whereas for the minimization of the relative error (left panel), the time interval is implied by the decay threshold D, it was chosen self-consistently for the absolute error to assure that the error is bound for all times $\tau \in [0, \infty]$. The plot suggests a remarkable (nearly) exponential convergence up to a certain value of N. For larger N (gray dots) it is not clear if this behavior truly changes or if the corresponding better fit was not found yet. See App. C for explicit values of the fits.

of the fits generated using the same technique decreases with N, the brute force approach has returned better fits breaking the pattern. Further details have not been investigated since the accuracy of the known fits is sufficient for many applications, in particular those discussed in Ch. 4 and Ch. 5.

The error of the currently best known fits (relative and absolute) is shown in Fig. 3.10 for various parameters s of the SD. With less than $N = 12$ summands, a relative error of 10^{-3} can be reached while following the algebraic decay over up to $\mathrm{D} = 4$ orders of magnitude. Concerning the absolute fits, the error quickly drops below 10^{-3} and reaches 10^{-4}. This reveals that remarkably accurate exponential representations of the (sub-) Ohmic BCF are possible with less than a dozen terms. For the fits shown in Fig. 3.10 the fit data is provided in App. C.

Further increasing the number of summands N has led to only minor or even no improvements of the accuracy. This might be due to the increasing complexity of the global minimum search. However, finding even more accurate representations could become relevant in case of very strong system-environment interactions. Investigating more efficient algorithms and exploring the scaling properties of the error is left for future work.

3.3 Truncation of the Hierarchy

Another prerequisite to solve the HOPS numerically is the truncation of the infinite set of hierarchically structured differential equations, linear [Eq. (2.30)] or non-linear [Eq. (2.51) and Eq. (2.52)].

Analytic arguments to justify a truncation can be found for a discrete environment (see Sec. 2.3.3). In that case, it was shown that the auxiliary states can be related to the Fock-states of the finite set of modes [Eq. (2.93)]. For example, in case of a single mode, an auxiliary state of level l contains contributions with Fock-states $n \geq l$ only, i.e., $\psi^l = \sum_{n=l}^{\infty} c_n^l \langle n|\Psi\rangle$. Consequently, if the Hilbert space of the harmonic oscillator can be truncated at $l_{\max}$, that is, setting $\langle n|\Psi\rangle = 0$ for all $n > l_{\max}$ serves as a suitable approximation, auxiliary states with $l > l_{\max}$ can be neglected too since they do not contribute to the reduced state, by means of the same degree of approximation. Thus, the set of differential equations, the HOPS, becomes finite. Increasing the truncation level $l_{\max}$ will increase the accuracy of the reduced state. Note that since the random variable z^* is not bound, the coefficients $c_n^l \sim (z^*)^n \sqrt{(n+l)!}/n!$ can become arbitrarily large. This means that it is not guaranteed that ψ^l is indeed close to zero, even though $\langle n|\Psi\rangle \approx 0$ holds for all $n \geq l$. This hints to the general observation, discussed in the following, that simply considering the norm of the auxiliary states does not justify the truncation.

For the more relevant case of a truly continuous SD, the physically motivated argument from above justifying the truncation is not obvious. This holds true particularly for (sub-) Ohmic environments, where the exponential representation of the exact BCF (see Sec. 3.2) has a purely mathematical motivation. As a consequence, the physical interpretation of the auxiliary states is unclear. Nonetheless, the mathematical structure of the HOPS [Eq. (2.30)] indicates that high level auxiliary states have only a minor influence on the zeroth level, i.e., the stochastic pure state. The rough argument is that since $\partial_t \psi^{\mathbf{k}} \sim -\sum_\mu k_\mu W_\mu \psi^{\mathbf{k}}$, the rate of change for the intrinsic evolution increases with the hierarchy level $l = \sum_\mu k_\mu$. This can either mean a quick decay scaled by the real part of W_μ, which is always positive, or a fast oscillation

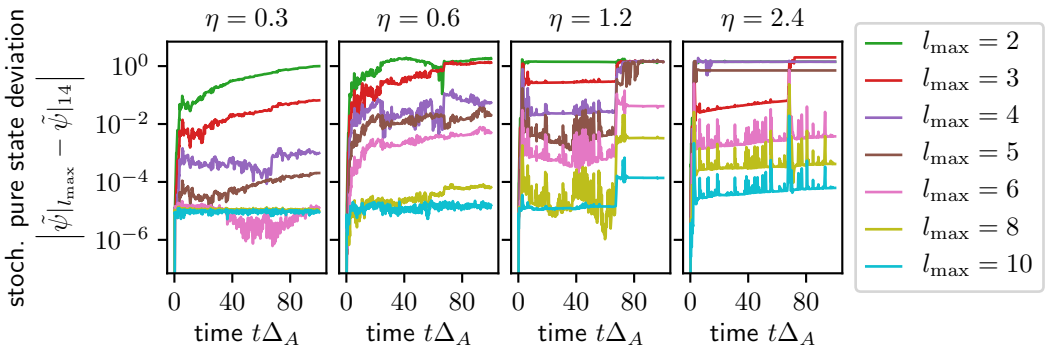

Fig. 3.11: The deviation of the normalized stochastic pure state $\tilde{\psi}|_{l_{\max}}$ from a reference calculation with $l_{\mathrm{ref}} = 14$ is shown for various truncation levels $l_{\max}$. The coupling strength η is increased from left to right. For each η, the deviation of $\tilde{\psi}$ becomes small for a sufficiently large $l_{\max}$. The shown graphs where obtained when solving the two-spin-boson model $H_{\mathrm{sys}} = -\Delta_A/2\sigma_x^A - \Delta_B/2\sigma_x^B$, $\Delta_B = 0.8\Delta_A$, $L = -1/2(\sigma_z^A + \sigma_z^B)$ with an Ohmic SD $J(\omega) = \eta\omega e^{-\omega/\omega_c}$, $\omega_c = 10\Delta_A$.

due to the imaginary part of W_μ. In either case, it is expected that the effect on the significantly slower dynamics of the zeroth level is small.

The following numerical investigation on the truncation of the HOPS confirms this vague line of reasoning. As an example, Fig. 3.11 shows the convergence of the stochastic pure state with respect to the truncation for the generic model of two qubits coupled in a spin-boson like manner to an Ohmic environment (see Sec. 5 for details of the model) where an expansion of the BCF with 4 terms was used. For reasons of simplicity, the so-called simplex truncation scheme is used which includes all auxiliary states with level $l \leq l_{\max}$ for a given truncation level $l_{\max}$. Note that since the non-linear variant of the HOPS is the numerical method of choice (see, e.g. Ref. [deV+05; HS17] and Sec. 4.5), it is referred to exclusively by the following examples. The effect of the truncation is analyzed by propagating the HOPS for a *fixed* stochastic process $\eta^*(t)$ while varying the truncation level $l_{\max}$. The deviation of the normalized stochastic pure state $\tilde{\psi}|_{l_{\max}} := \psi/|\psi|$, obtained when truncating at $l_{\max}$, from its correspondent using a suitably larger reference truncation at l_{ref}, i.e., $\left|\tilde{\psi}|_{l_{\max}} - \tilde{\psi}|_{l_{\mathrm{ref}}}\right|$, is used to examine the convergence.

It is shown in Fig. 3.11 that for a suitably large truncation level $l_{\max}$ the deviation becomes small. This justifies the use of the HOPS to calculate the stochastic pure state as being a solution of the NMQSD equation. In agreement with the case of a finite set of environmental modes (see Sec. 2.3.3), increasing the coupling strength requires a larger truncation level in order to maintain a certain degree of accuracy. It is worth noting that the deviation does not necessarily decrease monotonically with the truncation level. This behavior is often observed in the strong coupling regime where the norm of the stochastic pure state grows fast. Further, it is important to note that the ”population“ of the auxiliary states is hardly influenced by the coupling

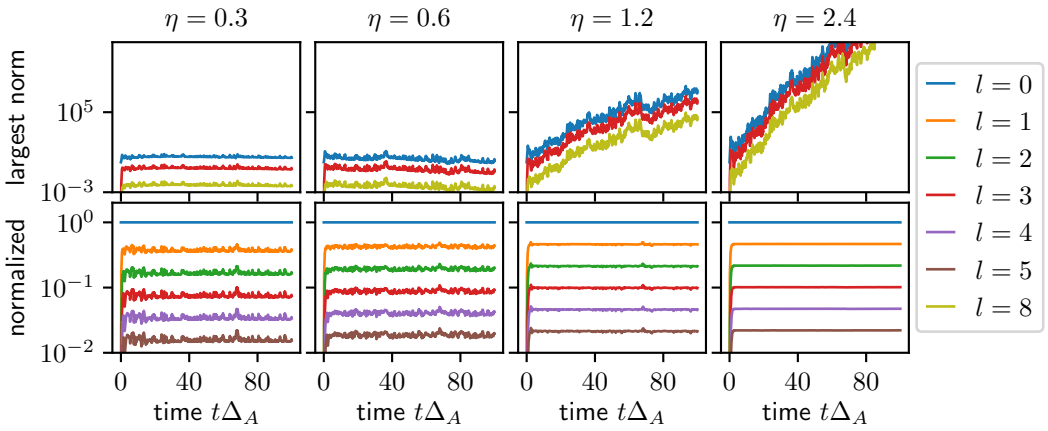

Fig. 3.12: In the upper row, the norm of the stochastic pure state $|\psi|$ (blue lines, $l = 0$, non-linear HOPS, not normalized) is shown. For large coupling strengths η, the norm grows rapidly. In addition, the largest norm of all auxiliary states within a given tire l of the hierarchy, $\max_{\mathbf{k}:l(\mathbf{k})=l}|\psi^{\mathbf{k}}|$, is shown with the aim to represent the "population" for each tire. For a better comparison, the lower row shows the largest norm of each tire scaled by $|\psi|^{-1}$. Thus, the lower row refers to the *normalized stochastic pure state* and the corresponding auxiliary states. The plot reveals that the "population" decreases with each hierarchy level l. However, the particular values are hardly influenced by the coupling strength and, thus, cannot be used as an indicator for the truncation of the HOPS. The same model parameters as in Fig. 3.11 were used.

strength (see Fig. 3.12). This leads, again, to the conclusion that the norm of the auxiliary states at different hierarchy levels cannot be used to deduce information for a suitable truncation. Note that since the norm of the full state vector of the hierarchy $|\Phi| = |(\tilde{\psi}, \ldots, \tilde{\psi}^{\mathbf{k}}, \ldots)|$ is not conserved, the term "population" must not be understood in the sense of a probability.

So far the convergence of the normalized stochastic pure state with respect to the truncation of the HOPS has been examined for a single realization. In general, the truncation level required to achieve a certain degree of accuracy might depend on the particular stochastic process. Therefore, for applications concerning the reduced dynamics, it is more convenient to base the truncation check on the reduced state rather than a single stochastic pure state. It seems sensible that using a few realizations only is sufficient to estimate a suitable truncation level.

A reduction of the number of auxiliary states and, with that, of the numerical cost may be achieved by refining the truncation scheme. For the fundamental discussion above it was sufficient to use the most simple simplex scheme which treats each index k_λ of the index vector $\mathbf{k} = (k_1, \ldots k_N)$ equally. The truncation condition, that only auxiliary states with a hierarchy level smaller or equal to a truncation level $l_{\max}$ are taken into account corresponds to the simplex condition $l(\mathbf{k}) = \sum_{\mu=1}^{N} k_\mu \leq l_{\max}$. The

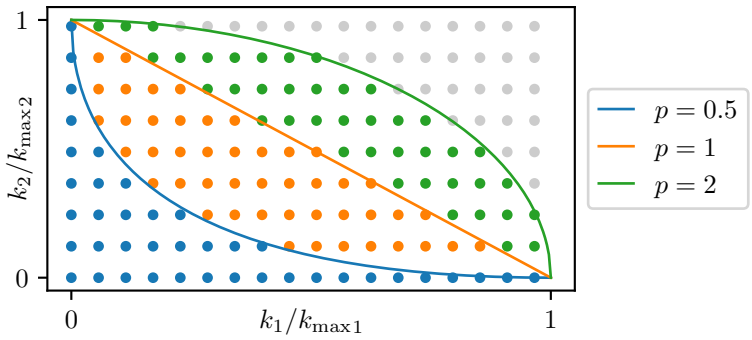

Fig. 3.13: The plot visualizes the generalized truncation scheme given in Eq. (3.33) in 2 dimension with exemplary values $k_{\max 1} = 17.6$ and $k_{\max 2} = 8.2$.

following expression has turned out to be a useful generalization of the truncation condition

$$\sum_{\mu=1}^{N} \left(\frac{k_\mu}{k_{\max \mu}} \right)^p \leq 1 \, . \tag{3.33}$$

The power p generalizes the simplex structure where $p < 1$ allows for auxiliary states with higher level on the index axes $\mathbf{e}_\mu$ compared to states "between" the axes. For $p > 1$ the opposite holds true. For $p = 1$ the simplex structure is recovered. The *truncation vector* $\mathbf{k}_{\max}$ allows to weight each index separately (see also Fig. 3.13 for visualization).

It seem plausible that the optimal choice of $\mathbf{k}_{\max}$ is related to the structure of the hierarchy [Eq. (2.30) or Eq. (2.51)] determined by the parameters G_μ, specifying the "coupling" between different auxiliary states $\dot{\psi}^{\mathbf{k}} \sim \sum_\mu G_\mu \psi^{\mathbf{k}+\mathbf{e}_\mu}$, and W_μ, determining the internal damping and/or oscillatory dynamics $\dot{\psi}^{\mathbf{k}} \sim -\sum_\mu k_\mu W_\mu \psi^{\mathbf{k}}$. Therefore, the truncation vector component $k_{\max_\mu}$ should increase with $|G_\mu|$ but decrease with $|W_\mu|$ which is accounted for most simply by setting $k_{\max_\mu} \sim (|G_\mu|/|W_\mu|)^q$. The requirement for a unitless component $k_{\max_\mu}$ also suggests the so-called "square root" truncation vector $k_{\max_\mu} \sim \left(\sqrt{|G_\mu|}/|W_\mu| \right)^q$. The exponent q has been introduced as an additional parameter which weights the asymmetry between the axes.

The following aim is to tune the parameters p and q for the class of sub-Ohmic and Ohmic SDs. To quantify the quality of the truncation scheme the convergence rate of the reduced state with respect to the number of auxiliary states is used. This convergence rate is estimated using the maximum deviation of the reduced state from a reference calculation involving significantly more auxiliary states over a suitably large time interval, i.e.,

$$d := \max_{t \in [0,T]} |\rho_{N_{\text{aux}}}(t) - \rho_{\text{ref}}(t)| \, . \tag{3.34}$$

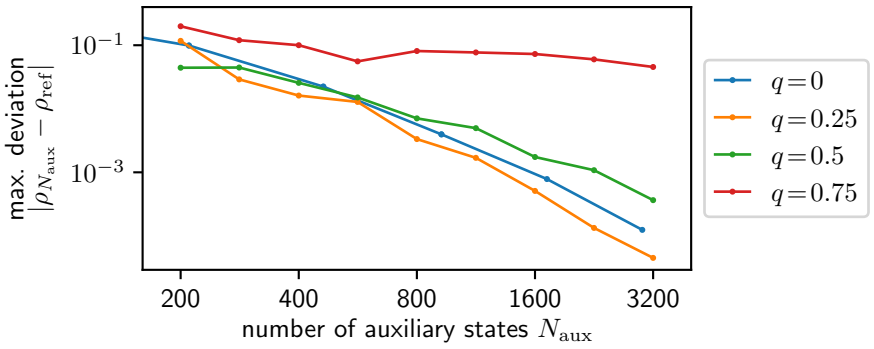

Fig. 3.14: The maximum deviation of the reduced state is shown using 16 samples. The deviation decreases with the number of auxiliary states which signifies convergence of the reduced state. The rate of convergence depends on the truncation scheme, here modified in terms of q. The Hilbert-Schmidt norm was used as matrix norm for $|\rho_{N_{\mathrm{aux}}}(t) - \rho_{\mathrm{ref}}(t)|$.

The Hilbert-Schmidt norm is used as matrix norm. Since the deviation, and not the reduced state itself, is the quantify of interest, a small number of realizations yields a good estimate already. To compare different truncation schemes, the calculations are done for a *fixed* ensemble of stochastic processes (see Fig. 3.14 for an example).

A detailed examination of the influence of the generalized truncation scheme on the convergence of the reduced state is shown in Fig. 3.15. The same relations as in the previous Fig. 3.14 are plotted, however, for a large variety of truncation schemes. The graphs suggest that $q \approx 0.5$ yields the most rapid convergence. Conveniently, this holds for various coupling strength and the sub-Ohmic as well as the Ohmic case.

Based on that, Fig. 3.16 shows all graphs with $q = 0.5$ in one plot. It is evident that the square root scaling $k_{\max_\mu} \sim \left(\sqrt{|G_\mu|/|W_\mu|}\right)^q$ is highly favorable. Further, the convergence rate does not depend significantly on the parameter p for $1 \lesssim p \lesssim 1.5$. A small difference between the various values of p becomes visible for the larger value of the coupling strength, i.e., $\eta = 1.2\Delta^{1-s}$. In that case the plots suggest that the optimal choice of p might also depend on the particular value of s. It should be noted that the coupling strengths used for investigating the convergence rate are very strong with respect to weak coupling perturbative regime. Thus, in order to examine non-trivial dynamics far beyond the weak coupling regime we use $p = 1$. When increasing the coupling strength much further, a more detailed investigation on the truncation parameter p might become relevant.

In addition (not shown), the convergence rate was examined when using the real part of W_μ instead of its absolute value $|W_\mu|$ to define the truncation vector, i.e., $k_{\max_\mu} \sim \left(\sqrt{|G_\mu|/\mathrm{Re}(W_\mu)}\right)^q$. Whereas in the Ohmic case a slight advantage of this truncation scheme becomes evident, the opposite holds true in case of a sub-Ohmic

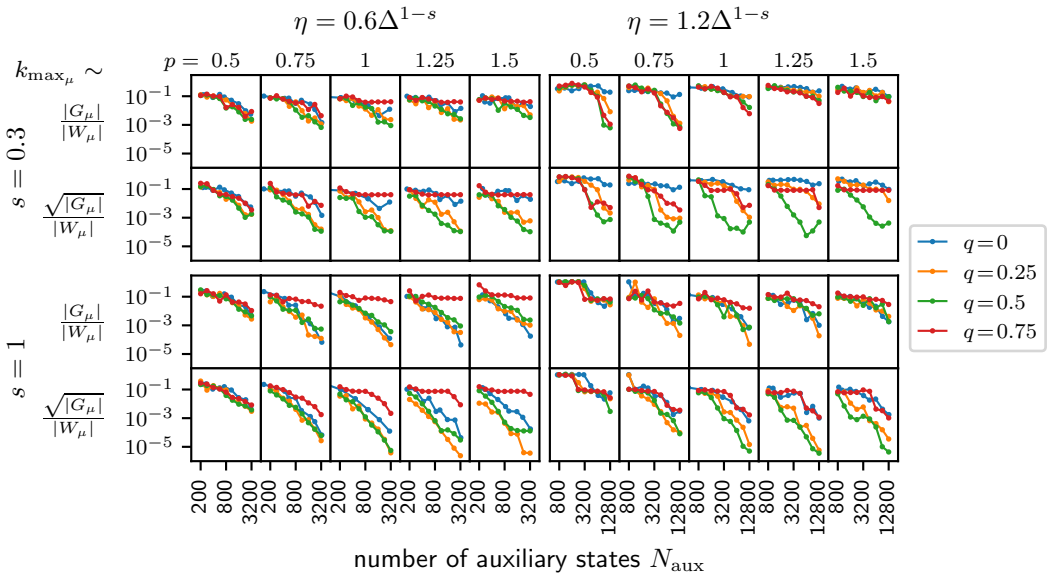

Fig. 3.15: The convergence of the reduced state is shown by means of the maximum deviation d. We distinguish between the sub-Ohmic ($s = 0.3$, upper two rows) and the Ohmic case (lower two rows) as well as two different coupling strengths η (left and right blocks). The plots reveal the influence of q (colors), p (columns) and the truncation vector $\mathbf{k}_{\max}$ (rows in each block), see Eq. (3.33), on the convergence rate. For nearly all cases shown, $q \approx 0.5$ yields the fastest convergence. Also, choosing the square root truncation seems highly beneficial. As reference truncation $q = 0.5$, $p = 1$ and $k_{\max_\mu} \sim (\sqrt{|G_\mu|}/|W_\mu|)^q$ was used with $N_{\text{ref}} = 25600$ auxiliary states for $\eta = 0.6\Delta^{1-s}$ and $N_{\text{ref}} = 102400$ for $\eta = 1.2\Delta^{1-s}$. A fit with 6 exponential terms minimizing the absolute difference was used (see App. C). Two qubits serve as exemplary model with $H_{\text{sys}} = -\Delta/2(\sigma_x^A + 0.8\sigma_x^B)$, $L = -1/2(\sigma_z^A + \sigma_z^B)$, a (sub-) Ohmic environment ($\omega_c = 10\Delta$) at zero temperature and a propagation up to $t\Delta = 100$.

SD with $s = 0.3$. Therefore this scheme is not used for the applications of the HOPS discussed in Ch. 4 and Ch. 5.

A final remark is devoted to so-called n-mode approximation [ZBE18] which provides an additional scheme to reduce the number of auxiliary states. The idea is that only n out of N modes are allowed to be excited simultaneously which has been shown useful for investigating molecular aggregates [ZBE18]. The n-mode approximation corresponds to the condition that the index vector $\mathbf{k}$ must consist of at most n out of N non-zero indices. However, as shown in Fig. 3.17, for spin systems strongly coupled to a (sub-) Ohmic environment, as considered in Ch. 4 and Ch. 5, the n-mode approximation does not provide an advantage.

To conclude, the numerical results gathered for sub-Ohmic and Ohmic SD confirms that the zeroth order hierarchy state, i.e., the sought after stochastic pure state, converges with respect to the number of auxiliary states when solving the truncated HOPS. Consequently, the numerical error induced by truncation method can be made arbitrarily small which qualifies the HOPS methods to be exact. Referring

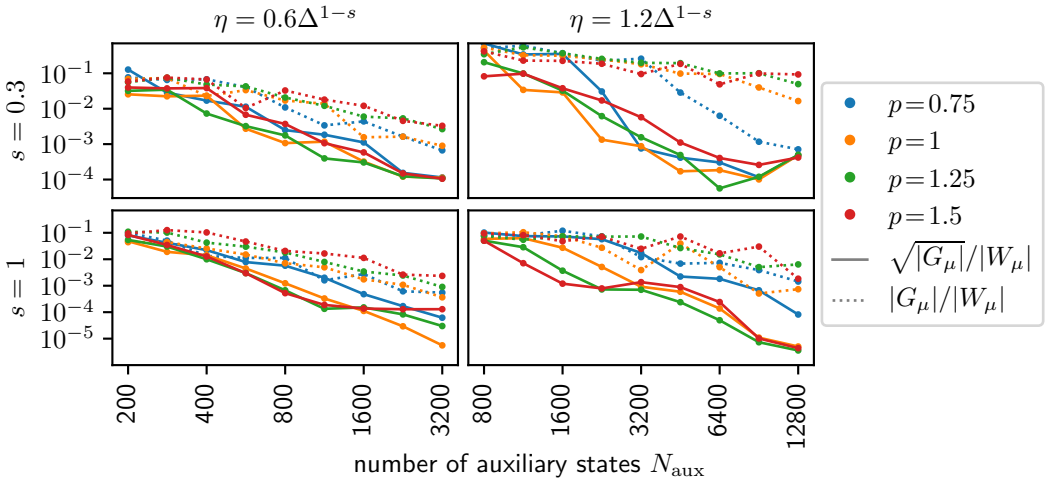

Fig. 3.16: The convergence of the reduced state is shown by means of the maximum deviation d as in Fig. 3.15. Here, however, the parameter $q = 0.5$ is held constant to compare the influence of the other parameters of the truncation scheme on the convergence rate. Most obvious, using the square root truncation is highly favorable. On a rough scale the dependence on p is minor. Thus, for the applications of the HOPS in Ch. 4 and Ch. 5 we use $p = 1$. Reliably identifying the best choice will require a more thorough investigation which is, however, not necessary here.

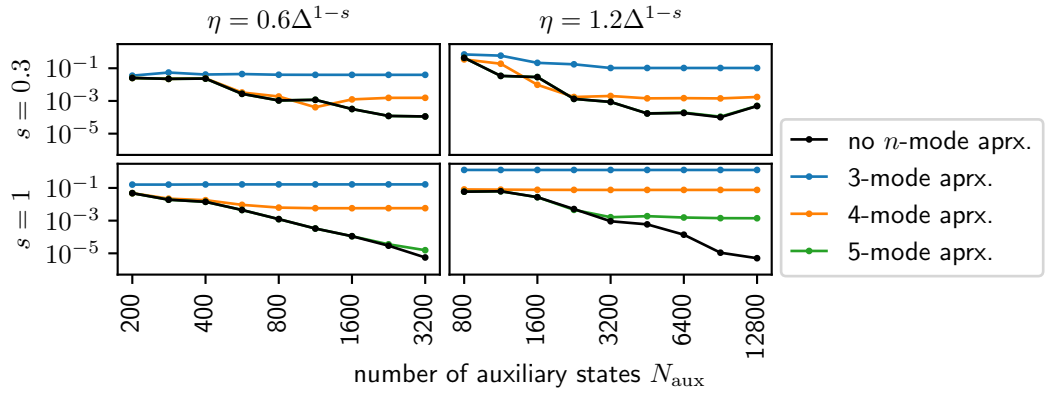

Fig. 3.17: The effect of the n-mode approximation for the hierarchy truncation on the convergence rate is shown. Here, the n-mode approximation is applied in addition to the truncation scheme with $q = 0.5$, $p = 1$ and the "square root" truncation vector (see Fig. 3.15 and Fig. 3.16). The graphs show that the n-mode approximation does not enhance the converge properties. Two qubits where use as generic example with the model parameters as in Fig. 3.15.

to the class of sub-Ohmic and Ohmic SDs, using the specialized truncation scheme [Eq. (3.33)] with the "square root" truncation vector $k_{\max_\mu} \sim \left(\sqrt{|G_\mu|}/|W_\mu|\right)^q$ and parameters $p = 1$, and $q = 0.5$, yields the fastest convergence for a wide range of coupling strengths. If not mentioned differently, this particular truncation scheme is used as standard for the calculations presented in the following chapters.

3.4 Non-Zero Temperature

The derivation of the NMQSD Equation (2.20) (Sec. 2.1.1) and, therefore, the HOPS formalism, too, requires an initial product state of the form $|\Psi\rangle = |\psi\rangle_{\mathrm{sys}} \otimes |\mathbf{0}\rangle_{\mathrm{env}}$ where $|\psi\rangle_{\mathrm{sys}}$ denotes an arbitrary state of the system Hilbert space and $|\mathbf{0}\rangle_{\mathrm{env}}$ the multi-mode ground state. Thus, the environmental initial condition is that of a canonical ensemble at zero temperature. So far, two approaches have been developed to treat an initial canonical ensemble at non-zero temperature. Both have in common that they map the $T > 0$ case to an effective $T = 0$ scenario where the original formalism is applicable. In particular, for a Hermitian coupling operator, i.e., $L = L^\dagger$, the thermo field (TF) method [SU83; TU96] yields the same NMQSD equation as for zero temperature, however, with the BCF $\alpha(\tau)$ simply taking the form of the thermal BCF $\alpha(\beta, \tau)$ [Eq. (2.72)] [DGS98]. The stochastic potential (SP) approach, introduced in Sec. 2.2.2, mimics the influence of non-zero temperature by an additional stochastic Hermitian contribution to the system Hamiltonian. Both approaches are exact. However, in terms of numerical applicability the SP method is highly favorable. As shown in 3.18, the convergence of the reduced state with respect to the number of auxiliary states is significantly faster compared to the TF method. As an example, whereas the for the SP approach the difference of the $\langle\sigma_z\rangle$ dynamics using 128 and 265 auxiliary states can hardly be distinguished, the TF method, using 1024 auxiliary states, results in an evolution which significantly deviates after a certain time. Note, in contrast to the previous investigation concerning the truncation scheme (Sec. 3.3), here the convergence of the reduced state cannot be based on a few realizations only since the noise processes are different. Instead, 2^{18} samples were used to ensure that the stochastic uncertainty is below the deviation between the reduces dynamics obtained using different truncation criterion.

To draw contact to earlier results presented in Ref. [HS17], the dynamics using the TF method in combination with the most simple simplex truncation ($p = 1$, $q = 0$) are shown as well (dotted lines in Fig. 3.18). The obvious difference emphasizes the advantage of a suitable truncation scheme, again.

The disadvantage of the TF approach in combination with the HOPS can be traced back to the increased real part of the thermal BCF compared to its zero-temperature equivalent (see Fig. 3.19) as seen by the particular form of the thermal BCF given in Eq. (2.72). Explicit expressions of the (sub-) Ohmic BCFs can be found in App. B. Since the magnitude of the thermal BCF is reflected by the magnitude of parameters G_μ of its exponential representation, increasing temperature effectively increases the coupling strength between the auxiliary states. This in turn requires more auxiliary states to reach a sufficiently degree of convergence and explains the behavior observed in Fig. 3.18.

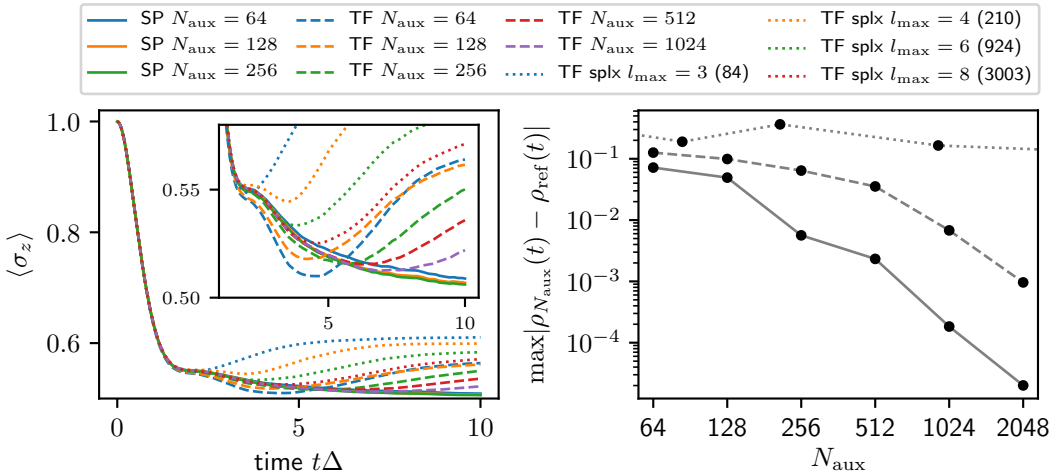

Fig. 3.18: Focusing on the two different approaches (stochastic potential (SP) and thermo field (TF)) to incorporate a thermal initial environmental, the convergence is shown (similar to Fig 3.15). The striking difference is visible for the dynamics of $\langle \sigma_z \rangle$ (left panel) and quantified by the maximum deviation of the reduced state (right panel). The SP approach (solid lines) requires significantly less auxiliary states for an acceptable accuracy. The dynamics obtained using the TF method (dashed lines) agrees with the converged result up to a certain time before it starts to deviate. Increasing the number of auxiliary states increases that time, eventually agreeing with the converged dynamics. Note that in addition to the advanced truncation scheme (Sec. 3.3), for the TF method results using the simplex truncation (TF splx) are shown, too (dotted lines). This emphasizes again the advantage of the advanced truncation, here applied on an exponential representation for the thermal BCF. The spin-boson model with a sub-Ohmic environment is used a generic example ($H_{\mathrm{sys}} = \Delta\sigma_x$, $L = \sigma_z$, $\eta = 0.745\Delta^{1-s}$, $s = 0.5$, $\omega_c = 10\Delta$, $T = \Delta$, $N_{\mathrm{BCF}} = 6$, 2^{18} samples).

Note that the noise generation for the TF approach, such that $\mathcal{M}(\eta(t)\eta^*(s)) = \alpha(\beta, t-s)$ with $\beta = 1/T$, is challenging for sub-Ohmic SD using the Fourier transform method (Sec. 3.1.2), although the thermal BCF [Eq. (2.72)] can in be written as the Fourier transform of an effective thermal SD $J(\beta, \omega)$ including negative frequencies,

$$\begin{aligned} \alpha(\beta,\tau) &:= \int_0^\infty \mathrm{d}\omega\, \frac{J(\omega)}{\pi} \left(\coth(\beta\omega/2)\cos(\omega\tau) - \mathrm{i}\sin(\omega\tau)\right) \\ &\equiv \int_{-\infty}^\infty \mathrm{d}\omega\, \frac{J(\beta,\omega)}{\pi} e^{-\mathrm{i}\omega\tau} \quad \text{with} \quad J(\beta,\omega) := \frac{J(\omega)}{1-e^{-\beta\omega}} \,. \end{aligned} \tag{3.35}$$

Here, the microscopic SD $J(\omega)$ is extended to negative frequencies by $J(\omega) := \mathrm{sig}(\omega)J(|\omega|)$ and $\bar{n}$ denotes the Bose-Einstein distribution. As discussed in Sec. 3.1, the divergence of $J(\beta,\omega) \sim |\omega|^{s-1}$ for $s < 1$ at $\omega = 0$ (see also Fig. 3.19) results in very poor convergence of the midpoint rule implied by the FFT method (Sec. 3.1.2.1). Although, an extension of the tanh-sinh (TS) scheme (Sec. 3.1.2.2) treating positive and negative frequencies separately is feasible, the example shown in Fig. 3.18 makes use of the Karhunen-Loève approach (Sec. 3.1.1) which is based on the BCF only. We note this here, because all calculation shown in the following chapters use either of the Fourier Transform method, FFT or TS, since they allow for

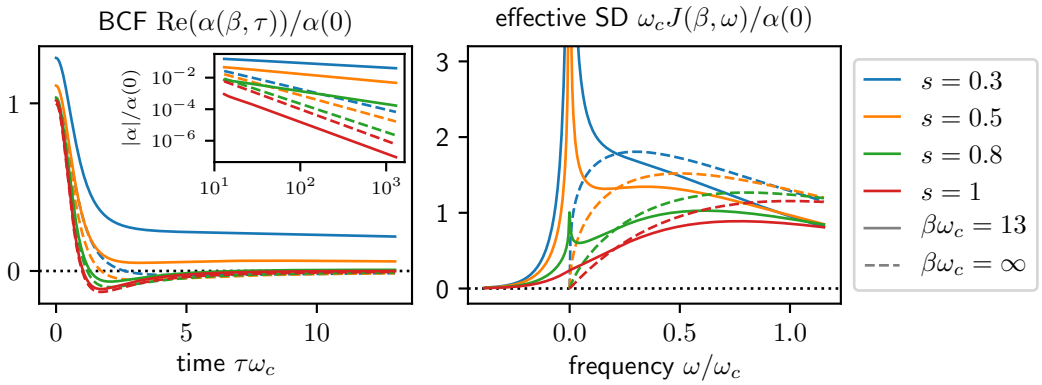

Fig. 3.19: The effect of non-zero temperature on the BCF and the related effective SD is shown for various parameters s of the (sub-) Ohmic SD. As shown in the left panel, the real part of the BCF at $\tau = 0$ increases with temperature. The imaginary part is not effected (not shown). For a sub-Ohmic SD ($s < 1$) the temperature dependent contribution $\alpha_\beta(\tau)$ to the thermal BCF $\alpha(\beta,\tau)$ [(2.72)] decays like τ^{-s} and, thus, dominates the asymptotic behavior of $\alpha(\beta,\tau)$ as shown by the inset of the left panel. The right panel shows the effective SD which diverges for $s < 1$ (see also App. B for a detailed analytic discussion).

larger time intervals. Note that the effective SD $\bar{n}(\omega\beta)J(\omega)$ of the thermal noise $\xi(t)$ occurring in the SP approach diverges at $\omega = 0$ for $s < 1$, too. However, since only positive frequencies are involved, the singularity is at the border of the integration interval and, thus, the TS method as presented Sec. 3.1.2 can be used. We conclude from thie investigation that the SP approach is the preferred way to account for non-zero temperatures in the HOPS formalism.

4 Comparing HOPS with Other Approaches

This chapter concerns the dynamics of the very fundamental model of a single qubit, i.e., a two-state quantum system, under the influence of a continuous environment (see Sec. 4.1 for introduction of the model). It might seem peculiar that with the general HOPS approach for open quantum system dynamics at hand, we focus on the most simple system. But, solving this so-called spin-boson model (SBM) has been a matter of research for theoreticians since decades [Leg+87; KM96; BTV03; TPG04; Nes+07; WT10] and still is. In particular, the exact dynamics in the strong coupling regime remains challenging [Str+18; Lam+19]. Therefore, the SBM represents an ideal test bed for novel methods, such as ours. Despite that, the long lasting interest is far from academical. The SBM appears as simplification of many physical scenarios where a complex quantum system is effectively restricted to two states only [Kal+83; Bru+96; Wal+00; MSS01; Por+08; Mag+18; HBR20]. Beyond that, many experiments aim to explicitly design such effective two-state systems, e.g, by using trapped ions [Sch17] or superconducting materials [Fag06; Per+10]. A reason for this is that qubits are the basic building blocks for quantum information or metrology devices [Ben+08; DS13; Bar+14] and other possible future technologies. Another goal of these “artificial atoms” is to realize a wide range of qubit-environment interactions. In that way the theory for light-matter interaction can be probed far beyond the usual context of atoms in the electromagnetic field with prospects of unexplored physics [Nie+10; Gus+14; Yos+17; For+17; Mag+18]. Furthermore, comprehensive experimental control of the system parameters paves the way for so-called quantum simulators [Bar+11; Hem+18]. Since exact calculations for open quantum system are costly, using a tunable quantum system as an investigative tool might be beneficial, too.

With this brought context in mind, we show in the following that the HOPS formalism qualifies to solve the SBM for a wide range of parameters. This includes the bias of the two-level system, the coupling strength to the environment and the temperature of the initial environmental state. The commonly used Ohmic as well as sub-Ohmic SD serves as model for the environmental structure. Importantly, agreement with various very distinct methods including a perturbative master equation (Sec. 4.2), the HEOM [Tan+15] (Sec. 4.3) as well as the multilayer MCTDH (ML-MCTDH) approach [WT10] (Sec. 4.4) is demonstrated with high accuracy. Notably, since

the algebraic decay of the BCF scales with the parameter s of the (sub-) Ohmic SD like $|\alpha(\tau)|\sim (\omega_c\tau)^{-(s+1)}$, the smaller s the slower the decay. As a consequence, long-ranging temporal environmental correlations causing memory effects on the system are expected if ω_c is of the order coupling strength or smaller. This regime is practically inaccessible by any method based on a rapid decay of the BCF, such as the perturbative Redfield [Red57; Dav20] or coarse graining [SB08] approach, or the QUAPI / TEMPO [MM95; Str+18] approach.

Although interesting on its own, here, we use the SBM mainly for testing purposes. Our primary physical interest lies in the entanglement dynamics of two qubits interacting with a common environment discussed in Ch. 5.

4.1 The Spin-Boson Model

Traditionally, the spin-boson model (SBM) originates from the scenario of a trapped particle where the potential energy shows two minima separated by a barrier (double well potential, see Fig. 4.1 for a sketch). For a sufficiently large spacing of the energy spectrum compared to the thermal energy of the environment, considering the two lowest energy eigenstates only is sufficient. The effective two-state system is described by the Hamiltonian [Leg+87; Wei08]

$$H_{\mathrm{sys}} = -\frac{\Delta}{2}\sigma_x + \frac{\epsilon}{2}\sigma_z \tag{4.1}$$

in terms of the Pauli matrices σ_x and σ_z where Δ corresponds to the tunneling frequency and a possible energy difference between the left and right localized state is given by the bias ϵ (see also Fig. 4.1). Thinking of the particle being confined to these two states only, its position Q is represented by σ_z where $\langle\sigma_z\rangle = \pm 1$ means that the particle is in the right/left well. For $\Delta/\epsilon \ll 1$ the eigenstates of H_{sys} are eigenstates of σ_z and, thus, if the particle is localized in one of the minima it will remain in that state for a long-time. On the contrary, for $\Delta/\epsilon \gg 1$ the eigenstates are symmetric / anti-symmetric superposition of the σ_z eigenstates. They correspond to states where the particle is delocalized. Consequently, if the particle is initially localized, its probability to be in one well oscillates with frequency Δ.

It has been argued that the influence of a continuous environment can be modeled by a set of harmonic oscillators with a linear coupling in the oscillator coordinates q_λ [Leg+87]. This motivates the specific form of the open two level system

$$H = H_{\mathrm{sys}} + L\sum_\lambda c_\lambda q_\lambda + \sum_\lambda \left(\frac{p_\lambda^2}{2m_\lambda} + \frac{m_\lambda\omega_\lambda^2 q_\lambda^2}{2}\right) \tag{4.2}$$

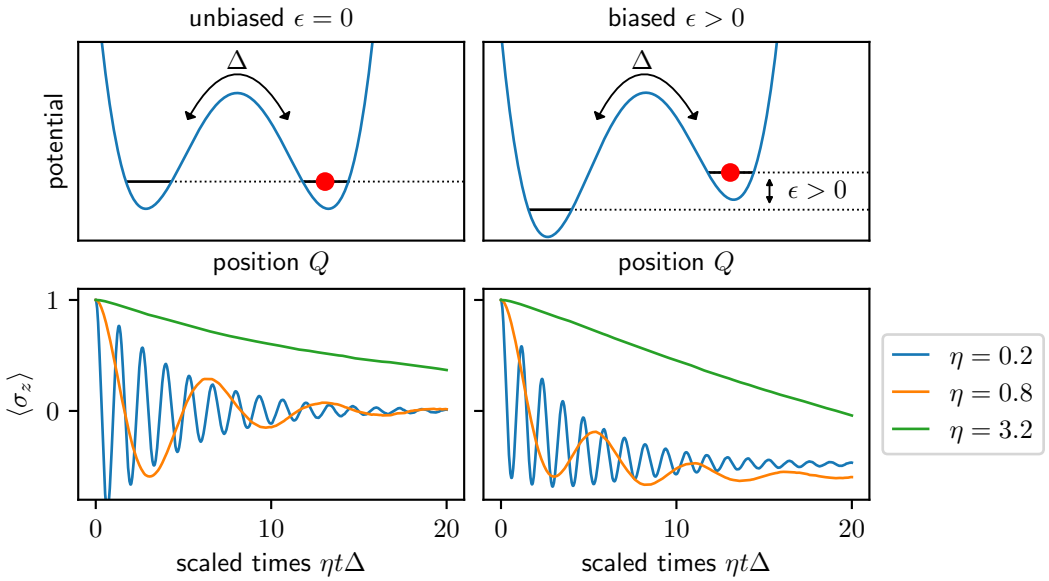

Fig. 4.1: The SBM as the low temperature limit of a particle confined in a double well potential is shown, distinguishing the unbiased (left panels) and the biased (right panel) case. The oscillation between the wells is damped by the influence of the environment (here at zero temperature). For a sufficiently strong coupling the oscillations vanish (green lines). The dynamics becomes overdamped. Further, it is sensible that the particle relaxes to a low-energy state. This suits the shown dynamics. In the biased case, the long-time dynamics indicates that the probability of measuring the particle in the left well is higher. In contrast, for the unbiased case, the asymptotic state has equal probability to find the particle in either well. This changes, however, once the coupling reaches a critical value which is related to known phase transition of the SBM [Leg+87; Wei08].

where c_λ denotes the individual coupling strength to the mode λ and m_λ, ω_λ, q_λ and p_λ its mass, frequency, position and momentum. The Hermitian system coupling operator $L = L^\dagger$ is still unspecified. Obviously, when changing from position and momentum to the creation/annihilation operator representation, this model takes the form of the microscopic model [Eq. 2.1] used to derive the HOPS

$$H = H_{\text{sys}} + L \sum_\lambda g_\lambda (a_\lambda + a_\lambda^\dagger) + \sum_\lambda \omega_\lambda a_\lambda a_\lambda^\dagger \quad \text{with} \quad g_\lambda = \frac{c_\lambda}{\sqrt{2 m_\lambda \omega_\lambda}} \,. \tag{4.3}$$

The specific choice of L models different physical circumstances.

For example, the case where L commutes with H_{sys} is, up to a unitary transformation, equivalent to $H_{\text{sys}} \sim \sigma_z \sim L$. This is one of the rare cases where the open system can be solved analytically [Unr95; PES96; BP07]. The dynamics of the reduced state exhibits pure dephasing, that is, the diagonal elements remain constant while the off-diagonal elements decay like $e^{-\Gamma(t)t}$ with some integral expression for $\Gamma(t)$.

In spirit of a particle being trapped in the double well potential, it is sensible to consider the system coupling operator to be the position Q of the particle and, thus,

$L = Q \sim \sigma_z$. This case is referred to as the SBM. The resulting Qq_λ coupling is known from the classical Langevin equation describing Brownian motion [Ull66]. In that sense, the SBM can be seen as the limiting case of a quantum Brownian particle confined to the two lowest energy eigenstates of a double well potential. Aside from that, the SBM appears in many physical scenarios related to condensed matter and atomic physics (see Ref. [GZC92; Bru+96; Hay+03; Por+08; Nie+10; Mag+18] for a few examples). The resulting spin-boson Hamiltonian

$$H = -\frac{\Delta}{2}\sigma_x + \frac{\epsilon}{2}\sigma_z + \sigma_z \sum_\lambda g_\lambda (a_\lambda + a_\lambda^\dagger) + \sum_\lambda \omega_\lambda a_\lambda a_\lambda^\dagger \tag{4.4}$$

is non-trivial to solve for general parameters. For the standard parameterization of the SD with a power law behavior for the low frequency modes [Leg+87], as introduced in Sec. 3.2 and named Ohmic ($s = 1$) or sub-Ohmic ($s < 1$) SD [Eq. (3.25)],

$$\pi \sum_\lambda g_\lambda^2 \delta(\omega - \omega_\lambda) \equiv J(\omega) = \eta \omega^s e^{-\frac{\omega}{\omega_c}} \quad , \tag{4.5}$$

the reduced dynamics shows rich behavior reaching from oscillatory to overdamped motion and to localization [Leg+87; WT08; WT10] (see also the example dynamics in Fig. 4.1). Note that the dimension of the SD is, by definition, energy. Therefore, for a sub-Ohmic SD the coupling strength η has the dimension $[\eta] = [\omega]^{1-s}$ and, thus, $\eta\Delta^{s-1}$ is dimensionless. This follows our choice to provide all quantities in units of Δ.

In the following subsections 4.2 to 4.4, the reduced dynamics of the SBM is calculated using the HOPS and compared to various other approaches found in the literature. The results, signifying a broad range of applicability of the HOPS formalism, have been published in the Journal of Chemical Theory and Computation [HS17].

4.2 Weak Coupling – the Quantum Optical Master Equation

First we compare the exact population dynamics $\langle\sigma_z\rangle(t)$ gained from HOPS with the dynamics calculated using so-called quantum optical master equation (QOME) which reads,

$$\frac{\mathrm{d}}{\mathrm{d}t}\rho_{\mathrm{sys}}(t) = -\,\mathrm{i}[H_{\mathrm{sys}} + H_{\mathrm{lamb}}, \rho_{\mathrm{sys}}(t)] + \sum_{\omega}\Big(J(\beta,\omega)[L_\omega\rho_{\mathrm{sys}}(t), L_\omega^\dagger] + \mathrm{h.c.}\Big)\ . \tag{4.6}$$

This master equation is of Gorini-Kossakowski-Sudarshan-Lindblad (GKSL) kind stating that the reduced dynamics is completely positive which, in turn, guarantees a positive reduced state for any initial condition at any time. The equation can be deduced from the general microscopic model Hamiltonian [Eq. (2.1)] in the weak coupling limit by applying a Born, Markov and rotating wave approximation (RWA) [Dav74; CDG98; BP07; KC08]. The derivation can be found in App. D.2. The so-called Lindblad operators L_ω are gained from the decomposition of the coupling operator L in terms of projectors of the energy eigenstates of the system Hamiltonian

$$L_\omega := \sum_{\varepsilon-\varepsilon' \,:\, \omega=\varepsilon'-\varepsilon} |\varepsilon\rangle\langle\varepsilon|L|\varepsilon'\rangle\langle\varepsilon'|\ . \tag{4.7}$$

In case of the two-level system [Eq. (4.1)] the eigenvalues $\pm\varepsilon = \pm\sqrt{\epsilon^2+\Delta^2}/2$ result in the possible values $-2\varepsilon, 0$ and 2ε for the transition frequency ω and the corresponding operators read

$$\begin{aligned} L_0 &= \cos(2\theta)(\cos(2\theta)\sigma_z + \sin(2\theta)\sigma_x), \\ L_{2\varepsilon} &= \sin(2\theta)\left(\frac{\sin(2\theta)}{2}\sigma_z + \sin^2(\theta)\sigma_+ - \cos^2(\theta)\sigma_-\right) \\ \text{and}\quad L_{-2\varepsilon} &= L_{2\varepsilon}^\dagger \quad \text{with} \quad \tan(2\theta) = \frac{\Delta}{\epsilon}\ . \end{aligned} \tag{4.8}$$

The so-called Lamb-shift Hamiltonian

$$H_{\mathrm{lamb}} := \sum_{\omega} S(\beta,\omega) L_\omega^\dagger L_\omega \tag{4.9}$$

and the dissipator in Eq. (4.6) depend on the values of the half-sided Fourier transform of the BCF (see also App. B)

$$F(\beta,\omega) \equiv J(\beta,\omega) + \mathrm{i}S(\beta,\omega) := \int_0^\infty \mathrm{d}\tau\, \alpha(\beta,\tau) e^{\mathrm{i}\omega\tau} \quad , \tag{4.10}$$

where, for completeness, the thermal BCF depends on the SD $J(\omega)$ and the inverse temperature β as given in Eq. (2.72). It can bee seen that the real part of F

determines the non-unitary damping whereas the imaginary part influences the environmentally induced unitary contribution of the reduced dynamics.

The validity of the QOME is limited to the weak coupling regime such that $\tau_{\mathrm{bcf}} \ll \tau_{\mathrm{ind}}$ and $\tau_{\mathrm{RWA}} \ll \tau_{\mathrm{ind}}$ are fulfilled simultaneously [KC08; HS20a], where τ_{bcf} denotes the time scale of the decay of the BCF and τ_{RWA} scales like

$$\frac{1}{\tau_{\mathrm{RWA}}} \sim \min_{\omega,\omega':\omega\neq\omega'} |\omega - \omega'| \tag{4.11}$$

with ω and ω' taking the values of the transition frequencies of the H_{sys}. Both of these timescales have to be smaller than τ_{ind}, the timescale of the dynamics induced by the influence of the environment, that is, the time scale on which the reduced state changes in the interaction picture. Since this time scale is governed by the coupling strength $\tau_{\mathrm{ind}}\Delta \sim \frac{1}{\eta\Delta^{s-1}}$ both conditions can be met if the coupling is sufficiently weak. More details can be found in App. D.

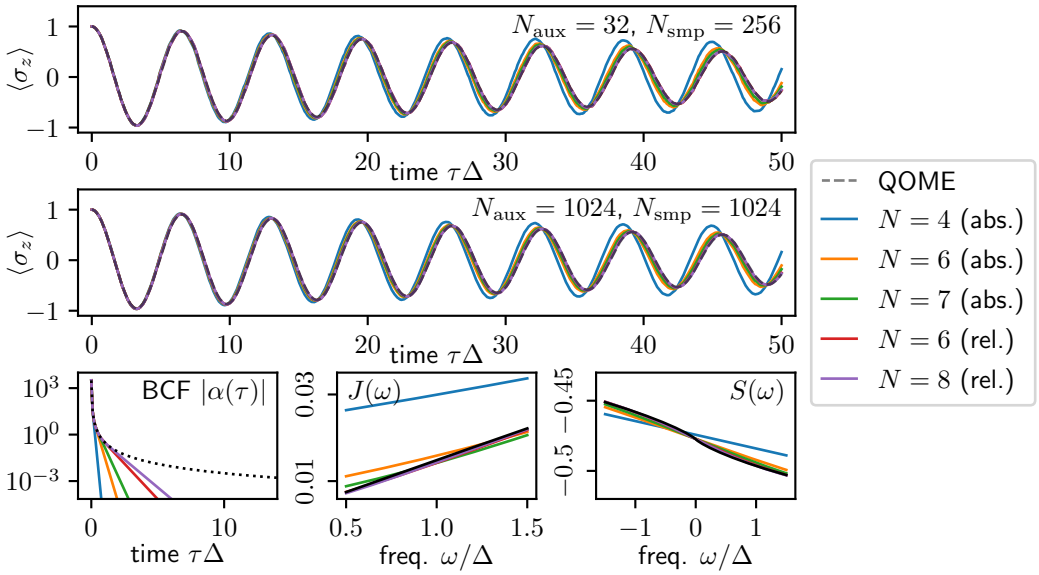

Fig. 4.2: The dynamics of the unbiased SBM ($\epsilon = 0$) is shown for an Ohmic SD with weak coupling ($\eta = 0.015$) and a fast decay of environmental correlations ($\omega_c = 100\Delta$). In that regime the QOME is applicable and, thus, agreement with the HOPS method is seen. Already, for $N_{\mathrm{aux}} = 32$ auxiliary states and $N_{\mathrm{smp}} = 256$ samples the dynamics has converged (no visible difference between plots in the upper and middle panel). Since the QOME is applicable, the dynamics is essentially determined by the SD $J(\omega)$ at $\omega = \pm\Delta$ (and the related function $S(\omega)$, Eq. (4.10)). This is also reflected by the exponential representation of the BCF. Sufficiently many terms are required to follow the algebraic decay in order to yield good agreement in frequency domain (see lower panels).

The expected agreement between the HOPS of the QOME for that regime is shown in Fig. 4.2 using an Ohmic environment. As a consequence of the weak coupling, several hundred samples only and a very small hierarchy depth are sufficient to achieve converged results (compare top and middle panel in Fig. 4.2). However,

the damped oscillation obtained from the HOPS is very sensitive to the exponential representation of the Ohmic BCF (see Sec. 3.2). Although the fit using 4 terms to minimize the absolute difference reaches an error of almost 10^{-3} (see Fig. 3.10) a difference in the dynamics between the HOPS and the QOME is clearly visible. Using more terms for a better approximation of the BCF results in better agreement with the QOME dynamics. Notably, small deviations between the dynamics resulting from 6 and 7 terms are visible, so the results cannot be claimed to have converged yet. In contrast, using fits minimizing the relative difference over $D = 4$ orders of magnitude yields no noticeable difference between 6 and 8 exponential terms. The HOPS has converged already using $N = 6$ exponential terms (rel. fit) and, as expected, agrees with the dynamics obtained from the QOME with high precision.

The slower convergence of the fits minimizing the absolute difference can be understood by recalling that the parameter regime was chosen such that Born- and Markov-approximation is fulfilled

$$0.01 = \Delta/\omega_c \sim \tau_{\mathrm{bcf}}\Delta \ll \tau_{\mathrm{ind}}\Delta \sim \Delta/\eta \approx 50\ . \tag{4.12}$$

Therefore, the value of the half-sided Fourier transform of the BCF at $\omega = \pm 2\varepsilon = \pm\Delta$ (unbiased case $\epsilon = 0$) determines the dynamics effectively (Eq. (4.6) and Eq. (4.10)). As shown in the bottom panel of Fig. 4.2 the faulty long-time behavior of the exponential representation for the actually algebraic decay of the Ohmic BCF results in a noticeable difference of J and S, the real and imaginary part of the half-sided Fourier transform, for $\omega = \pm\Delta$, especially for $N = 4$ (abs. fit). The fits minimizing the relative difference over 4 order of magnitude (red and purple lines in Fig. 4.2), which follow the algebraic decay longer but with less accuracy, yield more accurate values for the half-sided Fourier transform and, thus, more accurate dynamics.

Based on that, Fig. 4.3 shows the population dynamics of the SBM for various temperatures and different values of the detuning using the $N = 6$ (rel. fit) exponential representation and $N_{\mathrm{aux}} = 32$ auxiliary states only. In all cases the HOPS method and the QOME agree with high precision. Note that since the amplitude of the noise related to the stochastic potential approach for non-zero temperature scales with the temperature (see Sec. 2.2.2), the number of required samples scales with temperature, too (see Fig. 4.4).

For a sub-Ohmic environment at non-zero temperature the QOME as specified in Eq. (4.8) is not well defined. Both, the effective SD $J(\beta, \omega)$ and the corresponding imaginary part $S(\beta, \omega)$ diverge at $\omega = 0$ (see App. B). However, the formalism can

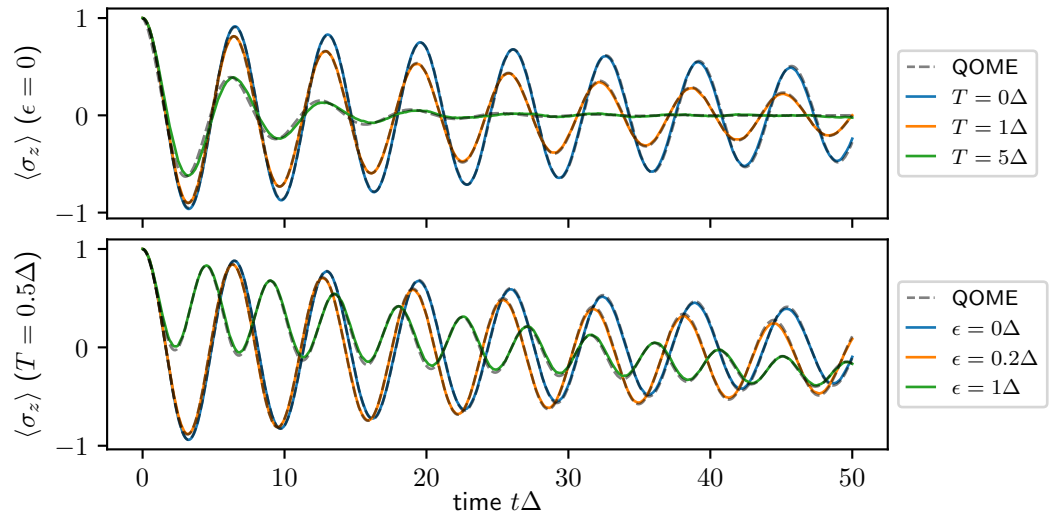

Fig. 4.3: For weak coupling ($\eta = 0.015$) and a fast decaying Ohmic BCF ($\omega_c = 100\Delta$) the QOME is applicable. As expected, agreement with the exact dynamics of the HOPS method for various temperatures T and different values of the bias ϵ was found.

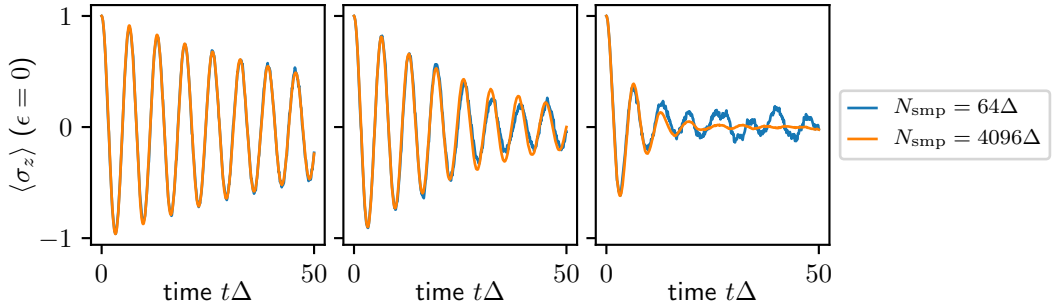

Fig. 4.4: Since the thermal fluctuations, directly accounted for by the stochastic potential term in the HOPS methods (see Sec. 2.2.2), increase with T, a higher temperature requires more samples (N_{smp}) to obtain converged results.

still be applied when "undoing" the $\int_0^t \to \int_0^\infty$ approximation used to derive the QOME [NF14]. This results in the time-dependent coefficients (TDC)

$$J_{\beta,\omega}(t) + \mathrm{i}S_{\beta,\omega}(t) := \int_0^t \mathrm{d}\tau\, \alpha(\beta,\tau)e^{\mathrm{i}\omega\tau} \quad , \tag{4.13}$$

simply replacing their asymptotic values $J(\beta,\omega)$ and $S(\beta,\omega)$ in the QOME. The comparison between the QOME with TDC and the HOPS shows agreement in all combinations of temperature and bias. As in the Ohmic case, a small hierarchy depth and a few hundred samples are sufficient for the HOPS to obtain converged results. Notably, as of the slower decay of the sub-Ohmic BCF compared to the Ohmic case, the coupling strength had to be chosen even smaller for the Born- and Markov-approximation to be applicable.

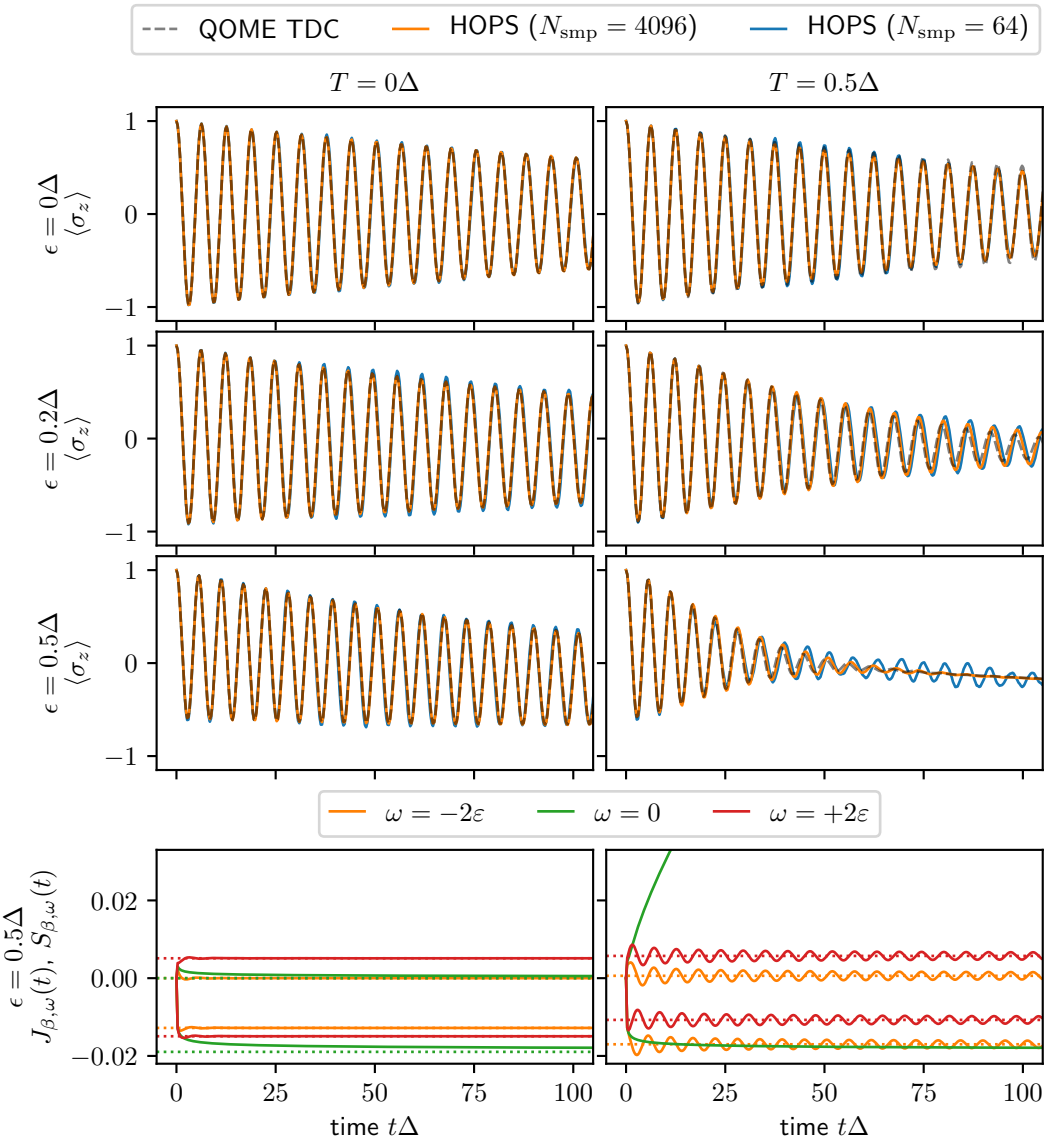

Fig. 4.5: The $\langle\sigma_z\rangle$ dynamics of the SBM with a sub-Ohmic environment ($s = 0.3$, $\eta = 0.005\Delta^{1-s}$, $\omega_c = 100\Delta$, $N = 8$ (rel. fit) exponential representation of the BCF) is shown for zero and non-zero temperature T and different values of the bias ϵ. As expected, agreement between the HOPS method and the QOME with time-dependent coefficients (TDC) is found. A few hundred samples and $N_{\mathrm{aux}} = 32$ auxiliary states are sufficient to obtain converged results. The bottom panels show the time-dependent coefficients (TDC) ($J_{\beta,\omega}(t) \geq 0$, $S_{\beta,\omega}(t) \leq 0$) and their asymptotic values (dotted lines). For $T = 0.5\Delta$ the rapid increase of $J_{\beta,\omega=0}(t)$ is well seen (upper green line) and directly reflected by the strong damping of the dynamics as compared to the zero-temperature environment. Note that the value of $J_{\beta,\omega=0}(t)$ is independent of the bias ϵ. However, since the operator L_0 scales with ϵ, i.e., $L_0 \sim \epsilon/\sqrt{\Delta^2 + \epsilon^2}$, the actual damping does depend on the bias, as seen particularly in the right panels from top to bottom.

4.3 Classical Noise – Hierarchical Equations of Motion and its extension

The next regime considered is the classical noise limit where presumably the influence of the environment can be accounted for by a stochastic force alone. This is the case whenever the real part of the BCF dominates the imaginary part. From Feynman-Vernon's path integral approach [FV63] it follows that when simply neglecting the imaginary part of the BCF the reduced dynamics can be obtained by averaging over the solutions of the stochastic Schrödinger equation

$$\mathrm{i}\partial_t\psi(t) = (H_{\mathrm{sys}} + \sigma_z F(t))\psi(t) \tag{4.14}$$

with the real valued noise process $F(t)$ obeying $\mathcal{M}(F(t)F(s)) = \mathrm{Re}(\alpha(\beta, t-s))$ [CCS13; MC13; Tan+15]. As a remark, in the high temperature limit, this expression is consistent with the stochastic potential (SP) formalism for non-zero temperature introduced in Sec. 2.2.2 and which can be seen as follows. Recalling that the thermal BCF $\alpha(\beta, t-s)$ contains a zero temperature contribution and a purely real thermal contribution [Eq. (2.73)], for large temperatures $\beta\omega_c \ll 1$, the thermal contribution scales linear with the temperature $T = 1/\beta$

$$\alpha_\beta(\tau) = \frac{1}{\pi}\int_0^\infty \mathrm{d}\omega\; 2\bar{n}(\beta\omega)J(\omega)\cos(\omega\tau) \approx \frac{1}{\beta\pi}\int_0^\infty \mathrm{d}\omega\; 2\frac{J(\omega)}{\omega}\cos(\omega\tau)\;. \tag{4.15}$$

Since the magnitude of the BCF, set by the scale η of the SD and the temperature, determines the strength of the environmental influence, it is sensible to consider the high temperature limit $T \to \infty$ while keeping ηT constant. In that limit, the real part of the thermal BCF becomes the thermal contribution and the zero temperature BCF tends to zero. Consequently, in the SP formalism, the zero temperature influence of the environmental can be neglected and only the stochastic potential remains with

$$\mathcal{M}(\tilde{\xi}(t)\tilde{\xi}(s)) = \alpha_\beta(t-s) \overset{T\to\infty}{\to} \mathrm{Re}(\alpha(\beta, t-s)) = \mathcal{M}(F(t)F(s))\;. \tag{4.16}$$

The parameters for the SBM with dynamics shown in Fig. 4.6 are motivated by the discussion on sub-Ohmic SD done by Tang et al. [Tan+15]. With the stochastic Hamiltonian approach [Eq. (4.14)] as reference, they discuss the insufficiency of the commonly used Meier-Tannor decomposition (MTD) [MT99] to obtain a multi-exponential representation of the sub-Ohmic BCF when used for the HEOM approach [TK89; Tan06]. Further, they show that this difficulty can be overcome by expanding the BCF in terms of harmonic oscillator wave functions instead of exponential terms which yields the so-called extended HEOM (eHEOM) method. In Fig. 4.6 we compare the results from Tang et al. [Tan+15] with the dynamics

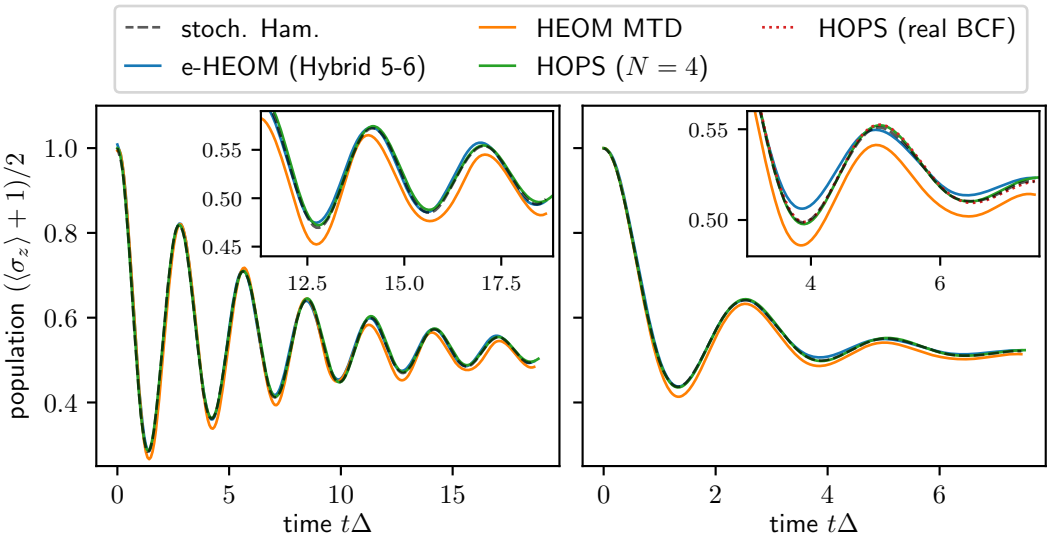

Fig. 4.6: In the high temperature limit environmental influences can be treated via stochastic forces (stoch. Ham. method, Eq. (4.14)). For the unbiased (ϵ=0) spin-boson model the population dynamics obtained from the HOPS, the HEOM and its extension the eHEOM approach are shown. In the left panel ($\eta = 0.304\Delta^{1-s}$, $\omega_c = 0.531\Delta$, $T = 2.09\Delta$, $s = 0.5$) eHEOM and HOPS match well the reference data from the stoch. Ham. method, whereas the usual HEOM yields slightly different dynamics as pointed out in Ref. [Tan+15]. In the right panel ($\eta = 0.192\Delta^{1-s}$, $\omega_c = 1.33\Delta$, $T = 5.21\Delta$, $s = 0.5$) the zoomed in view of the inset reveals that the HOPS matches the reference closely, whereas the eHEOM deviates slightly. Therefore, even more basis function and / or a higher hierarchy depth are required for the eHEOM approach to yield the same degree of accuracy as the HOPS. For an additional consistency check, the HOPS was setup also by fitting the non-zero temperature real valued BCF (red dots) which matches the reference data, too. The numeric values of the parameters (specified in units of Δ) are given with accuracy of three digits and correspond to the parameters given in Ref. [Tan+15] Fig. 5d and Fig. 5b.

obtained by solving the HOPS. Agreement with the reference stochastic Hamiltonian method is found while still making use of an exponential representation of the BCF. The difference is that the representation used by the HOPS is obtained by directly fitting the BCF in time domain (as explained in detail in Sec. 3.2) and not via MTD. Noteworthily, for the particular example, the eHEOM approach requires 31 basis functions to decompose the BCF sufficiently well. Also, a hierarchy depth of 6 is needed for convergence which results in a set of 31.675.182 coupled differential equations. In contrast, the HOPS has converged for 4 exponential terms and a hierarchy depth of 5 which yields a set of 252 coupled differential equations only.

Furthermore, considering the parameter set corresponding to the right panel in Fig. 4.6 a small discrepancy between the eHEOM and the stochastic Hamiltonian method is observed. However, the fully quantum mechanical calculation using the HOPS matches the dynamics gained from the stochastic Hamiltonian method very well, supporting the validity of neglecting the imaginary part of the BCF. Thus, the eHEOM approach has not fully converged yet for the parameters shown. To check

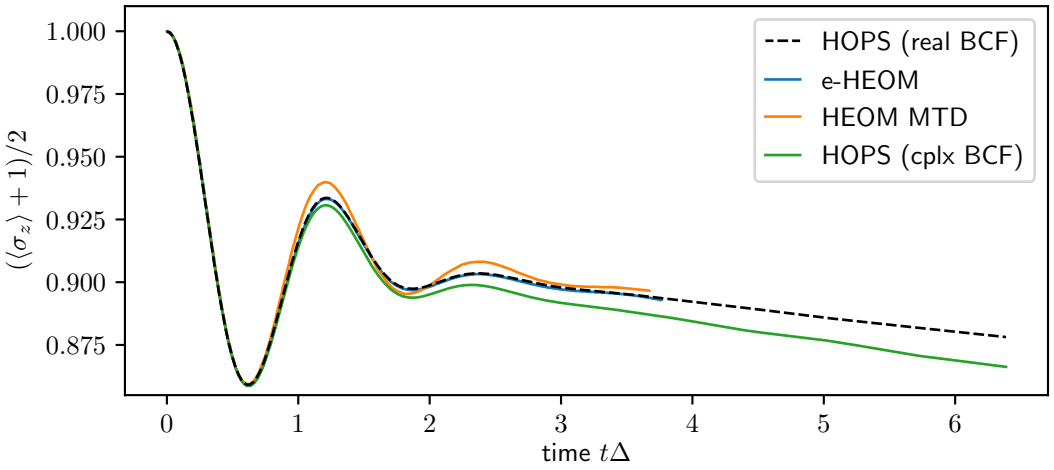

Fig. 4.7: The biased ($\epsilon = 2.5\Delta$) spin-boson model is considered with parameters $\eta = 0.0272\Delta^{1-s}$, $\omega_c = 2.65\Delta$, $T = 10.4\Delta$, $s = 0.5$ corresponding to the parameters from Ref. [Tan+15] Fig. 6a. The population dynamics gained from the fully quantum mechanical calculation using HOPS (green line) decays faster than the dynamics resulting from the other methods neglecting the imaginary part of the BCF. This example shows that it is not straight forward to tell a priory whether the imaginary part of the BCF can be neglected or not. Again, the usual HEOM with a MTD of the SD yields an even larger discrepancy with respect to the exact HOPS result.

consistency the HOPS has also been set up for the real valued non-zero temperature BCF (red dotted line) $\mathrm{Re}(\alpha(\beta,\tau)) = \frac{1}{\pi}\int_0^\infty \mathrm{d}\omega\, J(\omega)\coth(\beta\omega/2)\cos(\omega\tau)$ by fitting this particular BCF which, by construction, reproduces the dynamics from the stochastic Hamiltonian method exactly. As a reminder the fully quantum mechanical calculation via the HOPS involves fitting the zero temperature BCF and including temperature in a stochastic manner similar to the stochastic Hamiltonian method (see Sec. 2.2.2).

These results show that HOPS, which operates in the fully quantum regime, is very well capable of dealing with high temperature environments with a predominant classical influence (thermal fluctuations) on the quantum system. As of the stochastic potential approach to include thermal environments (Sec. 2.2.2) this was expected.

Additionally, in Fig. 4.7 a different set of parameters with a dominating bias ϵ, weak coupling and high temperature is shown. In Ref. [Tan+15] Fig. 6a these parameters serve as an example for the biased SBM. In contrast to the set of parameters discussed before, the HOPS reveals that the quantum nature of the environment yields a noticeable contribution to the dynamics. As a consistency check, we also use the HOPS with only the real part of BCF which yields the expected agreement with the stochastic Hamiltonian method and the eHEOM. However, invoking the HOPS with the actual complex valued BCF yields the same oscillatory behavior as the classic force approximation, however, with a slightly faster decay. Therefore, the

quantum nature of the bath is important for this particular set of parameters, even though the temperature is high.

4.4 Strong Coupling – Explicit Methods (time-dependent Hartree, Davidov)

In addition to the reduced approaches considered so far (master equations and HEOM) the SBM has been solved by means of explicit methods, too, which approximate the continuous environment by a finite number of discrete modes [ABV07; WT08; WT10; WG20]. The dynamics of the system and the environmental modes are solved explicitly such that the reduced dynamics follows simply from tracing out the environment. The very large dimension of the full Hilbert space is reduced by a suitable choice of a time depended basis whose dynamics follows from a variational principle. Among various choices, using a matrix product state representation has led to the successful ML-MCTDH method [Bec+00; WT03]. The zero temperature case for a sub-Ohmic environment, considered by Wang et al. [WT10], is highly relevant for our comparison. As of that we adapt the notation for the coupling strength in term of the dimensionless parameter $\alpha := \eta 2\eta\omega_c^{s-1}/\pi$. From the striking agreement shown Fig. 4.8 we conclude that the HOPS formalism, in combination with the tweaks discussed in Ch. 3, is indeed applicable in the strong coupling regime with

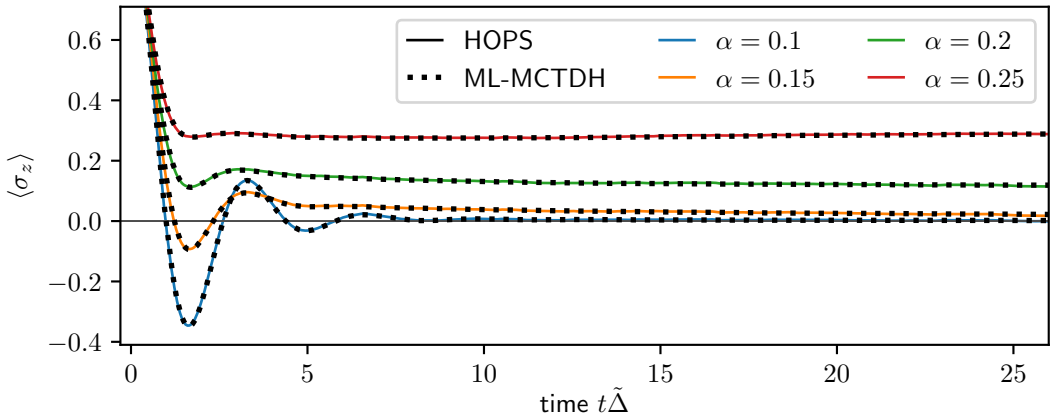

Fig. 4.8: The dynamics of $\langle \sigma_z \rangle$ is shown ($s = 0.5$, $\omega_c = 10\tilde{\Delta}$, $\epsilon = 0$, $T = 0$) various coupling strengths $\eta \equiv \pi\alpha\omega_c^{1-s}/2$. Agreement between the HOPS (colored lines) and the ML-MCTDH approach (dotted lines) is demonstrated with high precision. The graphs indicate that for $\alpha \geq 0.2$ the asymptotic state is localized. In contrast to an Ohmic environment, for $s < 1$ the initial damped oscillations do not vanish completely, even in the localized phase. A BCF fit minimizing the relative error up to time $15/\tilde{\Delta}$ with 5 terms and an accuracy below 2% was used. Convergence has been achieved for a simplex hierarchy truncation with depth $5(\alpha = 0.1)$, $6(\alpha = 0.15)$, $9(\alpha = 0.2)$ and $12(\alpha = 0.25)$ while averaging over 10^5 stochastic pure states. Note, parameters are given in units of $\tilde{\Delta} = \Delta/2$ and the dimensionless coupling strength α to match the parameterization used in Ref. [WT10].

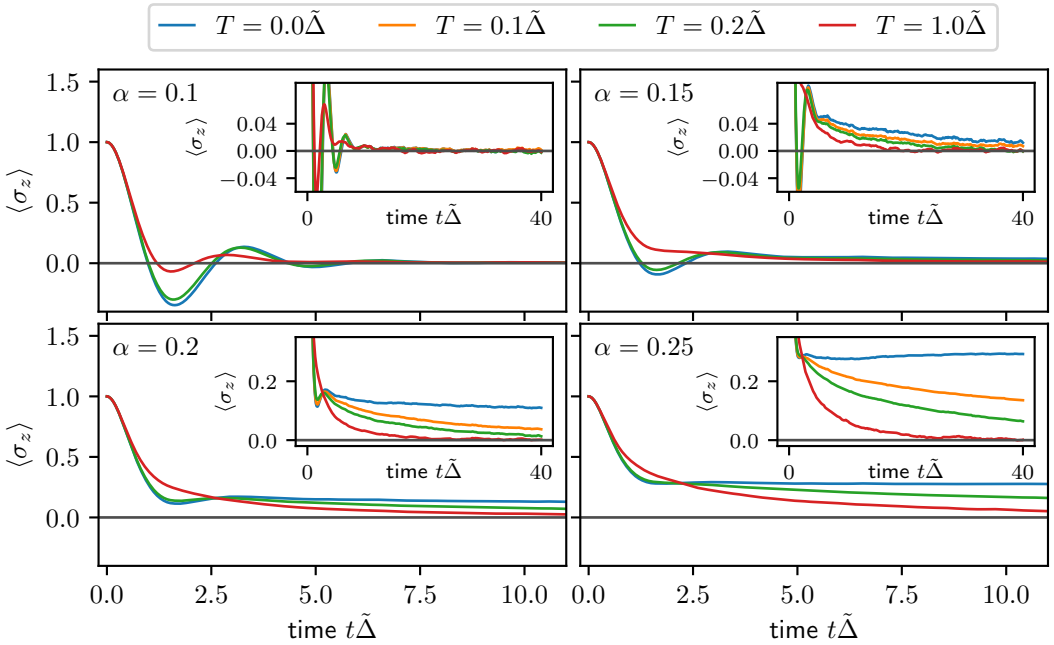

Fig. 4.9: The dynamics of $\langle\sigma_z\rangle$ is shown (same parameters as in Fig. 4.8) for various temperatures. The graphs reveal that increasing temperature weakens the initial oscillations until they vanish completely, which is sensible. Further, non-zero temperature accelerates the decay towards $\langle\sigma_z\rangle = 0$. Thus, it seem plausible that the critical coupling strength for localization to occur shift to larger values upon increasing temperature, which is in agreement with results from Ref. [ABV07].

a zero temperature environment while relying on an exponential representation of the BCF. Also, the strong coupling and zero temperature case is opposing to the previous discussions concerning weak coupling (Sec. 4.2) and high temperatures (Sec. 4.3), demonstrating a wide range of applicability for the HOPS method.

Concerning the relevant physics of the dynamics shown in Fig. 4.8, it is well known that the unbiased SBM exhibits a phase transition at a critical coupling strength [Leg+87; KM96; Wei08; ABV07]. For weak coupling the ground state is delocalized, i.e., $\langle\sigma_z\rangle = 0$. The particle can be found in either well with equal probability. For a coupling strength larger than a critical value, the ground state becomes degenerate with $\langle\sigma_z\rangle = \pm c$. Remarkably, this degeneracy is also reflected by the asymptotic value of the dynamics $\sigma_z(t)$. Depending on weather the particle is initially prepared in the right of the left well, $\sigma_z(t \to \infty)$ approaches either $+c_\infty$ or $-c_\infty$. This means that the particle is more likely to be found in one of the wells, it is said to be localized. The critical coupling strength for the qualitative change of the asymptotic state depends on the parameters modeling the environment such as the exponent s and the cutoff ω_c of the SD. In the limit of a large cutoff frequency $\Delta/\omega_c \gg 1$, i.e., a fast decaying BCF compared to the unperturbed dynamics of the spin, the Non-Interacting Blip Approximation (NIBA) yields an extensive picture for the dynamics of the SBM

[Leg+87]. However, if $\Delta/\omega_c \gg 1$ does not hold, solving the SBM in the regime of localization remains challenging, especially for the Ohmic case [WT10; Str+18].

In this spirit, the example shown in Fig. 4.8 deserves notice on its own, too, showing the transition from delocalization to localization of the asymptotic reduced state. In addition, the influence of non-zero temperature on the dynamics is shown in Fig. 4.9. For lower temperatures the effect is almost negligible for the initial oscillations but becomes evident in the long-time behavior suppressing the localization (see the insets of Fig. 4.9). Further increasing the temperature up to $T = \tilde{\Delta}$ results also in a stronger damping of the initial oscillations and a faster decay towards zero. Note that due to the enlarged view, small fluctuations of the dynamics originating from the stochastic nature of the HOPS method become visible. These fluctuations decrease in amplitude when increasing the number of samples.

4.5 Numeric Futility of the Linear HOPS

In this section we demonstrate that the use of the non-linear variant of the HOPS (Sec. 2.1.2) becomes nearly inevitable for strong couplings. For $\alpha = 0.2$ (as in Fig. 4.8) the dynamics of the SBM obtained from the linear HOPS is compared to its non-linear variant in Fig. 4.10. For 1000 samples already, the fluctuations due to the stochastic nature of the HOPS method are significantly smaller for the non-linear HOPS compared to the linear version. Even more severe, increasing the number of samples by a factor of 20 hardly decrease the fluctuations in the linear formalism. It seems unfeasible to obtain converged dynamics in particular at times where the

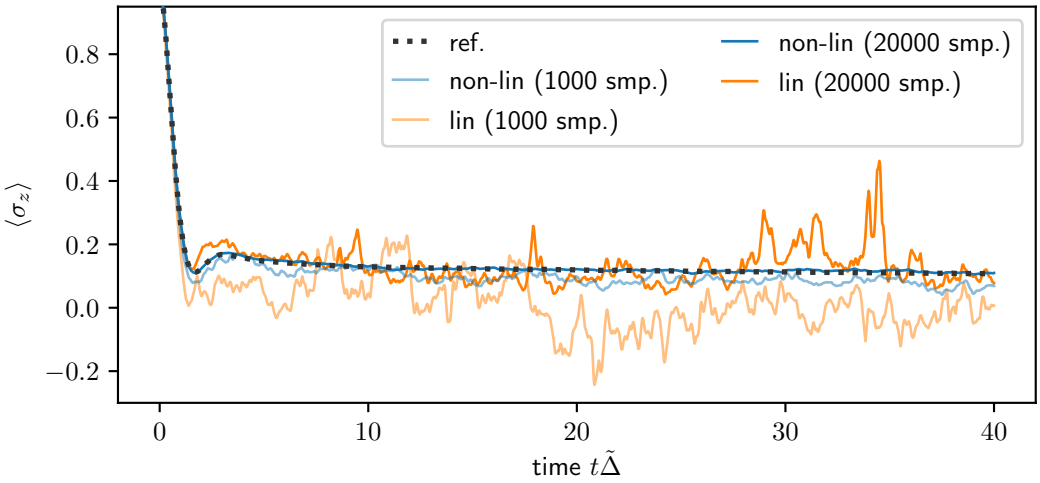

Fig. 4.10: Comparison of the convergence properties for the linear HOPS (orange line) and the non-linear HOPS (blue line) in the strong coupling regime ($\alpha = 0.2$, $s = 0.5$, $\omega_c = 10\tilde{\Delta}$, $\epsilon = 0$, $T = 0$). As reference (gray dashed line) the non-linear HOPS method with 10^5 samples was used which coincides well with ML-MCTDH dynamics.

dynamics has relaxed. The bad statistical convergence is explained by the unequal weight with which the stochastic pure state dyads contribute to the reduced state. As shown in Sec. 2.1.3, this weight corresponds to the squared norm of the stochastic pure state. Since in the strong coupling regime the norm varies strongly between different realizations, only a small portion of samples contributes effectively, which explains the large fluctuation of the orange lines shown in Fig 4.10. In contrast, the average over the normalized states from the non-linear NMQSD equation yields dynamics (blue lines) for which the fluctuations cannot be resolved on the scale shown in Fig. 4.10. Thus, the stochastic convergence is much better.

5 Entanglement Dynamics of the Two-Spin-Boson Model

The extensive survey concerning the applicability of the HOPS to solve the spin-boson model (SBM) for Ohmic and sub-Ohmic environments, done in the previous chapter, has shown that the HOPS serves as universal method. It is, thus, the main goal of this last chapter to address questions yet to be settled related to the dynamics of open quantum systems using the HOPS method. The overall scope is the evolution of entanglement of two qubits coupled to a common environment (see Fig. 5.1 for a sketch of the model). Many aspects of the following investigation have been published in the Quantum journal [HS20b].

Considering a bipartite system, such as the two qubits sketched in Fig. 5.1, the superposition principle of quantum mechanics allows for states which cannot be factorized as a single tensor product of contribution belonging to either of the parties. Such inseparable states are called *entangled states* [Hor+09]. As a consequence of the necessity to considered the state as whole, a local state modification, e.g., a local measurement, generally alters the whole state and with that the state of other party, too, no matter how far the two parties have been separated. This phenomenon, known as Einstein-Podolsky-Rosen-Paradoxon [EPR35], manifests quantum features not occurring in the classical world. Their experimental realizations (see Ref. [CS78; AGR82; Hen+15] for a small selection) pave the way to utilize entanglement as a resource for quantum information tasks [Hor+09] with the aim to ultimately exceed the capabilities of their classical equivalents [NC00].

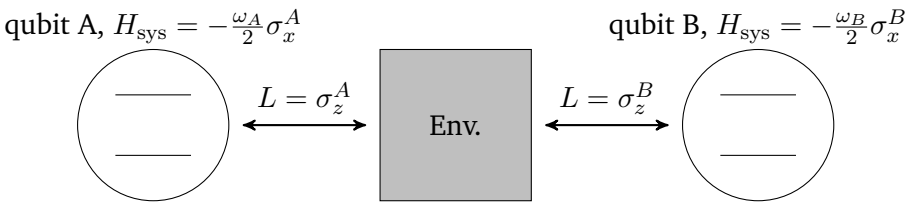

Fig. 5.1: The Schematic setup of two independent qubits experiencing an interaction mediated by the common environment is shown. The model extends the usual SBM to two qubits and, thus, allows us to study the influence of an environment on the entanglement dynamics.

The common challenge for all practical implementation exploiting entanglement are environmental influences which can destroy, but also induce, entanglement. It has been argued on general grounds that a quantum system can become effectively classical as a consequence of its interaction with an environment [Zur03]. That is, the noise induced by the environment causes the superposition state, featuring entanglement, to loose coherence and eventually approach the classical statistical mixture featuring no entanglement anymore. This behavior of the reduced dynamics is captured when modeling the environmental influence in terms of a master equation where the non-unitary contribution leads to decoherence and dephasing, destroying entanglement [Min+05; YE09]. On the other hand, the interaction with a common environment also features the capability to induce entanglement [DS98; Bra02; Kim+02; Isa09; Maz+09], which can even last for arbitrary long times [BF06; ZQK09; SM13]. For the perturbative master equation regime, the generation of entanglement can be explained by the environmentally induced unitary contribution (often called Lamb-shift Hamiltonian) which mediates an effective interaction between the qubits.

This motivates the following investigation of these non-trivial competing environmental effects. With the exact dynamics from the HOPS at hand, we point at the pitfalls of perturbative approaches (Sec. 5.1), show unexpected entanglement generation in the adiabatic regime (Sec. 5.2), demonstrate that a substantial amount of entanglement is generated for a wide range of model parameters including non-zero temperature (Sec. 5.3) and analyze the asymptotic entanglement while referring to the known phase transition of the open two-qubit system (Sec. 5.4).

As particular model the SBM (see also Sec. 4.1) is simply extended by another spin, in the following called two-spin-boson model (2SBM) [Ort+10; HL16]. The particular microscopic model Hamiltonian for the open quantum system (as in Eq. (2.1)) then reads

$$\begin{aligned} H &= H_{\mathrm{sys}} + L \otimes \sum_\lambda g_\lambda (a_\lambda + a_\lambda^\dagger) + \sum_\lambda \omega_\lambda a_\lambda^\dagger a_\lambda \\ \text{with} \quad H_{\mathrm{sys}} &= -\frac{\omega_A}{2}\sigma_x^A - \frac{\omega_B}{2}\sigma_x^B \quad \text{and} \quad L = \frac{1}{2}(\sigma_z^A + \sigma_z^B) \,. \end{aligned} \tag{5.1}$$

In spirit of the single SBM, each qubit (A and B) is modeled by the Pauli matrix σ_x and tunneling frequency ω (see also Fig. 5.1) assuming no energy bias. Further, no direct interaction between the qubits is present. If the tunneling frequencies are the same ($\omega_A = \omega_B$) the qubits are referred to be resonant, otherwise they are called detuned. The qubits are coupled with equal strength via σ_z to the common bosonic

environment. The (sub-) Ohmic SD, introduced in Sec. 3.2, modeling the continuous environment is reiterated for completeness

$$\pi \sum_{\lambda} g_\lambda^2 \delta(\omega - \omega_\lambda) = J(\omega) = \eta \omega^s e^{-\omega/\omega_c} \,. \tag{5.2}$$

To examine the entanglement dynamics, focusing on its generation, the two-qubit product state $|\psi_0\rangle = |\uparrow\rangle_A \otimes |\uparrow\rangle_B \equiv |\uparrow\uparrow\rangle$ is chosen as initial condition where $|\uparrow\rangle$ ($|\downarrow\rangle$) denotes the eigenvector of σ_z with eigenvalue $+1$ (-1). Note that for the unbiased single qubit Hamiltonian considered here, i.e., no σ_z contribution in the system Hamiltonian, the initial state $|\downarrow\downarrow\rangle$ yields the same entanglement dynamics. Also, the symmetry of the resonant Hamiltonian (5.1) ($\omega_A = \omega_B$) results in a decoherence free subspace spanned by the Bell-state $|\Phi_-\rangle \sim |\uparrow\downarrow\rangle - |\downarrow\uparrow\rangle$. Therefore, since the states $|\uparrow\downarrow\rangle$ and $|\downarrow\uparrow\rangle$ contain a contribution belonging to this decoherence free subspace, it is not too surprising that entanglement is effectively generated if they serve as initial condition [SM13]. For this reason, they are not considered here either.

To quantify the two-qubit entanglement the measure *concurrence* [HW97; Hor+09] is used,

$$c \coloneqq \lambda_1 - \lambda_2 - \lambda_3 - \lambda_4 \tag{5.3}$$

where λ_i are the decreasingly sorted eigenvalues of the matrix $R = \sqrt{\sqrt{\rho}\tilde{\rho}\sqrt{\rho}}$ with $\tilde{\rho} = \sigma_y^A \sigma_y^B \rho^* \sigma_y^A \sigma_y^B$. Strictly speaking, only the positive values of c quantify entanglement, however, when comparing the dynamics of c it seems more convenient to show its negative values, too. As a remark, the meaning of c as an entanglement measure is inevitably related to the semidefinite positivity of the statistical operator ρ, i.e., ρ represents a physical state. For negative ρ the meaning of c is futile and c, as defined above, can become complex valued. This becomes relevant for master equations well motivated in a perturbative sense which, however, do not guarantee positivity for the approximate reduced state such as the Redfield equation (RFE) (see Ref. [Dav20; HS20b] and below).

5.1 Perturbative Master Equations

In a weak coupling regime and/or for a fast decaying BCF the reduced dynamics of the microscopic model (Eq. (2.1) in general and Eq. (5.1) in particular) can be obtained approximately by solving a time local ordinary differential equation for the reduced state, that is, a time local master equation. Various such perturbative master equations have been proposed based on various assumptions. As of their simple structure, master equations are valuable, allowing for a fast evaluation and to gain insights in the relevant mechanisms. However, as we enlighten in the following,

their range of validity has to be checked carefully, in particular for quantum systems beyond a single qubit. With reference to the exact dynamics obtained from the HOPS, the applicability of the quantum optical master equation (QOME) (Born-Markov approximation and rotating wave approximation (RWA)) [BP07; KC08], its variation with only a partial rotating wave approximation (PRWA) [VJC13; Jes+15; TB15], the Redfield equation (RFE) (no RWA at all) [Red57], the very recent geometric-arithmetic master equation (GAME) (GKSL kind equation based on the RFE) [Dav20] and a coarse-graining master equation (CGME) [SB08; BFM10; Maj+13] is examined. The derivation of such master equations can be found in App. D.

5.1.1 The Rotating Wave Approximation

The great success of the QOME to describe the dynamics of a single qubit encourages the use of the same formalism for two qubits, too. Since the QOME is of GKSL form positivity of the reduced state is assured for all times and any initial condition. For resonant qubits $\omega_A = \omega_B$, the build-up of entanglement and its decay is shown in Fig. 5.2 and Fig. 5.3 (top panel). The generation of entanglement is easily explained by the unitary contribution of the QOME (Lamb-shift term, see also App. D.2)

$$H_{\mathrm{Lamb}} = H_{\mathrm{local}} + \frac{S(\omega_A) + S(-\omega_A)}{8} \left(\sigma_z^A \sigma_z^B + \sigma_y^A \sigma_y^B\right) \tag{5.4}$$

mediating an effective coupling between the qubits [LW06; STP07; McC+09; SM13]. Here, S denotes the imaginary part of the half sided Fourier transform of the BCF (see App. B.2 for details). Since the local contribution H_{local} acts on a single qubit only, it does not influence the entanglement dynamics and is, thus, not further specified.

Importantly, as of the RWA, for detuned qubits $\omega_A \neq \omega_B$ the Lamb-shift term consists of the local part only. Therefore entanglement generation is not featured by the QOME for detuned qubits [BFM10] (see 5.2 and Fig. 5.3, middle and lower panel). However, the exact dynamics obtained from the HOPS shows that for slightly detuned qubits entanglement *is* generated in a very similar manner as in the resonant case (see also Ref. [Fle+10; Ma+12; Eas+16; HS20a] for more detailed discussions on the severe consequences of the RWA on bipartite correlations). Assuming that the QOME provides a suitable approximation in some weak coupling regime, it seems contradictory that an infinitesimal change of the system parameters results in a significant change of the dynamics. The inconsistency can be resolved by recalling that a small detuning introduces a new very slow system time scale. Only for a decay time scale (inverse of the coupling strength) much larger than this slow system time scale, hence a sufficiently weak coupling, the RWA and therefore the QOME is

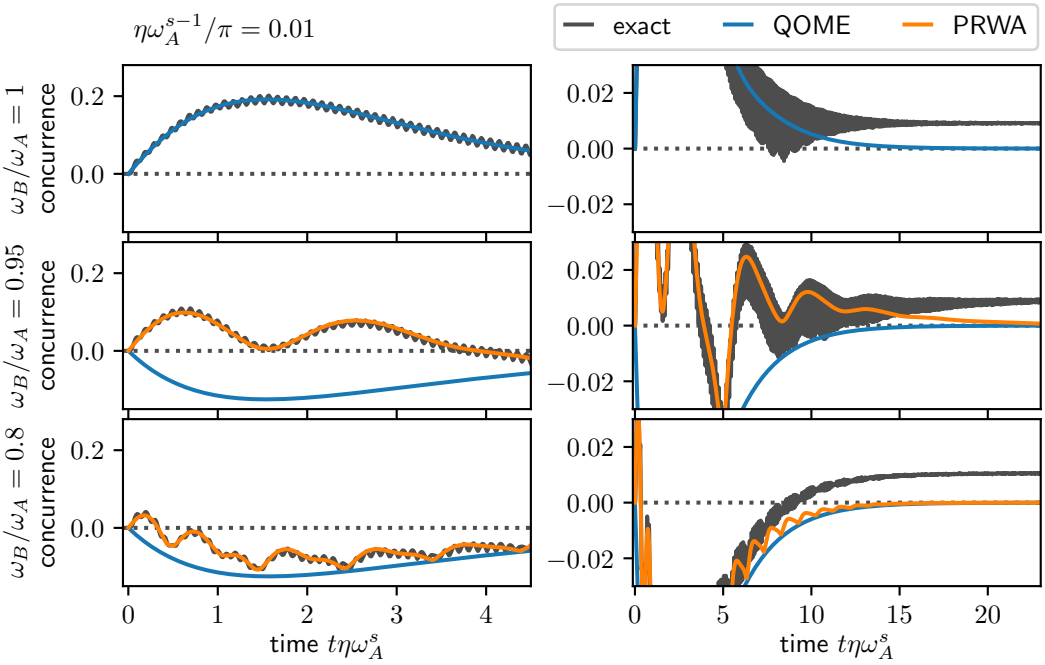

Fig. 5.2: The entanglement dynamics obtained from the QOME, the PRWA approach and the HOPS is shown for a sub-Ohmic environment ($s = 0.3$, $\omega_c = 10\omega_A$, $\eta\omega_A^{s-1}/\pi = 0.01$). The short-time dynamics (left column), long-time dynamics (right column) and different detunings ω_B/ω_A (rows) are considered. Note that the QOME and the PRWA coincide in the resonant case. Whereas the QOME does not predict the entanglement generation for detuned qubits, the PRWA approach shows overall agreement with the exact dynamics. Both master equations yield a vanishing asymptotic entanglement, which is in contrast to the exact finite value.

applicable. This highlights that the applicability of the QOME depends crucially on the system parameters. Only in the limit of zero coupling (in combination with a rescaled time, the so called scaling, van Hove or Davies limit) the QOME becomes exact [Dav76; SL07]. This also means, that for a sufficiently weak coupling strength the entanglement generation vanishes for any detuning, but remains in the resonant case. This feature can, to some extent, be seen by the exact dynamics for the weak coupling example shown in Fig. 5.2.

As of the severe problems for the detuned case, other perturbative approaches circumventing the RWA are considered next. A first one, very similar to the QOME, makes use of the RWA only partially [VJC13; Jes+15; TB15] which results in a master equation of GKSL kind also. The resulting equation, for any kind of detuning, involves the same non-local Lindblad operators occurring in the QOME for resonant qubits (see App. D.3). Henceforth, the Lamb-shift term is non-local and features entanglement generation also in the detuned case. The PRWA for the 2SBM rests on the assumption that $S(\omega_A) \approx S(\omega_B)$ which is best fulfilled for a small detuning.

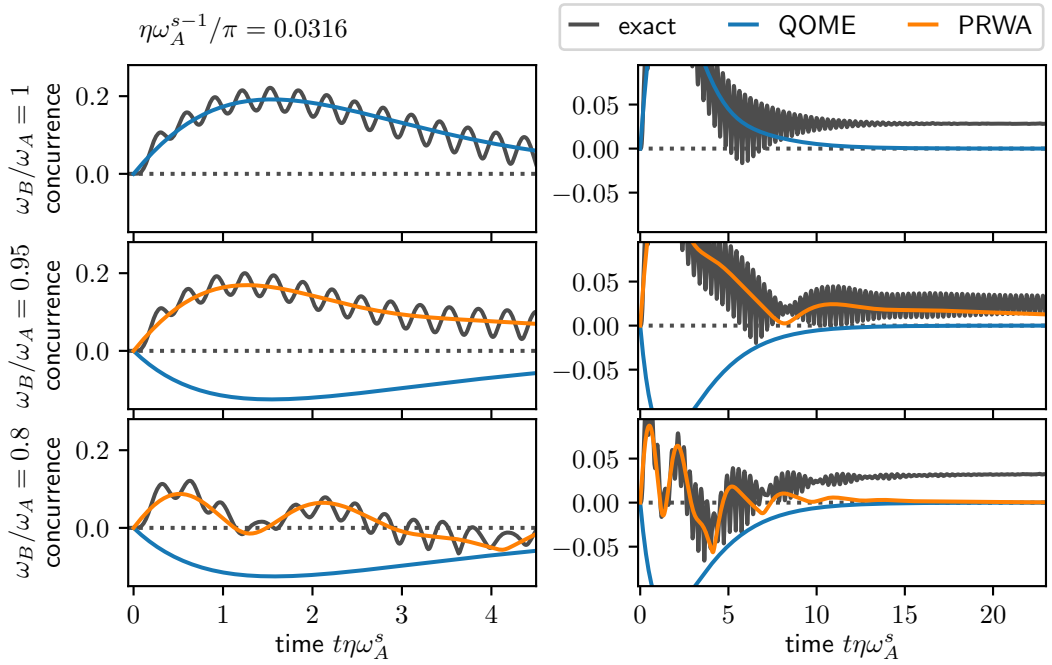

Fig. 5.3: The entanglement dynamics is shown for the same parameters as in Fig. 5.2, except for a larger coupling strength $\eta\omega_A^{s-1}/\pi = 0.0316$. As expected, larger deviations from the exact dynamics are evident. For the initial dynamics the PRWA still yield acceptable results.

The initial entanglement dynamics obtained from the PRWA master equation agrees quantitatively, up to some fast oscillation, with the exact dynamics obtained by the HOPS method (see Fig. 5.2 and Fig. 5.3). The fast superimposed oscillation are not captured because the PRWA still neglects some secular terms. Keeping all secular terms yields the RFE considered next. Both, the QOME and the PRWA approach yield a vanishing asymptotic entanglement which is in disagreement with the exact dynamics.

5.1.2 The Redfield Equation

It has been argued that for an initial product state of the system and the environment a physically consistent reduced dynamics is necessarily completely positive [Pec94; AL07]. Consequently, if the reduced dynamics is governed by a master equation, that master equation needs to be of GKSL form [Lin76]. Since the RFE (see App. D.1) is not of that form, at first glance it may disqualify as a suitable evolution equation. However, in terms of a perturbative treatment of the microscopic open system Hamiltonian [Eq. 2.1], the RFE involves less approximations compared to the QOME / PRWA. Therefore, although positivity of the reduced state is not guaranteed, the resulting dynamics can be expected to approximate the exact dynamics with higher accuracy. For two qubits and a common Lorentzian environment, we have confirmed this expectation in Ref. [HS20a] (not included here). Notably, when also using time

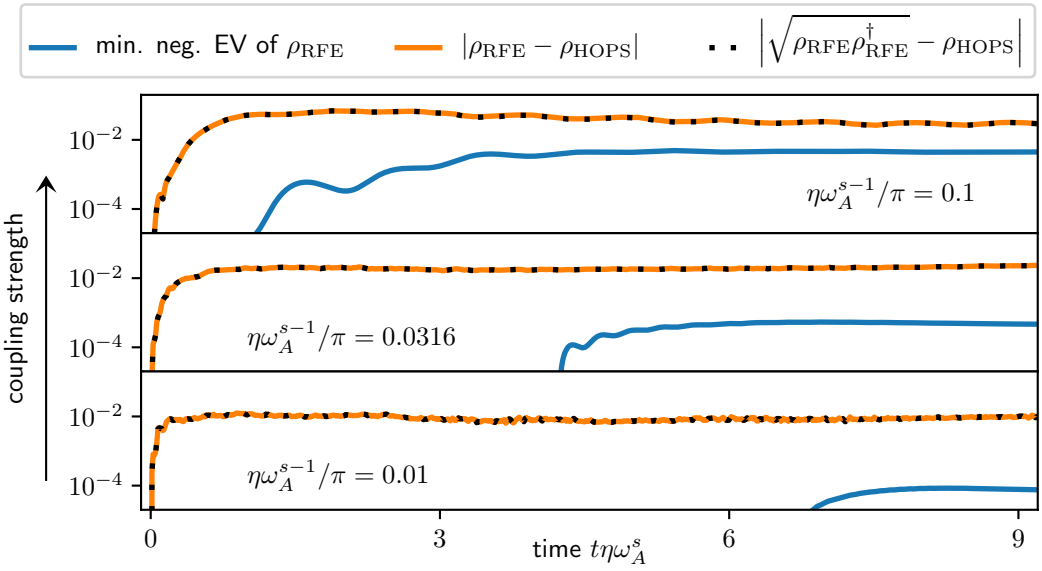

Fig. 5.4: The absolute value of the smallest negative eigenvalue is shown (blue lines) along with the error of the reduced state obtained from the RFE (orange lines). The error is quantified by means of the Hilbert-Schmidt-norm. Since the negative contribution to the reduced density matrix is small compared to the error, the matrix $\sqrt{\rho\rho^\dagger}$ which is positive by construction, approximates the exact state on the same level of accuracy (black dots). The same environmental parameters as in Fig. 5.2 were used.

dependent coefficients for the RFE (see also App. D.1), we found that a violation of positivity occurs only in the regime where the Redfield formalism is not applicable anyway. Therefore, the violation of positivity should not be seen as a defect but rather as a hallmark signaling the breakdown of the involved approximations [HS20a].

Unfortunately, for (sub-) Ohmic environments, as considered here, this feature is missing. It can be seen in Fig. 5.4 that the reduced state develops a negative eigenvalue after some time, even in the regime where the error between the perturbative RFE and the exact HOPS dynamics is small (here $\approx 1\%$). For such "states" with a negative eigenvalue it is ambiguous to calculate the concurrence. However, the plots in Fig. 5.4 also reveal that the magnitude of the negative eigenvalue remains significantly smaller than the error of the Redfield dynamics. It is, thus, consistent within a perturbative treatment to use the positive matrix $R := \sqrt{\rho\rho^\dagger}$ as approximation for the reduced state and estimate the concurrence based on R (see Fig. 5.5 for an example). The deviation of ρ and R from the exact state, shown in Fig. 5.4, is indistinguishable. As a remark, R is not necessarily normalized. However, the deviation of the norm from unity is of the order of the negative eigenvalues.

Including these considerations when quantifying the entanglement by means of the concurrence, the dynamics shown in Fig. 5.6 confirms that the high degree of accuracy of the RFE also holds for the sub-Ohmic environment considered here.

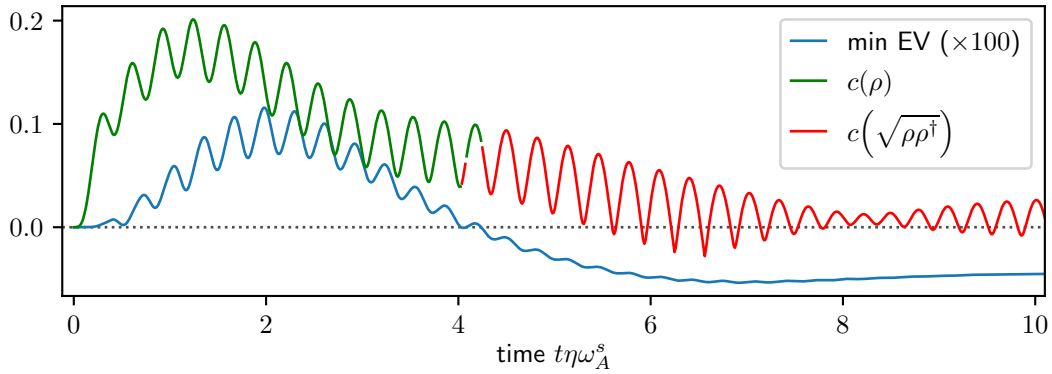

Fig. 5.5: The evolution of the concurrence and the smallest eigenvalue (scaled by a factor of 100) of the "reduced state" obtained using the RFE with time dependent coefficients is shown. When the eigenvalue turns negative, it is consistent within the perturbative treatment to base the concurrence on the positive matrix $\sqrt{\rho\rho^\dagger}$ which coincides with ρ for positive ρ. The same environmental parameters as in Fig. 5.2 were used with $\eta\omega_A^{s-1}/\pi = 0.0316$.

In particular, the initial build-up of entanglement agrees very well with the exact dynamics, independent of the detuning. In contrast to the PRWA, the fast oscillations are featured with high precision. Although the asymptotic entanglement is non-zero, it deviates from the exact value. Notably, the exact value of the asymptotic entanglement increases linearly with the coupling strength (see Sec. 5.4). So does the overall error of the RFE, with or without time dependent coefficients, which is reflected especially by the accuracy of the long-time dynamics [HS20a]. As a consequence, even though the RFE is the most accurate among the perturbative approaches considered here, it cannot predict the dependence of the asymptotic state on the coupling strength correctly. That is, the slope of the linear dependence of the asymptotic entanglement on the coupling strength is not accessible by the RFE.

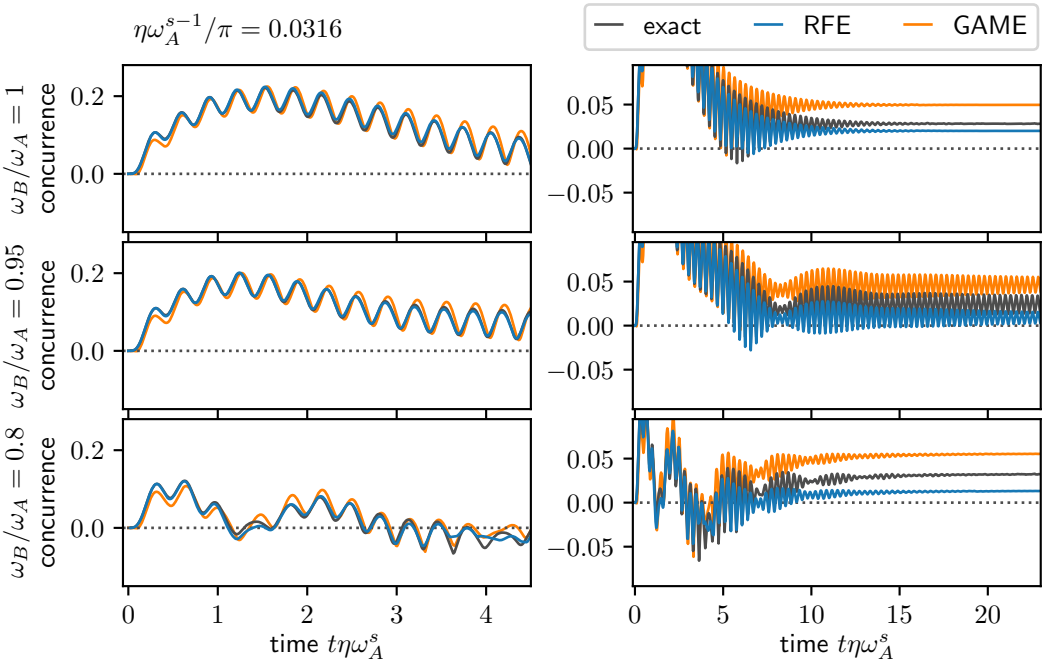

Fig. 5.6: The entanglement dynamics obtained from the RFE ($\rho \to \sqrt{\rho\rho^\dagger}$), the GAME and the exact HOPS is shown for the same parameters as in Fig. 5.3. For all three detuning parameters the RFE matches the exact dynamics very well over a significant period of time. For longer times deviations become apparent. Although slightly less accurate, the GAME yields similar results.

5.1.3 Geometric-Arithmetic Master Equation

In a recent publication the failure to quantify entanglement of a non-positive state in an approximative sense has been addressed as well [Dav20]. The proposed GAME (see also App. D.5) modifies the RFE such that it becomes a master equation of GKSL type. Crucially, the environmentally induced unitary influence on the system is identified from the RFE before the additional approximation is applied. The justification of the GAME is based on the relaxation time scale in the interaction picture, roughly given by the inverse of the coupling strength, and properties of the SD only. In contrast to the QOME, the particular spectrum of the system Hamiltonian is irrelevant. It is, thus, expected and confirmed in Fig. 5.6 that the entanglement generation is well captured for any detuning of the qubits. The GAME mimics also the fast oscillations of the entanglement dynamics, however, slightly less accurate compared to the positive matrix constructed from the RFE dynamics (see Fig. 5.7). Since the GAME is based on the RFE, it is consistent that the asymptotic entanglement deviates from the exact value on the same scale as the RFE result (see Fig. 5.6), although the value is overestimated. The comparison with the GAME results in the conclusion that the positivity issues related to the quantification of entanglement can be cured slightly more accurate using the Redfield formalism with $\sqrt{\rho\rho^\dagger}$ approximating the reduced state than applying the additional approximation invoked by the GAME.

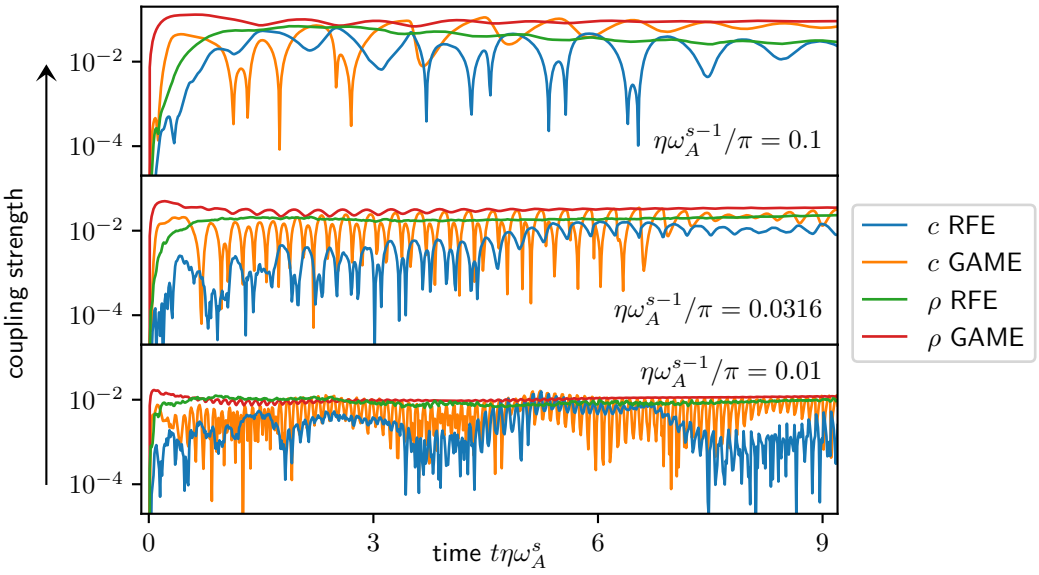

Fig. 5.7: The absolute error of the concurrence and the reduced state, quantified by means of the Hilbert-Schmidt-norm, is shown for the RFE and the GAME respectively. For the RFE $\sqrt{\rho\rho^\dagger}$ is used as approximation for the reduced state. For both approaches, the error of the concurrence (blue and orange lines) exceeds the error of the state (green and red lines) only marginally. The RFE is slightly more accurate compared the GAME. Nonetheless, the GAME outperforms the other GKSL kind equations considerably (not shown here).

5.1.4 The Coarse-Graining Master Equations

An alternative path towards a master equation for the microscopic model which assures positive dynamics is the so-called coarse-graining procedure [SB08; BFM10; Maj+13] (see also App. D.4). It has been proposed precisely with the aim to overcome the limitations due to the RWA. For two detuned qubits the generation of entanglement has been demonstrated using such a CGME [BFM10]. However, the quantitative comparison for a sub-Ohmic environment with $s = 0.3$ and $\omega_c = 10\omega_A$ (see Fig. 5.8 and Fig. 5.9) shows that the CGME does not reach the accuracy of the PRWA and the GAME. The error is related to the applicability condition $\tau_{\mathrm{env}} \ll \tau \ll \tau_{\mathrm{ind}}$ discussed in App. D.4 and Ref. [HS20a]. Since the timescale of the induced dynamics can be estimated from the exact entanglement dynamics, the separation of time scales can be checked explicitly. For the case with $\eta\omega_A^{s-1}/\pi = 0.01$ (Fig. 5.8) it follows $\tau_{\mathrm{ind}} \approx 0.5/(\eta\omega_A^s) \approx 16\omega_A^{-1}$. Although the decay time of the BCF scales with the cutoff frequencies $\tau_{\mathrm{env}} \sim \omega_c^{-1}$ the particular time at with the BCF has decayed over, for example, 2 orders of magnitude is $\tau_{\mathrm{env},2} \approx 10^{2/(s+1)}\omega_c^{-1}$. For the example considered here it follows $\tau_{\mathrm{env},2} \approx 3.5\omega_A^{-1}$. Obviously, there exists no coarse graining parameter τ such that a clear separation of the three timescales is justified. For the even stronger coupling $\eta\omega_A^{s-1}/\pi = 0.0316$ shown in Fig. 5.9 the time scale of the dynamics $\tau_{\mathrm{ind}} \approx 5\omega_A^{-1}$ becomes even smaller, which is directly reflected in a larger error.

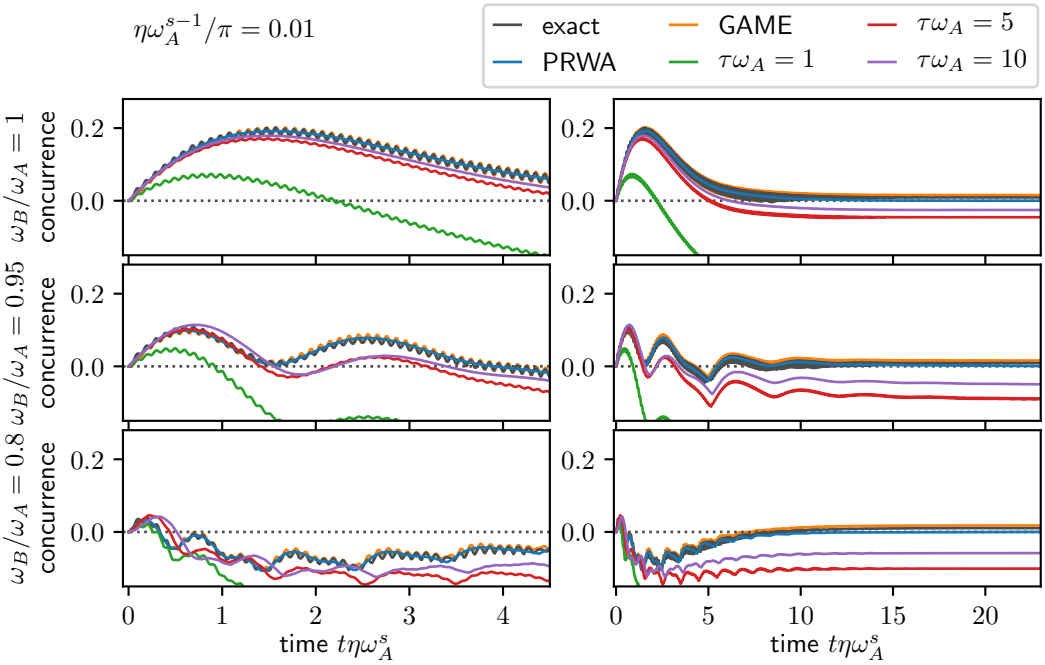

Fig. 5.8: The entanglement dynamics of the CGME is shown for comparison with the PRWA, the GAME and the exact dynamics (same environmental parameters as in Fig. 5.2). Since the QOME is applicable in the resonant case it is not surprising that for large coarse-graining parameters τ the CGME yields good results, too. For the detuned case the entanglement generation is still visible, in contrast to the QOME (not shown). However, the PRWA and the GAME agree better with the exact results.

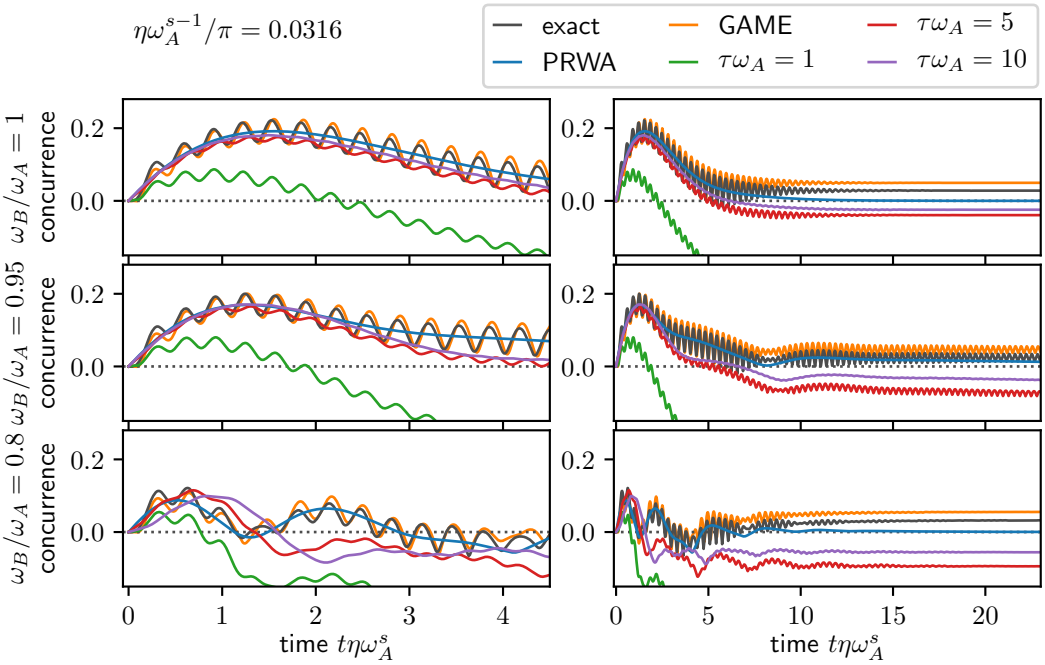

Fig. 5.9: The same plot as in Fig. 5.8 but with a stronger coupling η. The insufficient separation of time scales (see the main text) becomes visible even more in terms of the inaccurate dynamics. For the largest detuning considered $\omega_B/\omega_A = 0.8$, no coarse graining parameter τ yields in an acceptable agreement for the dynamics.

5.1.5 Summary

As expected, the approach with the least approximations, namely the RFE with time dependent coefficients, yields the most accurate results for the entanglement dynamics of two qubits coupled to a common sub-Ohmic environment. Positivity violations can consistently be healed by using the positive matrix $\sqrt{\rho\rho^\dagger}$ to estimate the concurrence. The PRWA, which coincides with the QOME in the resonant case, yields the correct overall dynamics while missing faster oscillations. The CGME is less appropriate for the set of parameters considered here. The recent GAME outperforms the other GKSL type master equations in terms of accuracy. Even the fast superimposed oscillation are captured, however, slightly less accurate compared to the RFE.

Both, the PRWA master equation as well as the GAME qualify as a suitable approximation scheme to describe the entanglement dynamics of the 2SBM, also for detuned qubits. As of the GKSL structure of the master equation the unitary as well the dissipative contribution can be calculated explicitly (see App. D). This allows one to use these approaches together with the exact results to elucidate the influence of the counterterm on the entanglement dynamics in the next section. Notably, none of the perturbative approaches predicts the asymptotic value of the entanglement correctly. It will be shown in Sec. 5.4 that the exact asymptotic entanglement scales linearly with the coupling strength. Although the RFE as well as the GAME show a linear behavior, too, they cannot predict the slope correctly. This is in fact expected since the overall error of the perturbative approaches scales linearly with the coupling strength, too [FC11; HS20a; Dav20; Tup+21], i.e., the reduced state, and with that the entanglement dynamics, is correct up to zeroth order only.

5.2 Influence of the Counterterm

To recapitulate the expression for the counterterm, which is intended to compensate the environmentally induced unitary effect on the system dynamics, a particle with position q and momentum p moving in a potential $V(q)$ and coupled to a set of harmonic oscillators with position (momentum) x_λ (p_λ) is considered. The linear coupling $-\sum_\lambda F_\lambda(q)x_\lambda$ to the environmental modes does not only result in damping but also contributes to the potential affecting the particle. It has been argued that in the adiabatic regime (instantaneous adjustment of the environmental modes to the particle position) the effective potential becomes [Wei08]

$$V_{\text{eff}}(q) = V(q) - \sum_\lambda \frac{F_\lambda(q)^2}{2m_\lambda\omega_\lambda^2} \,. \tag{5.5}$$

For a mode independent coupling operator $F_\lambda(q) = c_\lambda F(q)$, as in Eq. (5.1), the Hamiltonian

$$H = \frac{p^2}{2M} + V(q) + \sum_\lambda \left[\frac{p_\lambda^2}{2m_\lambda} + \frac{m_\lambda \omega_\lambda^2}{2} \left(x_\lambda - \frac{c_\lambda}{m_\lambda \omega_\lambda^2} F(q) \right)^2 \right] \tag{5.6}$$

compensates the change of the potential in the adiabatic regime.

It is plausible that the same line of reasoning holds true, too, when casting the above Hamiltonian to the more abstract form of the 2SBM Hamiltonian [Eq. (5.1)], as assumed also in Ref. [KA14]. In that case the induced change of the potential corresponds to the so-called Lamb-shift Hamiltonian contributing to the system Hamiltonian. Expressions for this Lamb-shift Hamiltonian can be deduced from the perturbative master equations considered in the previous Sec. 5.1 and are given explicitly for the PRWA [Eq. (D.23)] and the GAME [Eq. (D.42)] in the Appendix. In the adiabatic regime it is expected that this unitary environmental influence is compensated by the so-called counterterm H_c corresponding to the above change of the potential. Therefore, H_c is said to renormalize the system Hamiltonian. Using the relations $g_\lambda \sqrt{2 m_\lambda \omega_\lambda} = c_\lambda$ and $L = -F(q)$ yields as general expression

$$H_\mathrm{c} := \sum_\lambda \frac{c_\lambda^2 F(q)^2}{2 m_\lambda \omega_\lambda^2} = \sum_\lambda \frac{g_\lambda^2}{\omega_\lambda} L^2 = \frac{1}{\pi} \int_0^\infty \mathrm{d}\omega \, \frac{J(\omega)}{\omega} L^2 \, . \tag{5.7}$$

For the class of (sub-) Ohmic SD, as given in Eq. (5.2), the counterterm evaluates to

$$H_c = \frac{1}{\pi} \eta \omega_c^s \Gamma(s) L^2 \, . \tag{5.8}$$

It follows that if the entanglement generation of two non-interacting qubits in contact with a common environment is primarily due to the environmentally induced unitary interaction, i.e., the Lamb-shift Hamiltonian, as indicated in the previous Sec. 5.1, then it is expected that including the counterterm will suppress the generation of entanglement in the adiabatic regime. In the following we will show and explain that this is indeed the general behavior. However, for a deep sub-Ohmic environment ($s < 0.5$) the adiabatic regime is reached much slower compared to the Ohmic case, i.e., a significantly larger cutoff frequency ω_c is required to reach the regime where the counterterm cancels the Lamb-shift Hamiltonian effectively. Remarkably, for two *resonant* qubits and a deep sub-Ohmic environment we report the anomalous behavior that even in the adiabatic limit ($\omega_c \to \infty$) entanglement generation due to the Lamb-shift Hamiltonian remains significant when including the counterterm in the microscopic model. Thus, an effective cancellation is never observed.

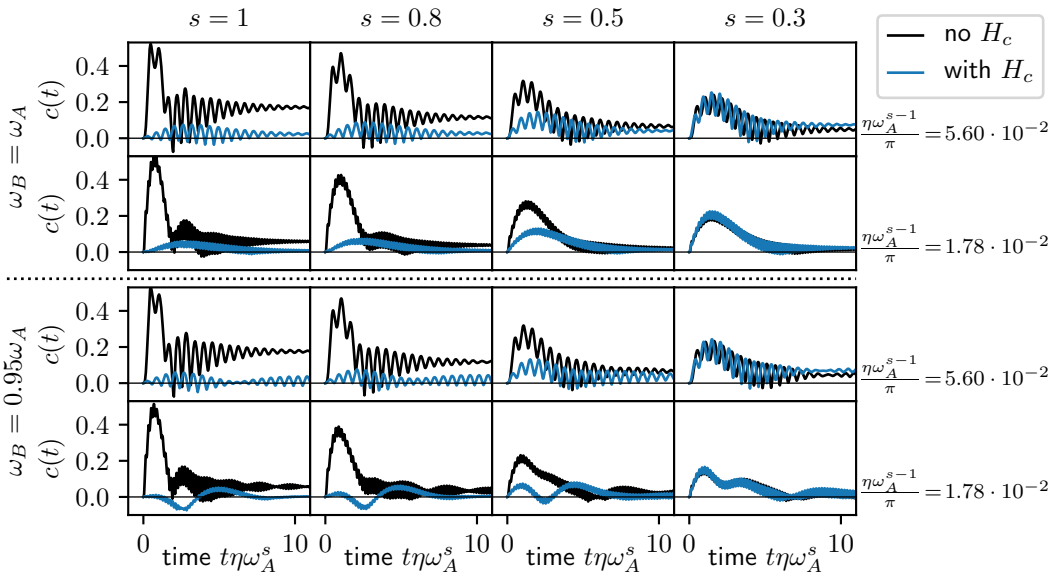

Fig. 5.10: The influence of the counterterm H_c on the entanglement dynamics for two qubits, distinguishing the resonant (upper panels) and the detuned case (lower panels), is shown. The parameter s of the (sub-) Ohmic environment ($\omega_c = 10\omega_A$) is lowered from left to right. Also, two different coupling strengths η are considered. For the weak and intermediate coupling strength shown, an effect of the counterterm is evidently visible in the Ohmic case ($s = 1$), however, it diminishes in the deep sub-Ohmic regime.

The effect of the counterterm on the entanglement dynamics obtained from the exact HOPS propagation is shown in Fig. 5.10 for various parameters s of the SD, two different coupling strengths and detuned as well as resonant qubits. A preliminary look reveals that whereas for $s = 1$ and $s = 0.8$ the initial build-up of entanglement is suppressed significantly, the entanglement generation remains nearly unchanged for $s = 0.3$, independent of the other parameters under consideration. Since within the HOPS formalism it is not obvious how to distinguish between the unitary (Lamb-shift) and the dissipative influence of the environment, a clear relation between the unitary contribution and the counterterm cannot be established at this stage.

Thus, to further enlighten the relevant mechanisms, we focus on weak coupling where perturbative approaches (see Sec. 5.1 and App. D), with a clear expression for the Lamb-shift and the dissipative contribution, are applicable. In that way the effect of the Lamb-shift Hamiltonian and the dissipator can be considered separately. The top row in Fig. 5.11 shows, again, the entanglement dynamics without the counterterm (gray lines) where a significant amount of entanglement generation is observed on an initial time scale. Note that the general case of two detuned qubits is considered. This initial phase coincides well with the joint unitary dynamics of the system and the Lamb-shift Hamiltonian (green lines), yielding the periodic entanglement dynamics shown in the middle row of Fig. 5.11. This allows for the conclusion that the initial major build-up of entanglement has its origin in

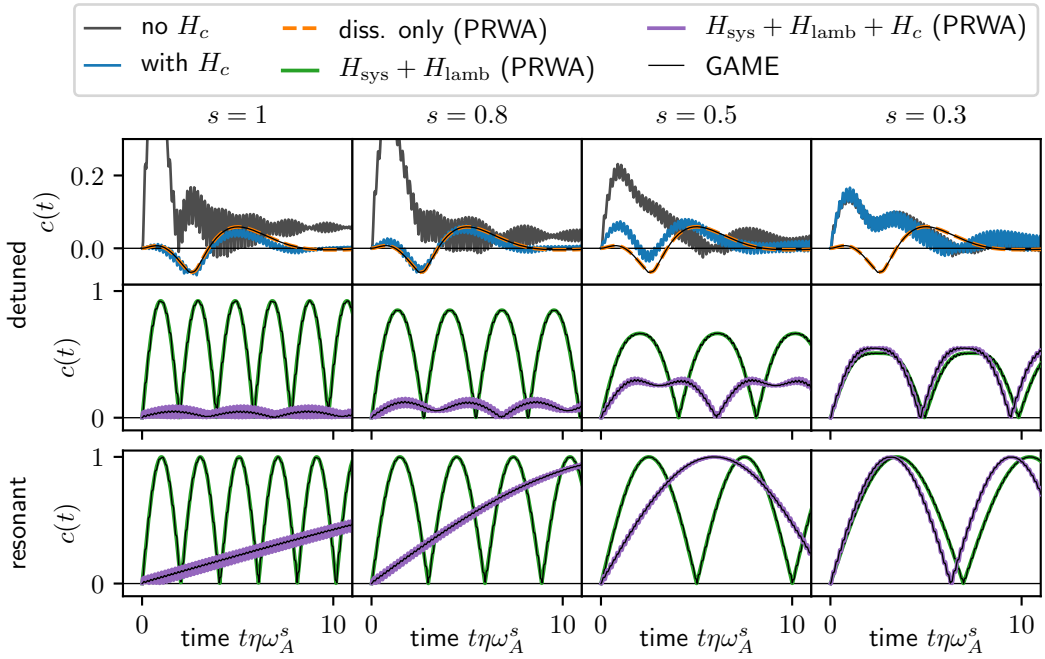

Fig. 5.11: The entanglement dynamics of the 2SBM (upper row, with and without H_c), and the entanglement due to the joint unitary dynamics of the system and Lamb-shift Hamiltonian, with and without H_c, is shown (detuned qubits: middle row, resonant qubits: lower row). If the exact entanglement dynamics including the counterterm (blue lines) is well mimicked by the action of the system Hamiltonian and the dissipator only (orange dashed lines), it can be concluded that the counterterm compensates the induced Lamb-shift contribution to some extend. As shown, the degree of compensation depends crucially on the parameter s of the SD. Further, the compensation is shown consistently by the joint unitary dynamics. The parameters for the 2SBM read $\eta\omega_A^{s-1}/\pi = 0.0178$, $\omega_c = 10\omega_A$ and, for the detuned case, $\omega_B = 0.95\omega_A$.

the environmentally induced Lamb-shift Hamiltonian. The additional dissipative effects reduce the amount of entanglement over time. Including the counterterm to the unitary contribution (purple lines) has different effects depending on the parameter s of the SD. Whereas for the Ohmic case ($s = 1$) the amplitude of the periodic entanglement pattern is suppressed significantly, it is marginally influenced in the deep sup-Ohmic regime ($s \lesssim 0.5$). This is consistently reflected by the exact entanglement dynamics including the counterterm (blue lines) which, in the Ohmic case, is mimicked well by the entanglement dynamics under the action of the *dissipator only* (dashed orange lines), which means that the Lamb-shift Hamiltonian and the counterterm nearly cancel each other. In contrast, for the deep sub-Ohmic regime, the dissipator-only dynamics behaves entirely different compared to the exact dynamics including the counterterm, thus, the counterterm does note compensate the induced Lamb-shift contribution.

Before we explain this behavior, several remarks are worth noting. First, as shown by the bottom row of Fig. 5.11, for resonant qubits the entanglement dynamics

due to the joint unitary evolution including the counterterm ($H_{\mathrm{sys}} + H_{\mathrm{lamb}} + H_c$, purple lines) nearly reaches one. This is in contrast to the detuned case where the amplitude of the entanglement dynamics becomes small. For the Ohmic case $s = 1$, however, the rate at which entanglement is generated in the microscopic model including the counterterm is slow compared the case without the counterterm and, even more importantly, slow compared to the timescale of the dissipation. Thus, the generation of entanglement is suppressed effectively, as seen also for the exact dynamics shown in the upper row of Fig. 5.10. Notably, the rate at which the entanglement is generated, including the counterterm, increases while decreasing s. For $s = 0.3$ this rate becomes even larger under the action of the counterterm. It seams reasonable that this rate corresponds to the difference between H_{lamb} and H_c and, thus, reflects how well the two terms compensate each other. A further investigation on this hypothesis follows below.

A second remark concerns the Lamb-shift Hamiltonian which generally depends on the system Hamiltonian. Consequently, the microscopic model with and without the counterterm yields different Lamb-shift Hamiltonians. However, since in the weak coupling regime the counterterm ($H_c \sim \eta$, Eq. (5.8)) is small compared to the system Hamiltonian, the leading order of the Lamb-shift Hamiltonian is independent of the counterterm.

As a final remark, the exact form of the Lamb-shift Hamiltonian and the dissipator depends on the particular master equation. Based on the discussion of the previous Sec. 5.1, the PRWA and the GAME may be employed which both yield to the agreeing results shown in Fig. 5.11. Since the RFE is not of GKSL form it does not reveal the unitary and the dissipative contribution unambiguously.

Nonetheless, the RFE can still be used to understand the compensation of the Lamb-shift Hamiltonian and the counterterm in general and to explain the sensitivity of that compensation on the parameter s of the SD. Using asymptotic coefficients, the RFE reads (see App. D.1)

$$\dot{\rho}(t) = -\mathrm{i}[H_{\mathrm{sys}}, \rho(t)] + \sum_i \left(F(\omega_i)[L_{\omega_i}\rho(t), L] + \mathrm{h.c.}\right) \ . \tag{5.9}$$

The real part of $F(\omega) = \int_0^\infty \mathrm{d}\tau\, \alpha_{\mathrm{bcf}}(\tau) e^{\mathrm{i}\omega\tau} = J(\omega) + \mathrm{i}S(\omega)$, which corresponds to the SD, accounts for dissipation whereas the imaginary part determines the unitary contribution, which is of relevance here. Under the assumption that the particular values $S(\omega_i)$ can be approximated by $S(0)$ (recall ω_i takes the value of all possible

transition frequencies of the system Hamiltonian) the corresponding contribution in the RFE becomes

$$\mathrm{i}\sum_i \left(S(\omega_i)[L_{\omega_i}\rho(t), L] + \mathrm{h.c.}\right) \approx -\mathrm{i}S(0)[L^2, \rho(t)] \,, \tag{5.10}$$

where it has been used that by definition $L = \sum_i L_{\omega_i}$.

Using the equivalent Cauchy principal value $\mathcal{P}$ expression for $S(\omega)$, which is based on the SD rather than the BCF,

$$S(\omega) = -\frac{1}{\pi}\mathcal{P}\int_{-\infty}^{\infty} \mathrm{d}\omega' \, \frac{J(\omega')}{\omega' - \omega} \,, \tag{5.11}$$

yields that the above approximate unitary contribution is exactly the negative of the counterterm. Therefore, given that $S(\omega_i) \approx S(0)$ holds the unitary contribution in the perturbative treatment (Lamb-shift term) is approximately canceled by the counterterm

$$H_{\mathrm{Lamb}} \approx S(0)L^2 = -\frac{1}{\pi}\int_0^{\infty} \mathrm{d}\omega' \, \frac{J(\omega')}{\omega'} L^2 = -H_c \,. \tag{5.12}$$

For the class of (sub-) Ohmic SD the validity of the assumption $S(\omega_i) \approx S(0)$ depends on the parameter s in a very sensitive way. To see that, it is convenient to expand the function $S(\omega)$ around $\omega = 0$. Expressing $F(\omega)$ analytically and expanding the incomplete gamma function for small values $x := \omega/\omega_c$ yields (see App. B.2.1)

$$\begin{aligned} S(\omega) &= -\frac{\eta\omega_c^s\Gamma(s)}{\pi} e^{-x} f(s,x) \\ f(s,x) &= \begin{cases} 1 + sg(s,x)\Gamma(-s)|x|^s + \frac{sx}{s-1} + \mathcal{O}(x^2) & s < 1 \\ 1 - x\ln(|x|) + (1-e_\gamma)x + \mathcal{O}(x^2) & s = 1 \end{cases} \\ g(s,x) &= \cos(\pi s)\Theta(x) + \Theta(-x) \end{aligned} \tag{5.13}$$

where e_γ denotes the Euler–Mascheroni constant and Θ the Heaviside step function. The expansion shows that the leading order behaves like $|w|^s$ in the sub-Ohmic and $w\log(|w|)$ in the Ohmic case (see Fig. 5.12 for examples). In addition, for positive x the term $\sim |x|^s$ changes its sign at $s = 0.5$ which results in a pointed minimum at $S(0)$ for $s < 0.5$.

It follows that the approximation $S(\omega_i) \approx S(0)$ becomes better when increasing ω_c since $f = 1 + \mathcal{O}(|\omega/\omega_c|^s)$. However, the approximation becomes significantly worse when changing from the Ohmic ($s = 1$) to the deep sub-Ohmic ($s < 0.5$) regime. This behavior explains that the cancellation of the Lamb-shift by the counterterm

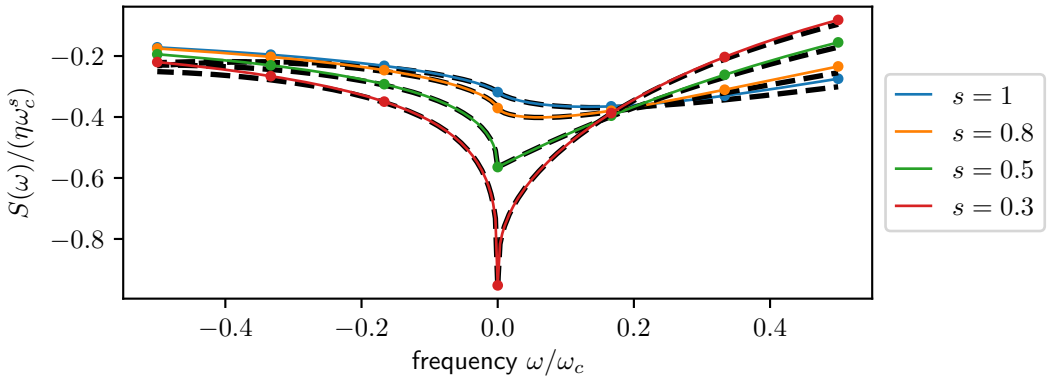

Fig. 5.12: The behavior of the imaginary part of the half-sided Fourier transform of the BCF $S(\omega)$ is shown for different parameters s and $\omega_c = 10\omega_A$. (solid lines: exact analytic expression, dashed lines: expansion around zero, dots: numeric Fourier integral)

fails spectacularly for small s and the cutoff frequency $\omega_c = 10\omega_A$ considered in the above examples.

Nonetheless, the above reasoning suggests that in the limit $\omega_c \to \infty$, where the approximation $S(\omega_i) \approx S(0)$ becomes exact, the counterterm should truly cancel the Lamb-shift contribution also in the deep sub-Ohmic regime. For two detuned qubits this behavior is confirmed by the example shown in the left column of Fig. 5.13. The entanglement dynamics (red lines) approaches the purely dissipative dynamics (blue lines) when increasing the cutoff frequency. The unitary effect of the Lamb-shift H_{lamb} (green lines) is compensated by the counterterm H_c (orange lines) where the degree of compensation increases with the cutoff frequency ω_c (top to bottom). Therefore, the entanglement induced by the Lamb-shift Hamiltonian vanishes in the adiabatic limit $\omega_c \to \infty$.

Remarkably, this does not hold true for resonant qubits (see right column in Fig. 5.13). To affirm that this effect remains even in the adiabatic limit it can be argued as follows. The remaining Hermitian contribution $H_{\text{Lamb}} + H_c$ scales in lowest order like

$$\Delta S = S_0 - S(\omega_A) \sim S_0 \left(\frac{\omega_A}{\omega_c}\right)^s \tag{5.14}$$

which sets the timescale on which the remaining environmentally induced unitary interaction takes place. Obviously, increasing ω_c while keeping S_0 constant increases that timescale which could mean an effective cancellation if the damping takes place on a faster time scale. It turns out, however, that this is not the case since the damping rate γ, determined by the SD at ω_A, scales with ω_c in the same manner.

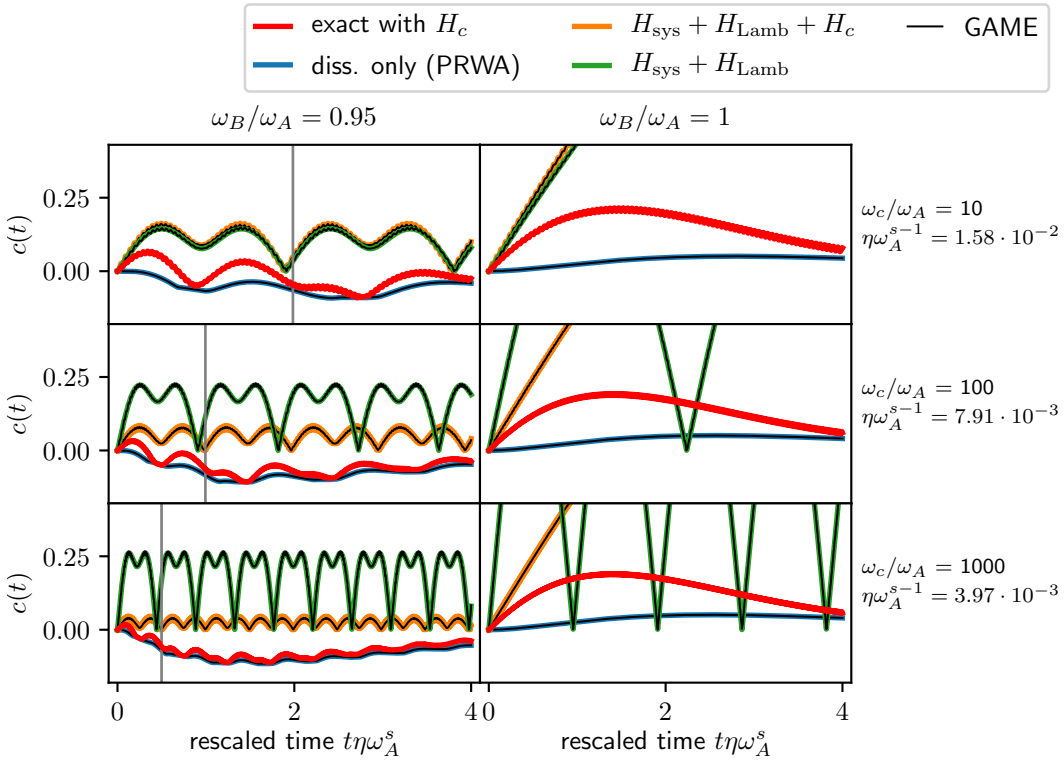

Fig. 5.13: The entanglement dynamics (including the counterterm) is shown (red lines) for a sub-Ohmic environment with $s = 0.3$ and $|S(0)|/\omega_A = 0.03 = \eta\omega_c^s\Gamma(s)/\omega_A/\pi$ while increasing the cutoff frequency ω_c from top to bottom, hence η decreases. As expected, for detuned qubits increasing ω_c results in a more effective compensation of the Lamb-shift contribution by the counterterm (orange lines). Consequently, the exact entanglement dynamics (red lines) approaches the dynamics obtained by the action of the dissipator only (blue lines). Remarkably, for resonant qubits (right column) this expectation is not fulfilled. In that case the joint unitary dynamics $H_{\mathrm{sys}} + H_{\mathrm{Lamb}} + H_c$ (orange lines) builds up entanglement on the same time scale as the dissipation takes place, independently of the cutoff frequency ω_c. The exact dynamics cannot be mimicked by the dissipator only dynamics (blue lines). This qualitative difference originates from the time scale set by the detuning which is independent of ω_c (gray vertical lines). Note, this time scale decreases on the rescaled time $t\eta\omega_A^s$ while increasing ω_c. Since the entanglement dynamics of the joint unitary part is periodic on that time scale, but the build-up takes place on the time scale set by $\Delta S \propto S_0$ (constant on the rescaled time), the generation of entanglement is effectively suppressed. In the limit of zero detuning that time scale becomes infinite. i.e., it is not present.´

This can be seen by expressing the coupling strength in terms of S_0 and expanding the SD in lowest order in ω_A/ω_c

$$\gamma \sim J(\omega_A) \sim S_0 \left(\frac{\omega_A}{\omega_c}\right)^s . \tag{5.15}$$

As a remark, in the adiabatic limit, the rate for the entanglement generation as well as the damping rate becomes infinitely slow. Therefore, taking the limit $\omega_c \to \infty$ while keeping S_0 constant makes sense only in combination with a rescaled time $t \cdot (\omega_A/\omega_c)^s$, similar to the scaling limit of the QOME.

In summary, we find the counter-intuitive result that for two resonant qubits and a sub-Ohmic environment the effect of the Lamb-shift contribution is not compensated by the counterterm, even in the limit $\omega_c \to \infty$ which is usually considered the adiabatic limit. Consequently, entanglement generation beyond the purely dissipative contribution remains for any ω_c. This, in particular, stays in contrast with the results presented in Ref. [KA14]. The authors claim that for sufficiently weak coupling the model including the counterterm (as in Eq. 5.6) does not result in any entanglement generation for the two qubits.

5.3 Strong Coupling

In this section we calculate the entanglement dynamics of the 2SBM beyond the perturbative regime. Noteworthily, the presumably exact treatment of the 2SBM by means of other numerical methods can be found in the literature with primary focus on the phase transition (delocalization to localization, see also next Sec. 5.4) [Ort+10; Bon13; WR14; HL16; Zho+18] as being a reminiscence of the well studied (single) SBM. In a recent work by N. Zhou et. al [Zho+18] noticeable difference between various approaches are addressed. Thus, we regard our exact results obtained utilizing the HOPS as a significant contribution to the field. This is further underlined by explicitly finding disagreement with path integral Monte Carlo results from Ref. [KA14] (not shown here). Besides that, the investigation of the dynamics of the 2SBM usually includes an explicit qubit-qubit interaction [Ort+10; WYS13] of an a-priory given strength. Here, however, we retain the case of no direct interaction where only the continuous environment mediates an effective interaction featuring the buildup of entanglement and its persistence. Of course, in case of including the counterterm [Eq. 5.8], a direct qubit-qubit interaction is present. Still, its strength is not a free parameter but scales with the coupling strength.

First, an environmental initial condition of zero temperature is considered, while varying the coupling strength, the detuning and the parameter s of the SD. The plots shown in Fig. 5.14 show various aspects. In general, a significant amount of entanglement builds up. The overall generation of entanglement is accompanied by oscillations with a time scale set by the system Hamiltonian, i.e., $\sim \omega_A^{-1}$, resulting in the known phenomenon of sudden death and revivals of entanglement [YE09; Maz+09; WYS13]. Recalling the discussion about the perturbative approaches (Sec. 5.1), for detuned qubits and a sufficiently weak coupling, entanglement is not generated. This tendency is seen already in the plots shown in Fig. 5.14. Beyond the weak coupling regime the detuning has only a minor influence on the entanglement dynamics. The kind of environmental model, i.e., sub-Ohmic ($s = 0.3$) or Ohmic, primarily effects the time scale of the initial entanglement dynamics. For the Ohmic

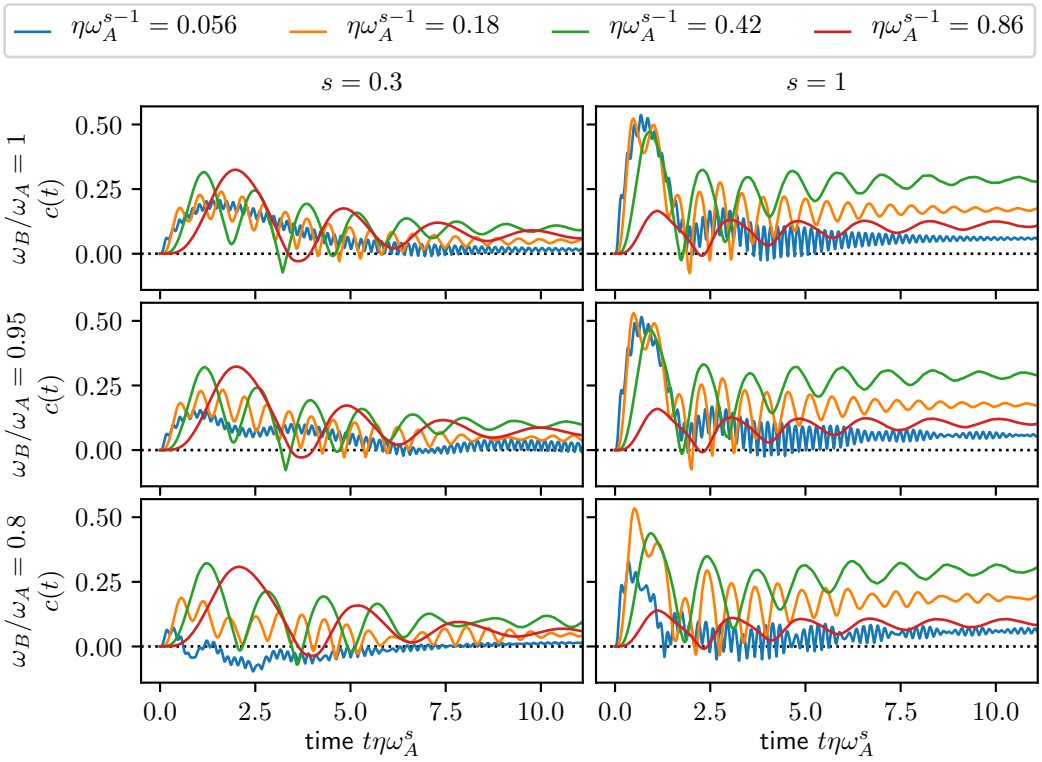

Fig. 5.14: The entanglement dynamics of the 2SBM is shown for a zero temperature initial environmental state and a fixed cutoff frequency $\omega_c = 10\omega_A$ while varying the coupling strength η, the detuning ω_B/ω_A and the parameter s of the SD. Except for the case of detuned qubits and weak coupling, due to the environmental influence a significant amount of entanglement develops, followed by oscillatory behavior and a non-vanishing asymptotic value.

environment, a full period of entanglement growth and decrease, due to the joint unitary effect of the system and the Lamb-shift Hamiltonian (compare Fig. 5.11), is visible before relaxational contributions dominate the dynamics. In case of the sub-Ohmic environment the entanglement build-up is slower which also results in a smaller maximum amount of entanglement being generated. This can be understood as follow. Whereas the relaxation towards the asymptotic state takes place on roughly the same time scale, the rate at which entanglement is generated initially can be inferred from the Lamb-shift Hamiltonian whose magnitude scales with $S(\omega)$ (imaginary part of the half-sided Fourier transform of the BCF). It is shown in App. B.2 that for small ω/ω_c the function $S(\omega)$ scales with $\eta\omega_c^s\Gamma(s)$. As a consequence, for the example shown in Fig. 5.14 choosing $\omega_c = 10\omega_A$, the magnitude of $S(\omega)$, and with that the rate at which entanglement is generated, differs roughly by a factor of two (see also Fig. 5.12) with respect to the sub-Ohmic and the Ohmic SD. In contrast, for a very strong coupling $\eta\omega_c^{s-1} \gtrsim 0.5$ and $\omega_c = 10\omega_A$ the sub-Ohmic environment features a larger amount of maximum entanglement compared to the Ohmic case. However, for strong coupling the overall dynamics hardly depends on the parameter s nor the detuning. In addition it is seen in Fig. 5.14 that the asymptotic entanglement exhibits a maximum (details in Sec. 5.4).

Next, the influence of the counterterm (see Sec. 5.2 for model details) beyond the weak coupling regime is shown in Fig. 5.15. As observed already for weak coupling, its effect for a sub-Ohmic environment is significantly less compared to an Ohmic one. In any case, rich entanglement dynamics is observed, featuring the initial build up of entanglement, followed by oscillatory behavior with complete loss of entanglement and a non-vanishing asymptotic value. In this sense the dynamics is very similar to the model without the counterterm. All of this is plausible because the parameters considered, i.e., strong coupling and a cutoff frequency which is not too large ($\omega_c = 10\omega_A$), are far away from the adiabatic regime.

Furthermore, the temperature dependence of the entanglement dynamics is shown in Fig. 5.16. In general, increasing the temperature of the initial environmental Gibbs state lowers the amount of entanglement which develops over time. This behavior seems intuitive since increasing the temperature amounts to more states contributing to the statistical mixture of the Gibbs state. Still, for the examples shown in Fig. 5.16, where the thermal energy is smaller or comparable to the single qubit energy $T \lesssim \omega_A$, initial entanglement build-up can be observed. Of course,

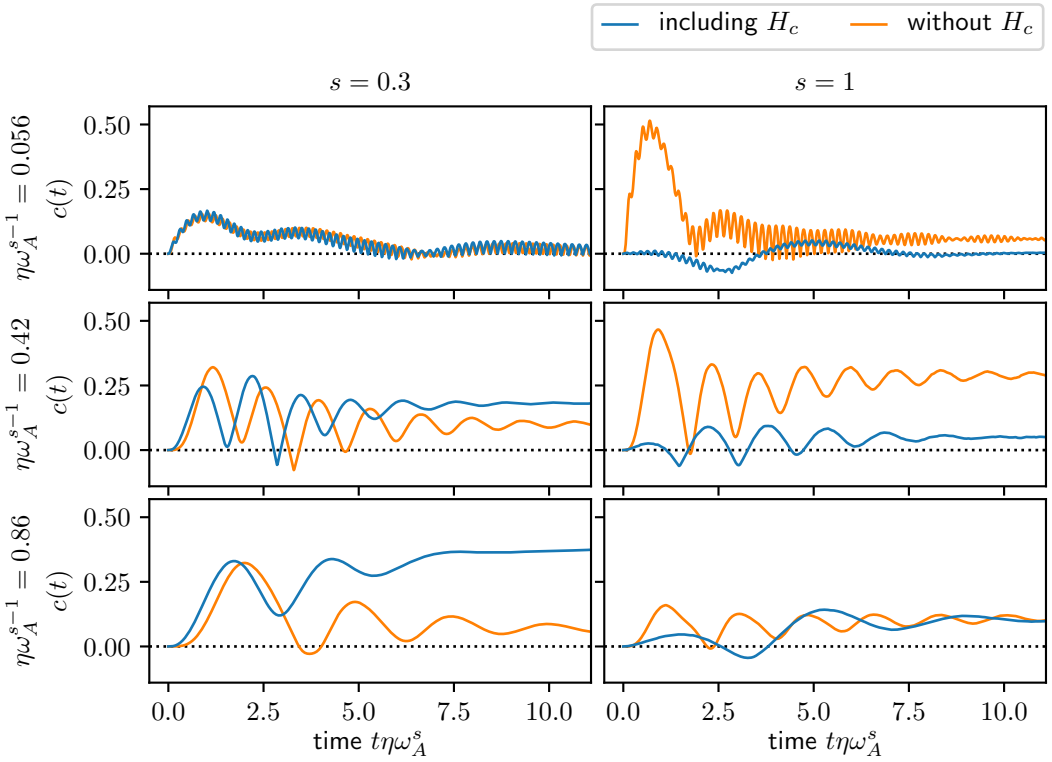

Fig. 5.15: The entanglement dynamics of the 2SBM is shown, highlighting the differences between the model with and without the counterterm. Here we show the general case of slightly detuned qubits $\omega_B/\omega_A = 0.95$ for a zero temperature initial environmental state and a cutoff frequency $\omega_c = 10\omega_A$. The expected suppression of entanglement generation can partly be observed for the Ohmic case ($s = 1$). However, in case of strong coupling and/or a sub-Ohmic SD, its effect is far from counteracting the build-up of entanglement.

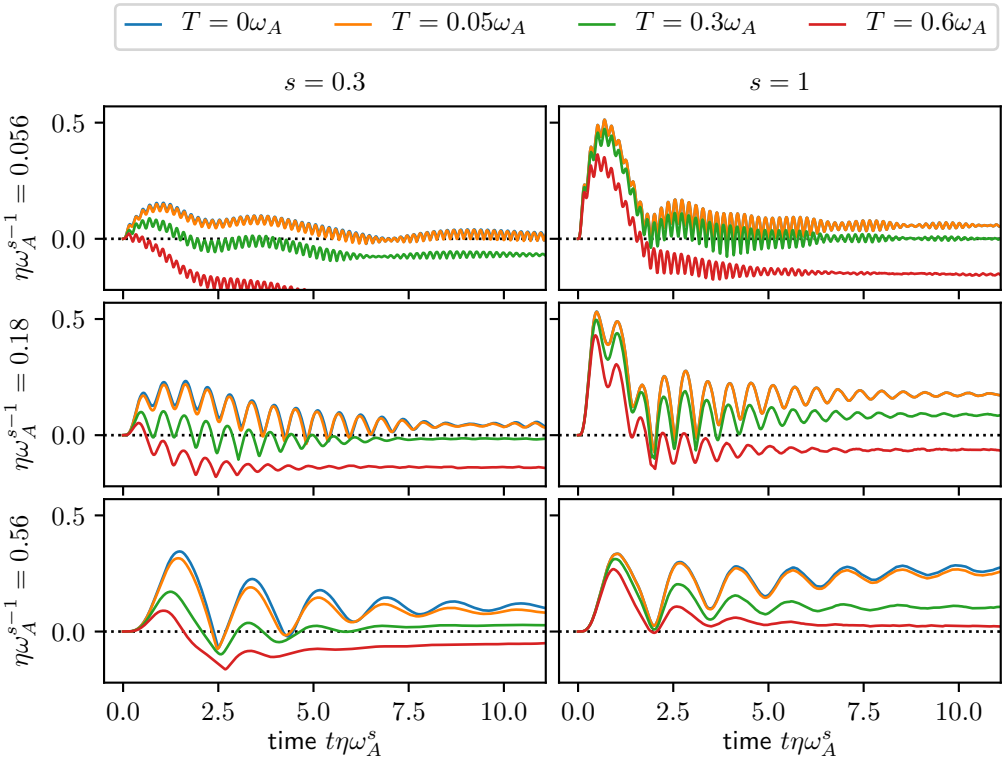

Fig. 5.16: The entanglement dynamics of the 2SBM is shown for different temperatures of the initial environmental Gibbs state. As in Fig. 5.15, slightly detuned qubits $\omega_B/\omega_A = 0.95$ and a cutoff frequency $\omega_c = 10\omega_A$ are chosen as example. The sensible tendency that increasing temperature results in less entanglement generation can be seen nicely.

revivals appear less prominent or not at all. Nonetheless, the calculation shows that environmentally induced entanglement generation is far from being a zero temperature phenomenon.

5.4 Asymptotic Entanglement

As already mentioned in the previous section and shown for example in Fig. 5.14, the two qubits relax towards an asymptotic state which exhibits entanglement. The properties of this so-called asymptotic entanglement are discussed in this section.

If the coupling is not too strong $\eta\omega_A^{s-1} \lesssim 0.3$ the plots in Fig. 5.17 suggest that in general the asymptotic entanglement increases linearly with the coupling strength, where in the limit $\eta \to 0$ the asymptotic entanglement vanishes. This seems plausible since it corresponds to the case of two non-interacting isolated qubits. This is also consistent with the widely used perturbative approach involving the full rotating wave approximation (RWA), which becomes exact in that limit of zero coupling strength (see also Sec. 5.1.1). It is known that the resulting QOME yields the local

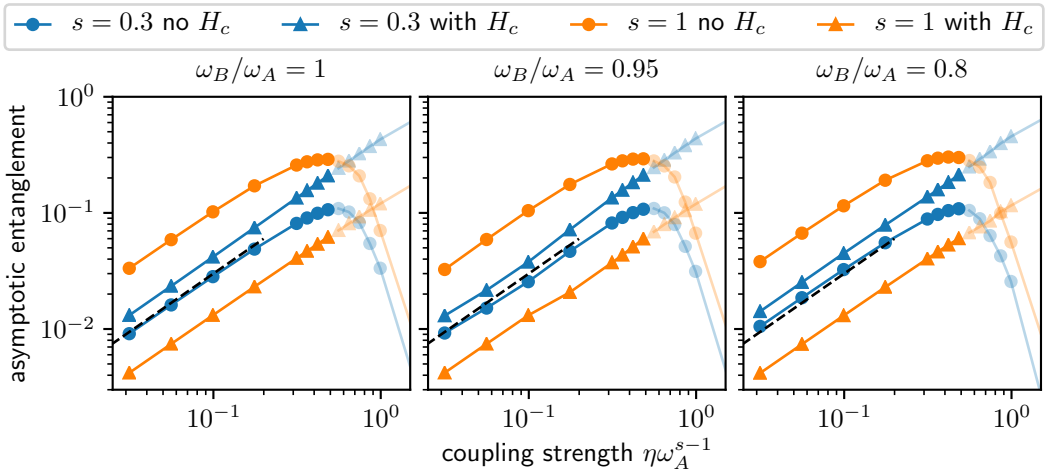

Fig. 5.17: The asymptotic entanglement (concurrence) is shown as a function of the coupling strength. The linear dependence (black dashed lines) in the weak coupling regime is well visible. Although the magnitude is effected when including the counterterm, remarkably, the linear dependence remains. Beyond the weak coupling regime, whereas a maximum is reached without the counterterm, the asymptotic entanglement increases further and eventually saturated when including the counterterm. Notably, the asymptotic behavior is largely independent of the detuning of the qubits, which does not hold true for the dynamics in general ($\omega_c = 10\omega_A$).

Gibbs ensemble as asymptotic state [BP07] which is, for two non-interacting qubits, a separable state.

The plots shown in Fig. 5.17 further reveal that the asymptotic entanglement is nearly independent of the detuning. This is remarkable when recalling that in the weak coupling regime the actual dynamics depends strongly on the detuning (see Fig. 5.14). In addition, the effect of the counterterm on the asymptotic entanglement is shown, too. Similar to the influence on the dynamics discussed in Sec. 5.2, for an Ohmic environment including the counterterm suppresses the asymptotic entanglement, here, by roughly a factor of 10. In contrast, in the sub-Ohmic case $s = 0.3$ the value is slightly increased, which seems counter intuitive, but has been explained in Sec. 5.2.

Beyond this linear regime, the presence of the counterterm results in a different qualitative behavior. Whereas without the counterterm the asymptotic entanglement reaches a maximum, it increases further and eventually saturates when the counterterm is present. Note, this qualitative difference is shown in light colors in Fig. 5.14 only, indicating that the results might not have fully converged yet in terms of numerics (see below). Nonetheless, the overall trend can be deduced. It is indeed plausible that the asymptotic entanglement for the model without the counterterm approaches zero when the coupling strength, and with that the interaction Hamiltonian, becomes large compared the system Hamiltonian. This can be seen when considering the very

crude approximation of simply neglecting the system Hamiltonian. For that case the reduced dynamics can be evaluated explicitly as for a general dephasing model [Gor+04]. Since the initial state considered here $\psi_0 = |\uparrow\uparrow\rangle$ is an eigenstate of the coupling operator $L \sim \sigma_z^A + \sigma_z^B$, the reduced state remains unchanged for that model. Thus, no entanglement generation can be observed. Note, this argument could be refined by treating the system Hamiltonian perturbatively, which is, however, out of scope here. In contrast, when including the counterterm, the system Hamiltonian cannot be neglected in the limit $\eta \to \infty$ because the counterterm scales with η, too, which gives rise to the qualitative difference between the two models.

As mentioned above, calculating the long-time dynamics in the very strong coupling regime turns our to be very demanding. In order to understand the difficulties and with that the degree of accuracy of the later plot showing the behavior of the asymptotic entanglement as a function of the coupling strength, special emphasize on the numeric convergence of the HOPS method are discussed next. Tightly connected, we show the single qubit expectation value $\langle \sigma_z^A \rangle$ which signifies the known phase transition from delocalization $\langle \sigma_z^A \rangle = 0$ to localization $\langle \sigma_z^A \rangle > 0$. Due to the qualitative differences, we distinguish between the sub-Ohmic and the Ohmic environment.

Sub-Ohmic Environment ($s = 0.3$) First of all, from the long-time dynamics shown in Fig. 5.18 we deduced that for any coupling strength the initial damped oscillations nearly vanish at $\tau_1 \eta \omega_A^s \approx 10$ (vertical dashed line). Further, for $\eta \omega_A^{s-1} \gtrsim 0.5$ another

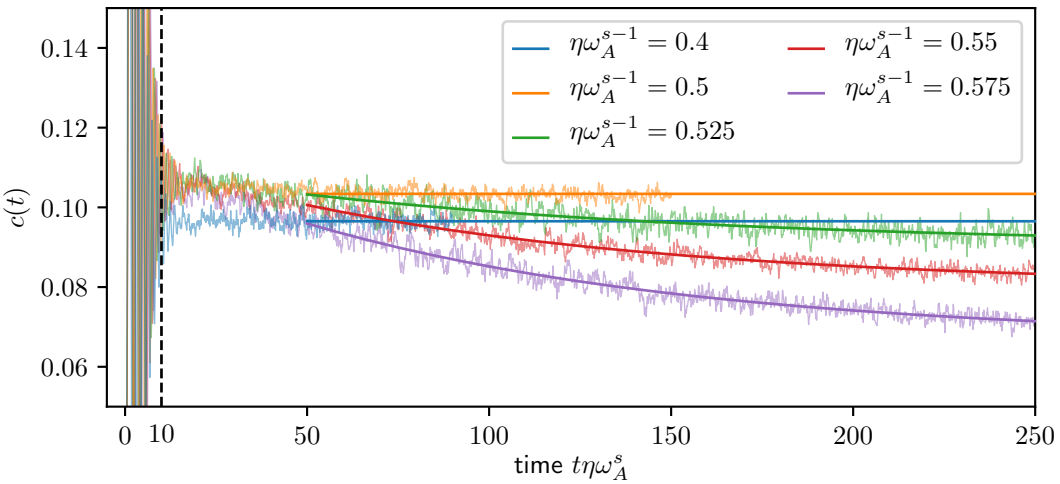

Fig. 5.18: The long-time dynamics of the concurrence is shown for a sub-Ohmic environment with $s = 0.3$. At $\eta_c \omega_A^{s-1} \approx 0.5$ the long-time dynamics reaches its largest value. Also, increasing the coupling strength beyond that value results in a qualitative change from quickly reaching the asymptotic value to a slow, presumably exponential decay. Here, quickly refers to the time scale of the damping of the initial oscillations. It is governed by the coupling strength and, thus, remains constant (≈ 10) with respect to the rescaled time $t\eta\omega_A^s$ ($\omega_B = \omega_A$, $\omega_c = 10\omega_A$).

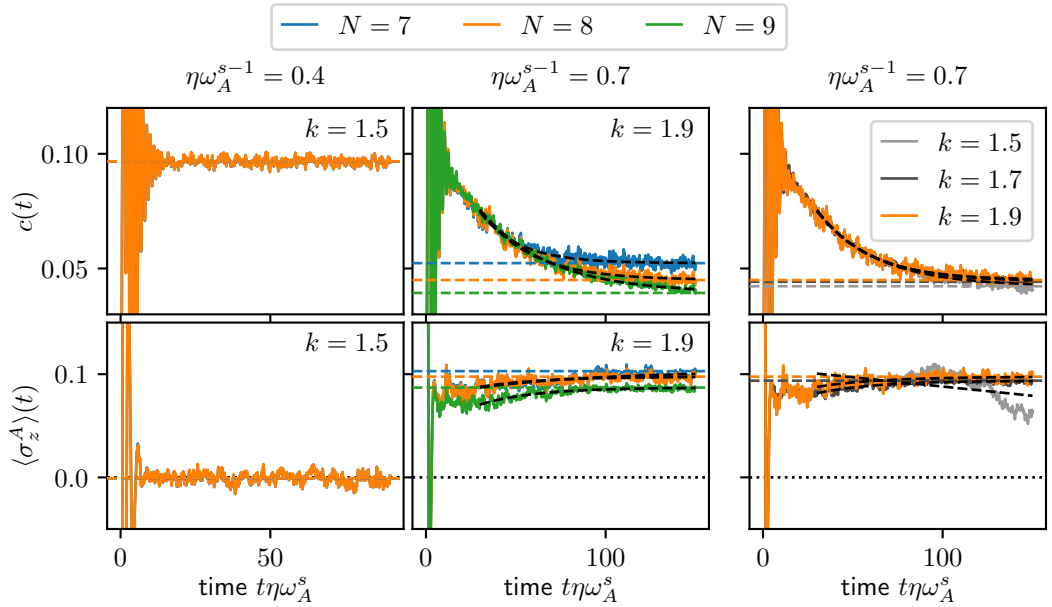

Fig. 5.19: Similar to Fig. 5.18, the long-time dynamics of the concurrence is shown (upper row, $s = 0.3$, $\omega_B = \omega_A$, $\omega_c = 10\omega_A$), here with emphasis on the sensitive dependence with respect to the accuracy of the BCF representation (number of exponential terms N). In the localized phase ($\eta\omega_A^{s-1} \gtrsim 0.5$) the long-time entanglement experiences a correction towards smaller values when using a more accurate representation, i.e., N is increased. In addition, the dynamics of $\langle\sigma_z\rangle$ is shown (lower row). The dependence on N seems not as crucial, however, an insufficient hierarchy depth k can yield in a faulty decay to zero. The dashed lines show the extrapolated asymptotic values.

kind of decay with an apparently larger time scale τ_2 emerges. The graphs shown in Fig. 5.18 motivate an estimation of the asymptotic entanglement by fitting an exponential behavior to the long-time dynamics such that

$$c(t) \approx c_\infty + c_1 e^{-t/\tau_2} \quad \text{for} \quad t \gg \tau_1 \,. \tag{5.16}$$

The appearance of this qualitatively new decay hints at the known delocalization/localized phase transition. This is underpinned by the behavior of the asymptotic spin polarization $\langle\sigma_z^A\rangle$ which becomes non-zero for coupling strengths where the exponential decay appears, too (see Fig. 5.21). Remarkably, the critical coupling strength amounts to the simple value of $\eta_c \approx 0.5\omega_A^{1-s}$.

Importantly, it is shown in Fig. 5.19 that the additional exponential decay, and with that the asymptotic entanglement, too, is very sensitive to the accuracy of the exponential representation of the BCF (see Sec. 3.2). Therefore, substantially more computational power is required when increasing the coupling strength $\eta\omega_A^{s-1}$ beyond 0.5 to obtained reliable results. In contrast, we observe that the required hierarchy depth k only increases moderately with the coupling strength.

Reiterating the results presented in Sec. 3.3, the truncation scheme [Eq. (3.33)] with parameters $p = 1$, $q = 0.5$ and

$$k_{\max_\mu} = k\frac{1}{\mathcal{N}}\left(\sqrt{|G_\mu|}/|W_\mu|\right)^q \tag{5.17}$$

with the normalization $\mathcal{N} = \min_\mu \left(\sqrt{|G_\mu|}/|W_\mu|\right)^q$ is used. By increasing the hierarchy depth k the number of auxiliary states increases, too.

As shown in the right panel of Fig. 5.19, the influence of the hierarchy depth k on the dynamics of the spin polarization $\langle\sigma_z^A\rangle(t)$ (lower row) is more severe compared to the entanglement dynamics (upper row). We found empirically that an insufficient hierarchy depth often yields a faulty decay of $\langle\sigma_z^A\rangle$ to zero whereas the converged dynamics remains at a non-zero value. This makes it challenging to deduce the critical coupling strength from the dynamics of $\langle\sigma_z^A\rangle$. For an Ohmic environment discussed next, it is even more difficult to obtain converged results in the localized phase.

Ohmic Environment The long-time dynamics of the expectation value $\langle\sigma_z^A\rangle$ for an Ohmic environment is shown in the lower panels of Fig. 5.20. Although the critical coupling strength where $\langle\sigma_z^A\rangle$ becomes non-zero asymptotically is hard to access, the lower left panel indicates that $\eta_c\omega_A^{s-1} > 0.9$ should hold. Thus, the critical coupling strength is larger as in the sub-Ohmic case, a behavior known from the (single) SBM, too [BTV03]. For a coupling strength near the critical value the spin polarization $\langle\sigma_z^A\rangle$ approaches its asymptotic value very slowly (lower middle panel) which is characteristic for the Ohmic case [WT08; Str+18]. As of that, its asymptotic value is very hard to access. Here, we constrain our analysis to a first estimate using a single exponential fit for extrapolation (black dashed lines). To rigorously justify this choice the propagation time should be much longer. Although the accuracy of the BCF representation (number of exponential terms N) seems to effect the dynamics $\langle\sigma_z^A\rangle(t)$ only minor, as of the slow decay the estimate for the asymptotic value varies drastically (lower middle panel). The same holds true when checking convergence with respect to the hierarchy depth k (lower right panel). Consequently, showing the phase transition is numerically very costly. As a remark, this difficulty has been noted for the (single) SBM as well for a variety of other approaches [WS19]. Although the plots in Fig. 5.20 suggest a non-vanishing asymptotic value $\langle\sigma_z^A\rangle$ at $\eta = 1.1$, due to our primary focus on the entanglement dynamics, reliably determining the critical coupling strength is left for further investigations.

As seen in the top panels of Fig. 5.20, the effect of the hierarchy depth on the long-time entanglement dynamics (top right panel) is not as crucial, compared to the dynamics of $\langle\sigma_z^A\rangle$. The same holds true for the influence of the accuracy of the

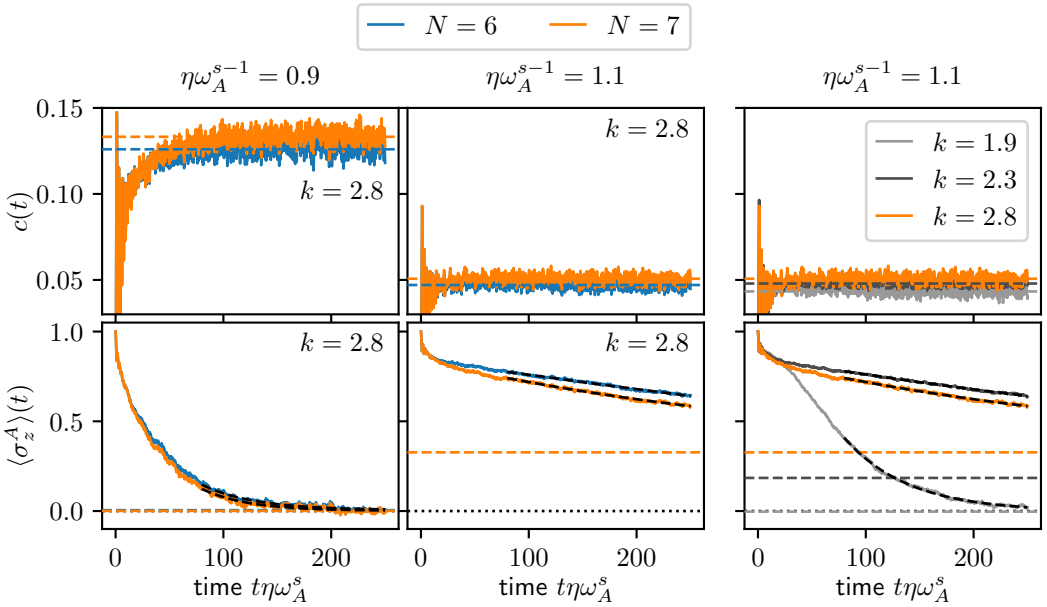

Fig. 5.20: Similar to Fig. 5.19 the long-time dynamics of the concurrence and $\langle\sigma_z^A\rangle$ are shown for an Ohmic environment ($\omega_B = \omega_A$, $\omega_c = 10\omega_A$). The entanglement approaches its asymptotic value quickly. Convergence with respect to the accuracy of the BCF representation (number of exponential terms N) and the hierarchy depth k can be achieved easily. For $\langle\sigma_z^A\rangle$, however, near the critical coupling strength the decay becomes very slow. As a consequence the asymptotic values (dashed lines) obtained by extrapolation are very sensitive to N (middle panel) and k (right panel).

BCF representation (top middle panel). In that sense we claim that the asymptotic value for the entanglement has been determined reliably for $\eta = 1.1$. Note that the qualitative change in the entanglement dynamics when passing the critical coupling strength has not been observed (see the paragraph on the sub-Ohmic case). It remains an open question if this qualitative change is simply not present in the Ohmic case or if $\eta = 1.1$ is still smaller than the critical coupling strength. The later would lead to the hypothesis that the qualitative change in the entanglement dynamics is more suited to detect the phase transition than the asymptotic spin polarization.

Asymptotic Values Finally, in Fig. 5.21 we show the asymptotic entanglement (solid lines) and the asymptotic spin polarization (dashed lines) over a broad range of coupling strengths, comparing the sub-Ohmic and the Ohmic environment. As expected, in both cases the asymptotic entanglement exhibits a maximum. For the sub-Ohmic case ($s = 0.3$) this maximum is located at $\eta_{\max}\omega_A^{s-1} \approx 0.5$ and reads $c_{\max} \approx 0.1$. For $s = 1$ it appears slightly earlier at $\eta_{\max} \approx 0.45$ and takes a significantly larger value $c_{\max} \approx 0.3$. Remarkably, for the sub-Ohmic environment the change from $\langle\sigma_z^A\rangle = 0$ to $\langle\sigma_z^A\rangle > 0$, signaling the phase transition, appears roughly at the position of the maximum. Also, the qualitative change in the entanglement

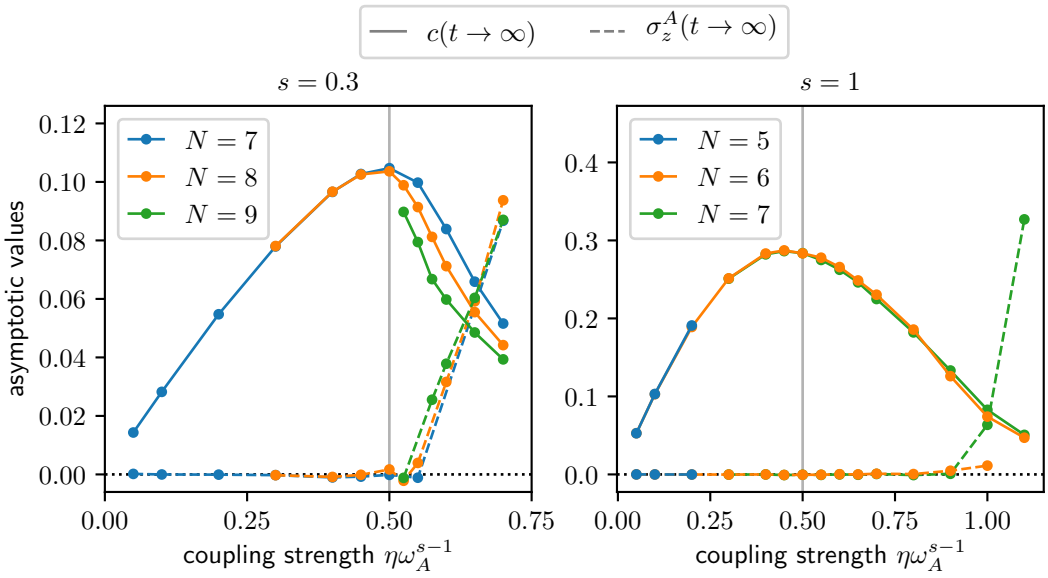

Fig. 5.21: The asymptotic values of the entanglement (solid lines) and the spin polarization $\langle\sigma_z^A\rangle$ (dashed lines) obtained from extrapolating the long-time dynamics are shown as a function of the coupling strength ($\omega_B = \omega_A$, $\omega_c = 10\omega_A$). For both environmental models (left: sub-Ohmic, right: Ohmic) the asymptotic entanglement exhibits a maximum near $\eta\omega_A^{s-1} = 0.5$. In case of the sub-Ohmic environment the maximum coincides with the critical coupling strength for the known delocalization / localization phase transition. As of that, the asymptotic entanglement shows a kink at that point. Also, beyond the maximum a sensitive dependence of the entanglement on the accuracy of the BCF representation (number of exponential terms N) becomes visible. For the Ohmic case the critical coupling strength has not been determined reliably. (See the main text also for a more detailed discussion of the graphs.)

dynamics, i.e., the additional "slow decay" discussed above, has been observed for $\eta > \eta_c = 0.5\omega_A^{1-s}$. Therefore we conjecture that the maximum coincides with the critical coupling strength of the phase transition. As a consequence of the additional "slow decay" the asymptotic entanglement as a function of the coupling strength exhibits a kink at $\eta_{\max} = \eta_c$. Importantly, the kink becomes visible only for a sufficiently accurate approximation of the sub-Ohmic BCF, i.e, a sufficiently large N.

Although the location of the maximum $\eta_{\max}$ for the Ohmic environment marginally differs from the sub-Ohmic case, a kink at the maximum is not observed. This is not too surprising because the phase transition, indicated by the asymptotic value of $\langle\sigma_z^A\rangle$, appears at a larger coupling strength $\eta_c > 0.9$. Since the critical coupling strength has not been determined reliably, so far a statement about a kink at η_c for an Ohmic environment is not possible. What we can say is that for $\eta = 1.1$ the long-time entanglement dynamics shows no qualitative difference compared to the dynamics for smaller coupling strengths, i.e., no additional "slow decay" is seen. However, a first crude estimate of the asymptotic spin polarization at $\eta = 1.1$ suggests a non-vanishing value indicating the phase transition.

Putting our findings in a broader context, we find that the asymptotic behavior of $\langle \sigma_z^A \rangle$ as well as the concurrence agree qualitatively with the behavior obtained when examining the ground state of the microscopic model [Ort+10], although there the sub-Ohmic SD has been modeled with a sharp cutoff. This comparison is in the spirit of the fundamental issue addressing the relation between the asymptotic (steady) state and statistical properties of a small system in contact with a large environment. In classical statistical mechanics it well known that the small system will thermalize, i.e., its asymptotic state is the local thermal state (canonical ensemble) with a temperature corresponding to the bath temperature. However, referring to the microscopic model for an open quantum system it has been shown that this statement holds approximately only in the weak coupling regime [Tas98; Gol+06; Wei08]. Beyond the perturbative regime rigorous statements are rare. What has been shown recently is that under the assumption that the microscopic Hamiltonian (system and environment) has non-degenerate energy gaps, the system reaches indeed a steady (equilibrium) state which is, however, not necessarily the local thermal state of the system [Lin+09; GE16]. However, it seems plausible that if the environment is initially in the ground state (zero temperature) and the system is initially excited then the presumably small energy contribution of the system will distribute over the many environmental degrees of freedom without a major effect on the environment. This suggests that the system should reach a steady state which is close to the reduced state obtained from the global ground state of the microscopic model. Of course, since in our formalism for the reduced dynamics a product state as initial condition is evolved unitarily, the global state cannot evolve to the global ground state. Following this line of reasoning makes is plausible that properties, such as the spin polarization, of the ground state are reflected by the asymptotic state, too, as we have shown above, although the asymptotic state may not agree exactly with the "ground state". Noteworthy, in the plausibility argument above the energy contribution from the interaction Hamiltonian has not been accounted for. In particular, for strong system-environment interactions, e.g., the regime of localization, where this contribution becomes large, further clarification is needed. In this respect the previous explanation for finding signs of the phase transition in the asymptotic state is not satisfying. It seems more reasonable that the phase transition is not only reflected by the ground state but rather by the entire spectrum of the microscopic Hamiltonian, thus, leading to the qualitative change in the dynamics. We are confident that the HOPS approach in general is well suited to perform "numerical experiments" shedding further light on quantum mechanical equilibration and thermalization.

As a final note, since we have considered the resonant case, $\langle \sigma_z^B \rangle$ shows the exact same behavior as $\langle \sigma_z^A \rangle$ and could have been used instead as an indicator for the phase transition. The plots in Fig. 5.17 and a comment in Ref. [Ort+10] give rise to the expectation that slightly detuned qubits behave similar.

6 Conclusion and Outlook

Many modern experimental setups engineer quantum systems which are strongly coupled to their environment [Nie+10; Mag+18]. This underlines the fundamental interest in describing the dynamics of such open quantum system exactly [FV63; Tan06]. Building on the theory of non-Markovian quantum state diffusion (NMQSD) [SDG99], the hierarchy of pure states (HOPS) provides a promising approach suitable for a numeric treatment [SES14; HS17]. Due to its stochastic nature, the HOPS approach is ideally suited for distributed computing on modern large scale computer systems which paves the way for the strong coupling regime. The methodical details which make the HOPS approach exact have been explained extensively. As a particular application of the HOPS method, we have focused on the entanglement dynamics of the open two-qubit system over a broad range of coupling strengths between the qubits and their environment.

A time-discrete scheme has been employed to derive the NMQSD / HOPS formalism in an independent and highly transparent manner. This includes the non-linear theory which ensures that the stochastic contributions assembling the reduced state, i.e., the dyads of the stochastic pure states, have equal weight. Furthermore, we have lifted the restriction for the harmonic environment to be initially prepared in its ground state by allowing for coherent states, too. This, in turn, led us to model non-zero temperature effects by means of a stochastic Hermitian contribution to the system Hamiltonian, an approach which has turned out highly favorable for the HOPS with strong system-environment interaction, but is also suitable for any zero temperature formalism.

In addition to the HOPS formalism, we have also derived various aspects of the underlying NMQSD equation which appear very promising for future methodical investigation. By using the Karhunen–Loève expansion to represent the stochastic process, we have derived a Schrödinger equation for the microscopic model where the environment consists of a *countably* infinite set of bosonic modes with a time dependent system-environment coupling. The reduced dynamics of that system corresponds exactly to the dynamic of the original model involving a truly continuous environment. Since the coupling to the modes decreases with the mode index, approximate solutions follow naturally. The full potential of this so-called Karhunen-Loève expansion Schrödinger equation (KLESEQ) approach has yet to be explored. A different point of view on the dynamics of open quantum systems was found from

the time-discrete formalism mentioned above. Taking the time-discrete equation literally yields a dynamical picture for the reduced dynamics. Instead of a static coupling to the environmental modes, in the so-called time oscillator picture the system interacts with a new oscillator at each time step, i.e., it moves to the next oscillator. Additional interactions with past oscillators account for memory effects. The reduced state is obtained by taking some *non-standard* trace over the time oscillators. Furthermore, we have derived a second kind of hierarchy of pure states based on higher order derivatives of the bath correlation function (BCF) rather than an exponential representation required by the "standard" variant. As we have elucidated, there are cases where the long time dynamics depends crucially on the accuracy of this exponential representation. Consequently, it remains an exciting project to explore the benefits of this alternative approach as a numerical method.

Referring again to the "standard" hierarchy, it has been at the heart of this thesis to show that the HOPS qualifies as a numerically exact approach, i.e., there are numerical errors only which can, in principle, be made arbitrarily small. This includes the sampling of stochastic processes, the exponential representation of (sub-) Ohmic BCFs and the truncation of the hierarchy.

For the well studied spin-boson model (SBM) [Leg+87], which remains challenging to treat exactly in the strong coupling regime [Str+18; WS19], we have demonstrated agreement between our HOPS implementation and various other open system approaches. The test cases include weak and strong coupling to the environment as well as zero and high temperatures for the initial thermal environmental state. Thus, we have concluded that the HOPS method is well suited for a wide range of situations.

Based on that confidence, we have investigated the generation of entanglement between two non-interacting qubits due to their interaction with a common environment. Starting with the weak coupling regime where perturbative master equations are expected to give reasonable results, we have demonstrated that the entanglement dynamics may differ significantly between such master equations. With the HOPS results as a reference, we have shown that the RFE is the most accurate perturbative method and that the commonly applied rotating wave approximation (RWA) is of very limited use only. The Coarse Graining approach [SB08] and the Geometric-Arithmetic approximation [Dav20], both intended to restore complete positivity without applying the RWA, have their regime of applicability. However, they do not reach the accuracy of the RFE. This is not surprising since the RFE involves the least approximations. We have found that the often criticized non-positivity of the reduced state obtained from the RFE is of no relevance since the positive matrix $\sqrt{\rho_{\mathrm{RFE}}^{\dagger} \cdot \rho_{\mathrm{RFE}}}$ approximates the reduced state to the same degree of accuracy as ρ_{RFE}. Therefore, the approximate entanglement dynamics can be obtained unam-

biguously using the RFE. Notably, we have reported that any of the perturbative approaches under consideration fails to faithfully predict the dependence of the steady state entanglement on the coupling strength. This is indeed in agreement with recent investigations showing that any second-order master equation (in the interaction Hamiltonian) yields a reduced state which is exact up to zeroth-order only [FC11; Tup+21].

Furthermore, we have investigated the effect of the renormalizing counterterm, a manually introduced contribution to the system Hamiltonian intended to compensate for the environmentally induced Hermitian contribution to the system dynamics (the so-called Lamb-shift Hamiltonian) [Wei08]. Since the Lamb-shift Hamiltonian is the primary mechanism for the generation of entanglement, it can be expected that the buildup of entanglement is suppressed by the counterterm. Employing the HOPS, we have investigated the effect of the counterterm non-perturbatively. We have found significant entanglement suppression due to the counterterm for an Ohmic environment but nearly no effect in the deep sub-Ohmic regime (setting $s = 0.3$, while leaving all other model parameters the same). Thus, the common expectation seems to fail for the sub-Ohmic regime. We have shown that, in general, the degree to which the counterterm cancels the Lamb-shift Hamiltonian is related to the "flatness" of $S(\omega)$ near $\omega = 0$ ($S(\omega)$ denotes the imaginary part of the half-sided Fourier transform of the BCF). The pointed minimum at $\omega = 0$ for a deep sub-Ohmic SD ($s < 0.5$), thus, explains the unexpected behavior. Note that since $S(\omega) \sim S(0) + |\omega/\omega_c|^s$ (ω_c: cutoff frequency the (sub-)Ohmic SD), $S(\omega)$ becomes effectively flat in the limit of large ω_c. In this adiabatic limit the counterterm and the lamb-shift Hamiltonian eventually add up to zero. Still, we have shown that for two resonant qubits and a deep sub-Ohmic SD, even in the adiabatic limit a small qubit-qubit interaction remains, yielding significant entanglement generation which cannot be explained by purely dissipative effects. This so-called anomalous behavior in the adiabatic regime essentially relates to the order in which the long-time and the adiabatic limits are taken.

Beyond the perturbative regime, we have shown that the detuning of the qubits hardly influences the entanglement dynamics. Additionally, we have found that a significant amount of entanglement remains in the steady state. Further, we have calculated the entanglement dynamics for non-zero temperatures of the environment, showing that the generation of entanglement is far from being a zero-temperature phenomenon.

Last but not least, we have focused on the properties of the steady state. We have found that the asymptotic entanglement, as a function of the coupling strength, increases linearly in the weak coupling regime. As mentioned above, this behavior is not faithfully accessible in lowest order perturbation theory. We have found that the

asymptotic entanglement exhibits a maximum at an intermediate coupling strength. For the two particular examples considered here ($s = 0.3$ and $s = 1$) the maximum appears at almost the same coupling strength. It remains an interesting question whether or not this holds more generally. For the sub-Ohmic environment ($s = 0.3$) it has turned out that the location of the maximum coincides with the critical coupling strength of the delocalization-to-localization phase transition [Ort+10; WR14]. In addition to the known properties of the spin polarization, we have observed a qualitative change in the long time entanglement dynamics when passing the critical coupling strength. On the one hand, for values smaller than the critical coupling strength, the steady state entanglement is reached quickly, i.e., on a time scale set by the inverse of the coupling strength. On the other hand, for larger values, an additional exponential decay with a much slower decay rate compared to the initial relaxation governs the long time dynamics. As a consequence, the asymptotic entanglement exhibits a kink at the critical coupling strength and, with that, at the maximum. Noteworthily, for coupling strengths larger than the critical value, the asymptotic entanglement depends very sensitively on the accuracy of the BCF representation. For the Ohmic case, the phase transition takes place at a larger coupling strength and, thus, not at the position of the maximum. So far, the exact value of the critical coupling strength has not been determined reliably within the HOPS formalism. As a remark, calculating the point of the phase transition for a single qubit and an Ohmic environment is known to be very challenging for other approaches, too [WS19]. It remains an open question whether the phase transition for two qubits and an Ohmic environment is accompanied by a kink in the asymptotic entanglement as well.

Investigating the entanglement dynamics of the open two-qubit system over a broad range of model parameters, especially for large system-environment interactions, has been possible utilizing the HOPS method. Thus, the HOPS approach can readily be used for many current topics in the field of open quantum system dynamics such as transport through quantum systems and their equilibration, real world application focusing on quantum information and quantum metrology as well as many others.

Although possible with current techniques, the numerical effort to obtain the long time dynamics in the strong coupling regime, necessary to draw conclusions about the phase transition, has been huge. This hints at future methodical directions of research related to the HOPS formalism. As a rather abstract goal, a variant of the HOPS, or even a novel approach obtained from the underlying NMQSD formalism specifically suited for the strong coupling regime would complete the stochastic description of the exact reduced dynamics. It remains for investigation whether or not the hierarchy based on time derivatives is advantageous in that respect. Furthermore, a stochastic steady state solver based on pure states is very desirable. A straight forward approach, however, is unclear, since the stochastic pure states,

i.e., solutions of the NMQSD equation, do not reach a steady state. Despite of that, progress might be achievable by exploiting the fact that the long time dynamics of the pure state projector is, in many cases, independent of the initial condition, which has been noted recently [HS21]. Also, it has been argued that if the steady state is unique, the time averaged projector of a single pure state realization approaches the steady state in the long time limit. Surely, there are a multitude of further interesting directions of research branching off the stochastic pure state description of open quantum stems dynamics in terms of the NMQSD and the HOPS formalism.

Acknowledgments

Throughout the time working on my theses, I have been accompanied by numerous great people. It is a pleasure to thank all of them for their inspiring support.

In particular, special gratitude is expressed to my doctoral adviser, Walter Strunz. His insights in the field of open quantum system dynamics have paved the way for the HOPS approach to mature. Even more sparkling have been the in depth discussions which often lead to fundamental questions in physics. At least equally admirable has been his support on non-academical matters which has allowed me to find a sustainable balance between work and my family.

I also thank Kimmo Luoma, Valentin Link, Nina Megier, Konstantin Bayer, Doran Bennett and Alex Eisfeld for the fruitful conversations regarding current issues on open quantum systems. Furthermore it has been a pleasure to develop a tool for distributed computing (`github.com/cimatosa/jobmanager`) and to discuss the numeric progress at weakly pizza events with Paul Müller. Inspiring in any sense, this regards issues of theoretical physics and far beyond, has also been my friendship with Simon Milz.

I appreciate the International Max Planck Research School at the MPI-PKS Dresden for their support and the Center for Information Services and High Performance Computing (ZIH) at TU Dresden for providing access to the Bull Cluster. During development and testing of the code frequent use was made of the `mpmath` library [Joh+21] which, thus, deserves special credit here.

Appendix

A HOPS for Multi-Partite Systems and Multiple Environments

The NMQSD equation (2.20) as well as the HOPS formalism (Sec. 2.1.2) can be generalized to the scenario where the system is partitioned into sub-systems and the environment consists of several independent environments, each one modeled by an infinite set of harmonic oscillators (see Fig. A.1).

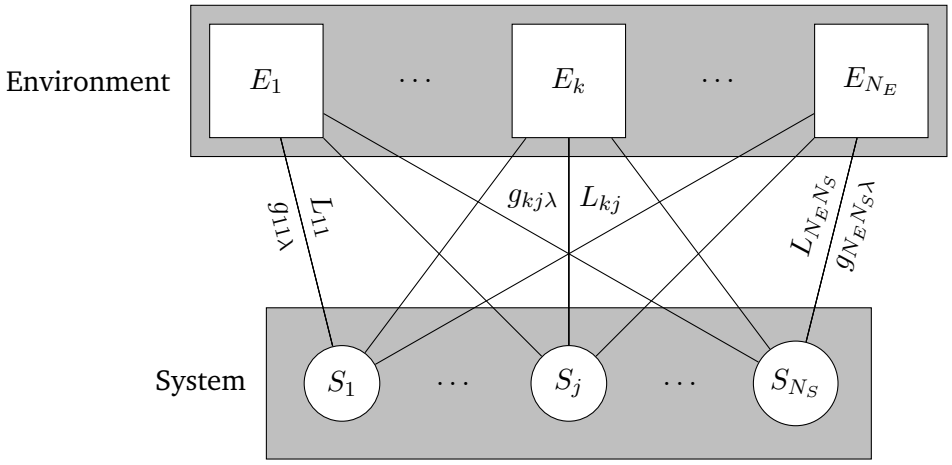

Fig. A.1: A schematic plot of the generalized microscopic model is shown. The system is partitioned in N_S sub-systems where each part is allowed to interact with N_E independent environments. As usual, the environments are modeled by a possibly infinite number of harmonic oscillators. In general each sub-system j couples to the modes of the environment k with individual coupling constants $g_{kj\lambda}$, i.e., an individual SD $J_{kj}(\omega) = \pi \sum_\lambda |g_{kj\lambda}|^2 \delta(\omega - \omega_{k\lambda})$.

The Hamiltonian of the microscopic model for the system and the environment takes the form

$$H = H_{\text{sys}} + \sum_{k=1}^{N_E} \sum_{j=1}^{N_S} \sum_\lambda \left(g^*_{kj\lambda} L_{kj} a^\dagger_{k\lambda} + \text{h.c.} \right) + \sum_{k=1}^{N_E} \sum_\lambda \omega_{k\lambda} a^\dagger_{k\lambda} a_{k\lambda} \,. \tag{A.1}$$

The index k enumerates the different environments, the index λ the harmonic oscillators within each of the environments and the index j the sub-system. The coefficients $g_{kj\lambda}$ assemble the SD which models the influence of the k-th environment

on the j-th sub-system, i.e., $J_{kj}(\omega) \equiv \pi \sum_\lambda |g_{kj\lambda}|^2 \delta(\omega - \omega_{k\lambda})$ or, equivalently, the BCF $\alpha_{kj}(\tau) \coloneqq \sum_\lambda |g_{kj\lambda}|^2 e^{-\mathrm{i}\omega_{k\lambda}\tau}$. Changing to the interaction picture with respect to the environment yields for the stochastic pure state

$$\partial_t \psi(\mathbf{z}^*, t) = \Bigg[-\mathrm{i}H_{\mathrm{sys}} + \sum_{k,j} \eta^*_{kj}(\mathbf{z}^*_k, t) L_{kj} - \mathrm{i} \sum_{k,j} L^\dagger_{kj} \sum_\lambda g_{kj\lambda} e^{-\mathrm{i}\omega_{k\lambda}t} \partial_{z^*_{k\lambda}} \Bigg] \psi(\mathbf{z}^*, t) \; . \tag{A.2}$$

Different stochastic processes $\eta^*_{kj}(t)$ have been introduced with their microscopic definition $\eta^*_{kj}(\mathbf{z}^*_k, t) \coloneqq -\mathrm{i} \sum_\lambda g^*_{kj\lambda} z^*_{k\lambda} e^{\mathrm{i}\omega_{k\lambda}t}$. Their (normal) second moments

$$\mathcal{M}\left(\eta_{kj}(t)\eta^*_{kj}(s)\right) = \alpha_{kj}(t-s) \tag{A.3}$$

correspond to the known relation from the Sec. 2.1.1. However, since each sub-system can interact with a particular environment simultaneously, also cross correlations appear. This is captured by the Gaussian statistics of a vector valued stochastic process (η^*_{kj} are the components), which is uniquely determined by the normal second moment

$$\mathcal{M}\left(\eta_{kj}(t)\eta^*_{k'j'}(s)\right) = \delta_{k,k'} \sum_\lambda g_{kj\lambda} g^*_{kj'\lambda} e^{-\mathrm{i}\omega_{k\lambda}(t-s)} = \delta_{k,k'} \alpha_{kjj'}(t-s) \; . \tag{A.4}$$

Note that due to the cross correlations the so-called generalized BCF $\alpha_{kjj'}(\tau)$ has three components Following the same line of arguments as in Sec. 2.1.1 the time-discrete NMQSD equation is obtained, i.e.,

$$\psi_{n+1}(\eta^*_{kj}|^n_0) = \Bigg[1 + \Delta t \Bigg(-\mathrm{i}H_{\mathrm{sys}} + \sum_{k,j} \eta^*_{kj}(t_n) L_{kj} - \sum_{k,j,j'} L^\dagger_{kj} \sum_{m=0}^{n-1} \alpha_{kjj'}(t_n - t_m) \partial_{\eta^*_{kj'}(t_m)} \Bigg) \Bigg] \psi_n(\eta^*_{kj}|^{n-1}_0) \; , \tag{A.5}$$

which yields in differential form

$$\partial_t \psi[\eta^*_{kj}(t)]_t = \Bigg[-\mathrm{i}H_{\mathrm{sys}} + \sum_{k,j} \eta^*_{kj}(t) L_{kj} - \sum_{k,j,j'} L^\dagger_{kj} \int_0^t \mathrm{d}s \, \alpha_{kjj'}(t-s) \frac{\delta}{\delta \eta^*_{kj'}(s)} \Bigg] \psi[\eta^*_{kj}(t)]_t \; . \tag{A.6}$$

For a multi-exponential representation of the generalized BCF, i.e., $\alpha_{kjj'}(\tau) = \sum_\mu G_{kjj'\mu} e^{-W_{kjj'\mu}\tau}$ for $\tau \geq 0$, the HOPS reads

$$\begin{aligned} \dot{\psi}_t^{\mathbf{h}} &= A\psi_t^{\mathbf{h}} + \sum_{k,j,j',\mu} B_{kj} G_{kjj'\mu} \psi_t^{\mathbf{h}+\mathbf{e}_{kjj'\mu}} + \sum_{k,j,j',\mu} C_{kj'} h_{kjj'\mu} \psi_t^{\mathbf{h}-\mathbf{e}_{kjj'\mu}} \\ \text{with} \quad A &= -\mathrm{i}H_{\mathrm{sys}} - \sum_{k,j,j',\mu} h_{kjj'\mu} W_{kjj'\mu} + \sum_{k,j} \eta_{kj}^*(t) L_{kj}, \\ B_{kj} &= -L_{kj}^\dagger \text{and} \quad C_{kj'} = L_{kj'} \, . \end{aligned} \tag{A.7}$$

For completeness, the Gaussian statistics of the stochastic processes involved are determined by

$$\begin{aligned} \mathcal{M}(\eta_{kj}^*(t)) = 0, \quad \mathcal{M}(\eta_{kj}^*(t)\eta_{k'j'}^*(s)) = 0 = \mathcal{M}(\eta_{kj}(t)\eta_{k'j'}(s)) \\ \text{and} \quad \mathcal{M}(\eta_{kj}(t)\eta_{k'j'}^*(s)) = \delta_{kk'}\alpha_{kjj'}(t-s) \, . \end{aligned} \tag{A.8}$$

Note that the index vector $\mathbf{h}$ has four indices $kjj'\mu$. Therefore the dimension of $\mathbf{h}$ is $N_E \cdot N_S^2 \cdot N_\mu$. For simplicity it has been assumed that each component of the generalized BCF $\alpha_{kjj'}$ is expressed with N_μ exponential terms, which can of course be relaxed.

A.1 Importance Sampling (Non-Linear HOPS)

In the following, the main steps to derive the non-linear variant of the NMQSD equation are reiterated, however using the microscopic model for a multi-partied system and multiple environments as specified in Eq. (A.1).

The relation between the norm of the stochastic pure state and the environmental Husimi function becomes

$$Q(\mathbf{z},\mathbf{z}^*,t) = \mathcal{N}\langle \mathbf{z}|\rho_{\mathrm{env}}(t)|\mathbf{z}\rangle = \mathcal{N}\langle \mathbf{z}|\mathrm{Tr}_{\mathrm{sys}}|\Psi(t)\rangle\langle\Psi(t)||\mathbf{z}\rangle = \mathcal{N}\langle\psi(\mathbf{z},t)|\psi(\mathbf{z}^*,t\rangle \tag{A.9}$$

with

$$\mathcal{N}(\mathbf{z},\mathbf{z}^*) = \prod_{k,\lambda} \frac{e^{-z_{k\lambda}z_{k\lambda}^*}}{\pi} \, . \tag{A.10}$$

The boldface is short hand notation for the product structure $|\mathbf{z}\rangle = \prod_{k\lambda}|z_{k\lambda}\rangle$ enumerated by the environment index k and the mode index λ. The evolution equation for Q takes the form of a first order partial differential equation

$$\partial_t Q(\mathbf{z},\mathbf{z}^*,t) = -\sum_{k,j,\lambda} \mathrm{i}g_{kj\lambda} e^{-\mathrm{i}\omega_{k\lambda}t} \partial_{z_{k\lambda}^*} \langle L_{kj}^\dagger\rangle_t Q(\mathbf{z},\mathbf{z}^*,t) - \mathrm{h.c.} \tag{A.11}$$

where the expectation value $\langle L_{kj}^\dagger \rangle_t$ denotes the normalized expectation value with respect to the stochastic pure state, i.e.,

$$\langle L_{kj}^\dagger \rangle_t := \langle \psi(\mathbf{z},t)|L_{kj}^\dagger|\psi(\mathbf{z}^*,t)\rangle / \langle \psi(\mathbf{z},t)|\psi(\mathbf{z}^*,t)\rangle \ . \tag{A.12}$$

This allows us to view the evolution of Q in terms of "phase space" trajectories $\mathbf{z}^*(t)$ (see Sec. 2.1.3) where the components obey

$$\dot{z}_{k\lambda}^*(t) = \mathrm{i} e^{-\mathrm{i}\omega_{k\lambda}t} \sum_j g_{kj\lambda} \langle L_{kj}^\dagger \rangle_t \tag{A.13}$$

with $\mathbf{z}^*(0) = \mathbf{z}_0^*$ being Gaussian distributed according to $Q(\mathbf{z}_0, \mathbf{z}_0^*, 0) = \mathcal{N}(\mathbf{z}_0, \mathbf{z}_0^*)$. For the stochastic pure states with co-moving coherent state label, i.e., $\psi(\mathbf{z}^*,t)|_{\mathbf{z}^*=\mathbf{z}^*(t)}$, it follows that

$$\begin{aligned}
&\dot{\psi}(\mathbf{z}^*(t),t) = \partial_t \psi(\mathbf{z}^*(t),t) + \sum_{k,\lambda} \dot{z}_{k\lambda}^*(t) \partial_{z_{k\lambda}^*} \psi(\mathbf{z}^*(t),t) \\
&= \left[-\mathrm{i}H_{\mathrm{sys}} + \sum_{k,j} \tilde{\eta}_{kj}^*(\mathbf{z}_k^*(t),t) L_{kj} - \mathrm{i} \sum_{k,j,\lambda} \left(L_{kj}^\dagger - \langle L_{kj}^\dagger \rangle_t \right) g_{kj\lambda} e^{-\mathrm{i}\omega_{k\lambda}t} \partial_{z_{k\lambda}^*} \right] \psi(\mathbf{z}^*(t),t) \ .
\end{aligned} \tag{A.14}$$

This equations is remarkably similar to its linear variant (Eq. (A.2)) and, thus, yields by similar reasoning the non-linear NMQSD equation

$$\begin{aligned}
\dot{\psi}[\eta_{kj}^*(t)]_t = \Bigg[&-\mathrm{i}H_{\mathrm{sys}} + \sum_{k,j} \tilde{\eta}_{kj}^*(t) L_{kj} \\
&- \sum_{k,j,j'} \left(L_{kj}^\dagger - \langle L_{kj}^\dagger \rangle_t \right) \int_0^t \mathrm{d}s \, \alpha_{kjj'}(t-s) \frac{\delta}{\delta \eta_{kj'}^*(s)} \Bigg] \psi[\eta_{kj}^*(t)]_t
\end{aligned} \tag{A.15}$$

however, with stochastic processes $\tilde{\eta}_{kj}^*(\mathbf{z}_k^*(t),t)$ depending on the co-moving coherent state labels. Using the formal solution

$$z_{k\lambda}^*(t) = z_{k\lambda}^*(0) + \mathrm{i} \int_0^t \mathrm{d}s \, e^{-\mathrm{i}\omega_{k\lambda}s} \sum_j g_{kj\lambda} \langle L_{kj}^\dagger \rangle_s \tag{A.16}$$

the stochastic process becomes

$$\begin{aligned}
\tilde{\eta}_{kj}^*(\mathbf{z}_k^*(t),t) &= -\mathrm{i} \sum_\lambda g_{kj\lambda}^* z_{k\lambda}^*(0) e^{\mathrm{i}\omega_{k\lambda}t} + \int_0^t \mathrm{d}s \sum_{j'} \sum_\lambda g_{kj\lambda}^* g_{kj'\lambda} e^{\mathrm{i}\omega_{k\lambda}(t-s)} \langle L_{kj'}^\dagger \rangle_t \\
&= \eta_{kj}^*(\mathbf{z}_k^*(0),t) + \int_0^t \mathrm{d}s \sum_{j'} \alpha_{kjj'}^*(t-s) \langle L_{kj'}^\dagger \rangle_s \ .
\end{aligned} \tag{A.17}$$

This shows that the stochastic process with co-moving coherent state labels consists of the original stochastic process with

$$\mathcal{M}(\eta_{kj}(\mathbf{z}_k(0),t)\eta^*_{k'j'}(\mathbf{z}^*_{k'}(0),s)) = \delta_{kk'}\alpha_{kjj'}(t-s) \tag{A.18}$$

and a shift contribution. The shift can be obtained numerically by solving its differential form along with the equations of the HOPS where the multi-exponential representation of the generalized BCF is used again, i.e.,

$$\begin{aligned} \eta^*_{kj,\mathrm{sh}}(t) &:= \int_0^t \mathrm{d}s \sum_{j'} \alpha^*_{kjj'}(t-s)\langle L^\dagger_{kj'}\rangle_s = \sum_{\mu,j'} \eta^*_{kjj'\mu,\mathrm{sh}}(t) \\ \text{with} \quad \eta^*_{kjj'\mu,\mathrm{sh}}(t) &:= \int_0^t \mathrm{d}s\, G^*_{kjj'\mu} e^{-W^*_{kjj'\mu}(t-s)} \langle L^\dagger_{kj'}\rangle_s \end{aligned} \tag{A.19}$$

which obviously obeys

$$\dot{\eta}^*_{kjj'\mu,\mathrm{sh}}(t) = G^*_{kjj'\mu}\langle L^\dagger_{kj'}\rangle_t - W^*_{kjj'\mu}\eta^*_{kjj'\mu,\mathrm{sh}}(t) \quad \text{with} \quad \eta^*_{kjj'\mu,\mathrm{sh}}(t) = 0\,. \tag{A.20}$$

Very similar to the results obtained in Sec. 2.1.3.2, the HOPS for the non-linear NMQSD equation is the same as in the linear case given in Eq. (A.7) except for replacements $L^\dagger_{kj} \to L^\dagger_{kj} - \langle L^\dagger_{kj'}\rangle_t$ and $\eta^*_{kj}(t) \to \tilde{\eta}^*_{kj}(t)$.

A.2 Special Cases

The general form of the HOPS [Eq. (A.7)] for many sub-systems coupled to various independent environments contains two special cases worth noting. First, assuming that the coupling operator L_{kj} for a particular sub-system is the same for each environment, i.e., $L_{kj} = L_j$, the summation over k can be performed. Consequently, an effective single environment remains. For example, this case is encountered when several groups of atoms are trapped in different locations in a multi-mode lossy cavity in the spirit of the dissipative Hubbard-Holstein model [FDD21]. Since the coupling operator σ_x does not distinguish between the cavity modes, the multi-mode cavity can be described effectively by a single environment. Still, the individual coupling strength can depend on both, the mode and the particular group of the atoms.

Second, the condition $g_{kj\lambda} = \delta_{kj} g_{k\lambda}$ accounts for the case where each sub-system interacts with a single environment exclusively. This case includes the widely used model for quantum aggregates which, for examples, allows to describe the excitation dynamics in protein complexes occurring in biological light harvesting systems [IF09].

A.2.1 Effective Single Environment

The assumption that the coupling operator L_{kj} depends on the index j only, results in the following NMQSD equation

$$\partial_t \psi[\eta_j^*(t)]_t = \left[-\mathrm{i}H_{\mathrm{sys}} + \sum_j \eta_j^*(t) L_j - \sum_{jj'} L_j^\dagger \int_0^t \mathrm{d}s\, \alpha_{jj'}(t-s) \frac{\delta}{\delta \eta_{j'}^*(s)} \right] \psi[\eta_j^*(t)]_t \,. \tag{A.21}$$

The microscopic definition of the effective noise process $\eta_j^*(t)$ is simply the sum over k of the general noise processes, i.e.,

$$\eta_j^*(t) \coloneqq \sum_k \eta_{kj}^*(t) = -\mathrm{i} \sum_{k\lambda} g_{kj\lambda}^* z_{k_\lambda}^* e^{\mathrm{i}\omega_{k_\lambda} t} \,. \tag{A.22}$$

Note that for the effective single environment case the sum over k may be infinite $N_E = \infty$. It follows consistently that

$$\mathcal{M}\left(\eta_j(t)\eta_{j'}^*(s)\right) = \sum_{kk'} \mathcal{M}\left(\eta_{kj}(t)\eta_{k'j'}^*(s)\right) = \alpha_{jj'}(t-s) \tag{A.23}$$

with the effective BCF $\alpha_{jj'}(t-s) \coloneqq \sum_k \alpha_{kjj'}(t-s)$. Expressing this effective BCF in terms of a multi-exponential expansion, i.e, $\alpha_{jj'}(\tau) = \sum_\mu G_{jj'\mu} e^{-W_{jj'\mu}\tau}$ for $\tau \geq 0$, the HOPS becomes

$$\begin{aligned} \dot{\psi}_t^{\mathbf{h}} &= A\psi_t^{\mathbf{h}} + \sum_{jj'\mu} B_j G_{jj'\mu} \psi_t^{\mathbf{h}+\mathbf{e}_{jj'\mu}} + \sum_{jj'\mu} C_{j'} h_{jj'\mu} \psi_t^{\mathbf{h}-\mathbf{e}_{jj'\mu}} \quad \text{with} \\ A = -\mathrm{i}H_{\mathrm{sys}} - \sum_{jj'\mu} h_{jj'\mu} W_{jj'\mu} + \sum_j \eta_j^*(t) L_j, &\quad B_j = -L_j^\dagger \quad \text{and} \quad C_{j'} = L_{j'} \,. \end{aligned} \tag{A.24}$$

As a consequence of the assumption $L_{kj} \to L_j$ the index vector $\mathbf{h}$ has three indices $jj'\mu$ instead of four as for the general case.

For the non-linear HOPS it follows that $B_j = -(L_j^\dagger - \langle L_j^\dagger \rangle)_t$ and $\eta_j^*(t) \to \tilde{\eta}_j^*(t) = \eta_j^*(t) + \eta_{j,\mathrm{sh}}^*(t)$ with

$$\begin{aligned} \mathcal{M}\left(\eta_j(t)\eta_{j'}^*(s)\right) &= \alpha_{jj'}(t-s) \,, \\ \eta_{j,\mathrm{sh}}^*(t) &= \int_0^t \mathrm{d}s \sum_{j'} \alpha_{jj'}^*(t-s) \langle L_{j'}^\dagger \rangle_s = \sum_{\mu,j'} \eta_{jj'\mu,\mathrm{sh}}^*(t) \,, \\ \eta_{jj'\mu,\mathrm{sh}}^*(t) &\coloneqq \int_0^t \mathrm{d}s\, G_{jj'\mu}^* e^{-W_{jj'\mu}^*(t-s)} \langle L_{j'}^\dagger \rangle_s \,, \\ \text{and} \quad \dot{\eta}_{jj'\mu,\mathrm{sh}}^*(t) &= G_{jj'\mu}^* \langle L_{j'}^\dagger \rangle_t - W_{jj'\mu}^* \eta_{jj'\mu,\mathrm{sh}}^*(t) \,. \end{aligned} \tag{A.25}$$

Referring to the multi-mode lossy cavity case, the j-th group of atoms interacts with the k-th lossy mode which amounts to a Lorentzian SD for the k-th environment, i.e., $J_{kj}(\omega) = c_{kj}\gamma_k/(\gamma_k+(\omega-\omega_{0k})^2)$ and a corresponding BCF $\alpha_{kjj}(\tau) = c_{kj}e^{-\mathrm{i}\omega_{0k}\tau-\gamma_k|\tau|}$. Note that the frequency of the mode ω_k and its damping rate γ_k is independent of the atoms, i.e., the index j. Still, c_{kj} denotes the individual coupling strength between the j-th clump and k-th mode. This allows us to easily evaluate the non-diagonal elements of the generalized BCF, i.e.,

$$\alpha_{kjj'}(\tau) = \int \mathrm{d}\omega\, \sqrt{J_{kj}(\omega)J_{kj'}(\omega)}e^{-\mathrm{i}\omega\tau} = \sqrt{c_{kj}c_{kj'}}e^{-\mathrm{i}\omega_{0k}\tau-\gamma_k|\tau|}\,. \tag{A.26}$$

The expression shows that each component of the generalized BCF for a multi-Lorentzian environment takes the form of a single exponential with $G_{jj'k} = \sqrt{c_{kj}c_{kj'}}$ and $W_{jj'k} = \gamma_k - \mathrm{i}\omega_{0k}$. For the effective single environment scenario, considered here, the exponential structure inherent to the multi-Lorentzian environment results in a sum of exponential terms directly suitable for the HOPS scheme, i.e.,

$$\alpha_{jj'}(\tau) = \sum_k^{N_E} \alpha_{kjj'}(\tau) = \sum_k^{N_E} \sqrt{c_{kj}c_{kj'}}e^{-\mathrm{i}\omega_{0k}\tau-\gamma_k|\tau|} \equiv \sum_\mu^{N_E} G_{jj'\mu}e^{-W_\mu\tau} \tag{A.27}$$

for $\tau > 0$. Although the multi-mode environment can be regarded as an effective single environment, its BCF is assembled by N_E exponential terms, i.e., one term per mode. This corresponds to the intuitive picture that each Lorentzian environment is indeed accounted for by a different branch in the hierarchy.

A.2.2 An Exclusive Environment for Each Sub-System Interaction

An exclusive interaction between the sub-system j and the environment k is realized if $g_jk\lambda = 0$ for all $j \neq k$, thus, the coupling strengths have to be of the form $g_{kj\lambda} = \delta_{kj}g_{k\lambda}$. This condition effects the stochastic processes such that $\eta^*_{kj}(t) = \delta_{kj}\eta^*_k(t)$ with

$$\eta^*_k(t) := -\mathrm{i}\sum_\lambda g^*_{k_\lambda} z^*_{k\lambda}e^{-\mathrm{i}\omega_{k\lambda}t} \tag{A.28}$$

and the generalized BCF becomes $\alpha_{kjj'}(\tau) = \delta_{kj}\delta_{kj'}\alpha_k(\tau)$ with

$$\alpha_k(\tau) := \sum_\lambda |g_{k\lambda}|^2 e^{-\mathrm{i}\omega_{k\lambda}\tau}\,. \tag{A.29}$$

As a consequence, the NMQSD equation reads

$$\partial_t\psi[\eta^*_k(t)]_t = \left[-\mathrm{i}H_{\mathrm{sys}} + \sum_k \eta^*_k(t)L_k - \sum_k L^\dagger_k \int_0^t \mathrm{d}s\, \alpha_k(t-s)\frac{\delta}{\delta\eta^*_k(s)}\right]\psi[\eta^*_k(t)]_t \tag{A.30}$$

and the HOPS becomes

$$\begin{aligned} \dot{\psi}_t^{\mathbf{h}} &= A\psi_t^{\mathbf{h}} + \sum_{k\mu} B_k G_{k\mu} \psi_t^{\mathbf{h}+\mathbf{e}_{k\mu}} + \sum_{k\mu} C_k h_{k\mu} \psi_t^{\mathbf{h}-\mathbf{e}_{k\mu}} \quad \text{with} \\ A &= -\mathrm{i}H_{\mathrm{sys}} - \sum_{k\mu} h_{k\mu} W_{k\mu} + \sum_k \eta_k^*(t) L_k, \quad B_k = -L_k^\dagger \quad \text{and} \quad C_k = L_k \end{aligned} \tag{A.31}$$

where the parameters $G_{k\mu}$ and $W_{k\mu}$ correspond to the multi-exponential representation of the BCF

$$\alpha_k(\tau) = \sum_\mu G_{k\mu} e^{-W_{k\mu}\tau} \quad \text{for} \quad \tau \geq 0\,. \tag{A.32}$$

The index vector $\mathbf{h}$ has only two indices instead of four as for the general case.

For the non-linear HOPS it follows that $B_k = -(L_k^\dagger - \langle L_k^\dagger \rangle)_t$ and $\eta_k^*(t) \to \tilde{\eta}_k^*(t) = \eta_k^*(t) + \eta_{k,\mathrm{sh}}^*(t)$ with

$$\begin{aligned} \mathcal{M}\left(\eta_k(t)\eta_{k'}^*(s)\right) &= \delta_{kk'}\alpha_k(t-s), \\ \eta_{k,\mathrm{sh}}^*(t) &= \int_0^t \mathrm{d}s\, \alpha_k^*(t-s)\langle L_k^\dagger \rangle_s = \sum_\mu \eta_{k\mu,\mathrm{sh}}^*(t), \\ \eta_{k\mu,\mathrm{sh}}^*(t) &:= \int_0^t \mathrm{d}s\, G_{k\mu}^* e^{-W_{k\mu}^*(t-s)} \langle L_k^\dagger \rangle_s \\ \text{and} \quad \dot{\eta}_{k\mu,\mathrm{sh}}^*(t) &= G_{k\mu}^* \langle L_k^\dagger \rangle_t - W_{k\mu}^* \eta_{k\mu,\mathrm{sh}}^*(t)\,. \end{aligned} \tag{A.33}$$

B The BCF and its Half-Sided FT for (Sub-)Ohmic Spectral Densities

The class of (sub-) Ohmic SDs, characterized by a power law behavior ω^s for small frequencies and an exponential cutoff at large frequencies, takes the form

$$J(\omega) = \eta\omega^s e^{-\frac{\omega}{\omega_c}} \tag{B.1}$$

where η denotes the coupling strength and ω_c the cutoff frequency. The following discussion of the corresponding bath correlation function (BCF) and its half-sided Fourier transform (FT) distinguishes between the sub-Ohmic ($s < 1$) and the Ohmic ($s = 1$) case.

First the analytic expression of the BCF in terms of the Riemann zeta function is examined. In particular, the asymptotic decay is investigated. Furthermore, efficient numeric methods to evaluate the half-sided FT of the BCF are presented. Whereas for zero temperature it is sufficient to evaluate the incomplete gamma function, for non-zero temperature the integral expression of the Cauchy principal value (CPV)

needs to be evaluated numerically. Additionally, special emphasis is given to the series expansion around $\omega = 0$.

To reiterate, for a given SD $J(\omega)$, the BCF for a given inverse temperature β is defined as [Wei08]

$$\alpha(\beta,\tau) := \frac{1}{\pi}\int_0^\infty \mathrm{d}\omega\, J(\omega)\left(\coth(\beta\omega/2)\cos(\omega\tau) - \mathrm{i}\sin(\omega\tau)\right)\ . \tag{B.2}$$

Using that $\coth(\beta\omega/2) = 1 + 2\bar{n}(\beta\omega)$ with the Bose-Einstein distribution $\bar{n}(\beta\omega) = (e^{\beta\omega}-1)^{-1}$ yields to the alternative form (as introduced in Eq. (2.72) already)

$$\alpha(\beta,\tau) = \frac{1}{\pi}\int_0^\infty \mathrm{d}\omega\, J(\omega)\Big(2\bar{n}(\beta\omega)\cos(\omega\tau) + e^{-\mathrm{i}\omega\tau}\Big) = \alpha(\beta,\tau) + \alpha_\beta(\tau) \tag{B.3}$$

which shows that the thermal BCF splits into two parts, i.e., the zero temperature contribution

$$\alpha(\tau) := \frac{1}{\pi}\int_0^\infty \mathrm{d}\omega\, J(\omega)e^{-\mathrm{i}\omega\tau} \tag{B.4}$$

and a remainder

$$\alpha_\beta(\tau) := \frac{2}{\pi}\int_0^\infty \mathrm{d}\omega\, \bar{n}(\beta\omega)J(\omega)\cos(\omega\tau)\ . \tag{B.5}$$

The terminology is motivated by the fact that in the limit of zero temperature, i.e., $\beta\to\infty$, it holds that $\alpha_\beta(\tau)\to 0$ and, thus, $\alpha(\beta,\tau)\to\alpha(\tau)$. This splitting is useful to express the thermal BCF for (sub-) Ohmic SD analytically. Additionally, it turns out convenient to express the thermal BCF as the FT of an effective SD, i.e.,

$$J(\beta,\omega) := \frac{J(\omega)}{1-e^{-\beta\omega}} \quad \text{with} \quad J(\omega) := -J(-\omega) \quad \text{for} \quad \omega<0\ . \tag{B.6}$$

With this definition, the thermal BCF can also be expressed as

$$\alpha(\beta,\tau) = \frac{1}{\pi}\int_{-\infty}^\infty \mathrm{d}\omega\, J(\beta,\omega)e^{-\mathrm{i}\omega\tau}\ . \tag{B.7}$$

We employ this relation to evaluate the half-sided FT of the thermal BCF, i.e.,

$$F(\beta,\omega) := \int_0^\infty \mathrm{d}\tau\, \alpha(\beta,\tau)e^{\mathrm{i}\omega\tau} \equiv J(\beta,\omega) + \mathrm{i}S(\beta,\omega)\ . \tag{B.8}$$

Note that due to the oscillating integrand the above integral is not suited for an accurate numerical evaluation, especially for large ω. However, since the thermal BCF has been expressed in terms of the FT of an effective SD, this problem can be circumvented by using that the imaginary part $S(\beta,\omega)$ is related to the real part $J(\beta,\omega)$ by the Cauchy-Principal value, denoted by $\mathcal{P}$, of the integral

$$S(\beta,\omega) = -\frac{1}{\pi}\mathcal{P}\int_{-\infty}^\infty \mathrm{d}\omega'\,\frac{J(\beta,\omega')}{\omega'-\omega}\ . \tag{B.9}$$

B.1 Bath Correlation Function

For an inverse temperature β, the thermal BCF is most conveniently expressed as in Eq. (2.72), i.e.,

$$\begin{aligned} \alpha(\beta,\tau) &= \alpha(\tau) + \alpha_\beta(\tau) \quad \text{with} \\ \alpha(\tau) &= \frac{\eta}{\pi}\int_0^\infty \mathrm{d}\omega\, \omega^s e^{-\frac{\omega}{\omega_c}} e^{-\mathrm{i}\omega\tau} = \frac{\eta}{\pi}\Gamma(s+1)\left(\frac{\omega_c}{1+\mathrm{i}\omega_c\tau}\right)^{s+1} \\ \text{and} \quad \alpha_\beta(\tau) &= \frac{2\eta}{\pi}\mathrm{Re}\left[\int_0^\infty \mathrm{d}\omega\, \frac{\omega^s e^{-\frac{\omega}{\omega_c}}}{e^{\beta\omega}-1} e^{-\mathrm{i}\omega\tau}\right] \\ &= \frac{2\eta}{\pi\beta^{s+1}}\Gamma(s+1)\mathrm{Re}\left[\zeta\left(s+1, \frac{1+\beta\omega_c+\mathrm{i}\omega_c\tau}{\beta\omega_c}\right)\right] , \end{aligned} \tag{B.10}$$

with the obvious zero temperature limit

$$\lim_{\beta\to\infty} \alpha(\beta,\tau) = \alpha(\tau) \sim (1+\mathrm{i}\omega_c\tau)^{-(s+1)} \tag{B.11}$$

showing an algebraic decay of power $s+1$. Γ denotes the gamma function and ζ the Hurwitz zeta function [ON10].

Note that the ζ function with complex arguments is, for example, implemented by the arbitrary precision library Arb (`arblib.org`) [Joh17]. This library can be used to assure correct 64-bit results by using a higher intermediate working precision.

Introducing $z := (1+\mathrm{i}\omega_c\tau)/\beta\omega_c$ leads to for the compact notation,

$$\alpha(\beta,\tau) = \frac{\eta\Gamma(s+1)}{\pi\beta^{s+1}}\left(z^{-(s+1)} + 2\mathrm{Re}[\zeta(s+1,z+1)]\right) . \tag{B.12}$$

From the series expansion of ζ [ON10] in terms of the second argument, i.e.,

$$\zeta(s+1,a) = \frac{a^{-s}}{s} + \frac{a^{-(s+1)}}{2} + \mathcal{O}\left(a^{-(s+2)}\right) , \tag{B.13}$$

the leading order terms of the asymptotic (large τ) behavior of the thermal BCF is deduced. It is instructive rewrite the complex power as,

$$a^{-s} = (x+\mathrm{i}y)^{-s} = \left(\frac{x-\mathrm{i}y}{x^2+y^2}\right)^s = \frac{e^{-\mathrm{i}s\varphi}}{(x^2+y^2)^{s/2}} , \tag{B.14}$$

with $\tan(\varphi) = y/x$. In the asymptotic regime $\omega_c\tau \gg 1 \Leftrightarrow \varepsilon := x/y \ll 1$ the following relation holds,

$$y/x = \tan(\varphi) \approx \frac{1}{\pi/2-\varphi} \quad \Rightarrow \quad \varphi = \frac{\pi}{2} - \varepsilon , \tag{B.15}$$

and therefore,

$$(x+\mathrm{i}y)^{-s} = \frac{e^{-\mathrm{i}s\pi/2}}{y^s}\left(1+(\mathrm{i}s-s/2)\varepsilon+\mathcal{O}(\varepsilon^2)\right) . \tag{B.16}$$

Using this expression yields for the leading order terms of the asymptotic behavior of the BCF [Eq. (B.12)]

$$\alpha(\beta,\tau) \approx \frac{\eta\Gamma(s+1)}{\pi}\cos(s\pi/2)\left(\frac{2}{s\beta}\frac{1}{\tau^s}-\mathrm{i}\frac{1}{\tau^{s+1}}\right) . \tag{B.17}$$

For the Ohmic case ($s=1$), however, since $\cos(\pi/2)=0$, these terms vanish. Consequently, the asymptotic behavior is determined by the terms of next order, i.e.,

$$\alpha(\beta,\tau) \approx \frac{2\eta}{\pi}\left(\frac{1}{\beta\omega_c\tau^2}-\mathrm{i}\frac{1}{\omega_c\tau^3}\right) . \tag{B.18}$$

One sees that the asymptotic values are suppressed roughly by the factor $(\omega_c\tau)^{-1}$ compared to the sub-Ohmic case (see also Fig. 3.19) which means that the BCF decays much faster. Note that for $s\approx 1$ the leading order terms are scaled by $\cos(s\pi/2)$ which is then close to zero. Therefore, the different asymptotic scaling becomes noticeable only for sufficiently large τ.

B.2 Half-Sided Fourier Transform

In many perturbative approaches the half-sided FT of the BCF needs to be evaluated, i.e.,

$$F(\beta,\omega) := \int_0^\infty \mathrm{d}\tau\, \alpha(\beta,\tau)e^{\mathrm{i}\omega\tau} \equiv J(\beta,\omega)+\mathrm{i}S(\beta,\omega) . \tag{B.19}$$

Its real part simply corresponds to the effective SD $J(\beta,\omega)$ [Eq. (B.6)] whereas the imaginary part $S(\beta,\omega)$ needs to be deduced.

B.2.1 Zero Temperature

For the zero temperature BCF [Eq. (B.10)]

$$\alpha(\tau) = \frac{\eta\Gamma(s+1)}{\pi}\frac{\omega_c^{s+1}}{(1+\mathrm{i}\omega_c\tau)^{s+1}} \tag{B.20}$$

the half-sided FT can be written by means of the incomplete Gamma function (implemented for example by the Arb library [Joh17])

$$F(\omega) = \frac{\eta\Gamma(s+1)}{\pi}\frac{(-\mathrm{i}\omega)^s}{\mathrm{i}^{s+1}}e^{-\frac{\omega}{\omega_c}}\lim_{\epsilon\to 0}\Gamma\left(-s,-\left(\frac{\omega}{\omega_c}+\mathrm{i}\epsilon\right)\right) . \tag{B.21}$$

The limit assures the correct branch since the incomplete gamma function experiences a branch cut along the negative real axis. For $\omega > 0$ this expression can be rewritten as

$$\begin{aligned} F_>(\omega) =& \eta\omega^s e^{-\frac{\omega}{\omega_c}} F_\Gamma\left(\frac{\omega}{\omega_c}, s\right) \quad \text{with} \\ F_\Gamma(x,s) :=& \frac{\Gamma(s+1)}{\pi} e^{-\mathrm{i}\pi(s+1/2)} \lim_{\epsilon\to 0} \Gamma\left(-s, -(x+\mathrm{i}\epsilon)\right) \end{aligned} \tag{B.22}$$

where, indeed, the real part of F_Γ equals to 1. For negative ω the expression takes the form

$$F_<(\omega) = -\mathrm{i}\frac{\eta\Gamma(s+1)}{\pi}|\omega|^s e^{\frac{|\omega|}{\omega_c}} \Gamma\left(-s, \frac{|\omega|}{\omega_c}\right) . \tag{B.23}$$

Since the incomplete gamma function is purely real valued for a positive second argument, $F_<(\omega)$ is purely imaginary, as expected.

The regime $|\omega| \ll \omega_c$ follows from the series expansion in the second argument of the incomplete gamma function ($0 < s < 1$), i.e.,

$$\Gamma(-s,z) = \Gamma(-s) + \frac{1}{z^s}\left(\frac{1}{s} + \frac{z}{1-s} + \mathcal{O}(z^2)\right) . \tag{B.24}$$

Whereas the expansion of $F_<$ follows immediately ($x = |\omega|/\omega_c$)

$$F_<(\omega) = -\mathrm{i}\frac{\eta\Gamma(s)\omega_c^s}{\pi}\left(1 + s\Gamma(-s)x^s + \frac{1}{1-s}x + \mathcal{O}\left(x^{s+1}\right)\right) \tag{B.25}$$

the negative second arguments appearing in the expression for $F_>$ requires special care. Using

$$\lim_{\epsilon\to 0}\left(-(x+\mathrm{i}\epsilon)\right)^s = e^{-\mathrm{i}\pi s}x^s \tag{B.26}$$

and Euler's reflection formula $\Gamma(s+1)\Gamma(-s) = -\pi\sin^{-1}(\pi s)$ yields

$$\begin{aligned} F_\Gamma(x,s) =& -\mathrm{i}\frac{\Gamma(s+1)}{\pi}e^{-\mathrm{i}\pi s}\left(\Gamma(-s) + \frac{1}{s}\frac{e^{\mathrm{i}\pi s}}{x^s} - \frac{1}{1-s}\frac{e^{\mathrm{i}\pi s}}{x^{s-1}} + \mathcal{O}(x^{2-s})\right) \\ =& 1 - \mathrm{i}\left(\frac{\Gamma(s+1)}{\pi s x^s} - \cot(\pi s) - \frac{\Gamma(s+1)}{\pi(1-s)}x^{1-s} + \mathcal{O}(x^{2-s})\right) \end{aligned} \tag{B.27}$$

and, thus, ($x = \omega/\omega_c$)

$$F_>(\omega) = J(\omega) - \mathrm{i}\eta\omega_c^s\left(\frac{\Gamma(s)}{\pi} - \cot(\pi s)x^s - \frac{\Gamma(s)}{\pi(1-s)}x + \mathcal{O}(x^{s+1})\right) . \tag{B.28}$$

Finally, the series expansion of the imaginary part of the half-sided FT reads in compact notation

$$S(\omega) = -\frac{\eta\omega_c^s\Gamma(s)}{\pi}\left(1 - \Gamma(1-s)g(s,\omega)(|\omega|/\omega_c)^s - \frac{\omega}{\omega_c(1-s)} + \mathcal{O}((|\omega|/\omega_c)^{s+1})\right)$$
$$\text{with} \quad g(s,\omega) \coloneqq \cos(\pi s)\theta(\omega) + \theta(-\omega)\ , \tag{B.29}$$

where θ denotes the Heaviside step function.

For the Ohmic case ($s = 1$) the expansion of the incomplete gamma function reads

$$\Gamma(-1, z) = \frac{1}{z} - (1-\gamma) + \ln(z) + \frac{z}{2} + \mathcal{O}(z^2) \tag{B.30}$$

which results in

$$S(\omega) = -\frac{\eta\omega_c}{\pi}\left(1 - \left(\gamma + \ln(|\omega|/\omega_c)\right)\frac{\omega}{\omega_c} + \mathcal{O}((|\omega|/\omega_c)^2)\right) \tag{B.31}$$

where $\gamma = 0.577\ldots$ denotes the Euler–Mascheroni constant.

B.2.2 Non-Zero Temperature

For non-zero temperature the BCF is conveniently expressed as the FT of the effective SD $J(\beta,\omega)$ [Eq. (B.6) and Eq. (B.7)]. The half-sided FT splits in a real and an imaginary part, i.e.,

$$\int_0^\infty \mathrm{d}\tau\, \alpha(\beta,\tau)e^{\mathrm{i}\omega\tau} = F(\beta,\omega) \equiv J(\beta,\omega) + \mathrm{i}S(\beta,\omega) \tag{B.32}$$

where $S(\beta,\omega)$ can be evaluated in terms of the Cauchy principal value (CPV) $\mathcal{P}$ of the integral

$$S(\beta,\omega) = -\frac{1}{\pi}\mathcal{P}\int_{-\infty}^{\infty}\mathrm{d}\omega'\,\frac{J(\beta,\omega')}{\omega'-\omega}\ . \tag{B.33}$$

For a numeric treatment, this non-oscillatory expression is more suitable. The limit defining the CPV is simply incorporated by splitting the integral at ω and substituting $x = \omega' - \omega$,

$$\begin{aligned} I(\omega) &\coloneqq \mathcal{P}\int_{-\infty}^{\infty}\mathrm{d}\omega'\,\frac{J(\beta,\omega')}{\omega'-\omega} \\ &= \lim_{\epsilon\to 0}\left[\int_{-\infty}^{\omega-\epsilon}\mathrm{d}\omega'\,\frac{J(\beta,\omega')}{\omega'-\omega} + \int_{\omega+\epsilon}^{\infty}\mathrm{d}\omega'\,\frac{J(\beta,\omega')}{\omega'-\omega}\right] \\ &= \lim_{\epsilon\to 0}\int_{\epsilon}^{\infty}\mathrm{d}x\,\frac{J(\beta,\omega+x) - J(\beta,\omega-x)}{x}\ . \end{aligned} \tag{B.34}$$

By the additional substitution $y = x/|\omega| \geq 0$ the difficult points of the integrand are located at $y = 0$ (possible pole from the CPV) and $y = 1$ (singularity of the

effective SD at $\omega' = 0$ for sub-Ohmic SDs). Noting that $\omega \pm x = |\omega|(\mathrm{sgn}(\omega) \pm y) = \omega(1 \pm \mathrm{sgn}(\omega)y)$ holds, the CPV integral becomes,

$$\begin{aligned} I(\omega) &= \int_0^\infty \mathrm{d}y \, \frac{I_f(\omega, y)}{y} \\ I_f(\omega, y) &:= \frac{J(|\omega|(\mathrm{sgn}(\omega) + y))}{1 - e^{-\omega\beta(1+\mathrm{sgn}(\omega)y)}} - \frac{J(|\omega|(\mathrm{sgn}(\omega) - y))}{1 - e^{-\omega\beta(1-\mathrm{sgn}(\omega)y)}} \, . \end{aligned} \tag{B.35}$$

Realizing that for $\omega > 0$ this expressions reduces to

$$I_{f_>}(\omega, y) := \frac{J(|\omega|(1 + y))}{1 - e^{-\omega\beta(1+y)}} - \frac{J(|\omega|(1 - y))}{1 - e^{-\omega\beta(1-y)}} \tag{B.36}$$

whereas for $\omega < 0$, using the antisymmetry of $J(\omega)$ allows us to write $I_f(\omega, y)$ as

$$\begin{aligned} I_{f_<}(\omega, y) :=& \frac{J(|\omega|(-1 + y))}{1 - e^{-\omega\beta(1-y)}} - \frac{J(|\omega|(-1 - y))}{1 - e^{-\omega\beta(1+y)}} \\ =& \frac{-J(|\omega|(1 - y))}{1 - e^{-\omega\beta(1-y)}} + \frac{J(|\omega|(1 + y))}{1 - e^{-\omega\beta(1+y)}} = I_{f_>}(\omega, y) \, . \end{aligned} \tag{B.37}$$

In summary, the CPV integral becomes

$$\begin{aligned} I(\omega) =& \int_0^\infty \mathrm{d}y \, \frac{1}{y} \left(\frac{J(|\omega|(1 + y))}{1 - e^{-\omega\beta(1+y)}} - \frac{J(|\omega|(1 - y)}{1 - e^{-\omega\beta(1-y)}} \right) \\ =& \frac{|\omega|^s}{\omega\beta} \left[\int_0^1 \mathrm{d}y \, \frac{\omega\beta}{y} \left(\frac{(1 + y)^s e^{-\frac{|\omega|}{\omega_c}(1+y)}}{1 - e^{-\omega\beta(1+y)}} - \frac{(1 - y)^s e^{-\frac{|\omega|}{\omega_c}(1-y)}}{1 - e^{-\omega\beta(1-y)}} \right) \right. \\ &+ \left. \int_1^\infty \mathrm{d}y \, \frac{\omega\beta}{y} \left(\frac{(1 + y)^s e^{-\frac{|\omega|}{\omega_c}(1+y)}}{1 - e^{-\omega\beta(1+y)}} + \frac{(y - 1)^s e^{-\frac{|\omega|}{\omega_c}(y-1)}}{1 - e^{-\omega\beta(1-y)}} \right) \right] \end{aligned} \tag{B.38}$$

where $\omega\beta$ has been factored out such that the integrals remain finite at $\omega = 0$. It is convenient to define $\mu = |\omega|/\omega_c$ and $\nu = \omega\beta\omega_c/|\omega| = \omega\beta/\mu$ which leads to

$$I(\omega) = \frac{\omega_c^s}{\nu} \mu^{s-1} \Big(I_{01}(s, \mu, \nu) + I_{0\infty}(s, \mu, \nu) \Big) \, . \tag{B.39}$$

Introducing the helper functions

$$f(x, \mu, \alpha) := x^{s-1} g(\mu x, \alpha) \quad \text{and} \quad g(z, \alpha) := \frac{\alpha z e^{-z}}{1 - e^{-\alpha z}} \tag{B.40}$$

allows us to write the integrals in the compact notation

$$\begin{aligned} I_{01} &= \int_0^1 \mathrm{d}y \, \frac{f(y + 1, \mu, \nu) - f(1 - y, \mu, +\nu)}{y} \, , \\ I_{1\infty} &= \int_1^\infty \mathrm{d}y \, \frac{f(y + 1, \mu, \nu) - f(y - 1, \mu, -\nu)}{y} \, . \end{aligned} \tag{B.41}$$

Due to the possible singularities, the TS integration scheme [Mor05] should be used for numerical integration which still yields very accurate results. For completeness,

since the singularities are best coped with if they are located at zero, the numerical evaluation is done by integrating three separate integrals (see also Fig. B.1), i.e.,

$$\begin{aligned} I_{01} =& I_{01,a} + I_{01,b} \quad \text{with} \\ I_{01,a} =& \int_0^{\frac{1}{2}} \mathrm{d}y \, \frac{f(y+1,\mu,\nu) - f(1-y,\mu,+\nu)}{y} \,, \\ I_{01,b} =& \int_0^{\frac{1}{2}} \mathrm{d}y \, \frac{f(2-y,\mu,\nu) - f(y,\mu,+\nu)}{1-y} \quad \text{and} \\ I_{0\infty} =& \int_0^{\infty} \mathrm{d}y \, \frac{f(y+2,\mu,\nu) - f(y,\mu,-\nu)}{1+y} \,. \end{aligned} \tag{B.42}$$

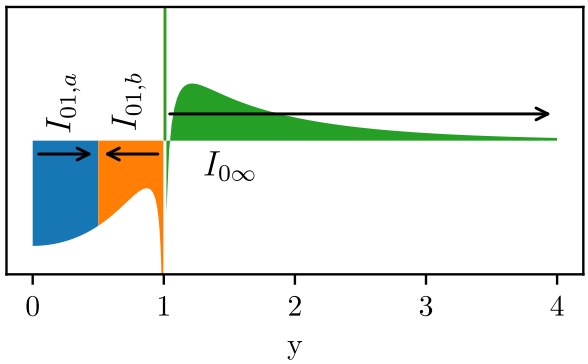

Fig. B.1: Sketch of the integral splitting suitable for the TS integration routine.

To correctly account for small, i.e., $\mu = |\omega|/\omega_c \ll 1$, the integrals need to be expanded around 0. For the sub-Ohmic case ($0 < s < 1$) the expansion reads

$$\begin{aligned} I_{01}(\mu) =& c_0 + c_1\mu + \mathcal{O}(\mu^2) \quad \text{with} \\ c_0 =& \int_0^{\frac{1}{2}} \mathrm{d}y \, \frac{(1+y)^{s-1} - (1-y)^{s-1}}{y} + \int_0^{\frac{1}{2}} \mathrm{d}y \, \frac{(2-y)^{s-1} - y^{s-1}}{1-y} \quad \text{and} \\ c_1 =& \frac{\nu-2}{2} \int_0^1 \mathrm{d}y \, \frac{(1+y)^s - (1-y)^s}{y} \,, \end{aligned} \tag{B.43}$$

as well as

$$\begin{aligned} I_{1\infty}(\mu) =& d_0 + d_s\mu^{1-s} + d_1\mu + \mathcal{O}(\mu^{2-s}) \quad \text{with} \\ d_0 =& \int_0^{\infty} \mathrm{d}y \, \frac{(y+2)^{s-1} - y^{s-1}}{y+1} \,, \\ d_s =& \frac{\nu}{1-s}(\Gamma(s) - \Gamma(s+1)) \quad \text{and} \\ d_1 =& \frac{\nu-2}{2s} \left[\int_0^1 \mathrm{d}y \, \left(\frac{1}{y}+1\right)^s - 2^{s+1} \right] - \frac{\nu+2}{2s} \int_0^1 \mathrm{d}y \, \left(\frac{1}{y}-1\right)^s \,. \end{aligned} \tag{B.44}$$

In case of an Ohmic SD ($s = 1$) it follows that

$$I_{01}(\mu) = c_0 + c_1\mu + \mathcal{O}(\mu^2) \quad \text{with} \quad c_0 = 0 \quad \text{and} \quad c_1 = \nu - 2 \,, \tag{B.45}$$

as well as

$$I_{1\infty}(\mu) = \nu + [\nu\gamma - 2b_0(\nu) + 2\ln(\mu)]\mu + \mathcal{O}(\mu^2) \quad \text{with}$$
$$b_0(\nu) = \int_0^\infty \mathrm{d}z\, g''(z,\nu)\ln(z)\ , \tag{B.46}$$

where $\gamma = 0.577\ldots$ denotes the Euler–Mascheroni constant. Note that the second derivative of g in the integral for b_0 needs special care when evaluated for z close to zero. This is related to the cancellation of precision of terms like $e^x - \sum_{k=0}^{n-1} x^k/k! \sim x^n + \mathcal{O}(x^{n+1})$ which is most dramatically for $x \leq 10^{-16/n}$ where the difference becomes numerically zero.

C Fit Data for the Exponential Expansion of (Sub-) Ohmic SDs

C.1 Relative Difference

The following tables show the fit data for G_μ and W_μ corresponding to the fits used in the left panel of Fig. 3.10. The accuracy A quantifies the *maximum relative* error such that $\epsilon = 10^{-A}$ over the time interval given by the decay threshold D [Eq. (3.31)].

- D = 2

$s = 0.1$	G_μ	real	imag	G_μ	real	imag	W_μ	real	imag	W_μ	real	imag
$N = 4$	1	-2.37062e-3	-3.88096e-2	2	+3.75720e-2	-1.88078e-1	1	+2.09791e-2	+1.26063e-3	2	+1.41558e-1	+1.75451e-2
A = 1.65	3	+5.92051e-1	-3.57569e-1	4	+3.91768e-1	+5.96105e-1	3	+5.78348e-1	+2.04310e-1	4	+1.55126e+0	+1.37439e+0
$N = 5$	1	-2.11021e-3	-3.05227e-2	2	+1.10752e-2	-1.19967e-1	1	+1.72661e-2	+1.02508e-3	2	+1.03266e-1	+9.60025e-3
A = 2.27	3	+2.11294e-1	-3.29215e-1	4	-1.69473e-2	+4.46271e-1	3	+3.62246e-1	+7.46272e-2	4	+2.13559e+0	+2.03959e+0
	5	+7.95847e-1	+3.87365e-2				5	+1.01896e+0	+4.77135e-1			
$N = 6$	1	-1.86246e-3	-2.52455e-2	2	+3.55113e-3	-8.75830e-2	1	+1.47116e-2	+8.69320e-4	2	+8.25642e-2	+6.57813e-3
A = 2.91	3	+8.38673e-2	-2.29588e-1	4	-1.55422e-1	+1.98214e-1	3	+2.58593e-1	+3.71272e-2	4	+2.73737e+0	+2.76113e+0
	5	+4.91297e-1	-2.93854e-1	6	+5.77363e-1	+4.38351e-1	5	+6.81506e-1	+1.98828e-1	6	+1.51535e+0	+8.50352e-1
$N = 7$	1	-1.67177e-3	-2.14287e-2	2	+6.20109e-4	-6.88329e-2	1	+1.27728e-2	+7.40772e-4	2	+6.90492e-2	+4.94753e-3
A = 3.51	3	-1.30049e-1	+3.72693e-2	4	+3.81276e-2	-1.65322e-1	3	+3.34701e+0	+3.49724e+0	4	+2.00653e-1	+2.22389e-2
	5	+2.45179e-1	-2.98643e-1	6	+1.82980e-1	+5.41438e-1	5	+4.89037e-1	+9.81346e-2	6	+2.04056e+0	+1.28855e+0
	7	+6.64632e-1	-2.47175e-2				7	+1.07092e+0	+3.93436e-1			

$s = 0.3$	G_μ	real	imag	G_μ	real	imag	W_μ	real	imag	W_μ	real	imag
$N = 4$	1	-1.24638e-2	-4.27082e-2	2	+2.55276e-2	-2.48146e-1	1	+4.37116e-2	+4.38070e-3	2	+2.45550e-1	+4.38858e-2
A = 1.8	3	+2.50856e-1	+6.47691e-1	4	+7.44116e-1	-3.43373e-1	3	+1.88995e+0	+1.77967e+0	4	+8.27197e-1	+3.52115e-1
$N = 5$	1	-9.93756e-3	-3.24427e-2	2	-7.09455e-3	-1.57123e-1	1	+3.61240e-2	+3.60527e-3	2	+1.85172e-1	+2.63636e-2
A = 2.48	3	-1.30168e-1	+3.85127e-1	4	+2.88947e-1	-4.16177e-1	3	+2.55100e+0	+2.56135e+0	4	+5.66325e-1	+1.53055e-1
	5	+8.55959e-1	+2.22996e-1				5	+1.36226e+0	+7.32490e-1			
$N = 6$	1	-8.17305e-3	-2.61038e-2	2	-1.33949e-2	-1.12965e-1	1	+3.08905e-2	+3.12090e-3	2	+1.50779e-1	+1.93145e-2
A = 3.17	3	-1.81059e-1	+1.06606e-1	4	+1.06482e-1	-3.12304e-1	3	+3.23907e+0	+3.41477e+0	4	+4.26298e-1	+8.66504e-2
	5	+6.59731e-1	-2.62584e-1	6	+4.35857e-1	+6.07020e-1	5	+9.91847e-1	+3.59283e-1	6	+1.95030e+0	+1.22659e+0
$N = 7$	1	-6.88935e-3	-2.17126e-2	2	-1.41717e-2	-8.76359e-2	1	+2.69811e-2	+2.75912e-3	2	+1.27972e-1	+1.55288e-2
A = 3.87	3	+4.01092e-2	-2.31113e-1	4	+3.70617e-1	-3.59356e-1	3	+3.43111e-1	+5.85857e-2	4	+7.59344e-1	+2.08148e-1
	5	+7.47224e-1	+1.91333e-1	6	-4.19021e-2	+5.27154e-1	5	+1.48925e+0	+6.70211e-1	6	+2.57224e+0	+1.82736e+0
	7	-9.49246e-2	-1.87573e-2				7	+3.94340e+0	+4.35150e+0			

$s = 0.5$	G_μ	real	imag	G_μ	real	imag	W_μ	real	imag	W_μ	real	imag
$N = 4$	1	-2.30979e-2	-4.50549e-2	2	+1.42756e-2	-3.14262e-1	1	+7.60300e-2	+1.10845e-2	2	+3.69536e-1	+8.69550e-2
A = 1.94	3	+1.21301e-1	+6.66241e-1	4	+8.88799e-1	-2.95390e-1	3	+2.20511e+0	+2.17970e+0	4	+1.07775e+0	+5.27688e-1
$N = 5$	1	-1.77355e-2	-3.29925e-2	2	-2.82220e-2	-1.97382e-1	1	+6.30497e-2	+9.20233e-3	2	+2.85764e-1	+5.59422e-2

$A = 2.66$	3	-2.05767e-1	+3.11814e-1	4	+3.88851e-1	-4.93282e-1	3	+2.93475e+0	+3.06752e+0	4	+7.86669e-1	+2.61038e-1
	5	+8.60771e-1	+4.12408e-1				5	+1.69321e+0	+1.01128e+0			
$N = 6$	1	-1.37977e-2	-2.58589e-2	2	-3.19165e-2	-1.38546e-1	1	+5.38679e-2	+8.43298e-3	2	+2.34716e-1	+4.43741e-2
$A = 3.4$	3	-1.74947e-1	+3.34362e-2	4	+1.43765e-1	-3.98068e-1	3	+3.71346e+0	+4.04667e+0	4	+6.12350e-1	+1.65362e-1
	5	+2.59580e-1	+7.07127e-1	6	+8.17201e-1	-1.78455e-1	5	+2.36167e+0	+1.62452e+0	6	+1.30283e+0	+5.60581e-1
$N = 7$	1	-1.12861e-2	-2.05713e-2	2	-3.07580e-2	-1.03383e-1	1	+4.66458e-2	+7.22022e-3	2	+1.98628e-1	+3.55020e-2
$A = 4.13$	3	+4.44907e-2	-2.99057e-1	4	+5.09481e-1	-3.94004e-1	3	+4.98993e-1	+1.16682e-1	4	+1.03085e+0	+3.50903e-1
	5	+7.53102e-1	+4.09629e-1	6	-2.06917e-1	+4.49655e-1	5	+1.88049e+0	+9.68301e-1	6	+3.05487e+0	+2.35255e+0
	7	-5.80542e-2	-4.22467e-2				7	+4.50396e+0	+5.18799e+0			

$s = 1$	G_μ	real	imag	G_μ	real	imag	W_μ	real	imag	W_μ	real	imag
$N = 4$	1	-4.96766e-2	-4.62328e-2	2	+4.14072e-3	-4.95114e-1	1	+1.93537e-1	+5.21517e-2	2	+7.23489e-1	+2.71841e-1
$A = 2.19$	3	-1.35525e-1	+6.24629e-1	4	+1.17658e+0	-7.86632e-2	3	+2.90446e+0	+3.15131e+0	4	+1.67280e+0	+1.04700e+0
$N = 5$	1	-3.54708e-2	-3.05365e-2	2	-2.80345e-1	+1.37315e-1	1	+1.61586e-1	+4.38557e-2	2	+3.77372e+0	+4.27130e+0
$A = 3.01$	3	-8.20466e-2	-3.08517e-1	4	+6.97903e-1	-6.05675e-1	3	+5.83764e-1	+1.94647e-1	4	+1.34332e+0	+6.36621e-1
	5	+6.99328e-1	+8.06701e-1				5	+2.44460e+0	+1.76507e+0			
$N = 6$	1	-2.69854e-2	-2.16956e-2	2	-1.04127e-1	-7.90134e-2	1	+1.39329e-1	+3.74378e-2	2	+4.90069e+0	+5.49211e+0
$A = 3.81$	3	-9.42500e-2	-2.08283e-1	4	+3.07626e-1	-6.42410e-1	3	+4.94837e-1	+1.52357e-1	4	+1.12988e+0	+4.45419e-1
	5	-2.17400e-1	+7.28106e-1	6	+1.13527e+0	+2.23258e-1	5	+3.38190e+0	+2.63369e+0	6	+2.09861e+0	+1.15274e+0
$N = 7$	1	-2.07927e-2	-1.55233e-2	2	-8.64337e-2	-1.43833e-1	1	+1.20860e-1	+3.15279e-2	2	+4.24088e-1	+1.23136e-1
$A = 4.42$	3	+8.68540e-2	-5.27435e-1	4	+9.90641e-1	-3.23219e-1	3	+9.56214e-1	+3.36265e-1	4	+1.77977e+0	+8.19865e-1
	5	+4.34348e-1	+9.70987e-1	6	-4.23245e-1	+8.31226e-2	5	+2.93767e+0	+1.82607e+0	6	+4.45226e+0	+3.66096e+0
	7	+1.86053e-2	-4.40760e-2				7	+6.29211e+0	+6.79231e+0			

- $D = 4$

$s = 0.1$	G_μ	real	imag	G_μ	real	imag	W_μ	real	imag	W_μ	real	imag
$N = 6$	1	-6.99951e-5	-4.48480e-4	2	-4.18890e-4	-2.84453e-3	1	+3.58817e-4	+5.09446e-7	2	+2.77759e-3	+1.17736e-5
$A = 1.4$	3	-1.94312e-3	-1.85600e-2	4	+1.04115e-2	-1.19787e-1	3	+1.56920e-2	+2.93207e-4	4	+8.63100e-2	+7.00748e-3
	5	+4.40759e-1	-4.11470e-1	6	+5.78923e-1	+5.58691e-1	5	+4.28034e-1	+1.32667e-1	6	+1.32056e+0	+1.18138e+0
$N = 7$	1	-5.84908e-5	-3.74349e-4	2	-2.82387e-4	-1.87671e-3	1	+3.12153e-4	+4.36805e-7	2	+2.11180e-3	+6.57407e-6
$A = 1.77$	3	-1.18311e-3	-9.31168e-3	4	-1.86164e-3	-4.71570e-2	3	+9.59154e-3	+1.02686e-4	4	+4.19214e-2	+1.61905e-3
	5	+6.09751e-2	-2.18075e-1	6	+2.68324e-1	+5.71411e-1	5	+1.79211e-1	+2.36723e-2	6	+1.66263e+0	+1.56443e+0
	7	+6.81687e-1	-2.84934e-1				7	+6.65504e-1	+2.61302e-1			
$N = 8$	1	-5.04653e-5	-3.22760e-4	2	-2.09958e-4	-1.37940e-3	1	+2.77029e-4	+3.85020e-7	2	+1.72209e-3	+4.36124e-6
$A = 2.14$	3	-7.63126e-4	-5.55265e-3	4	-2.06714e-3	-2.30307e-2	3	+6.70871e-3	+4.74658e-5	4	+2.46142e-2	+5.37094e-4
	5	+5.69627e-3	-9.44988e-2	6	+1.70101e-1	-3.08842e-1	5	+8.93493e-2	+5.90063e-3	6	+3.13033e-1	+5.86867e-2
	7	+3.31885e-2	+4.70206e-1	8	+7.93887e-1	-3.12739e-2	7	+2.01351e+0	+1.97149e+0	8	+9.32892e-1	+4.32693e-1
$N = 9$	1	-4.44533e-5	-2.84155e-4	2	-1.66717e-4	-1.08740e-3	1	+2.49268e-4	+3.43230e-7	2	+1.46576e-3	+3.18864e-6
$A = 2.5$	3	-5.32334e-4	-3.71897e-3	4	-1.49657e-3	-1.31452e-2	3	+5.11738e-3	+2.61429e-5	4	+1.64164e-2	+2.27310e-4
	5	-1.46885e-3	-4.67595e-2	6	+3.13128e-2	-1.58214e-1	5	+5.19988e-2	+1.95824e-3	6	+1.62910e-1	+1.61387e-2
	7	-1.00750e-1	+3.23987e-1	8	+3.31025e-1	-3.43226e-1	7	+2.37088e+0	+2.39626e+0	8	+4.84914e-1	+1.17832e-1
	9	+7.40580e-1	+2.44121e-1				9	+1.22129e+0	+6.40675e-1			

$s = 0.3$	G_μ	real	imag	G_μ	real	imag	W_μ	real	imag	W_μ	real	imag
$N = 6$	1	-2.30987e-4	-4.62206e-4	2	-1.59009e-3	-3.36175e-3	1	+1.39918e-3	+5.92910e-6	2	+8.77681e-3	+8.86847e-5
$A = 1.58$	3	-8.86792e-3	-2.39788e-2	4	-5.06292e-3	-1.69360e-1	3	+4.01900e-2	+1.42754e-3	4	+1.76144e-1	+2.21233e-2
	5	+6.01806e-1	-4.42220e-1	6	+4.29737e-1	+6.52839e-1	5	+6.68981e-1	+2.59604e-1	6	+1.66855e+0	+1.58466e+0
$N = 7$	1	-1.89229e-4	-3.78238e-4	2	-1.06377e-3	-2.20706e-3	1	+1.22218e-3	+5.17900e-6	2	+6.89166e-3	+5.44401e-5
$A = 1.99$	3	-4.96113e-3	-1.18120e-2	4	-1.55601e-2	-6.53723e-2	3	+2.63287e-2	+5.80310e-4	4	+9.54386e-2	+6.32858e-3
	5	+7.91244e-2	-3.08291e-1	6	+9.32348e-2	+5.75560e-1	5	+3.32261e-1	+6.29356e-2	6	+2.06775e+0	+2.05318e+0
	7	+8.49930e-1	-1.79294e-1				7	+9.77554e-1	+4.60311e-1			
$N = 8$	1	-1.60112e-4	-3.19813e-4	2	-7.86172e-4	-1.61386e-3	1	+1.08699e-3	+4.61508e-6	2	+5.73690e-3	+3.85897e-5
$A = 2.4$	3	-3.10957e-3	-6.97710e-3	4	-1.04541e-2	-3.11746e-2	3	+1.93448e-2	+2.99480e-4	4	+6.05231e-2	+2.45094e-3
	5	-8.81081e-3	-1.37573e-1	6	-1.08389e-1	+3.97883e-1	5	+1.85536e-1	+1.94478e-2	6	+2.47645e+0	+2.54413e+0
	7	+2.63271e-1	-4.06333e-1	8	+8.66274e-1	+1.88480e-1	7	+5.37858e-1	+1.36403e-1	8	+1.31217e+0	+7.08181e-1
$N = 9$	1	-1.38327e-4	-2.76091e-4	2	-6.19004e-4	-1.26172e-3	1	+9.78573e-4	+4.09055e-6	2	+4.94476e-3	+2.93623e-5
$A = 2.81$	3	-2.13875e-3	-4.63701e-3	4	-6.78277e-3	-1.74285e-2	3	+1.52714e-2	+1.77577e-4	4	+4.26682e-2	+1.14213e-3
	5	-1.48644e-2	-6.66716e-2	6	+3.39303e-2	-2.33182e-1	5	+1.16762e-1	+7.36774e-3	6	+3.13074e-1	+4.53318e-2
	7	-1.81806e-1	+2.16848e-1	8	+5.01944e-1	-3.83112e-1	7	+2.89576e+0	+3.04211e+0	8	+7.83192e-1	+2.42776e-1
	9	+6.69205e-1	+4.89745e-1				9	+1.66566e+0	+9.87627e-1			

$s = 0.5$	G_μ	real	imag	G_μ	real	imag	W_μ	real	imag	W_μ	real	imag
$N = 6$	1	-4.06855e-4	-4.23326e-4	2	-3.17755e-3	-3.60407e-3	1	+3.86079e-3	+3.65331e-5	2	+2.07052e-2	+3.99109e-4
$A = 1.73$	3	-1.88817e-2	-2.94166e-2	4	-2.15671e-2	-2.32211e-1	3	+8.12998e-2	+4.63471e-3	4	+2.99589e-1	+5.16317e-2
	5	+2.73283e-1	+7.04312e-1	6	+7.76702e-1	-4.24343e-1	5	+2.00597e+0	+1.99718e+0	6	+9.29895e-1	+4.23462e-1
$N = 7$	1	-3.26394e-4	-3.39012e-4	2	-2.11295e-3	-2.33128e-3	1	+3.38159e-3	+3.22239e-5	2	+1.66167e-2	+2.62170e-4
$A = 2.18$	3	-1.04652e-2	-1.39823e-2	4	-3.51457e-2	-8.79102e-2	3	+5.60030e-2	+2.10357e-3	4	+1.76587e-1	+1.73711e-2
	5	+1.20012e-1	-4.13054e-1	6	-5.62827e-2	+5.35043e-1	5	+5.24420e-1	+1.28614e-1	6	+2.45830e+0	+2.54468e+0
	7	+9.81642e-1	-1.24931e-2				7	+1.30136e+0	+6.97414e-1			
$N = 8$	1	-2.70707e-4	-2.80742e-4	2	-1.54992e-3	-1.68165e-3	1	+3.01183e-3	+2.85535e-5	2	+1.40209e-2	+1.92540e-4
$A = 2.63$	3	-6.53611e-3	-8.06629e-3	4	-2.30915e-2	-4.03291e-2	3	+4.25961e-2	+1.16535e-3	4	+1.18584e-1	+7.46475e-3

	5	-2.60095e-2	-1.94523e-1	6	-1.98868e-1	+3.03600e-1	5	+3.19748e-1	+4.63922e-2	6	+2.91438e+0	+3.10930e+0
	7	+4.02018e-1	-4.87075e-1	8	+8.52356e-1	+4.28765e-1	7	+8.00861e-1	+2.50628e-1	8	+1.69372e+0	+1.01756e+0
$N = 9$	1	-2.28413e-4	-2.34440e-4	2	-1.19409e-3	-1.28204e-3	1	+2.69768e-3	+1.66248e-5	2	+1.21058e-2	+1.32516e-4
$\mathrm{A} = 3.13$	3	-4.37438e-3	-5.22959e-3	4	-1.45598e-2	-2.15606e-2	3	+3.41620e-2	+8.14926e-4	4	+8.63298e-2	+4.11679e-3
	5	-3.49436e-2	-9.14615e-2	6	+4.93396e-2	-3.28109e-1	5	+2.12392e-1	+1.95428e-2	6	+5.06705e-1	+9.53511e-2
	7	+7.06043e-1	-3.55745e-1	8	+5.07022e-1	+6.87755e-1	7	+1.11169e+0	+4.09478e-1	8	+2.10096e+0	+1.36595e+0
	9	-2.07655e-1	+1.15370e-1				9	+3.38892e+0	+3.68077e+0			

$s = 1$	G_μ	real	imag	G_μ	real	imag	W_μ	real	imag	W_μ	real	imag
$N = 5$	1	-1.11571e-3	-1.13362e-4	2	-1.58710e-2	-4.94491e-3	1	+2.44831e-2	+8.41471e-4	2	+1.11631e-1	+7.86456e-3
$\mathrm{A} = 1.54$	3	-1.10814e-1	-1.48545e-1	4	+6.90871e-1	-6.99669e-1	3	+3.94352e-1	+7.63372e-2	4	+1.12768e+0	+5.54962e-1
	5	+4.47964e-1	+8.76912e-1				5	+2.23953e+0	+2.32935e+0			
$N = 6$	1	-8.00051e-4	-7.71852e-5	2	-8.70875e-3	-2.04588e-3	1	+2.10777e-2	+7.33477e-4	2	+8.66699e-2	+4.87592e-3
$\mathrm{A} = 2.07$	3	-6.04564e-2	-4.19271e-2	4	-4.02882e-2	-4.54874e-1	3	+2.63733e-1	+3.26289e-2	4	+7.17669e-1	+2.04606e-1
	5	-7.89155e-2	+6.88243e-1	6	+1.18432e+0	-1.82947e-1	5	+2.79693e+0	+3.02790e+0	6	+1.60538e+0	+9.40320e-1
$N = 7$	1	-6.07565e-4	-5.68297e-5	2	-5.60023e-3	-1.09020e-3	1	+1.85468e-2	+6.55299e-4	2	+7.18536e-2	+3.55620e-3
$\mathrm{A} = 2.6$	3	-3.32656e-2	-1.57897e-2	4	-1.10966e-1	-1.73240e-1	3	+1.97253e-1	+1.78624e-2	4	+4.90529e-1	+9.11637e-2
	5	-2.89400e-1	+3.38965e-1	6	+3.63373e-1	-6.84975e-1	5	+3.36781e+0	+3.75323e+0	6	+1.10520e+0	+4.06703e-1
	7	+1.07413e+0	+5.35794e-1				7	+2.10730e+0	+1.38835e+0			
$N = 8$	1	-4.77791e-4	-4.20760e-5	2	-3.95891e-3	-6.55139e-4	1	+1.65483e-2	+5.65247e-4	2	+6.17820e-2	+2.70384e-3
$\mathrm{A} = 3.15$	3	-2.04159e-2	-7.28470e-3	4	-7.84717e-2	-6.89911e-2	3	+1.58283e-1	+1.10483e-2	4	+3.63310e-1	+4.69817e-2
	5	-2.62149e-1	+7.31195e-2	6	-5.17030e-2	-4.14915e-1	5	+3.94364e+0	+4.48354e+0	6	+7.83963e-1	+1.91604e-1
	7	+9.02135e-1	-5.05668e-1	8	+5.14817e-1	+9.23779e-1	7	+1.53581e+0	+6.67741e-1	8	+2.62539e+0	+1.87304e+0

C.2 Absolute Difference

The following tables show the fit data for G_μ and W_μ corresponding to the fits used for the right panel of Fig. 3.10. The accuracy A quantifies the maximum *absolute error* such that $\epsilon = 10^{-A}$ for all times $\tau \in [0, \infty]$.

$s = 0.1$	G_μ	real	imag	G_μ	real	imag	W_μ	real	imag	W_μ	real	imag
$N = 4$	1	+4.94961e-4	-6.07184e-2	2	+1.84023e-1	-3.21137e-1	1	+2.80945e-2	+2.36555e-3	2	+2.42205e-1	+6.68317e-2
$\mathrm{A} = 2.5$	3	+2.33768e-2	+3.78319e-1	4	+7.91195e-1	+6.59844e-3	3	+2.00206e+0	+2.26706e+0	4	+8.92503e-1	+5.41010e-1
$N = 5$	1	-1.80631e-3	-2.30558e-2	2	+2.92837e-2	-1.54105e-1	1	+1.16463e-2	+4.70862e-4	2	+1.06164e-1	+1.52575e-2
$\mathrm{A} = 2.92$	3	-9.01922e-2	+2.29451e-1	4	+3.93161e-1	-3.50635e-1	3	+2.42174e+0	+2.79962e+0	4	+4.55916e-1	+1.57589e-1
	5	+6.68544e-1	+2.98812e-1				5	+1.23920e+0	+8.23901e-1			
$N = 6$	1	-1.15826e-3	-9.11561e-3	2	+1.97238e-4	-6.46635e-2	1	+5.02657e-3	+6.50619e-5	2	+4.67717e-2	+3.03224e-3
$\mathrm{A} = 3.32$	3	-1.17395e-1	+1.22286e-1	4	+9.32767e-2	-2.44967e-1	3	+2.79926e+0	+3.24552e+0	4	+2.17573e-1	+3.85453e-2
	5	+5.68441e-1	-2.63184e-1	6	+4.56234e-1	+4.59527e-1	5	+6.87268e-1	+2.62223e-1	6	+1.56880e+0	+1.08288e+0
$N = 7$	1	-4.99283e-4	-3.88744e-3	2	-1.73669e-3	-2.75292e-2	1	+2.31738e-3	+4.30159e-5	2	+2.15567e-2	+9.83565e-4
$\mathrm{A} = 3.69$	3	-1.02396e-1	+4.94397e-2	4	+1.51785e-2	-1.16084e-1	3	+3.15009e+0	+3.70755e+0	4	+1.01890e-1	+1.11276e-2
	5	+1.95110e-1	-2.96773e-1	6	+2.36524e-1	+4.88045e-1	5	+3.47122e-1	+8.18079e-2	6	+1.86525e+0	+1.37358e+0
	7	+6.57721e-1	-9.33573e-2				7	+9.09705e-1	+4.01381e-1			
$N = 8$	1	-2.20818e-4	-1.80444e-3	2	-1.45637e-3	-1.26589e-2	1	+1.15444e-3	+3.72552e-5	2	+1.06938e-2	+2.70391e-4
$\mathrm{A} = 4.02$	3	-1.09115e-4	-5.50726e-2	4	-7.72721e-2	+4.56786e-3	3	+5.09123e-2	+2.95840e-3	4	+3.53521e+0	+4.14145e+0
	5	+4.67302e-2	-1.75364e-1	6	+4.20287e-2	+4.42924e-1	5	+1.78976e-1	+2.45639e-2	6	+2.20312e+0	+1.66684e+0
	7	+3.22419e-1	-3.11848e-1	8	+6.67885e-1	+1.09187e-1	7	+5.06939e-1	+1.38443e-1	8	+1.16814e+0	+5.57302e-1
$N = 9$	1	-1.39100e-4	-1.03807e-3	2	-9.38248e-4	-7.37159e-3	1	+6.98168e-4	+1.50269e-5	2	+6.51874e-3	+1.21825e-4
$\mathrm{A} = 4.26$	3	-1.65263e-3	-3.25031e-2	4	-4.26437e-2	-1.27215e-2	3	+3.13579e-2	+1.32107e-3	4	+3.85182e+0	+4.77917e+0
	5	+1.26553e-2	-1.09160e-1	6	+1.28262e-1	-2.64102e-1	5	+1.11765e-1	+1.06880e-2	6	+3.25978e-1	+5.71190e-2
	7	-1.09999e-1	+3.21103e-1	8	+4.89160e-1	-2.47511e-1	7	+2.54972e+0	+2.03313e+0	8	+7.82930e-1	+2.28451e-1
	9	+5.25313e-1	+3.53299e-1				9	+1.52754e+0	+7.44882e-1			

$s = 0.3$	G_μ	real	imag	G_μ	real	imag	W_μ	real	imag	W_μ	real	imag
$N = 4$	1	-1.24673e-2	-6.18827e-2	2	-3.05782e-2	+3.68123e-1	1	+5.24549e-2	+6.49454e-3	2	+2.26317e+0	+2.68838e+0
$\mathrm{A} = 2.61$	3	+1.89481e-1	-3.76616e-1	4	+8.52039e-1	+7.23097e-2	3	+3.52581e-1	+1.19641e-1	4	+1.10387e+0	+7.44590e-1
$N = 5$	1	-7.05864e-3	-2.09185e-2	2	+1.08650e-2	-1.71904e-1	1	+2.32839e-2	+1.53255e-3	2	+1.67428e-1	+3.39302e-2
$\mathrm{A} = 3.07$	3	-1.18312e-1	+2.01632e-1	4	+4.45849e-1	-3.91668e-1	3	+2.69494e+0	+3.27497e+0	4	+6.07869e-1	+2.57513e-1
	5	+6.67819e-1	+3.82897e-1				5	+1.47229e+0	+1.09071e+0			
$N = 6$	1	-3.40903e-3	-7.48794e-3	2	-1.35707e-2	-6.67405e-2	1	+1.08918e-2	+9.85700e-5	2	+8.06677e-2	+7.51729e-3
$\mathrm{A} = 3.5$	3	-1.28647e-1	+8.76841e-2	4	+8.57341e-2	-2.87298e-1	3	+3.13001e+0	+3.78162e+0	4	+3.19357e-1	+7.60166e-2
	5	+4.00539e-1	+5.37959e-1	6	+6.59140e-1	-2.64333e-1	5	+1.84939e+0	+1.40491e+0	6	+8.86218e-1	+4.04464e-1
$N = 7$	1	-1.42457e-3	-3.17818e-3	2	-8.50287e-3	-2.80549e-2	1	+5.61245e-3	+1.39794e-4	2	+4.19789e-2	+3.03098e-3
$\mathrm{A} = 3.88$	3	-9.52753e-2	+2.13577e-2	4	+2.42815e-4	-1.38059e-1	3	+3.49081e+0	+4.33308e+0	4	+1.70469e-1	+2.79196e-2
	5	+2.34968e-1	-3.54971e-1	6	+1.33473e-1	+5.14859e-1	5	+5.05808e-1	+1.56896e-1	6	+2.18825e+0	+1.77555e+0
	7	+7.36506e-1	-1.20554e-2				7	+1.17023e+0	+6.10143e-1			
$N = 8$	1	-7.58760e-4	-1.61275e-3	2	-5.43060e-3	-1.40776e-2	1	+3.35268e-3	+5.85062e-5	2	+2.51564e-2	+1.03292e-3
$\mathrm{A} = 4.17$	3	-4.42513e-2	-2.53913e-2	4	-1.21398e-2	-7.19508e-2	3	+4.27285e+0	+5.10133e+0	4	+1.03428e-1	+1.06903e-2

	5	+5.77062e-2	-2.41982e-1	6	-1.23822e-1	+3.65184e-1	5	+3.16210e-1	+6.64579e-2	6	+2.76443e+0	+2.30967e+0
	7	+4.66308e-1	-3.38418e-1	8	+6.62424e-1	+3.28241e-1	7	+7.79045e-1	+2.83436e-1	8	+1.58950e+0	+9.06683e-1
$N = 9$	1	-4.76370e-4	-7.72144e-4	2	-3.04038e-3	-6.67347e-3	1	+2.00729e-3	-1.38026e-4	2	+1.46060e-2	-1.93215e-4
$A = 4.43$	3	-9.64342e-3	-3.46560e-2	4	-3.96686e-2	-4.33665e-3	3	+5.96950e-2	+3.60053e-3	4	+3.77177e+0	+5.29858e+0
	5	+5.72922e-3	-1.27950e-1	6	-5.71423e-2	+2.63464e-1	5	+1.85276e-1	+2.99373e-2	6	+2.54677e+0	+2.58572e+0
	7	+1.77999e-1	-2.63386e-1	8	+4.99474e-1	-1.30517e-1	7	+4.55264e-1	+1.47606e-1	8	+9.10563e-1	+4.85706e-1
	9	+4.26766e-1	+3.04801e-1				9	+1.58816e+0	+1.20231e+0			

$s = 0.5$	G_μ	real	imag	G_μ	real	imag	W_μ	real	imag	W_μ	real	imag
$N = 4$	1	-2.46076e-2	-6.18372e-2	2	-7.40343e-2	+3.53925e-1	1	+8.52890e-2	+1.42010e-2	2	+2.49902e+0	+3.09335e+0
$A = 2.7$	3	+1.96625e-1	-4.29863e-1	4	+9.00358e-1	+1.38851e-1	3	+4.70710e-1	+1.87557e-1	4	+1.30319e+0	+9.57968e-1
$N = 5$	1	-1.20460e-2	-1.87041e-2	2	-1.55697e-2	-1.96986e-1	1	+4.08192e-2	+3.53914e-3	2	+2.46646e-1	+5.66231e-2
$A = 3.2$	3	-1.45383e-1	+1.73972e-1	4	+5.12732e-1	-4.44052e-1	3	+2.97457e+0	+3.72024e+0	4	+7.85067e-1	+3.60460e-1
	5	+6.59669e-1	+4.85550e-1				5	+1.72265e+0	+1.34352e+0			
$N = 6$	1	-5.08118e-3	-6.30271e-3	2	-3.08510e-2	-7.19199e-2	1	+2.07948e-2	+8.74328e-4	2	+1.30096e-1	+1.56279e-2
$A = 3.64$	3	-1.37998e-1	+5.80214e-2	4	+7.51989e-2	-3.53365e-1	3	+3.44594e+0	+4.25596e+0	4	+4.54708e-1	+1.20086e-1
	5	+3.26981e-1	+6.26584e-1	6	+7.71669e-1	-2.53231e-1	5	+2.14813e+0	+1.69436e+0	6	+1.12383e+0	+5.44791e-1
$N = 7$	1	-2.02794e-3	-2.52575e-3	2	-1.43945e-2	-2.73479e-2	1	+1.13213e-2	+6.56019e-4	2	+7.00345e-2	+8.00183e-3
$A = 4.03$	3	-9.05959e-2	+7.82265e-4	4	-1.38494e-2	-1.56158e-1	3	+3.82120e+0	+4.85774e+0	4	+2.48535e-1	+5.67707e-2
	5	+2.72590e-1	-4.07188e-1	6	+4.82708e-2	+5.31312e-1	5	+6.63178e-1	+2.53362e-1	6	+2.49161e+0	+2.13919e+0
	7	+8.00031e-1	+6.10445e-2				7	+1.41328e+0	+8.26402e-1			
$N = 8$	1	-1.02655e-3	-1.17277e-3	2	-7.42600e-3	-1.29372e-2	1	+6.96200e-3	+1.20019e-4	2	+4.30597e-2	+4.52622e-3
$A = 4.36$	3	-5.06682e-2	-1.39529e-2	4	-1.71821e-2	-7.30188e-2	3	+4.06878e+0	+5.49256e+0	4	+1.51849e-1	+3.16337e-2
	5	+5.50618e-2	-2.46159e-1	6	-8.87373e-2	+3.73030e-1	5	+4.03960e-1	+1.32115e-1	6	+2.74868e+0	+2.60011e+0
	7	+4.60448e-1	-3.31361e-1	8	+6.49548e-1	+3.05553e-1	7	+8.88894e-1	+4.22344e-1	8	+1.67241e+0	+1.12800e+0

$s = 1$	G_μ	real	imag	G_μ	real	imag	W_μ	real	imag	W_μ	real	imag
$N = 4$	1	-5.24536e-2	-5.82591e-2	2	-1.53070e-1	+3.13214e-1	1	+2.00828e-1	+5.50627e-2	2	+3.01477e+0	+4.04811e+0
$A = 2.89$	3	+2.19825e-1	-5.55609e-1	4	+9.84414e-1	+3.00531e-1	3	+7.80901e-1	+4.10809e-1	4	+1.75909e+0	+1.51249e+0
$N = 5$	1	-2.12358e-2	-1.21821e-2	2	-1.72838e-1	+1.10546e-1	1	+1.11643e-1	+1.89225e-2	2	+3.54897e+0	+4.80949e+0
$A = 3.44$	3	-6.74051e-2	-2.48812e-1	4	+6.76090e-1	-5.15468e-1	3	+4.75015e-1	+1.66319e-1	4	+1.19276e+0	+7.06478e-1
	5	+5.85227e-1	+6.65589e-1				5	+2.24681e+0	+2.03466e+0			
$N = 6$	1	-8.12969e-3	-2.87953e-3	2	-6.51413e-2	-8.01954e-2	1	+6.62243e-2	+7.38414e-3	2	+2.93112e-1	+7.09275e-2
$A = 3.91$	3	-1.15364e-1	-4.03041e-3	4	+9.93156e-2	-4.76469e-1	3	+4.16684e+0	+5.59224e+0	4	+7.89167e-1	+3.32839e-1
	5	+1.16286e-1	+6.85707e-1	6	+9.73105e-1	-1.22221e-1	5	+2.76330e+0	+2.60270e+0	6	+1.61906e+0	+1.05619e+0
$N = 7$	1	-3.41938e-3	-1.19963e-3	2	-3.32995e-2	-3.07209e-2	1	+4.27878e-2	+5.30407e-3	2	+1.91510e-1	+4.46372e-2
$A = 4.28$	3	-5.33754e-2	-2.16946e-2	4	-4.32204e-2	-2.36708e-1	3	+4.44007e+0	+6.43728e+0	4	+5.27067e-1	+1.96477e-1
	5	-1.33009e-1	+4.29896e-1	6	+4.56843e-1	-4.86407e-1	5	+3.12810e+0	+3.26207e+0	6	+1.12086e+0	+6.15014e-1
	7	+8.09484e-1	+3.46827e-1				7	+1.99961e+0	+1.53180e+0			

D Derivation of the Perturbative Master Equations

As a preliminary to provide explicit expressions for various master equations aiming for approximate solutions of the dynamics of the unbiased two-spin-boson model (2SBM), the eigenvalues and eigenstates of the system Hamiltonian [Eq. (5.1)], i.e.,

$$H_{\rm sys} = -\frac{\omega_A}{2}\sigma_x^A - \frac{\omega_B}{2}\sigma_x^B \,, \tag{D.1}$$

are required. Using the eigenstates of the Pauli matrix σ_x, i.e.,

$$\sigma_x|\psi_\pm\rangle = \sigma_x\frac{1}{\sqrt{2}}(|\uparrow\rangle \pm |\downarrow\rangle) = \frac{1}{\sqrt{2}}(|\downarrow\rangle \pm |\uparrow\rangle) = \pm|\psi_\pm\rangle\};, \tag{D.2}$$

the 4 eigenstates of $H_{\rm sys}$ follow immediately

$$H_{\rm sys}|\psi_\pm\rangle^A|\psi_\pm\rangle^B = -\frac{1}{2}\left((\pm)^A\omega_A(\pm)^B\omega_B\right)|\psi_\pm\rangle^A|\psi_\pm\rangle^B \,, \tag{D.3}$$

where the eigenvalues can also be expressed as $\mp\Delta, \mp\delta$ with $\Delta = (\omega_A + \omega_B)/2$ and $\delta = (\omega_A - \omega_B)/2$. It turns out useful to decompose the coupling operator

$$L = \frac{1}{2}\left(\sigma_z^A + \sigma_z^B\right) \tag{D.4}$$

in terms of eigenstate projectors of $H_{\text{sys}}|\epsilon\rangle = \epsilon|\epsilon\rangle$ and group summands with an equal energy difference (transition frequency) $\omega = \epsilon' - \epsilon$, i.e.,

$$L = \sum_{\epsilon,\epsilon'} |\epsilon\rangle\langle\epsilon|L|\epsilon'\rangle\langle\epsilon'| = \sum_w L_w \quad \text{with} \quad L_w := \sum_{\epsilon,\epsilon':\epsilon'-\epsilon=\omega} |\epsilon\rangle\langle\epsilon|L|\epsilon'\rangle\langle\epsilon'| \,. \tag{D.5}$$

The possible energy differences $\omega = \epsilon' - \epsilon$, given in the following table

$\epsilon\backslash\epsilon'$	$-\Delta$	$-\delta$	δ	Δ
$-\Delta$	0	ω_B	ω_A	$\omega_A + \omega_B$
$-\delta$	$-\omega_B$	0	$\omega_A - \omega_B$	ω_A
δ	$-\omega_A$	$\omega_B - \omega_A$	0	ω_B
Δ	$-\omega_A - \omega_B$	$-\omega_A$	$-\omega_B$	0

(D.6)

and the action $\sigma_z|\psi_\pm\rangle = \sigma_z \frac{1}{\sqrt{2}}(|+\rangle \pm |-\rangle) = \frac{1}{\sqrt{2}}(|+\rangle \mp |-\rangle) = |\psi_\mp\rangle$ allows us to evaluate the operators L_w, i.e.,

$$\begin{gathered} L_0 = 0, \quad L_{\pm(\omega_A+\omega_B)} = 0, \quad L_{\pm(\omega_A-\omega_B)} = 0, \\ L_{\omega_B} = \frac{1}{2}\mathbb{1}^A|\psi_+\rangle^B\langle\psi_-|^B = L_{-\omega_B}^\dagger \quad \text{and} \quad L_{\omega_A} = \frac{1}{2}|\psi_+\rangle^A\langle\psi_-|^A\mathbb{1}^B = L_{-\omega_A}^\dagger \,. \end{gathered} \tag{D.7}$$

Note that for resonant qubits, i.e., $\Delta = \omega_A = \omega_B$, the two non-vanishing contributions above joint into the single operator

$$L_\Delta = \frac{1}{2}\left(\mathbb{1}^A|\psi_+\rangle^B\langle\psi_-|^B + |\psi_+\rangle^A\langle\psi_-|^A\mathbb{1}^B\right) = L_{-\Delta}^\dagger \,. \tag{D.8}$$

It is useful to introduce X_+ and X_- as the ladder operators with respect to the eigenstates of σ_x, i.e.,

$$X_+ := |\psi_+\rangle\langle\psi_-| = \frac{1}{2}(\sigma_z - \mathrm{i}\sigma_y) \quad \text{and} \quad X_- := |\psi_-\rangle\langle\psi_+| = \frac{1}{2}(\sigma_z + \mathrm{i}\sigma_y) = X_+^\dagger \,. \tag{D.9}$$

Also the following relations turn out useful, too,

$$\begin{aligned} X_+X_- &= |\psi_+\rangle\langle\psi_+| = \frac{1}{4}(\sigma_z - \mathrm{i}\sigma_y)(\sigma_z + \mathrm{i}\sigma_y) = \frac{1}{2}(\mathbb{1} + \sigma_x) \quad \text{and} \\ X_-X_+ &= |\psi_-\rangle\langle\psi_-| = \frac{1}{2}(\mathbb{1} - \sigma_x) \,. \end{aligned} \tag{D.10}$$

D.1 The Redfield Equation

To derive an approximate evolution equation for the reduced state [BP07; KC08; Whi08] the Nakajima-Zwanzig projection formalism [Nak58; Zwa60; Gra06] may be used as starting point. In lowest order of the coupling strength the following expression is obtained

$$\dot{\tilde{\rho}}(t) = -\int_0^t \mathrm{d}s\, \mathrm{Tr}_{\mathrm{env}}[\tilde{V}(t), [\tilde{V}(s), \tilde{\rho}(s) \otimes \rho_{\mathrm{env}}]] \,. \tag{D.11}$$

Here $\tilde{\rho}$ and $\tilde{V}$ denote the reduced state and the interaction Hamiltonian in the interaction picture with respect to the system and the environment Hamiltonian. Also an initial product state of the form $\rho_{\mathrm{tot}}(0) = \rho(0) \otimes \rho_{\mathrm{env}}$ has been assumed. For the microscopic model Hamiltonian [Eq. (2.1)] with a Hermitian coupling operator $L = L^\dagger$ it follows explicitly that $\tilde{V}(t) = \sum_\lambda g_\lambda \tilde{L}(t)(a_\lambda e^{-\omega_\lambda t} + a_\lambda^\dagger e^{\omega_\lambda t})$. To note in passing, the following steps can easily be generalized for a non-Hermitian coupling operator which yields two different integral kernels α_1 and α_2. Abbreviating $F(t) \coloneqq \sum_\lambda a_\lambda e^{-\mathrm{i}\omega_\lambda t} + a_\lambda^\dagger e^{\mathrm{i}\omega_\lambda t}$ and assuming a thermal initial state $\rho_{\mathrm{env}} \sim e^{-\beta H_{\mathrm{env}}}$, the evolution equation Eq. (D.11) becomes

$$\dot{\tilde{\rho}}(t) = -\int_0^t \mathrm{d}s\, \Big(\alpha(\beta, t-s)[\tilde{L}(t), \tilde{L}(s)\tilde{\rho}(s)] + \mathrm{h.c.}\Big) \tag{D.12}$$

with the bath correlation function (BCF)

$$\begin{aligned} \alpha(\beta,\tau) &\coloneqq \mathrm{Tr}_{\mathrm{env}} F(t)F(t+\tau)\rho_{\mathrm{env}} \\ &= \sum_\lambda g_\lambda^2((2\bar{n}(\beta\omega)+1)\cos(\omega\tau) - \mathrm{i}\sin(\omega\tau)) \end{aligned} \tag{D.13}$$

where $\bar{n}(x) = (e^x - 1)^{-1}$ denotes the Bose-Einstein distribution. For a continuous environment, i.e., $\sum_\lambda |g_\lambda|^2 \to \frac{1}{\pi}\int_0^\infty \mathrm{d}\omega\, J(\omega)$, the BCF becomes the previously introduced integral expression (see for example App. B, Eq. (B.3)). For a BCF which decays faster than the time scale of the reduced dynamics in the interaction picture, $\tilde{\rho}(s)$ may well be approximated with $\tilde{\rho}(t)$ under the integral. Finally, substituting $\tau = t - s$ and transforming back to the Schrödinger picture yields

$$\dot{\rho}(t) = -\mathrm{i}[H_{\mathrm{sys}}, \rho(t)] + \int_0^t \mathrm{d}\tau\, \Big(\alpha(\beta,\tau)[\tilde{L}(-\tau)\rho(t), L] + \mathrm{h.c.}\Big) \,. \tag{D.14}$$

The remaining interaction picture contribution $\tilde{L}(-\tau)$ can be made explicit by decomposing $L = \sum_\omega L_\omega$ where ω runs over all possible transition frequencies of H_{sys} (see Eq. (D.5)). In follows that an operator L in the interacting picture can be written as

$$\tilde{L}(t) = e^{\mathrm{i}H_{\mathrm{sys}}t} L e^{-\mathrm{i}H_{\mathrm{sys}}t} = \sum_\omega e^{-\mathrm{i}\omega t} L_\omega \,. \tag{D.15}$$

The resulting master equation is known as the *Redfield Master Equation* with time-dependent coefficients (RFEtdc) where the coefficients $F(\omega,t)$ can be obtained conveniently by propagating $F(\omega,t)$ along with the reduced state, i.e.,

$$\begin{aligned}\dot{\rho}(t) &= -\mathrm{i}[H_{\mathrm{sys}},\rho(t)] + \sum_{\omega}\Big(F(\beta,\omega,t)[L_{\omega}\rho(t),L] + \mathrm{h.c.}\Big) \quad \text{with} \\ &\qquad F(\beta,\omega,t) := \int_0^t \mathrm{d}\tau\, \alpha(\beta,\tau)e^{\mathrm{i}\omega\tau} \\ \Leftrightarrow \quad &\dot{F}(\beta,\omega,t) = \alpha(\beta,t)e^{\mathrm{i}\omega t} \quad \text{and} \quad F(\beta,\omega,0) = 0\,.\end{aligned} \tag{D.16}$$

In contrast to master equations involving the RWA (discussed next), grouping all contribution with the same transition frequency is of no importance for the RFE since the operators L_w enter the master equation linearly. Therefore, $\sum_{\omega}$ could be replaced by $\sum_{\epsilon,\epsilon'}$ equally well.

For a sufficiently fast decaying BCF, the asymptotic values $F(\beta,\omega,t\to\infty) = J(\beta,\omega) + \mathrm{i}S(\beta,\omega)$ may be used instead of the actual time dependent coefficients. We have shown in App. B how to obtain these values for the class of (sub-)Ohmic SDs. This leads to the *Redfield Master Equation* with asymptotic coefficients (RFEac). Both variants of the RFE are not of Gorini-Kossakowski-Sudarshan-Lindblad (GKSL)-form which implies that the solution may develop negative eigenvalues over time. Note that these negative and, thus, unphysical contributions are of the order of the perturbative error. This justifies the use of the RFE which has been discussed controversially in the literature. Since many attempts to restore complete positivity of the dynamics involve additional approximation on top of the RFE, it is not too surprising these approaches are less accurate (see Ref. [HS20a] for details).

Also, for the same perturbative regime (including time dependent coefficients) a positivity preserving stochastic quantum trajectory description is available by means of a perturbative treatment of the NMQSD equation [Yu+99; deV+05].

D.2 Quantum Optical Master Equation

With the aim to enforce the GKSL-form for the master equation, Eq. (D.12) is rewritten with $\tilde{L}(t) = \sum_{\omega} e^{\mathrm{i}\omega t}L_{\omega}^{\dagger}$ and $\tilde{L}(s) = \sum_{\omega'} e^{-\mathrm{i}\omega' s}L_{\omega'}$. As before, for a sufficiently fast decaying BCF the integral can be approximated by replacing $\tilde{\rho}(s)$ with $\tilde{\rho}(t)$. The resulting equation (D.12) takes the form

$$\dot{\tilde{\rho}}(t) = \sum_{\omega,\omega'} e^{-\mathrm{i}(\omega-\omega')t}F(\omega',t)[L_{\omega'}\tilde{\rho}(t),L_{\omega}^{\dagger}] + \mathrm{h.c.}\,. \tag{D.17}$$

If the magnitude of $F(\omega',t)$, which scales with the coupling strength, is significantly smaller than the smallest non-zero frequency ($\min_{\omega\neq\omega'}|\omega-\omega'|$), it can be argued that

due to the oscillating phase so-called secular terms (summands with $\omega \neq \omega'$) average to zero. This motivates to keep terms only with $\omega = \omega'$. Furthermore, replacing $F(\beta, \omega', t)$ by the asymptotic values $F(\beta, \omega') = J(\beta, \omega') + \mathrm{i}S(\beta, \omega')$ yields, in the Schrödinger picture, the well-known quantum optical master equation (QOME) which is of GKSL-form

$$\dot{\rho}(t) = -\mathrm{i}[H_{\mathrm{sys}} + \sum_{\omega} S(\omega) L_\omega^\dagger L_\omega, \rho(t)] + \sum_{\omega} \left(J(\omega)[L_\omega \rho(t), L_\omega^\dagger] + \mathrm{h.c.} \right) . \tag{D.18}$$

In contrast to the RFE, the so-called Lindblad Operators L_ω appear non-linearly in the master equation (products of L_ω and $L_\omega^\dagger$). Therefore the grouping of contributions with the same transition frequency effects the resulting master equation significantly. In the general case ($\omega_A \neq \omega_B$), the non-trivial terms for L_ω are the single qubit operators (see Eq. (D.7)) $L_{\omega_{A/B}}$ and $L_{-\omega_{A/B}}^\dagger$. As a consequence the Lamb-shift Hamiltonian (ignoring terms proportional to the identity matrix)

$$\begin{aligned} H_{\mathrm{Lamb}} &= \sum_{\omega \in \{\pm\omega_A, \pm\omega_B\}} S(\omega) L_\omega^\dagger L_\omega \\ &= \frac{S(-\omega_A) - S(\omega_A)}{8} \sigma_x^A + \frac{S(-\omega_B) - S(\omega_B)}{8} \sigma_x^B \end{aligned} \tag{D.19}$$

contains local contributions only. However, for resonant qubits ($\omega_A = \omega_B = \Delta$), since the Lindblad operator consists of the sum of the above local contributions, i.e.,

$$L_\Delta = L_{\omega_A} + L_{\omega_B} = \frac{1}{4}(\sigma_z^A + \sigma_z^B - \mathrm{i}\sigma_y^A - \mathrm{i}\sigma_y^B) = L_{-\Delta}^\dagger , \tag{D.20}$$

the Lamb-shift Hamiltonian contains additional, in particular, non-local terms mediating an effective interaction between the qubits, i.e.,

$$\begin{aligned} H_{\mathrm{Lamb}} &= \sum_{\omega \in \{\pm\Delta\}} S(\omega) L_\omega^\dagger L_\omega \\ &= \frac{S(\Delta) + S(-\Delta)}{4} (X_-^A X_+^B + X_+^A X_-^B) + H_{\mathrm{Lamb}}^{\mathrm{local}} \\ &= \frac{S(\Delta) + S(-\Delta)}{8} (\sigma_z^A \sigma_z^B + \sigma_y^A \sigma_y^B) + H_{\mathrm{Lamb}}^{\mathrm{local}} \\ \text{with} \quad H_{\mathrm{Lamb}}^{\mathrm{local}} &= \frac{S(-\Delta) - S(\Delta)}{8} (\sigma_x^A + \sigma_x^B) + \sim \mathbb{1} . \end{aligned} \tag{D.21}$$

Even for infinitesimally detuned qubits, these non-local terms are missing due to the secular approximation which particularly influences the entanglement dynamics of the two qubits as discussed in Sec. 5.1.

As a remark, the Lamb-shift term of the QOME expressed by the ladder operators $X_\pm$ shows that the induced interaction is excitation conserving which is a clear signature of the RWA. Without the RWA, additional terms, proportional to $X_+^A X_+^B$

and $X_-^A X_-^B$, contribute to the environmentally qubit-qubit interaction as shown, e.g., by the GAME [Eq. (D.42)].

D.3 Partial Rotating Wave Approximation

For a small detuning the unphysical discontinuity in the Lamb-shift Hamiltonian can be circumvented by using the Lindblad operators of the resonant case [Eq. (D.8)] also for the detuned case. Formally this corresponds to a way of deriving a master equation of GKSL kind where the rotating wave approximation (RWA) is applied only partially [VJC13; Jes+15; TB15]. As for the derivation of the QOME (full RWA), Eq. (D.17) serves as starting point. Given that the transition frequencies ω cluster into groups such that for each member ω of the group $G_{\bar{\omega}}$ the approximation $F(\bar{\omega}) \approx F(\omega)$ holds, Eq. (D.17) becomes

$$\dot{\tilde{\rho}}(t) = \sum_{\bar{\omega},\bar{\omega}'} e^{-\mathrm{i}(\bar{\omega}-\bar{\omega}')t} F(\bar{\omega}', t)[L_{\bar{\omega}'}\tilde{\rho}(t), L_{\bar{\omega}}^\dagger] + \mathrm{h.c.} \tag{D.22}$$

where $L_{\bar{\omega}} = \sum_{\omega \in G_{\bar{\omega}}} L_\omega$. If the mean frequencies $\bar{\omega}$ of each cluster differ significantly, applying the RWA on the basis of the frequencies $\bar{\omega}$ is well motivated. Transforming back to the Schrödinger picture yields the PRWA master equation

$$\dot{\rho}(t) = -\mathrm{i}[H_{\mathrm{sys}} + \sum_{\bar{\omega}} S(\bar{\omega}) L_{\bar{\omega}}^\dagger L_{\bar{\omega}}, \rho(t)] + \sum_{\bar{\omega}} \Big(J(\bar{\omega})[L_{\bar{\omega}}\rho(t), L_{\bar{\omega}}^\dagger] + \mathrm{h.c.} \Big) \tag{D.23}$$

which is of GKSL form. Note that due to the grouping, the Lindblad operators are, in general, different compared to the QOME. This results, for example, in significantly different entanglement dynamics as discussed in Sec. 5.1.1.

Applying this idea to the 2SBM works especially well for a small detuning $\delta \ll \Delta$. In that case ω_A and ω_B are grouped in the group with label $\Delta = (\omega_A + \omega_B)/2$. A second group exists for the negative values. Thus, $\bar{\omega}$ takes the values $\pm\Delta$ and the corresponding Lindblad operator corresponds to the QOME Lindblad operator for resonant qubits, i.e.,

$$L_\Delta = \frac{1}{2}(X_+^A + X_+^B) = \frac{1}{4}(\sigma_z^A + \sigma_z^B - \mathrm{i}\sigma_y^A - \mathrm{i}\sigma_y^B) = L_{-\Delta}^\dagger \,, \tag{D.24}$$

here, however, used for the detuned case.

D.4 Coarse-Graining Master Equation

Applying a coarse-graining procedure provides yet another way to improve on the limitation of the RWA for detuned qubits while keeping the GKSL-property of the master equation [SB08; BFP03; Maj+13]. The method is based on a second order

expansion of the time evolution operator $U(t, t+\tau)$ in the full interaction picture which yields

$$\tilde{\rho}(t+\tau) - \tilde{\rho}(t) \approx -\mathrm{i}\int_t^{t+\tau} \mathrm{d}s\, [\tilde{H}(s), \tilde{\rho}(t)] - \int_t^{t+\tau} \mathrm{d}s \int_t^s \mathrm{d}u\, [\tilde{H}(s), [\tilde{H}(u), \tilde{\rho}(t)]]\,, \tag{D.25}$$

where $\tilde{H}(s)$ is the remaining interaction Hamiltonian in the interaction picture. As before, evaluating the trace over the environment on the right hand side is done approximately by assuming that $\tilde{\rho}(t)$ can be replaced by $\tilde{\rho}_{\mathrm{sys}}(t) \otimes \tilde{\rho}_{\mathrm{env}}$ under the integral. Given that $\mathrm{Tr}_{\mathrm{env}}[\tilde{H}(s), \tilde{\rho}_{\mathrm{sys}}(t) \otimes \tilde{\rho}_{\mathrm{env}}] = 0$ holds true[1] this yields

$$\begin{aligned} \tilde{\rho}_{\mathrm{sys}}(t+\tau) - \tilde{\rho}_{\mathrm{sys}}(t) &\approx \mathcal{Z}_\tau \tilde{\rho}(t) \quad \text{with} \\ \mathcal{Z}_\tau \tilde{\rho}(t) &:= -\int_t^{t+\tau} \mathrm{d}s \int_t^s \mathrm{d}u \left(\alpha(s-u)[\tilde{L}(s), \tilde{L}(u)\tilde{\rho}_{\mathrm{sys}}(t)] + \mathrm{h.c.}\right). \end{aligned} \tag{D.26}$$

If the product state assumption $\tilde{\rho}_{\mathrm{sys}}(t) \otimes \tilde{\rho}_{\mathrm{env}}$ is reasonable not only at t but also at any discrete $t_n = t + n\tau$, the above expression suggests to generate the time discrete dynamics by sequentially applying $\mathcal{Z}_\tau$ such that $\tilde{\rho}(t+n\tau) = (\mathcal{Z}_\tau)^n\, \tilde{\rho}(t)$. In this sense τ is related to the decay of bath correlations, that is the time scale on which correlations between the system and the environment are expected to become unimportant for the reduced dynamics.

However, it has been pointed out that the discrete map $\mathcal{Z}_\tau$ is not completely positive [SB08], yet it is a valid GKSL generator. Therefore, if the finite difference may well be approximated by the time derivative of the reduced state, Eq. (D.26) turns into a master equation of GKSL-type [SB08], i.e.,

$$\dot{\tilde{\rho}}_{\mathrm{sys}}(t) \approx \frac{\tilde{\rho}(t+\tau) - \tilde{\rho}(t)}{\tau} \approx \frac{\mathcal{Z}_\tau}{\tau} \tilde{\rho}_{\mathrm{sys}}(t)\,. \tag{D.27}$$

Notably, in the mathematical limit $\tau \to 0$ the double time integral in Eq. (D.26) scales as τ^2 which results in a vanishing and, thus, meaningless right hand side of the above equation. Therefore, for the CGME to be meaningful the time scale separation $\tau_{\mathrm{env}} \ll \tau \ll \tau_{\mathrm{ind}}$ is required. Again, τ_{ind} is the timescale on which the reduced state changes in the interaction picture, τ_{env} is the timescale set by the decay of the BCF and τ is in principle a free parameters of the coarse graining scheme.

To actually solve the CGME numerically, instead of writing the master equation in obvious GKSL-form as provided in Ref. [SB08; BFM09], it is advantageous to rewrite Eq. (D.27) solely in terms of the decomposition L_ω of the coupling operator. In the Schrödinger picture the CGME reads

$$\dot{\rho}_{\mathrm{sys}} = -\mathrm{i}[H_{\mathrm{sys}}, \rho] - \frac{1}{\tau} \sum_{\omega,\omega'} \left(G(\omega, \omega', \tau) \times [L_{\omega'}, L_\omega^\dagger \rho_{\mathrm{sys}}] + \mathrm{h.c.}\right) \tag{D.28}$$

[1] As for Eq. (D.11), for thermal states in combination with the usual interaction Eq. (2.1), this is valid.

where the coarse-graining parameter τ dependent coefficients

$$G(\omega,\omega',\tau)=\int_0^\tau \mathrm{d}s\int_0^s \mathrm{d}u\,\alpha(s-u)e^{\mathrm{i}(\omega' s-\omega u)} \tag{D.29}$$

have been introduced.

As for the RFE, the operators L_ω appear linearly only which makes the CGME insensitive to the grouping by transition frequencies involved to obtain L_ω.

D.5 Geometric-Arithmetic Master Equation

Based on the RFE [Eq. (D.16)] the geometric-arithmetic master equation (GAME) [Dav20] achieves complete positivity without any requirements on the system Hamiltonian and, thus, no RWA. In a first step, a unitary effect of the environment on the system is separated (referred as renormalization of the system Hamiltonian or Lamb-shift) by constructing a von-Neumann like contribution for the right hand side of the RFE with asymptotic coefficients [Eq. (D.16)], i.e.,

$$\begin{aligned}\sum_\omega\Big(F_\omega[L_\omega\rho,L]+\mathrm{h.c.}\Big)&\equiv -LL_f^\dagger\rho-\rho L_f L+L_f^\dagger\rho L+L\rho L_f\\ &\text{with}\quad L_f^\dagger:=\sum_\omega F(\omega)L_\omega\ ,\end{aligned} \tag{D.30}$$

by the following rewriting,

$$\begin{aligned}-LL_f^\dagger\rho-\rho L_f L&=-2\left(\frac{LL_f^\dagger\rho}{2}+\frac{\rho L_f L}{2}\right)+\frac{\rho LL_f^\dagger}{2}-\frac{\rho LL_f^\dagger}{2}+\frac{L_f L\rho}{2}-\frac{L_f L\rho}{2}\\ &=-\mathrm{i}\frac{\mathrm{i}}{2}[L_f L-LL_f^\dagger,\rho]-\frac{1}{2}\{L_f L+LL_f^\dagger,\rho\}\ ,\end{aligned} \tag{D.31}$$

where $H_{\mathrm{Lamb}}:=\frac{\mathrm{i}}{2}(L_f L-LL_f^\dagger)$ is indeed Hermitian. The RFE takes the form

$$\dot\rho+\mathrm{i}[H_{\mathrm{sys}}+H_{\mathrm{Lamb}},\rho]=-\frac{1}{2}\{L_f L+LL_f^\dagger,\rho\}+L_f^\dagger\rho L+L\rho L_f\ . \tag{D.32}$$

Recalling the definition of $L_f^\dagger=\sum_\omega F(\omega)L_\omega=\int_0^\infty \mathrm{d}\tau\,\alpha(\beta,\tau)\tilde L(-\tau)$ allows to write the above RFE in matrix components with respect to the eigenstates of the system Hamiltonian $H_{\mathrm{sys}}|n\rangle=\epsilon_n|n\rangle$, using

$$\begin{aligned}\langle n|L_f^\dagger|m\rangle&=\int_0^\infty \mathrm{d}\tau\,\alpha(\beta,\tau)\langle n|e^{-\mathrm{i}H_{\mathrm{sys}}\tau}Le^{\mathrm{i}H_{\mathrm{sys}}\tau}|m\rangle\\ &=\int_0^\infty \mathrm{d}\tau\,\alpha(\beta,\tau)e^{-\mathrm{i}(\epsilon_n-\epsilon_m)\tau}L_{nm}\\ &=F(\omega_{mn})L_{nm}\quad\text{with}\quad\omega_{mn}=\epsilon_m-\epsilon_n\\ \text{and}\quad\langle n|L_f|m\rangle&=\langle m|L_f^\dagger|n\rangle^*=F^*(\omega_{nm})L_{mn}^*=F^*(\omega_{nm})L_{nm}\end{aligned} \tag{D.33}$$

yields to

$$\begin{aligned}
&\dot{\rho}_{nm} + \mathrm{i}[H_{\mathrm{sys}} + H_{\mathrm{Lamb}}, \rho]_{nm} \\
=&\sum_{ij} \Big(-\frac{1}{2} F^*(\omega_{ni}) L^*_{in} L_{ij} \rho_{jm} - \frac{1}{2} L_{ni} F(\omega_{ji}) L_{ij} \rho_{jm} \\
&- \frac{1}{2} \rho_{ni} F^*(\omega_{ij}) L^*_{ji} L_{jm} - \frac{1}{2} \rho_{ni} L_{ij} F(\omega_{mj}) L_{jm} \\
&+ F(\omega_{in}) L_{ni} \rho_{ij} L_{jm} + L_{ni} \rho_{ij} F^*(\omega_{jm}) L^*_{mj} \Big) \, .
\end{aligned} \tag{D.34}$$

By using the hermicity of L it follows that

$$\begin{aligned}
\dot{\rho}_{nm} + \mathrm{i}[H_{\mathrm{sys}} + H_{\mathrm{Lamb}}, \rho]_{nm} = \sum_{ij} \Big(& L_{ni} \rho_{ij} L_{jm} (F(\omega_{in}) + F^*(\omega_{jm})) \\
& - \frac{1}{2} \rho_{ni} L_{ij} L_{jm} (F(\omega_{mj}) + F^*(\omega_{ij})) \\
& - \frac{1}{2} L_{ni} L_{ij} \rho_{jm} (F(\omega_{ji}) + F^*(\omega_{ni})) \Big) \, .
\end{aligned} \tag{D.35}$$

Ignoring the coefficients $F(\omega) + F^*(\omega')$ for a moment, the right hand side is already of GKSL kind $A^\dagger \rho A - \frac{1}{2}\{AA^\dagger, \rho\}$. The additional approximation made is based on the properties of the coefficients. Replacing the sum of the real parts (geometric mean) by the square root of their product (arithmetic mean) results in

$$F(\omega) + F^*(\omega') = J(\omega) + J(\omega') + \mathrm{i}(S(\omega) - S(\omega')) = 2\sqrt{J(\omega) J(\omega')} + f(\omega, \omega') \tag{D.36}$$

where, crucially, the remainder

$$f(\omega, \omega') = \left(\sqrt{J(\omega)} - \sqrt{J(\omega')} \right)^2 + \mathrm{i}(S(\omega) - S(\omega')) \tag{D.37}$$

becomes zero for $\omega = \omega'$. As a consequence of that (see Ref. [Dav20] for a thorough discussion), on a coarse grained time scale the influence of this remainder becomes small. Notably, the validity of this statement depends on the particular functions $J(\omega)$ and $S(\omega)$ and, thus, on the BCF only. Hence, for a sufficiently weak coupling strength, such that the reduced dynamics in the interaction picture takes place on a time scale slower than the coarse graining time scale needed to suppress the influence of the remainder, the following master equation is justified

$$\begin{aligned}
\dot{\rho}_{nm} + \mathrm{i}[H_{\mathrm{sys}} + H_{\mathrm{Lamb}}, \rho]_{nm} = \sum_{ij} \Big(& L^*_{in} \sqrt{J_{in}} \rho_{ij} L_{jm} \sqrt{J_{jm}} \\
& - \frac{1}{2} \left(\rho_{ni} L_{ij} \sqrt{J_{ij}} L^*_{mj} \sqrt{J_{mj}} + L_{ni} \sqrt{J_{ni}} L^*_{ji} \sqrt{J_{ji}} \rho_{jm} \right) \Big) \, .
\end{aligned} \tag{D.38}$$

Since $J(\omega)$ is non-negative, defining the Lindblad operator $A_{nm} = L_{nm} \sqrt{J(\omega_{nm})}$ results in the GAME

$$\dot{\rho} = -\mathrm{i}[H_{\mathrm{sys}} + H_{\mathrm{Lamb}}, \rho] + A^\dagger \rho A - \frac{1}{2}\{AA^\dagger, \rho\} \, , \tag{D.39}$$

which is of GKSL kind. Note that opposing to the claim in Ref. [Dav20], equivalency between the equation for the components and the final matrix equation can not be established for time dependent coefficients $F(\omega, t)$ since, in general, $\mathrm{Re}(F(\omega, t)) \geq 0$ does not hold true for all times.

Finally, we derive the Lamb-shift Hamiltonian of the GAME for the 2SBM. Using

$$L = \frac{1}{2}(\sigma_z^A + \sigma_z^B) = \frac{1}{2}(X_+^A + X_-^A + X_+^B + X_-^B) \tag{D.40}$$

yields to

$$\begin{aligned} LL_f^\dagger = \sum_\omega F(\omega) L L_\omega = \\ \frac{F(\omega_A)}{4}(X_-^A X_+^A + X_+^A(X_+^B + X_-^B)) + \frac{F(-\omega_A)}{4}(X_+^A X_-^A + X_-^A(X_+^B + X_-^B)) \\ + \frac{F(\omega_B)}{4}(X_-^B X_+^B + (X_+^A + X_-^A)X_+^B) + \frac{F(-\omega_B)}{4}(X_+^B X_-^B + (X_+^A + X_-^A)X_-^B)\,. \end{aligned} \tag{D.41}$$

The Lamb-shift Hamiltonian, thus, equates to

$$\begin{aligned} H_{\mathrm{Lamb}} &= \frac{\mathrm{i}}{2}(L_f L - L L_f^\dagger) = \frac{\mathrm{i}}{2}\sum_\omega (F(\omega)^* L_\omega^\dagger L - F(\omega) L L_\omega) \\ &= \frac{S(\omega_A)}{4} X_-^A X_+^A + \frac{S(-\omega_A)}{4} X_+^A X_-^A + \frac{S(\omega_B)}{4} X_-^B X_+^B + \frac{S(-\omega_B)}{4} X_+^B X_-^B \\ &+ \frac{S(\omega_A) + S(-\omega_A) + S(\omega_B) + S(-\omega_B)}{8}(X_-^A + X_+^A)(X_-^B + X_+^B) \\ &+ \mathrm{i}\frac{J(\omega_A) - J(-\omega_A)}{8}(X_-^A - X_+^B)(X_-^B + X_+^B) \\ &+ \mathrm{i}\frac{J(\omega_B) - J(-\omega_B)}{8}(X_-^A + X_+^B)(X_-^B - X_+^B) \end{aligned} \tag{D.42}$$

which is, up to some irrelevant contributions, equivalent to

$$\begin{aligned} H_{\mathrm{Lamb}} = \frac{S(-\omega_A) - S(\omega_A)}{8}\sigma_x^A + \frac{S(-\omega_B) - S(\omega_B)}{8}\sigma_x^B \\ + \frac{S(-\omega_A) + S(\omega_A) + S(-\omega_B) + S(\omega_B)}{8}\sigma_z^A \sigma_z^B \\ + \frac{(J(-\omega_A) - J(\omega_A))}{8}\sigma_y^A \sigma_z^B + \frac{J(-\omega_B) - J(\omega_B)}{8}\sigma_z^A \sigma_y^B\,. \end{aligned} \tag{D.43}$$

Bibliography

[ABV07] F. B. Anders, R. Bulla, and M. Vojta. „Equilibrium and Nonequilibrium Dynamics of the Sub-Ohmic Spin-Boson Model“. In: *Phys. Rev. Lett.* 98.21 (May 2007), p. 210402 (cit. on pp. 29, 87, 88).

[AGR82] A. Aspect, P. Grangier, and G. Roger. „Experimental Realization of Einstein-Podolsky-Rosen-Bohm Gedankenexperiment: A New Violation of Bell's Inequalities“. In: *Phys. Rev. Lett.* 49.2 (July 1982), pp. 91–94 (cit. on pp. 1, 91).

[AL07] R. Alicki and K. Lendi. *Quantum Dynamical Semigroups and Applications*. Springer, Apr. 2007 (cit. on pp. 32, 36, 96).

[AS05] F. B. Anders and A. Schiller. „Real-Time Dynamics in Quantum-Impurity Systems: A Time-Dependent Numerical Renormalization-Group Approach“. In: *Phys. Rev. Lett.* 95.19 (Oct. 2005), p. 196801 (cit. on pp. 10, 36).

[AS06] F. B. Anders and A. Schiller. „Spin Precession and Real-Time Dynamics in the Kondo Model: Time-Dependent Numerical Renormalization-Group Study“. In: *Phys. Rev. B* 74.24 (Dec. 2006), p. 245113 (cit. on p. 10).

[Bar+11] J. T. Barreiro, M. Müller, P. Schindler, et al. „An Open-System Quantum Simulator with Trapped Ions“. In: *Nature* 470.7335 (Feb. 2011), pp. 486–491 (cit. on p. 75).

[Bar+14] R. Barends, J. Kelly, A. Megrant, et al. „Superconducting Quantum Circuits at the Surface Code Threshold for Fault Tolerance“. In: *Nature* 508.7497 (Apr. 2014), pp. 500–503 (cit. on p. 75).

[Bar61] V. Bargmann. „On a Hilbert Space of Analytic Functions and an Associated Integral Transform Part I“. In: *Communications on Pure and Applied Mathematics* 14.3 (1961), pp. 187–214 (cit. on p. 12).

[Bay+17] A. Bayer, M. Pozimski, S. Schambeck, et al. „Terahertz Light–Matter Interaction beyond Unity Coupling Strength“. In: *Nano Lett.* 17.10 (Oct. 2017), pp. 6340–6344 (cit. on p. 10).

[Bec+00] M. H. Beck, A. Jäckle, G. A. Worth, and H. .-.-D. Meyer. „The Multiconfiguration Time-Dependent Hartree (MCTDH) Method: A Highly Efficient Algorithm for Propagating Wavepackets“. In: *Phys. Rep.* 324.1 (Jan. 2000), pp. 1–105 (cit. on p. 87).

[Bel64] J. S. Bell. „On the Einstein Podolsky Rosen Paradox“. In: *Physics Physique Fizika* 1.3 (Nov. 1964), pp. 195–200 (cit. on p. 1).

[Ben+08] J. Benhelm, G. Kirchmair, C. F. Roos, and R. Blatt. „Towards Fault-Tolerant Quantum Computing with Trapped Ions“. In: *Nature Physics* 4.6 (June 2008), pp. 463–466 (cit. on p. 75).

[BF05] F. Benatti and R. Floreanini. „Open Quantum Dynamics: Complete Positivity and Entanglement“. In: *Int. J. Mod. Phys. B* 19.19 (July 2005), pp. 3063–3139 (cit. on p. 5).

[BF06] F. Benatti and R. Floreanini. „Entangling Oscillators through Environment Noise“. In: *J. Phys. A: Math. Gen.* 39.11 (Mar. 2006), pp. 2689–2699 (cit. on p. 92).

[BFM09] F. Benatti, R. Floreanini, and U. Marzolino. „Environment-Induced Entanglement in a Refined Weak-Coupling Limit“. In: *EPL* 88.2 (2009), p. 20011 (cit. on pp. 6, 153).

[BFM10] F. Benatti, R. Floreanini, and U. Marzolino. „Entangling Two Unequal Atoms through a Common Bath“. In: *Phys. Rev. A* 81.1 (Jan. 2010), p. 012105 (cit. on pp. 5, 94, 100).

[BFP03] F. Benatti, R. Floreanini, and M. Piani. „Environment Induced Entanglement in Markovian Dissipative Dynamics“. In: *Phys. Rev. Lett.* 91.7 (Aug. 2003), p. 070402 (cit. on pp. 5, 152).

[Boh35] N. Bohr. „Can Quantum-Mechanical Description of Physical Reality Be Considered Complete?“ In: *Phys. Rev.* 48.8 (Oct. 1935), pp. 696–702 (cit. on p. 1).

[Bon13] J. Bonart. „Dissipative Phase Transition in a Pair of Coupled Noisy Two-Level Systems“. In: *Phys. Rev. B* 88.12 (Sept. 2013), p. 125139 (cit. on p. 110).

[BP07] H.-P. Breuer and F. Petruccione. *The Theory of Open Quantum Systems*. Oxford, New York: Oxford University Press, Jan. 2007 (cit. on pp. 1, 9, 77, 79, 94, 114, 149).

[Bra02] D. Braun. „Creation of Entanglement by Interaction with a Common Heat Bath“. In: *Phys. Rev. Lett.* 89.27 (Dec. 2002), p. 277901 (cit. on pp. 5, 92).

[Bru+96] M. Brune, F. Schmidt-Kaler, A. Maali, et al. „Quantum Rabi Oscillation: A Direct Test of Field Quantization in a Cavity“. In: *Phys. Rev. Lett.* 76.11 (Mar. 1996), pp. 1800–1803 (cit. on pp. 75, 78).

[BTV03] R. Bulla, N.-H. Tong, and M. Vojta. „Numerical Renormalization Group for Bosonic Systems and Application to the Sub-Ohmic Spin-Boson Model“. In: *Phys. Rev. Lett.* 91.17 (Oct. 2003), p. 170601 (cit. on pp. 45, 57, 59, 75, 117).

[CCS13] X. Chen, J. Cao, and R. J. Silbey. „A Novel Construction of Complex-Valued Gaussian Processes with Arbitrary Spectral Densities and Its Application to Excitation Energy Transfer“. In: *J. Chem. Phys.* 138.22 (June 2013), p. 224104 (cit. on pp. 31, 84).

[CDG98] C. Cohen-Tannoudji, J. Dupont-Roc, and G. Grynberg. *Atom-Photon Interactions: Basic Processes and Applications*. New York: Wiley-VCH, Mar. 1998 (cit. on pp. 9, 31, 79).

[CL83] A. O. Caldeira and A. J. Leggett. „Quantum Tunnelling in a Dissipative System“. In: *Annals of Physics* 149.2 (Sept. 1983), pp. 374–456 (cit. on p. 1).

[Col15] P. Coleman. *Introduction to Many-Body Physics*. Cambridge University Press, Nov. 2015 (cit. on p. 57).

[CS78] J. F. Clauser and A. Shimony. „Bell's Theorem. Experimental Tests and Implications“. In: *Rep. Prog. Phys.* 41.12 (Dec. 1978), pp. 1881–1927 (cit. on pp. 1, 91).

[CT06] A. Chin and M. Turlakov. „Coherent-Incoherent Transition in the Sub-Ohmic Spin-Boson Model“. In: *Phys. Rev. B* 73.7 (Feb. 2006), p. 075311 (cit. on p. 45).

[Cui+19] L. Cui, H.-D. Zhang, X. Zheng, R.-X. Xu, and Y. Yan. „Highly Efficient and Accurate Sum-over-Poles Expansion of Fermi and Bose Functions at near Zero Temperatures: Fano Spectrum Decomposition Scheme“. In: *J. Chem. Phys.* 151.2 (July 2019), p. 024110 (cit. on pp. 41, 57).

[Dav20] D. Davidović. „Completely Positive, Simple, and Possibly Highly Accurate Approximation of the Redfield Equation“. In: *Quantum* 4 (Sept. 2020), p. 326 (cit. on pp. 6, 10, 76, 93, 94, 99, 102, 122, 154–156).

[Dav74] E. B. Davies. „Markovian Master Equations“. In: *Commun. Math. Phys.* 39.2 (June 1974), pp. 91–110 (cit. on pp. 10, 79).

[Dav76] E. B. Davies. „Markovian Master Equations. II“. In: *Mathematische Annalen* 219.2 (June 1976), pp. 147–158 (cit. on p. 95).

[deV+05] I. deVega, D. Alonso, P. Gaspard, and W. T. Strunz. „Non-Markovian Stochastic Schrödinger Equations in Different Temperature Regimes: A Study of the Spin-Boson Model“. In: *J. Chem. Phys.* 122.12 (Mar. 2005), p. 124106 (cit. on pp. 20, 65, 150).

[DGS98] L. Diósi, N. Gisin, and W. T. Strunz. „Non-Markovian Quantum State Diffusion“. In: *Phys. Rev. A* 58.3 (Sept. 1998), pp. 1699–1712 (cit. on pp. 2, 4, 11–13, 20, 23, 24, 27, 36, 46, 71).

[Dod+18] A. Dodin, T. Tscherbul, R. Alicki, A. Vutha, and P. Brumer. „Secular versus Nonsecular Redfield Dynamics and Fano Coherences in Incoherent Excitation: An Experimental Proposal“. In: *Phys. Rev. A* 97.1 (Jan. 2018), p. 013421 (cit. on p. 5).

[DS13] M. H. Devoret and R. J. Schoelkopf. „Superconducting Circuits for Quantum Information: An Outlook“. In: *Science* 339.6124 (Mar. 2013), pp. 1169–1174 (cit. on pp. 3, 75).

[DS97] L. Diósi and W. T. Strunz. „The Non-Markovian Stochastic Schrödinger Equation for Open Systems“. In: *Phys. Lett. A* 235.6 (Nov. 1997), pp. 569–573 (cit. on p. 27).

[DS98] M. Dubé and P. C. E. Stamp. „Dynamics of a Pair of Interacting Spins Coupled to an Environmental Sea“. In: *Int. J. Mod. Phys. B* 12.11 (May 1998), pp. 1191–1245 (cit. on p. 92).

[Dua+17] C. Duan, Z. Tang, J. Cao, and J. Wu. „Zero-Temperature Localization in a Sub-Ohmic Spin-Boson Model Investigated by an Extended Hierarchy Equation of Motion“. In: *Phys. Rev. B* 95.21 (June 2017), p. 214308 (cit. on p. 16).

[Eas+16] P. R. Eastham, P. Kirton, H. M. Cammack, B. W. Lovett, and J. Keeling. „Bath-Induced Coherence and the Secular Approximation“. In: *Phys. Rev. A* 94.1 (July 2016), p. 012110 (cit. on pp. 5, 94).

[Eng+07] G. S. Engel, T. R. Calhoun, E. L. Read, et al. „Evidence for Wavelike Energy Transfer through Quantum Coherence in Photosynthetic Systems“. In: *Nature* 446.7137 (Apr. 2007), pp. 782–786 (cit. on p. 10).

[EPR35] A. Einstein, B. Podolsky, and N. Rosen. „Can Quantum-Mechanical Description of Physical Reality Be Considered Complete?“ In: *Phys. Rev.* 47.10 (May 1935), pp. 777–780 (cit. on pp. 1, 91).

[Eva10] L. C. Evans. *Partial Differential Equations*. American Mathematical Soc., Jan. 2010 (cit. on p. 21).

[EW92] R. Egger and U. Weiss. „Quantum Monte Carlo Simulation of the Dynamics of the Spin-Boson Model“. In: *Z. Physik B - Condensed Matter* 89.1 (Feb. 1992), pp. 97–107 (cit. on p. 59).

[Fag06] R. L. Fagaly. „Superconducting Quantum Interference Device Instruments and Applications“. In: *Review of Scientific Instruments* 77.10 (Oct. 2006), p. 101101 (cit. on p. 75).

[FC11] C. H. Fleming and N. I. Cummings. „Accuracy of Perturbative Master Equations“. In: *Phys. Rev. E* 83.3 (Mar. 2011), p. 031117 (cit. on pp. 6, 7, 102, 123).

[FDD21] S. Flannigan, F. Damanet, and A. J. Daley. „Many-Body Quantum State Diffusion for Non-Markovian Dynamics in Strongly Interacting Systems“. In: *arXiv:2108.06224 [quant-ph]* (Aug. 2021). arXiv: `2108.06224 [quant-ph]` (cit. on p. 133).

[Fle+10] C. Fleming, N. I. Cummings, C. Anastopoulos, and B. L. Hu. „The Rotating-Wave Approximation: Consistency and Applicability from an Open Quantum System Analysis“. In: *J. Phys. A: Math. Theor.* 43.40 (2010), p. 405304 (cit. on p. 94).

[For+17] P. Forn-Díaz, J. J. García-Ripoll, B. Peropadre, et al. „Ultrastrong Coupling of a Single Artificial Atom to an Electromagnetic Continuum in the Nonperturbative Regime“. In: *Nature Physics* 13.1 (Jan. 2017), pp. 39–43 (cit. on p. 75).

[Fri+19] A. Frisk Kockum, A. Miranowicz, S. De Liberato, S. Savasta, and F. Nori. „Ultrastrong Coupling between Light and Matter“. In: *Nat. Rev. Phys.* 1.1 (Jan. 2019), pp. 19–40 (cit. on p. 3).

[FV63] R. P. Feynman and F. L. Vernon Jr. „The Theory of a General Quantum System Interacting with a Linear Dissipative System“. In: *Ann. Phys.* 24.0 (Oct. 1963), pp. 118–173 (cit. on pp. 31, 84, 121).

[GE16] C. Gogolin and J. Eisert. „Equilibration, Thermalisation, and the Emergence of Statistical Mechanics in Closed Quantum Systems“. In: *Rep. Prog. Phys.* 79.5 (May 2016), p. 056001 (cit. on p. 120).

[Gol+06] S. Goldstein, J. L. Lebowitz, R. Tumulka, and N. Zanghì. „Canonical Typicality“. In: *Phys. Rev. Lett.* 96.5 (Feb. 2006), p. 050403 (cit. on p. 120).

[Gor+04] T. Gorin, T. Prosen, T. H. Seligman, and W. T. Strunz. „Connection between Decoherence and Fidelity Decay in Echo Dynamics“. In: *Phys. Rev. A* 70.4 (Oct. 2004), p. 042105 (cit. on p. 115).

[Gra06] H. Grabert. *Projection Operator Techniques in Nonequilibrium Statistical Mechanics*. Springer, Apr. 2006 (cit. on p. 149).

[Gro+16] F. Grossmann, M. Werther, L. Chen, and Y. Zhao. „Generalization of the Davydov Ansatz by Squeezing“. In: *Chemical Physics*. Quantum Dynamics and Femtosecond Spectroscopy Dedicated to Prof. Vladimir Y. Chernyak on the Occasion of His 60th Birthday 481 (Dec. 2016), pp. 99–107 (cit. on pp. 10, 33).

[GS12] R. G. Ghanem and P. Spanos. *Stochastic Finite Elements: A Spectral Approach*. Springer Science & Business Media, Dec. 2012 (cit. on pp. 32–34, 47).

[Gus+14] M. V. Gustafsson, T. Aref, A. F. Kockum, et al. „Propagating Phonons Coupled to an Artificial Atom". In: *Science* 346.6206 (Oct. 2014), pp. 207–211 (cit. on p. 75).

[GZC92] B. Golding, M. N. Zimmerman, and S. N. Coppersmith. „Dissipative Quantum Tunneling of a Single Microscopic Defect in a Mesoscopic Metal". In: *Phys. Rev. Lett.* 68.7 (Feb. 1992), pp. 998–1001 (cit. on p. 78).

[Har+19] R. Hartmann, M. Werther, F. Grossmann, and W. T. Strunz. „Exact Open Quantum System Dynamics: Optimal Frequency vs Time Representation of Bath Correlations". In: *J. Chem. Phys.* 150.23 (June 2019), p. 234105 (cit. on pp. 11, 27, 33, 36, 57, 58).

[Hay+03] T. Hayashi, T. Fujisawa, H. D. Cheong, Y. H. Jeong, and Y. Hirayama. „Coherent Manipulation of Electronic States in a Double Quantum Dot". In: *Phys. Rev. Lett.* 91.22 (Nov. 2003), p. 226804 (cit. on p. 78).

[HBR20] S. Haroche, M. Brune, and J. M. Raimond. „From Cavity to Circuit Quantum Electrodynamics". In: *Nature Physics* 16.3 (Mar. 2020), pp. 243–246 (cit. on p. 75).

[HC18] C.-Y. Hsieh and J. Cao. „A Unified Stochastic Formulation of Dissipative Quantum Dynamics. I. Generalized Hierarchical Equations". In: *The Journal of Chemical Physics* 148.1 (Jan. 2018), p. 014103 (cit. on p. 33).

[Hem+18] C. Hempel, C. Maier, J. Romero, et al. „Quantum Chemistry Calculations on a Trapped-Ion Quantum Simulator". In: *Phys. Rev. X* 8.3 (July 2018), p. 031022 (cit. on p. 75).

[Hen+15] B. Hensen, H. Bernien, A. E. Dréau, et al. „Loophole-Free Bell Inequality Violation Using Electron Spins Separated by 1.3 Kilometres". In: *Nature* 526.7575 (Oct. 2015), pp. 682–686 (cit. on pp. 1, 91).

[HL16] L. Henriet and K. Le Hur. „Quantum Sweeps, Synchronization, and Kibble-Zurek Physics in Dissipative Quantum Spin Systems". In: *Phys. Rev. B* 93.6 (Feb. 2016), p. 064411 (cit. on pp. 92, 110).

[Hor+09] R. Horodecki, P. Horodecki, M. Horodecki, and K. Horodecki. „Quantum Entanglement". In: *Rev. Mod. Phys.* 81.2 (June 2009), pp. 865–942 (cit. on pp. 91, 93).

[HS17] R. Hartmann and W. T. Strunz. „Exact Open Quantum System Dynamics Using the Hierarchy of Pure States (HOPS)". In: *J. Chem. Theory Comput.* 13.12 (Dec. 2017), pp. 5834–5845 (cit. on pp. 11, 18, 27, 65, 71, 78, 121).

[HS20a] R. Hartmann and W. T. Strunz. „Accuracy Assessment of Perturbative Master Equations: Embracing Nonpositivity". In: *Phys. Rev. A* 101.1 (Jan. 2020), p. 012103 (cit. on pp. 6, 7, 80, 94, 96–98, 100, 102, 150).

[HS20b] R. Hartmann and W. T. Strunz. „Environmentally Induced Entanglement – Anomalous Behavior in the Adiabatic Regime". In: *Quantum* 4 (Oct. 2020), p. 347 (cit. on pp. 6, 27, 91, 93).

[HS21] R. Hartmann and W. T. Strunz. „Open Quantum System Response from the Hierarchy of Pure States“. In: *J. Phys. Chem. A* 125.32 (Aug. 2021), pp. 7066–7079 (cit. on p. 125).

[HW97] S. Hill and W. K. Wootters. „Entanglement of a Pair of Quantum Bits“. In: *Phys. Rev. Lett.* 78.26 (June 1997), pp. 5022–5025 (cit. on p. 93).

[HXY10] J. Hu, R.-X. Xu, and Y. Yan. „Communication: Padé Spectrum Decomposition of Fermi Function and Bose Function“. In: *J. Chem. Phys.* 133.10 (Sept. 2010), p. 101106 (cit. on p. 57).

[IF09] A. Ishizaki and G. R. Fleming. „Theoretical Examination of Quantum Coherence in a Photosynthetic System at Physiological Temperature“. In: *PNAS* 106.41 (Oct. 2009), pp. 17255–17260 (cit. on p. 133).

[Isa09] A. Isar. „Entanglement Generation and Evolution in Open Quantum Systems“. In: *Open Systems & Information Dynamics* 16.02n03 (Sept. 2009), pp. 205–219 (cit. on pp. 5, 92).

[Jes+15] J. Jeske, D. J. Ing, M. B. Plenio, S. F. Huelga, and J. H. Cole. „Bloch-Redfield Equations for Modeling Light-Harvesting Complexes“. In: *The Journal of Chemical Physics* 142.6 (Feb. 2015), p. 064104 (cit. on pp. 94, 95, 152).

[JK03] S. Joe and F. Y. Kuo. „Remark on Algorithm 659: Implementing Sobol's Quasirandom Sequence Generator“. In: *ACM Trans. Math. Softw.* 29.1 (Mar. 2003), pp. 49–57 (cit. on p. 59).

[JK08] S. Joe and F. Y. Kuo. „Constructing Sobol Sequences with Better Two-Dimensional Projections“. In: *SIAM Journal on Scientific Computing* 30.5 (Jan. 2008), pp. 2635–2654 (cit. on p. 59).

[Joh+21] F. Johansson et al. *Mpmath: A Python Library for Arbitrary-Precision Floating-Point Arithmetic*. http://mpmath.org/. Oct. 2021 (cit. on p. 127).

[Joh17] F. Johansson. „Arb: Efficient Arbitrary-Precision Midpoint-Radius Interval Arithmetic“. In: *IEEE Transactions on Computers* 66.8 (Aug. 2017), pp. 1281–1292 (cit. on pp. 138, 139).

[KA14] D. Kast and J. Ankerhold. „Bipartite Entanglement Dynamics of Two-Level Systems in Sub-Ohmic Reservoirs“. In: *Phys. Rev. B* 90.10 (Sept. 2014), p. 100301 (cit. on pp. 6, 103, 110).

[Kal+83] Y. Kaluzny, P. Goy, M. Gross, J. M. Raimond, and S. Haroche. „Observation of Self-Induced Rabi Oscillations in Two-Level Atoms Excited Inside a Resonant Cavity: The Ringing Regime of Superradiance“. In: *Phys. Rev. Lett.* 51.13 (Sept. 1983), pp. 1175–1178 (cit. on p. 75).

[KC08] S. Kryszewski and J. Czechowska-Kryszk. „Master Equation - Tutorial Approach“. In: *arXiv:0801.1757 [quant-ph]* (Jan. 2008). arXiv: `0801.1757 [quant-ph]` (cit. on pp. 79, 80, 94, 149).

[Kim+02] M. S. Kim, J. Lee, D. Ahn, and P. L. Knight. „Entanglement Induced by a Single-Mode Heat Environment“. In: *Phys. Rev. A* 65.4 (Apr. 2002), p. 040101 (cit. on p. 92).

[KLS16] S. Kretschmer, K. Luoma, and W. T. Strunz. „Collision Model for Non-Markovian Quantum Dynamics“. In: *Phys. Rev. A* 94.1 (July 2016), p. 012106 (cit. on pp. 32, 36).

[KM96] S. Kehrein and A. Mielke. „On the Spin–Boson Model with a Sub–Ohmic Bath“. In: *Physics Letters A* 219.5-6 (Aug. 1996), pp. 313–318. arXiv: `cond-mat/9602022` (cit. on pp. 75, 88).

[KMT11] H. Kobayashi, B. L. Mark, and W. Turin. *Probability, Random Processes, and Statistical Analysis : Applications to Communications, Signal Processing, Queueing Theory and Mathematical Finance*. Cambridge: Cambridge University Press, 2011 (cit. on pp. 32–34, 47).

[Lam+19] N. Lambert, S. Ahmed, M. Cirio, and F. Nori. „Modelling the Ultra-Strongly Coupled Spin-Boson Model with Unphysical Modes“. In: *Nature Communications* 10.1 (Aug. 2019), p. 3721 (cit. on p. 75).

[Leg+87] A. J. Leggett, S. Chakravarty, A. T. Dorsey, et al. „Dynamics of the Dissipative Two-State System“. In: *Rev. Mod. Phys.* 59.1 (Jan. 1987), pp. 1–85 (cit. on pp. 3, 4, 9, 45, 57, 59, 75–78, 88, 89, 122).

[Lin+09] N. Linden, S. Popescu, A. J. Short, and A. Winter. „Quantum Mechanical Evolution towards Thermal Equilibrium“. In: *Phys. Rev. E* 79.6 (June 2009), p. 061103 (cit. on p. 120).

[Lin76] G. Lindblad. „On the Generators of Quantum Dynamical Semigroups“. In: *Commun.Math. Phys.* 48.2 (June 1976), pp. 119–130 (cit. on p. 96).

[LW06] K. Lendi and A. J. van Wonderen. „Davies Theory for Reservoir-Induced Entanglement in a Bipartite System“. In: *J. Phys. A: Math. Theor.* 40.2 (Dec. 2006), pp. 279–288 (cit. on pp. 5, 94).

[Ma+12] J. Ma, Z. Sun, X. Wang, and F. Nori. „Entanglement Dynamics of Two Qubits in a Common Bath“. In: *Phys. Rev. A* 85.6 (June 2012), p. 062323 (cit. on pp. 5, 94).

[Mag+18] L. Magazzù, P. Forn-Díaz, R. Belyansky, et al. „Probing the Strongly Driven Spin-Boson Model in a Superconducting Quantum Circuit“. In: *Nat. Commun.* 9.1 (Apr. 2018), p. 1403 (cit. on pp. 3, 7, 10, 45, 57, 75, 78, 121).

[Maj+13] C. Majenz, T. Albash, H.-P. Breuer, and D. A. Lidar. „Coarse Graining Can Beat the Rotating-Wave Approximation in Quantum Markovian Master Equations“. In: *Phys. Rev. A* 88.1 (July 2013), p. 012103 (cit. on pp. 94, 100, 152).

[Mak95] N. Makri. „Numerical Path Integral Techniques for Long Time Dynamics of Quantum Dissipative Systems“. In: *Journal of Mathematical Physics* 36.5 (May 1995), pp. 2430–2457 (cit. on pp. 1, 10, 39).

[Maz+09] L. Mazzola, S. Maniscalco, J. Piilo, K.-A. Suominen, and B. M. Garraway. „Sudden Death and Sudden Birth of Entanglement in Common Structured Reservoirs“. In: *Phys. Rev. A* 79.4 (Apr. 2009), p. 042302 (cit. on pp. 92, 110).

[MC13] J. M. Moix and J. Cao. „A Hybrid Stochastic Hierarchy Equations of Motion Approach to Treat the Low Temperature Dynamics of Non-Markovian Open Quantum Systems“. In: *J. Chem. Phys.* 139.13 (Oct. 2013), p. 134106 (cit. on pp. 31, 84).

[McC+09] D. P. S. McCutcheon, A. Nazir, S. Bose, and A. J. Fisher. „Long-Lived Spin Entanglement Induced by a Spatially Correlated Thermal Bath“. In: *Physical Review A* 80.2 (Aug. 2009), p. 022337 (cit. on p. 94).

[Mik+14] S. G. Mikhlin, I. N. Sneddon, M. Stark, and S. Ulam. *Integral Equations: And Their Applications to Certain Problems in Mechanics, Mathematical Physics and Technology*. Pergamon, July 2014 (cit. on p. 47).

[Min+05] F. Mintert, A. R. R. Carvalho, M. Kuś, and A. Buchleitner. „Measures and Dynamics of Entangled States“. In: *Physics Reports* 415.4 (Aug. 2005), pp. 207–259 (cit. on pp. 5, 92).

[MM13] Q. Meng and H.-D. Meyer. „A Multilayer MCTDH Study on the Full Dimensional Vibronic Dynamics of Naphthalene and Anthracene Cations“. In: *J. Chem. Phys.* 138.1 (Jan. 2013), p. 014313 (cit. on pp. 10, 33).

[MM95] N. Makri and D. E. Makarov. „Tensor Propagator for Iterative Quantum Time Evolution of Reduced Density Matrices. I. Theory“. In: *The Journal of Chemical Physics* 102.11 (Mar. 1995), pp. 4600–4610 (cit. on pp. 1, 10, 76).

[MMC90] H.-D. Meyer, U. Manthe, and L. S. Cederbaum. „The Multi-Configurational Time-Dependent Hartree Approach“. In: *Chem. Phys. Lett.* 165.1 (Jan. 1990), pp. 73–78 (cit. on p. 10).

[Mor05] M. Mori. „Discovery of the Double Exponential Transformation and Its Developments“. In: *Publications of the Research Institute for Mathematical Sciences* 41.4 (2005), pp. 897–935 (cit. on pp. 49, 55, 142).

[MSS01] Y. Makhlin, G. Schön, and A. Shnirman. „Quantum-State Engineering with Josephson-Junction Devices“. In: *Rev. Mod. Phys.* 73.2 (May 2001), pp. 357–400 (cit. on p. 75).

[MT99] C. Meier and D. J. Tannor. „Non-Markovian Evolution of the Density Operator in the Presence of Strong Laser Fields“. In: *J. Chem. Phys.* 111.8 (Aug. 1999), pp. 3365–3376 (cit. on pp. 4, 11, 57, 84).

[Nak58] S. Nakajima. „On Quantum Theory of Transport PhenomenaSteady Diffusion“. In: *Prog Theor Phys* 20.6 (Dec. 1958), pp. 948–959 (cit. on p. 149).

[NC00] M. A. Nielsen and I. L. Chuang. *Quantum Computation and Quantum Information*. Cambridge ; New York: Cambridge University Press, Oct. 2000 (cit. on pp. 1, 91).

[Nes+07] F. Nesi, E. Paladino, M. Thorwart, and M. Grifoni. „Spin-Boson Dynamics: A Unified Approach from Weak to Strong Coupling“. In: *EPL* 80.4 (2007), p. 40005 (cit. on p. 75).

[NF14] K.-J. Noh and U. R. Fischer. „Consistent perturbative treatment of the subohmic spin-boson model yielding arbitrarily small T_2/T_1 decoherence time ratios“. In: *Phys. Rev. B* 90.22 (Dec. 2014), p. 220302 (cit. on p. 82).

[Nie+10] T. Niemczyk, F. Deppe, H. Huebl, et al. „Circuit Quantum Electrodynamics in the Ultrastrong-Coupling Regime“. In: *Nat. Phys.* 6.10 (Oct. 2010), pp. 772–776 (cit. on pp. 10, 75, 78, 121).

[NMG16] R. A. Norte, J. P. Moura, and S. Gröblacher. „Mechanical Resonators for Quantum Optomechanics Experiments at Room Temperature“. In: *Phys. Rev. Lett.* 116.14 (Apr. 2016), p. 147202 (cit. on p. 3).

[NT10] P. Nalbach and M. Thorwart. „Ultraslow Quantum Dynamics in a Sub-Ohmic Heat Bath“. In: *Phys. Rev. B* 81.5 (Feb. 2010), p. 054308 (cit. on p. 29).

[ON10] F. W. J. Olver and National Institute of Standards and Technology (U.S.), eds. *NIST Handbook of Mathematical Functions*. Cambridge ; New York: Cambridge University Press : NIST, 2010 (cit. on p. 138).

[Ort+10] P. P. Orth, D. Roosen, W. Hofstetter, and K. Le Hur. „Dynamics, Synchronization, and Quantum Phase Transitions of Two Dissipative Spins“. In: *Phys. Rev. B* 82.14 (Oct. 2010), p. 144423 (cit. on pp. 8, 92, 110, 120, 124).

[PC99] V. Y. Pan and Z. Q. Chen. „The Complexity of the Matrix Eigenproblem“. In: *Proceedings of the Thirty-First Annual ACM Symposium on Theory of Computing*. STOC '99. Atlanta, Georgia, USA: Association for Computing Machinery, May 1999, pp. 507–516 (cit. on p. 51).

[Pec94] P. Pechukas. „Reduced Dynamics Need Not Be Completely Positive“. In: *Phys. Rev. Lett.* 73.8 (1994), pp. 1060–1062 (cit. on p. 96).

[Per+10] B. Peropadre, P. Forn-Díaz, E. Solano, and J. J. García-Ripoll. „Switchable Ultrastrong Coupling in Circuit QED“. In: *Phys. Rev. Lett.* 105.2 (July 2010), p. 023601 (cit. on p. 75).

[PES96] G. M. Palma, A. K. Ekert, and K. A. Suominen. „Quantum Computers and Dissipation“. In: *Proc. R. Soc. Lond., A* 452.quant-ph/9702001 (1996), p. 567 (cit. on p. 77).

[Por+08] D. Porras, F. Marquardt, J. von Delft, and J. I. Cirac. „Mesoscopic Spin-Boson Models of Trapped Ions“. In: *Phys. Rev. A* 78.1 (July 2008), p. 010101 (cit. on pp. 75, 78).

[Pre+07] W. H. Press, S. A. Teukolsky, W. T. Vetterling, and B. P. Flannery. *Numerical Recipes 3rd Edition: The Art of Scientific Computing*. Auflage: 3. Cambridge, UK ; New York: Cambridge University Press, Sept. 2007 (cit. on pp. 48, 49).

[RE14] G. Ritschel and A. Eisfeld. „Analytic Representations of Bath Correlation Functions for Ohmic and Superohmic Spectral Densities Using Simple Poles“. In: *J. Chem. Phys.* 141.9 (Sept. 2014), p. 094101 (cit. on p. 57).

[Red57] A. G. Redfield. „On the Theory of Relaxation Processes“. In: *IBM J. Res. Dev.* 1.1 (Jan. 1957), pp. 19–31 (cit. on pp. 10, 76, 94).

[RK19] H. Rahman and U. Kleinekathöfer. „Chebyshev Hierarchical Equations of Motion for Systems with Arbitrary Spectral Densities and Temperatures“. In: *J. Chem. Phys.* 150.24 (June 2019), p. 244104 (cit. on pp. 2, 10, 33).

[SB02] J. Stoer and R. Bulirsch. *Introduction to Numerical Analysis*. Springer Science & Business Media, Aug. 2002 (cit. on p. 54).

[SB08] G. Schaller and T. Brandes. „Preservation of Positivity by Dynamical Coarse Graining“. In: *Phys. Rev. A* 78.2 (Aug. 2008), p. 022106 (cit. on pp. 6, 10, 76, 94, 100, 122, 152, 153).

[Sch17] T. Schaetz. „Trapping Ions and Atoms Optically“. In: *J. Phys. B: At. Mol. Opt. Phys.* 50.10 (Apr. 2017), p. 102001 (cit. on p. 75).

[Sch35] E. Schrödinger. „Die gegenwärtige Situation in der Quantenmechanik“. In: *Naturwissenschaften* 23.48 (Nov. 1935), pp. 807–812 (cit. on p. 1).

[Sci+20] SciPy 1.0 Contributors, P. Virtanen, R. Gommers, et al. „SciPy 1.0: Fundamental Algorithms for Scientific Computing in Python“. In: *Nature Methods* 17.3 (Mar. 2020), pp. 261–272 (cit. on p. 61).

[SDG99] W. T. Strunz, L. Diósi, and N. Gisin. „Open System Dynamics with Non-Markovian Quantum Trajectories“. In: *Phys. Rev. Lett.* 82.9 (Mar. 1999), pp. 1801–1805 (cit. on pp. 2, 11–13, 24, 121).

[SES14] D. Suess, A. Eisfeld, and W. T. Strunz. „Hierarchy of Stochastic Pure States for Open Quantum System Dynamics“. In: *Phys. Rev. Lett.* 113.15 (Oct. 2014), p. 150403 (cit. on pp. 2, 11, 12, 18, 121).

[SG02] J. T. Stockburger and H. Grabert. „Exact c-Number Representation of Non-Markovian Quantum Dissipation“. In: *Phys. Rev. Lett.* 88.17 (Apr. 2002), p. 170407 (cit. on p. 31).

[SL07] H. Spohn and J. L. Lebowitz. „Irreversible Thermodynamics for Quantum Systems Weakly Coupled to Thermal Reservoirs“. In: *Advances in Chemical Physics*. Ed. by S. A. Rice. Hoboken, NJ, USA: John Wiley & Sons, Inc., Mar. 2007, pp. 109–142 (cit. on p. 95).

[SM13] M. M. Sahrapour and N. Makri. „Tunneling, Decoherence, and Entanglement of Two Spins Interacting with a Dissipative Bath“. In: *The Journal of Chemical Physics* 138.11 (Mar. 2013), p. 114109 (cit. on pp. 92–94).

[Sob67] I. M. Sobol'. „On the Distribution of Points in a Cube and the Approximate Evaluation of Integrals“. In: *USSR Computational Mathematics and Mathematical Physics* 7.4 (1967), pp. 86–112 (cit. on p. 59).

[STP07] D. Solenov, D. Tolkunov, and V. Privman. „Exchange Interaction, Entanglement, and Quantum Noise Due to a Thermal Bosonic Field“. In: *Physical Review B* 75.3 (Jan. 2007), p. 035134 (cit. on p. 94).

[Str+18] A. Strathearn, P. Kirton, D. Kilda, J. Keeling, and B. W. Lovett. „Efficient Non-Markovian Quantum Dynamics Using Time-Evolving Matrix Product Operators“. In: *Nature Communications* 9.1 (Aug. 2018), p. 3322 (cit. on pp. 1, 8, 10, 39, 45, 75, 76, 89, 117, 122).

[Str01] W. T. Strunz. „The Brownian Motion Stochastic Schrödinger Equation“. In: *Chemical Physics* 268.1 (June 2001), pp. 237–248 (cit. on p. 23).

[Str96] W. T. Strunz. „Linear Quantum State Diffusion for Non-Markovian Open Quantum Systems“. In: *Phys. Lett. A* 224.1 (Dec. 1996), pp. 25–30 (cit. on pp. 2, 11, 12).

[SU83] G. W. Semenoff and H. Umezawa. „Functional Methods in Thermofield Dynamics: A Real-Time Perturbation Theory for Quantum Statistical Mechanics“. In: *Nucl. Phys. B* 220.2 (June 1983), pp. 196–212 (cit. on pp. 4, 36, 71).

[Sun+15] K.-W. Sun, M. F. Gelin, V. Y. Chernyak, and Y. Zhao. „Davydov Ansatz as an Efficient Tool for the Simulation of Nonlinear Optical Response of Molecular Aggregates“. In: *J. Chem. Phys.* 142.21 (May 2015), p. 212448 (cit. on pp. 10, 33).

[Tan+15] Z. Tang, X. Ouyang, Z. Gong, H. Wang, and J. Wu. „Extended Hierarchy Equation of Motion for the Spin-Boson Model“. In: *J. Chem. Phys.* 143.22 (Dec. 2015), p. 224112 (cit. on pp. 2, 4, 10, 16, 41, 45, 75, 84–86).

[Tan06] Y. Tanimura. „Stochastic Liouville, Langevin, Fokker–Planck, and Master Equation Approaches to Quantum Dissipative Systems“. In: *J. Phys. Soc. Jpn.* 75.8 (2006), p. 082001 (cit. on pp. 2, 4, 10, 16, 33, 57, 84, 121).

[Tan14] Y. Tanimura. „Reduced Hierarchical Equations of Motion in Real and Imaginary Time: Correlated Initial States and Thermodynamic Quantities“. In: *J. Chem. Phys.* 141.4 (July 2014), p. 044114 (cit. on pp. 2, 4, 10, 57).

[Tan20] Y. Tanimura. „Numerically “Exact” Approach to Open Quantum Dynamics: The Hierarchical Equations of Motion (HEOM)“. In: *J. Chem. Phys.* 153.2 (July 2020), p. 020901 (cit. on p. 33).

[Tas98] H. Tasaki. „From Quantum Dynamics to the Canonical Distribution: General Picture and a Rigorous Example“. In: *Phys. Rev. Lett.* 80.7 (Feb. 1998), pp. 1373–1376 (cit. on p. 120).

[TB15] T. V. Tscherbul and P. Brumer. „Partial Secular Bloch-Redfield Master Equation for Incoherent Excitation of Multilevel Quantum Systems“. In: *J. Chem. Phys.* 142.10 (Mar. 2015), p. 104107 (cit. on pp. 6, 94, 95, 152).

[TK89] Y. Tanimura and R. Kubo. „Two-Time Correlation Functions of a System Coupled to a Heat Bath with a Gaussian-Markoffian Interaction“. In: *J. Phys. Soc. Jpn.* 58.4 (1989), pp. 1199–1206 (cit. on pp. 16, 33, 84).

[TM73] H. Takahasi and M. Mori. „Double Exponential Formulas for Numerical Integration“. In: *Publications of the Research Institute for Mathematical Sciences* 9.3 (1973), pp. 721–741 (cit. on p. 55).

[TPG04] M. Thorwart, E. Paladino, and M. Grifoni. „Dynamics of the Spin-Boson Model with a Structured Environment“. In: *Chemical Physics*. The Spin-Boson Problem: From Electron Transfer to Quantum Computing ... to the 60th Birthday of Professor Ulrich Weiss 296.2 (Jan. 2004), pp. 333–344 (cit. on p. 75).

[TU96] Y. Takahashi and H. Umezawa. „Thermo Field Dynamics“. In: *Int. J. Mod. Phys. B* 10.13n14 (June 1996), pp. 1755–1805 (cit. on pp. 4, 36, 71).

[Tup+21] D. Tupkary, A. Dhar, M. Kulkarni, and A. Purkayastha. „Fundamental Limitations in Lindblad Descriptions of Systems Weakly Coupled to Baths“. In: *arXiv:2105.12091 [cond-mat, physics:quant-ph]* (Aug. 2021). arXiv: 2105.12091 [cond-mat, physics:quant-ph] (cit. on pp. 6, 102, 123).

[Ull66] P. Ullersma. „An Exactly Solvable Model for Brownian Motion: I. Derivation of the Langevin Equation“. In: *Physica* 32.1 (Jan. 1966), pp. 27–55 (cit. on pp. 9, 78).

[Unr95] W. G. Unruh. „Maintaining Coherence in Quantum Computers“. In: *Phys. Rev. A* 51.2 (Feb. 1995), pp. 992–997 (cit. on p. 77).

[VJC13] N. Vogt, J. Jeske, and J. H. Cole. „Stochastic Bloch-Redfield Theory: Quantum Jumps in a Solid-State Environment“. In: *Physical Review B* 88.17 (Nov. 2013), p. 174514 (cit. on pp. 94, 95, 152).

[Wal+00] C. H. van der Wal, A. C. J. ter Haar, F. K. Wilhelm, et al. „Quantum Superposition of Macroscopic Persistent-Current States“. In: *Science* 290.5492 (Oct. 2000), pp. 773–777 (cit. on p. 75).

[Wei08] U. Weiss. *Quantum Dissipative Systems*. Singapore: World Scientific, Mar. 2008 (cit. on pp. 1, 6, 9, 27, 29, 76, 77, 88, 102, 120, 123, 137).

[WG18] M. Werther and F. Grossmann. „The Davydov D1.5 Ansatz for the Quantum Rabi Model“. In: *Phys. Scr.* 93.7 (June 2018), p. 074001 (cit. on p. 10).

[WG20] M. Werther and F. Großmann. „Apoptosis of Moving Nonorthogonal Basis Functions in Many-Particle Quantum Dynamics“. In: *Phys. Rev. B* 101.17 (May 2020), p. 174315 (cit. on pp. 33, 36, 87).

[Whi08] R. S. Whitney. „Staying Positive: Going beyond Lindblad with Perturbative Master Equations“. In: *J. Phys. A: Math. Theor.* 41.17 (2008), p. 175304 (cit. on p. 149).

[WR14] A. Winter and H. Rieger. „Quantum Phase Transition and Correlations in the Multi-Spin-Boson Model“. In: *Phys. Rev. B* 90.22 (Dec. 2014), p. 224401 (cit. on pp. 8, 110, 124).

[WS19] H. Wang and J. Shao. „Quantum Phase Transition in the Spin-Boson Model: A Multilayer Multiconfiguration Time-Dependent Hartree Study“. In: *J. Phys. Chem. A* 123.9 (Mar. 2019), pp. 1882–1893 (cit. on pp. 2, 117, 122, 124).

[WT03] H. Wang and M. Thoss. „Multilayer Formulation of the Multiconfiguration Time-Dependent Hartree Theory“. In: *J. Chem. Phys.* 119.3 (July 2003), pp. 1289–1299 (cit. on pp. 2, 10, 33, 36, 87).

[WT08] H. Wang and M. Thoss. „From Coherent Motion to Localization: Dynamics of the Spin-Boson Model at Zero Temperature“. In: *New J. Phys.* 10.11 (2008), p. 115005 (cit. on pp. 8, 45, 57, 78, 87, 117).

[WT10] H. Wang and M. Thoss. „From Coherent Motion to Localization: II. Dynamics of the Spin-Boson Model with Sub-Ohmic Spectral Density at Zero Temperature“. In: *Chem. Phys.* Dynamics of Molecular Systems: From Quantum to Classical 370.1–3 (May 2010), pp. 78–86 (cit. on pp. 2, 8, 57, 59, 75, 78, 87, 89).

[WYS13] L.-A. Wu, C. X. Yu, and D. Segal. „Exact Dynamics of Interacting Qubits in a Thermal Environment: Results beyond the Weak Coupling Limit“. In: *New J. Phys.* 15.2 (Feb. 2013), p. 023044 (cit. on p. 110).

[XDR02] Y. Xue, S. Datta, and M. A. Ratner. „First-Principles Based Matrix Green's Function Approach to Molecular Electronic Devices: General Formalism“. In: *Chemical Physics* 281.2 (Aug. 2002), pp. 151–170 (cit. on p. 57).

[YE09] T. Yu and J. H. Eberly. „Sudden Death of Entanglement“. In: *Science* 323.5914 (Jan. 2009), pp. 598–601 (cit. on pp. 5, 92, 110).

[Yos+17] F. Yoshihara, T. Fuse, S. Ashhab, et al. „Superconducting Qubit–Oscillator Circuit beyond the Ultrastrong-Coupling Regime“. In: *Nature Physics* 13.1 (Jan. 2017), pp. 44–47 (cit. on p. 75).

[Yu+99] T. Yu, L. Diósi, N. Gisin, and W. T. Strunz. „Non-Markovian Quantum-State Diffusion: Perturbation Approach“. In: *Phys. Rev. A* 60.1 (July 1999), pp. 91–103 (cit. on p. 150).

[ZBE18] P.-P. Zhang, C. D. B. Bentley, and A. Eisfeld. „Flexible Scheme to Truncate the Hierarchy of Pure States“. In: *The Journal of Chemical Physics* 148.13 (Apr. 2018), p. 134103 (cit. on p. 69).

[Zho+18] N. Zhou, Y. Zhang, Z. Lü, and Y. Zhao. „Variational Study of the Two-Impurity Spin–Boson Model with a Common Ohmic Bath: Ground-State Phase Transitions“. In: *Annalen der Physik* 530.10 (2018), p. 1800120 (cit. on pp. 7, 8, 110).

[ZQK09] T. Zell, F. Queisser, and R. Klesse. „Distance Dependence of Entanglement Generation via a Bosonic Heat Bath“. In: *Phys. Rev. Lett.* 102.16 (Apr. 2009), p. 160501 (cit. on p. 92).

[Zur03] W. H. Zurek. „Decoherence, Einselection, and the Quantum Origins of the Classical“. In: *Rev. Mod. Phys.* 75.3 (May 2003), pp. 715–775 (cit. on pp. 5, 92).

[Zwa60] R. Zwanzig. „Ensemble Method in the Theory of Irreversibility“. In: *J. Chem. Phys.* 33.5 (Nov. 1960), pp. 1338–1341 (cit. on p. 149).

Colophon

This thesis was typeset with LaTeX 2$_\varepsilon$. It uses the *Clean Thesis* style developed by Ricardo Langner. The design of the *Clean Thesis* style is inspired by user guide documents from Apple Inc.

Download the *Clean Thesis* style at `http://cleanthesis.der-ric.de/`.

Erklärung

Hiermit versichere ich, dass ich die vorliegende Arbeit ohne unzulässige Hilfe Dritter und ohne Benutzung anderer als der angegebenen Hilfsmittel angefertigt habe; die aus fremden Quellen direkt oder indirekt übernommenen Gedanken sind als solche kenntlich gemacht. Die Arbeit wurde bisher weder im Inland noch im Ausland in gleicher oder ähnlicher Form einer anderen Prüfungsbehörde vorgelegt.

Die vorliegende Arbeit wurde am Institut für Theoretische Physik der Technischen Universität Dresden unter der wissenschaftlichen Betreuung Prof. Dr. Walter Strunz durchgeführt.

Dresden, 8. November 2021

Richard Hartmann